

Dumitrita Spinu

Lignin to Bio-fuels via Fast Pyrolysis Process Assisted by Catalytic Upgrading of Volatiles

July 2019



Norwegian University of
Science and Technology

Lignin to Bio-fuels via Fast Pyrolysis Process Assisted by Catalytic Upgrading of Volatiles

Dumitrita Spinu

Chemical Engineering

Submission date: July 2019

Supervisor: Professor De Chen

Co-supervisor: Associate Professor Kumar Ranjan Rout

Norwegian University of Science and Technology
Department of Chemical Engineering

Abstract

The increase of energy consumption and noticeable climate change have made people focus progressively on more sustainable and environmentally friendly energy sources. The bio-oil production from lignin has become a very researched area as it is a promising precursor of the aromatic compounds required by the fuel and petrochemical plants. However, considering its thermal and physical resistant structures, as well as the instability, acidity and low heating value of the thermal generated oil, this material requires a detailed investigation of different conditions and a proper catalyst able to improve the oil yield and its properties, as well as to reduce the overall process energy consumption. The lignin used in this project is obtained as a by-product on the Etanolix plant, St1 company. Its thermal behavior was studied in two processes: fast pyrolysis (FP) and fast pyrolysis assisted by a subsequently catalytic upgrading of the volatiles (FP-CU). Three sets of catalysts were involved in the volatiles upgrading step. First set was consisted of 5, 10 and 15 wt% of Mo and 10wt% of MoCo, MoCu, MoFe, MoNi oxy phosphates impregnated on γ - Al_2O_3 support. The support was also tested in order to correctly evaluate the activity of the impregnated species. The second set was formed of different zeolites, namely HZSM-5 with Si/Al ratio of 30, 50, 80 and 280, HZSM-22, SAPO-11, SAPO-34, H β and HY. Different Si/Al ratios of HZSM-5 were studied in order to see the effect of the acid sites density on the products distribution. The influence of the zeolite structure and pore size, as well as the strength of the acidic sites on the products distribution were also investigated. The last set was consisted of Mo oxy phosphates (10 wt%) impregnated on HZSM-5(Si/Al=30), H β and HY, as well as Ni oxide (10 wt%) on HZSM-5(30). The goal was to identify if a higher surface area provided by the zeolites could improve the upgrading properties of MoP. The NiO/HZSM-5(30) was tested in order to see any upgrading improvements. Different techniques like XRD, BET, TGA and NH_3 -TPD were used for the catalyst's characterization. Two different reactors were involved in this study in order to test different conditions and catalysts: a microcopyrolizer (Py) coupled with the GC/MS and a fixed bed tubular reactor. The Py-GC/MS was used to test different temperatures of the FP of lignin, as well as to screen the activity of all the selected catalysts in the FP-CU process. However, this type of reactor is mostly used in the qualitative analysis. According to this, a fixed bed reactor with higher dimensions was used to generate the gas, liquid and solid yields at the temperature and in the presence of the most active catalysts found in the Py-GC/MS based on products distribution. Moreover, the gas and liquid products were quantified by using GC/FID/TCD/MS. The char and coke yields were also determined based on the total solid yield and the coke yield calculated by TGA of spent catalysts.

From the temperature analysis of lignin FP in the Py-GC/MS, 550 °C was the value selected for the FP-CU due to the generating of more Ph and MAH compared to 500 °C. A higher temperature was not selected as there was not observed a significant increase of the Ph and MAH. The MoP (10 wt%) manifested interesting deoxygenation properties in the FP-CU process by converting the PhA into a large content of Ph, MAH and DAH. However, it was not tested in the fixed bed reactor as the total area was much lower compared to tested zeolites, especially HZSM-5(30). When testing the Si/Al ratio of HZSM-5, it was noticed that by increasing the density of acid sites, more MAH and DAH are generated. Moreover, the HZSM-5(Si/Al=30) recorded the highest activity and selectivity for MAH compared to the rest of the zeolites. By realizing the NH_3 -TPD of HZSM-5(Si/Al=30), H β and HY, the HZSM-5 was found with stronger acid sites compared to the H β and HY. The

impregnation of MoP on the zeolites significantly decreased the total area compared to the area generated by the pure zeolite. Accordingly, they were not chosen for the testing in the fixed bed reactor, neither was NiO/HZSM-5(30) due to the high area fraction of PhA. By testing the Si/Al ratio of HZSM-5 in the fixed bed reactor, it was noticed that there was no variation of the oil yield, however, by decreasing the Si/Al ratio, more coke was generated and this is because of the density of the acid sites which promotes the bimolecular reaction. The activity of H β and HY was also analyzed in the fixed bed reactor. By comparing their results with HZSM-5(30), it was observed that HY generated the highest oil yield (53 wt%) due to its high internal pore space. However, the selectivity for aromatic hydrocarbons was lower compared to H β and HZSM-5(30). Moreover, HY produced the highest coke yield (22 wt%), which was also associated to its large pores and supercages.

The pathway of lignin was also developed based on seven model compounds. It was observed that the substituent in the para position of the guaiacol structure influenced the reactivity of the compound. In addition, when comparing the products generated in the FP of each model compound with the products of lignin FP, it was noticed that the products which were supposed to be found in large quantities in the lignin pyrolysis were not detected and this could be related to the synergy between different radicals derived from the various linkages and phenolic compounds of lignin.

Key words: Lignin; Fast Pyrolysis; Catalytic upgrading; Lignin pathway

Acknowledgments

I would like to express my sincere gratitude to my supervisor Professor De Chen, and my co-supervisor Associate Professor Kumar Ranjan Rout for their valuable and constructive feedback, as well as for their continuous encouragement and support throughout my MSc thesis.

Many thanks to PhD Issac Yeboah, Postdoc. Xiang Feng and Zhenping Cai for their useful suggestions, creative ideas and technical/data support.

I would like to offer also my special thanks to the St1 company for the provided lignin feedstock, as well as for their cooperation and valuable information.

Furthermore, I express my appreciation to Senior Engineer Estelle Marie M. Vanhaecke and Senior Advisor Anne Hoff for organizing the equipment training and keeping the laboratories secure and well maintained.

Table of Contents

List of Figures	ix
List of Tables	xv
List of Abbreviations	xvi
1 Introduction.....	1
1.1 Motivation	1
1.2 Objectives	3
2 Literature Survey & Theory	4
2.1 Lignocellulosic biomass	4
2.1.1 Cellulose.....	4
2.1.2 Hemicellulose	5
2.1.3 Lignin.....	5
2.1.3.1 Types of lignin	8
2.1.3.2 Physical properties of lignin	9
2.1.3.3 Various application of lignin and its derivatives	9
2.2 Lignocellulose processing	14
2.2.1 Physical Pretreatment.....	15
2.2.2 Chemical Pretreatment	16
2.2.3 Biological pretreatment.....	16
2.3 Thermal cracking of β -O-4 and C_{α} - C_{β}	17
2.4 Thermo-catalytic conversion processes of lignin	20
2.4.1 Gasification	20
2.4.2 Pyrolysis.....	21
2.4.3 Hydrogenolysis	30
2.5 Zeolites	32
2.5.1 Faujasite (FAU).....	34
2.5.2 Chabazite (CHA)	35
2.5.3 ZSM-5 (MFI)	36
2.5.4 Beta polymorphs *BEA and BEC	36
2.5.5 ZSM-22 (TON).....	37
2.5.6 SAPO-11.....	37
2.6 Synthesis	38
2.6.1 Incipient wetness impregnation.....	38
2.6.2 Calcination.....	38
2.7 Characterization	38
2.7.1 Surface area and the pore system - N ₂ adsorption.....	38
2.7.2 X-ray diffraction.....	42

2.7.3 Temperature Programmed Desorption Technique.....	44
2.7.4 Thermal Gravimetric Analysis-Mass Spectrometry.....	45
2.8 Activity.....	45
2.8.1 Py-GC/MS.....	45
2.9 GC-FID/TCD.....	47
2.9.1 Gas Chromatography/Thermal Conductivity Detector (TCD).....	47
2.9.2 Gas Chromatography/Flame Ionization Detector (FID).....	47
3 Material and Methods.....	48
3.1 Elemental Composition and Pretreatment of Lignin.....	48
3.2 Preparation of catalyst.....	48
3.2.1 Incipient wetness impregnation and calcination.....	48
3.2.2 Activation of zeolites.....	49
3.2.3 Oxides of transition metals supported on alumina.....	49
3.3 Characterization.....	49
3.3.1 Surface area and the pore system- N ₂ adsorption.....	49
3.3.2 X-ray Diffraction.....	50
3.3.3 Temperature Programmed Desorption Technique.....	50
3.3.4 Thermal Gravimetric Analysis-Mass Spectrometry.....	50
3.4 Activity.....	50
3.4.1 Py/GC-MS.....	50
3.4.2 Fixed bed reactor.....	51
3.4.3 Liquid Analysis: Gas Chromatography/ Flame Ionization Detector (FID)/Mass Spectrometry detector.....	54
3.4.4 Gas Analysis: Gas Chromatography/Thermal Conductivity Detector (TCD)/ Flame Ionization Detector (FID).....	55
4 Results & Discussion.....	56
4.1 Characterization.....	56
4.1.1 Surface area and the pore system- N ₂ adsorption.....	56
4.1.2 X-ray diffraction (XRD).....	59
4.1.3 Temperature Programmed Desorption Technique (NH ₃ -TPD).....	61
4.1.4 Thermal Gravimetric Analysis-Mass Spectrometry.....	62
4.2 Activity.....	67
4.2.1 Py-GC/MS.....	67
4.2.1.1 Temperature analysis (FP).....	68
4.2.1.2 Fast pyrolysis-upgrading of volatiles on metal-non-metal oxides supported on γ -Al ₂ O ₃	70
4.2.1.3 Fast pyrolysis- catalytic upgrading of volatiles on three different loadings of MoP oxides on γ -Al ₂ O ₃	73
4.2.1.4 Fast pyrolysis- catalytic upgrading of volatiles on HZSM-22, HZSM-5 (Si/Al=30, 50, 80 and 280), H β , SAPO-11, SAPO-34 and HY.....	73

4.2.1.5 Fast pyrolysis-catalytic upgrading of volatiles on MoP(10 %)/HZSM-5(30), NiO(10 %)/HZSM-5(30), MoP(10 %)/H β and MoP(10 %)/HY.....	78
4.2.2 Fixed bed reactor	79
4.2.2.1 Temperature analysis of the FP-CU process on HZSM-5(30).....	80
4.2.2.2 Nitrogen flow analysis of the FP-CU process on HZSM-5(30)	83
4.2.2.3 Catalyst:lignin ratio analysis of the FP-CU process on HZSM-5(30)	86
4.2.2.4 FP vs FP-CU.....	89
4.2.2.5 The effect of SiO ₂ /Al ₂ O ₃ ratio of HZSM-5 on the upgrading of the pyrolytic volatiles	92
4.2.2.6 The influence of the pore size and internal pore architecture on the upgrading of pyrolytic volatiles.....	94
4.2.2.7 The FP-CU of pine and polyethylene powder- process revision.....	96
5 Lignin Pathway.....	100
5.1 The pathway of lignin fast pyrolysis coupled with in-situ catalytic upgrading.....	100
5.1.1 Guaiacol	104
5.1.2 Creosol.....	108
5.1.3 Phenol, 4-ethyl-2-methoxy-.....	112
5.1.4 Phenol, 2-methoxy-4-propyl-	119
5.1.5 Trans-Isoeugenol	124
5.1.6 Vanillin	130
5.1.7 Apocynin	135
5.2 FP of model compounds vs FP of lignin	139
6 Conclusions	143
7 Bibliography	146
8 Appendix.....	152
A1. Introduction.....	152
A2. Literature Survey and Theory	153
A3. Material and Methods	157
A4. Results and Discussion	160

List of Figures

Figure 2.1 Lignocellulose structure. "GI" – glucuronic acid and "Fer" – esterification with ferulic acid[8].....	5
Figure 2.2 Structure of the three lignin monolignols[13].....	6
Figure 2.3 Three main lignin units obtained after polymerization[14].....	7
Figure 2.4 Examples of C-O-C and C-C linkages between the three units of the lignin structure[11]	7
Figure 2.5 The pathway of crude oil[16].....	10
Figure 2.6 Different applications of polypropylene[18].....	11
Figure 2.7 Different application of lignin polymer[26]	14
Figure 2.8 Alder-ene reaction[31]	17
Figure 2.9 Retro-ene reaction of PPE	18
Figure 2.10 Homolytic cleavage of C _β -O (A) and C _α - C _β (B)[29]	19
Figure 2.11 Concerted reaction pathways of the β-O-4 linkage in the pyrolytic process of model compound 1 [29].....	19
Figure 2.12 Thermochemical conversion processes of lignin into different products[34]	20
Figure 2.13 Simulation of catalytic fast pyrolysis and fast pyrolysis coupled with catalytic upgrading of volatiles[33]	23
Figure 2.14 The distribution of non-CFP and CFP products for the three zeolites[40].....	24
Figure 2.15 The selectivity of silica and aluminosilicate based catalysts[42]	25
Figure 2.16 Non-CFT and CFP of four lignin sources[43].....	26
Figure 2.17 The pathway of the non-CFP coupled with the catalytic upgrading[44].....	27
Figure 2.18 Carbon yield variation with different Fe loadings[45].....	28
Figure 2.19 The variation of products distribution with different loadings of MgO on the mesoporous Al-MCM-41 and unsupported MgO[48].....	29
Figure 2.20 The O/C ratio and H/C ratio of the crude oil, conventional fuels, three polymers of lignocellulose and other chemical and petrochemical compounds[51].....	30
Figure 2.21 Hydrodeoxygenation of phenols pathway[56].....	31

Figure 2.22 The structure and the pore dimensions of Faujasite, ZSM-12, ZSM-5 and Theta-1[61]	33
Figure 2.23 Some examples of CBUs with their name and pore symbols[62]	34
Figure 2.24 CHA framework structure and its channel system[62]	35
Figure 2.25 MFI framework structure and its channel system[62]	36
Figure 2.26 *BEA (a) and BEC (b) structures[62]	37
Figure 2.27 Physisorption isotherms (left side) and the hysteresis loops (right side) proposed by IUPAC[70]	40
Figure 2.28 Different pore shapes and the associated hysteresis loops[71]	40
Figure 2.29 The ideal form of Type II isotherm[68]	41
Figure 2.30 The BET plot[68]	41
Figure 2.31 Constructive and destructive interferences[74]	43
Figure 2.32 Bragg's Law[75]	44
Figure 2.33 a - PY-GC/MS system configuration; b - Multi-shot pyrolyzer[79]	46
Figure 3.1 (a)-Pyrolyzer-Gas Chromatography/Mass Spectrometry; (b)-Sample cup – simulates fast catalytic pyrolysis; (c)-Sample cup-simulates the fast pyrolysis and the fast pyrolysis coupled with the catalytic upgrading step	51
Figure 3.2 The flowsheet of the FP and FP-CU processes.....	53
Figure 4.1 N ₂ adsorption isotherms of HZSM-5(30) (left) and MoP(10%)/ HZSM-5(30) (right).....	57
Figure 4.2 N ₂ adsorption isotherm of MoP(10%)/β.....	58
Figure 4.3 N ₂ adsorption isotherms of HY (left) and MoP(10 %)/ HY (right)	58
Figure 4.4 N ₂ adsorption isotherms of SAPO-11 and ZSM-22.....	59
Figure 4.5 The diffractograms of HZSM-5(30) and MoP(10%)/HZSM-5(30)	60
Figure 4.6 The diffractograms of Hβ and MoP(10%)/Hβ	60
Figure 4.7 The diffractograms of HY and MoP(10%)/HY	61
Figure 4.8 The NH ₃ -TPD results for Hβ, HY and HZSM-5(30)	62
Figure 4.9 Weight loss of the spent HZSM-5 with Si/Al= 30, 50, 80 and 280 (FP-CU at 550 °C, C:L=1, N ₂ flow=40 mL/min)	63
Figure 4.10 The CO ₂ ion current (MS) and HDSC of HZSM-5(30) (A), HZSM-5 (50) (B), HZSM-5 (80) (C) and HZSM-5 (280) (D) (FP-CU at 550 °C, C:L=1, N ₂ flow=40 mL/min)	64

Figure 4.11 Weight loss of the spent HZSM-5(30), H β and HY(FP-CU at 550 °C, C:L=1, N ₂ flow=40 mL/min)	65
Figure 4.12 The CO ₂ ion current (MS) and HDSC of H β (A) and HY (B) (FP-CU at 550 °C, C:L=1, N ₂ flow=40 mL/min)	65
Figure 4.13 Weight loss of the spent HZSM-5(30) involved in the FP-CU at 450, 550 and 600 °C (C:L=1, N ₂ flow=40 mL/min)	66
Figure 4.14 The CO ₂ ion current (MS) and HDSC of HZSM-5 involved in FP-CU at 450 (A) and 600 °C (B) (C:L=1, N ₂ flow=40 mL/min)	67
Figure 4.15 The products distributions obtained from lignin in the FP at 500, 550, 600, 650 and 700 °C. Process was realized in a Py-GC/MS at helium flowrate of 2 mL/min.....	69
Figure 4.16 The yield variation with the temperature of the main PhA and Ph compounds. FP was realized in a Py-GC/MS at helium flowrate of 2 mL/min.....	70
Figure 4.17 The products distribution of FP (L) and FP-CU on γ -Al ₂ O ₃ and MoXP/ γ -Al ₂ O ₃ (X=Co, Cu, Ni or Fe) at 550 °C, Py-GC/MS	72
Figure 4.18 The products distribution of FP (L) and FP-CU on γ -Al ₂ O ₃ and MoXP (10 %)/ γ -Al ₂ O ₃ (X=Co, Cu, Ni or Fe) at 550 °C, Py-GC/MS	72
Figure 4.19 The products distribution of FP-CU on MoP (5 %)/ γ -Al ₂ O ₃ , MoP (10 %)/ γ -Al ₂ O ₃ and MoP (15 %)/ γ -Al ₂ O ₃ at 550 °C, Py-GC/MS.....	73
Figure 4.20 The products distribution of FP and FP-CU on HZSM-22, HZSM-5 with Si/Al=30, 50, 80 and 280, H β , SAPO-11, SAPO-34 HY (Py-GC/MS, 550 °C, C:L=3 (0.5 mg (lignin), 1.5 mg (catalyst)))	76
Figure 4.21 The products distribution of FP and FP-CU on HZSM-22, HZSM-5 with Si/Al=30, 50, 80 and 280, H β , SAPO-11, SAPO-34 HY (Py-GC/MS, 550 °C, C:L=3 (0.5 mg (lignin), 1.5 mg (catalyst)))	77
Figure 4.22 The products distribution (carbon number) of FP-CU on HZSM-22, HZS-5(30), H β and HY (Py-GC/MS, 550 °C, C:L=3 (0.5 mg (lignin), 1.5 mg (catalyst))).....	77
Figure 4.23 The products distribution of FP-CU on MoP(10%)/HZSM-5(30) and NiO(10 %)/HZSM-5(30) (Py-GC/MS, 550 °C, C:L=3 (0.5 mg (lignin), 1.5 mg (catalyst))).....	78
Figure 4.24 The products distribution of FP-CU on MoP (10 %)/H β and MoP (10 %)/HY (Py-GC/MS, 550 °C, C:L=3 (0.5 mg (lignin), 1.5 mg (catalyst))).....	79
Figure 4.25 Temperature analysis of the FP-CU process on HZSM-5(30) (N ₂ flow=40 mL/min, C:L=1). A-fixed bed reactor results. B-Fixed bed reactor and TGA results	81
Figure 4.26 Temperature effect on the products distribution of the liquid phase resulted in the FP-CU on HZSM-5(30) (N ₂ flow=40 ml/min, C:L=1)	82

Figure 4.27 Temperature effect on the products distribution of the gas phase resulted in the FP-CU on HZSM-5(30) (N ₂ flow=40 ml/min, C:L=1)	83
Figure 4.28 Nitrogen flowrate analysis of the FP-CU process on HZSM-5(30) (t=600 °C, C:L=1). A-fixed bed reactor results. B-Fixed bed reactor and TGA results....	84
Figure 4.29 Nitrogen flowrate effect on the products distribution of the liquid phase resulted in the FP-CU on HZSM-5(30) (t=600 °C, C:L=1).....	85
Figure 4.30 Nitrogen flowrate effect on the products distribution of the gas phase resulted in the FP-CU on HZSM-5(30) (t=600 °C, C:L=1).....	86
Figure 4.31 Catalyst to lignin ratio analysis of the FP-CU process on HZSM-5(30) (t=550 °C, nitrogen flowrate=40 mL/min). A-fixed bed reactor results. B-Fixed bed reactor and TGA results.....	87
Figure 4.32 Catalyst to lignin ratio effect on the products distribution of the liquid phase resulted in the FP-CU on HZSM-5(30) (t=550 °C, nitrogen flowrate=40 mL/min)	88
Figure 4.33 Catalyst to lignin ratio effect on the products distribution of the gas phase resulted in the FP-CU on HZSM-5(30) (t=550 °C, nitrogen flowrate=40 mL/min)	88
Figure 4.34 The effect of HZSM-5(30) on the oxygenated volatiles resulted in the FP at 550 and 600 °C (nitrogen flowrate=40 mL/min, a ratio of one was set for the HZSM-5(30)/lignin and SiO ₂ /lignin). A-fixed bed reactor results. B-Fixed bed reactor and TGA results.....	90
Figure 4.35 The products distribution of liquid phase resulted in the FP and FP-CU realized at 550 and 600 °C. HZSM-5(30) was used in the FP-CU and SiO ₂ in the FP. (nitrogen flowrate=40 mL/min, a ratio of one was set for the HZSM-5(30)/lignin and SiO ₂ /lignin)	91
Figure 4.36 The products distribution of gas phase resulted in the FP and FP-CU realized at 550 and 600 °C. HZSM-5(30) was used in the FP-CU and SiO ₂ in the FP. (nitrogen flowrate=40 mL/min, a ratio of one was set for the HZSM-5(30)/lignin and SiO ₂ /lignin)	91
Figure 4.37 The effect of SiO ₂ /Al ₂ O ₃ of HZSM-5 on the distribution of the three main products: gas, liquid and solid. The FP-CU was realized at 550 °C, nitrogen flowrate of 40 mL/min and C:L ratio of 1. A-fixed bed reactor results, B-fixed bed reactor and TGA results.....	92
Figure 4.38 The effect of SiO ₂ /Al ₂ O ₃ of HZSM-5 on the distribution of the liquid products. The FP-CU was realized at 550 °C, nitrogen flowrate of 40 mL/min and C:L ratio of 1	93
Figure 4.39 The effect of SiO ₂ /Al ₂ O ₃ of HZSM-5 on the distribution of the gas products. The FP-CU was realized at 550 °C, nitrogen flowrate of 40 mL/min and C:L ratio of 1	93
Figure 4.40 The effect of pore size and internal pore architecture on the distribution of the three main products: gas, liquid and solid. The pore size: HZSM-	

5(30)<H β <HY. The FP-CU was realized at 550 °C, nitrogen flowrate of 40 mL/min and C:L ratio of 1. A-fixed bed reactor results, B-fixed bed reactor and TGA results 94

Figure 4.41 The effect of pore size and internal pore architecture on the products distribution of liquid phase. The pore size: HZSM-5(30)<H β <HY. The FP-CU was realized at 550 °C, nitrogen flowrate of 40 mL/min and C:L ratio of 1 95

Figure 4.42 The effect of pore size and internal pore architecture on the products distribution of gas phase. The pore size: HZSM-5(30)<H β <HY. The FP-CU was realized at 550 °C, nitrogen flowrate of 40 mL/min and C:L ratio of 1 96

Figure 4.43 The products distribution of FP-CU of polyethylene powder in the fixed bed reactor (A) and Py-GC/MS (B). A: t=600 °C, nitrogen flowrate of 40 mL/min and catalyst to PE ratio of 1. The products were quantified based the effective carbon number approach. B: t=600 °C, helium flowrate of 2 mL/min and catalyst to PE ratio of 3 98

Figure 4.44 The products distribution of FP-CU of pine in the fixed bed reactor. The process was realized at 600 °C, nitrogen flowrate of 40 mL/min and catalyst to lignin ratio of 3. The products of liquid phase were analysed only by GC/MS 99

Figure 4.45 The products distribution of FP-CU of lignin in the fixed bed reactor. The process was realized at 700 °C, nitrogen flowrate of 100 mL/min and catalyst to lignin ratio of 1. The products of liquid phase were analysed only by GC/MS..... 99

Figure 5.1 The name and structure of the seven lignin model compounds (A) and the coniferyl alcohol monolignol (B[11]) 101

Figure 5.2 The main linkages of lignin network and the model lignin compound (A-1-(4-hydroxy-3-methoxyphenyl)-2-(2-methoxyphenoxy) propane-1,3-diol) (Me: methyl group)..... 102

Figure 5.3 Concerted retro-ene (Alder-ene) fragmentation of 1-(4-hydroxy-3-methoxyphenyl)-2-(2-methoxyphenoxy) propane-1,3-diol -1..... 102

Figure 5.4 The synthesis reactions of vanillin-7, tran-Isoeugenol-12, phenol, 4-ethyl-2-methoxy- 16, apocynin- 10, phenol, 2-methoxy-4-propyl- 14, creosol- 19..... 103

Figure 5.5 Guaiacol: the overlapped 550 °C and 650 °C pyrograms (A) and 650 °C and 650 °C-HZSM-5 pyrograms (B) 105

Figure 5.6 The guaiacol fast pyrolysis pathway..... 107

Figure 5.7 The pathway of guaiacol in the fast pyrolysis process coupled with the catalytic upgrading (HZSM-5 with SiO₂/Al₂O₃=30) 108

Figure 5.8 Creosol: the overlapped 550 °C and 650 °C pyrograms (A) and 650 °C and 650 °C-HZSM-5 pyrograms (B) 109

Figure 5.9 The creosol fast pyrolysis pathway 112

Figure 5.10 The pathway of creosol in the fast pyrolysis process coupled with the catalytic upgrading (HZSM-5 with SiO₂/Al₂O₃=30) 112

Figure 5.11 Phenol, 4-ethyl-2-methoxy-: the overlapped 550 °C and 650 °C pyrograms (A) and 650 °C and 650 °C-HZSM-5 pyrograms (B).....	114
Figure 5.12 The phenol, 4-ethyl-2-methoxy- fast pyrolysis pathway.....	118
Figure 5.13 The pathway of phenol, 4-ethyl-2-methoxy- in the fast pyrolysis process coupled with the catalytic upgrading (HZSM-5 with SiO ₂ /Al ₂ O ₃ =30).....	118
Figure 5.14 Phenol, 2-methoxy-4-propyl-: the overlapped 550 °C and 650 °C pyrograms (A) and 650 °C and 650 °C-HZSM-5 pyrograms (B).....	120
Figure 5.15 The phenol, 2-methoxy-4-propyl- fast pyrolysis pathway.....	123
Figure 5.16 The pathway of phenol, 2-methoxy-4-propyl- in the fast pyrolysis process coupled with the catalytic upgrading (HZSM-5 with SiO ₂ /Al ₂ O ₃ =30).....	124
Figure 5.17 Trans-Isoeugenol: the overlapped 550 °C and 650 °C pyrograms (A) and 650 °C and 650 °C-HZSM-5 pyrograms (B).....	125
Figure 5.18 The trans-Isoeugenol fast pyrolysis pathway.....	129
Figure 5.19 The pathway of trans-Isoeugenol in the fast pyrolysis process coupled with the catalytic upgrading (HZSM-5 with SiO ₂ /Al ₂ O ₃ =30).....	130
Figure 5.20 Vanillin: the overlapped 550 °C and 650 °C pyrograms (A) and 650 °C and 650 °C-HZSM-5 pyrograms (B)	131
Figure 5.21 The vanillin fast pyrolysis pathway	134
Figure 5.22 The pathway of vanillin in the fast pyrolysis process coupled with the catalytic upgrading (HZSM-5 with SiO ₂ /Al ₂ O ₃ =30)	134
Figure 5.23 Apocynin: the overlapped 550 °C and 650 °C pyrograms (A) and 650 °C and 650 °C-HZSM-5 pyrograms (B)	135
Figure 5.24 The apocynin fast pyrolysis pathway.....	138
Figure 5.25 The pathway of apocynin in the fast pyrolysis process coupled with the catalytic upgrading (HZSM-5 with SiO ₂ /Al ₂ O ₃ =30)	139
Figure 5.26 The possible reactions of different oxygenated compounds generated with a high area fraction in the FP of model compounds, but not in the FP of lignin	140

List of Tables

Table 2.1 Biological pretreatment of lignocellulose feedstock[27]	16
Table 2.2 The products distribution of the non-CFP and CFP. AL represents Alcell lignin and the % represents the loading of the catalyst*[32]	26
Table 2.3 Short information about FAU structure[62]	35
Table 2.4 Short information about CHA structure[62]	35
Table 2.5 Short information about MFI structure[62].....	36
Table 2.6 *BEA and BEC structure information [62]	37
Table 3.1 The elemental composition of lignin	48
Table 4.1 Surface area of the calcined catalysts.....	57
Table 4.2 The groups generated according to the resulted products.....	68
Table 4.3 The notations for the liquid products analysis	68
Table 4.4 The notations for the liquid products analysis	79
Table 4.5 The notations for the gas products analysis.....	80
Table 5.1 The guaiacol fast pyrolysis and fast pyrolysis coupled with catalytic upgrading products	107
Table 5.2 The creosol fast pyrolysis and fast pyrolysis coupled with catalytic upgrading products	111
Table 5.3 The phenol, 4-ethyl-2-methoxy- fast pyrolysis and fast pyrolysis coupled with catalytic upgrading products	117
Table 5.4 Phenol, 2-methoxy-4-propyl- fast pyrolysis and fast pyrolysis coupled with catalytic upgrading products	122
Table 5.5 Trans-Isoeugenol fast pyrolysis and fast pyrolysis coupled with catalytic upgrading products	129
Table 5.6 Vanillin fast pyrolysis and fast pyrolysis coupled with catalytic upgrading products	133
Table 5.7 Apocynin fast pyrolysis and fast pyrolysis coupled with catalytic upgrading products	138
Table 5.8 The most abundant compounds generated in the FP of the seven model compounds at 650 °C. The area fraction (%) is presented in the square brackets.....	142

List of Abbreviations

Py-GC/MS	Pyrolyzer-Gas Chromatography/Mass Spectrometry
XRD	X-ray diffraction
BET	Brunauer-Emmett-Teller
TPD	Temperature Programmed Desorption
TGA	Thermogravimetric Analysis
FP	Fast Pyrolysis
CU	Catalytic Upgrading
FID	Flame ionization detector
TCD	Thermal Conductivity Detector
CFP	Catalytic Fast Pyrolysis
HHV	Higher Heating Value
BTX	Benzene, Toluene, Xylenes
Si/Al	SiO ₂ /Al ₂ O ₃

1 Introduction

1.1 Motivation

The life is easier when you have a plastic bag to carry your groceries, but it becomes much easier when you have a plastic bag and a car. Car and plastic bags manufacturers are also looking for new ways to optimize and automate their industries. Same goes for other intermediate industries like paint, as well as the plastic monomer industry. These are all connected, together forming a huge framework. People's desire for comfort is increasing, this leading to a surplus in production nowadays, all at the cost of the environment. The evolution of human creativity is recorded in the things created throughout the history. A remarkable change started with the period of 1760-1840, both for mankind and for the environment. This period is called Industrial Revolution. It highlights the manual work that has been mechanized, the iron, cement, chemical, glass, machine tools, food industries that had been set up, the infrastructure, working conditions, sanitation, domestic conditions that had been improved, as well as the creation of steam engine and the gas lighting that had obviously made the life effortless and more interesting[1]. In the same range of time the population number was less than one billion, but due to the accentuated progress in different spheres of activity and to a more appropriate lifestyle, the population growth rate was stimulated. The 20th century was marked by an increase of population of approximately 4.6 billion (Figure 8.1, Appendix). Moreover, the beginning of this century triggered a temperature anomaly on the Earth that is observed due to climate change in different locations. Obviously, this is not a coincidence as the industrial economy has to cope with the population growth and with the human tendency to a more prosperous life. These are the two major factors that create an uncontrollable discomfort to the environment. By consuming enormous quantities of fossil resources in the energy and petrochemistry sectors, as well as in transportation, colossal amounts of greenhouse gases are emitted daily in the atmosphere. These gases are carbon dioxide, methane, water vapor and nitrous oxide. Their ability to absorb and emit the radiation from infrared spectrum contributes to the trapping of heat in the atmosphere. Carbon dioxide is the major problem as it is emitted in extremely large quantities, especially by the processes that involve the combustion of fossil fuels. Referring to what is said, the world is getting increasingly concerned regarding global warming. However, this is not the only concern, as the depletion of fossil resources is also a challenge for the population. In the Figure 8.2(Appendix), an estimation of the period when fossil fuels will run out is presented. Of course, this estimation is based on the current resource usage. Nevertheless, this forecast is closely related to the evolution of the existing technology. By improving the engine performance, the waste recycling all over the world, as well as the fossil sources detection and extraction technology, the period can be extended. However, this time range is not only for improving things, but is also for researching of new energy sources and not only, as the human life is based on the carbon-containing compounds.

Energy is one of the major sources of existence and in order to assure its sustainability, renewable sources provided by nature must be exploited. The sun, wind, water, biomass are the key sources that incorporate large quantities of energy and this energy is given every day around us, moreover, they are renewable and eco-friendly sources that will help to diminish the emissions of greenhouse gases into the atmosphere. In the past, people built up windmills to convert the wind power into mechanical energy that was used to grind

the grain or to pump the water, as well as the water mills that were driven by flowing waters and used for crushing the oil seeds, for producing cloths and for milling the corn[2, 3]. These energy sources, as well as the sun radiation have become very researched topics in the 21st century. The existing technology still requires improvement, as well as the storage of the energy that is not in use at the time of its capturing. However, the human creativity has no boundaries and different mechanisms of storing energy like thermal storage, compressed air, hydrogen production, pumped hydroelectric storage, batteries and many others are studied or implemented in different parts of the world[4]. In order to avoid the energy storage problem, the biomass started to be a very investigated field, and this is because it stores the sun energy in its bio-chemical structure through the photosynthesis process. Of course, this also requires many steps and high costs when the biofuels or different chemical intermediates are decided to be produced, nevertheless the biomass wastes are produced in huge amounts yearly and it is a cheap feedstock. Furthermore, the biomass is the second and the last source after fossil matter that can generate different organic compounds demanded by industries that produce pharmaceuticals, food, solvent, detergents, polymers, clothes and many other goods.

The transesterification of different oil-containing plants and the fermentation of sugar-containing plants are well known processes that produce biodiesel and ethanol. The plants that are usually used in these processes are sugarcane and corn for ethanol production and sunflower, soy, rapeseed for biodiesel production. These products are called first generation biofuels and they are not profitable anymore as the population number is very high and the prices of this feedstock are increased by the competition with food industry. Based on this, people started to focus to the second-generation biofuels that refers mainly to lignocellulosic biomass and to third generation biofuels represented by algae. The lignocellulosic biomass wastes like sawdust, sugarcane bagasse, wood, corn cobs manifest an interest due to their generation in large quantities and to their low price. However, these biomass wastes are still considered a low-grade fuel and are simply burnt to generate power. Of course, getting rid of it is not a choice as many valuable products can be obtained. According to this, many processes like gasification, pyrolysis, anaerobic digestion and fermentation are investigated.

In this project the conversion of lignin into bio-oil via the fast pyrolysis process coupled with the catalytic upgrading step was investigated. The lignin was chosen due to its large amounts which are generated in the paper and ethanol industries. It is obtained as a by-product and doesn't manifest an interest because of its complex structure and its toughness against physical and thermal treatment processes. Anyway, the lignin is a cheap feedstock and its phenolic structure is a very promising source for production of aromatic hydrocarbon and even of different oxygenated aromatic compounds. The lignin studied in this project was supplied by the St1 company that produces ethanol from feedstock like process residue from local bakeries and bread from shops[5].

1.2 Objectives

The main objectives for this project work are to gain insights into the fast pyrolysis and volatiles catalytic upgrading of lignin to biofuels. In other words, the main objectives are:

- To study the thermal behavior of lignin in the fast pyrolysis process with Py-GC/MS;
- To prepare, characterize and screen catalysts for the upgrading of lignin pyrolytic volatiles to biofuels with XRD, BET, TGA, NH₃-TPD and Py-GC/MS;
- To determine the product yields (gas, liquid and solid) in the fixed bed reactor at different process parameters and in the presence of the catalysts found with high deoxygenation properties in the Py-GC/MS;
- To quantify the gas products with GC/FID/TCD, the liquid products with GC/FID/MS and solid products (if developing FP-CU) with TGA-MS.
- To develop the lignin pathway based on different model compounds found in large amounts in the FP products.

2 Literature Survey & Theory

2.1 Lignocellulosic biomass

After fossil sources biomass is the next and the last source of carbon. The U.S national energy security regulations define biomass as a renewable organic substance which includes agriculture products and waste, aquatic plants, wood and wood waste, animal and urban waste[6]. It is well known that water, carbon dioxide and solar energy are the crucial elements for the plant photosynthesis. The energy is stored in the fat, starch, protein that are widely researched and utilized substances, as well as in lignocellulose which still represents a challenge for the research area due to its complexity[6]. The lignocellulosic source is a great material for producing different chemicals and fuels, furthermore, it does not compete with food. According to the information provided by Chen[6], the lignocellulosic material is produced yearly in huge amounts and it is a cheap renewable source. It is classified as waste in many countries in the world. In most cases this material is used as low-grade energy source, but this is not a good solution due to the depletion of fossil sources. Of course, fossil matter is still a basic source for energy production and many other chemicals required by industries for producing food, pharmaceuticals, clothes, detergents, fertilizers and many other products, but lignocellulose is the only other source that can substitute fossil matter in the mentioned applications and even more. It is a renewable source that can reduce carbon dioxide emissions and due to its high oxygen content, plenty of chemicals can be directly produced.

As it is well known, lignocellulose is consisted mainly of three polymers: cellulose, hemicellulose and lignin. Cellulose is the most abundant polymer and it is found in a range of 30-35 %, then comes hemicellulose with 25-30 % and lignin with 10 %[6]. These ranges are approximated as the composition differs from species to species. For example, poplar and pine contain cellulose up to 50 %, spruce contains lignin up to 28 %[7]. In Table 8.1 (Appendix) are presented some lignocellulosic species and their composition. Besides these polymers, lignocellulose has also some ash that represents 5 % and it is consisted mostly of silica, and the rest is water, lipid, protein[6].

2.1.1 Cellulose

Cellulose is consisted of D-glucose units disposed in a linear chain and, as it can be seen in the Figure 2.1, it builds up the cell wall of the plant tissue. These units can be found in a large amount in the cellulose macromolecule and, according to Chen[6], they can reach a value of 10,000. The interconnection of D-glucose monomers is realized by β (1-4) linkages. At ambient temperature this polymer is insoluble in diluted acidic and alkaline solutions and water. It is well known that cellulose is a very important product for producing paper and pulp, textile, as well as in the energy industry[6]. Cotton is consisted mostly of 100 % of cellulose and it is a very demanded plant species.

2.1.2 Hemicellulose

Hemicellulose polymer has a very interesting beginning of its story as its name is derived from a product that was considered a semi-finished product of cellulose or a cellulose precursor. Its structure is consisted of different types of glycosyl: L/D-configuration type, pyran type, furan type and so on[6]. It can be observed in Figure 2.1 that hemicellulose is formed of five-carbon sugars such as Arabinose and Xylose, as well as of six-carbon sugars such as Glucose, Galactose. Hemicellulose, compared to cellulose, can be easily degraded in acidic medium. This polymer, together with cellulose and lignin, play an important role in the plant tissue, they enhance the resistance against cell wall degradation. The main function of this polymer is to adjust the process of cell growth[6].

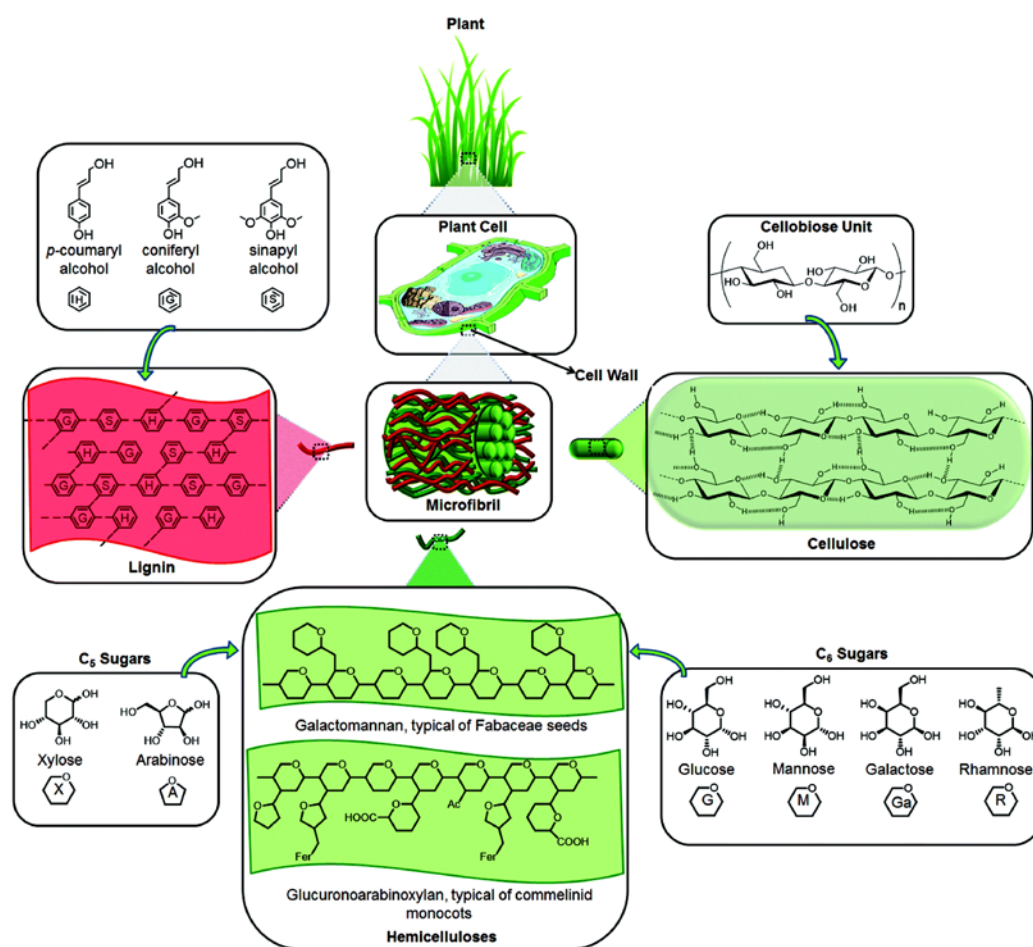


Figure 2.1 Lignocellulose structure. "GI" – glucuronic acid and "Fer" – esterification with ferulic acid[8]

2.1.3 Lignin

Lignin is a three-dimensional polymer which binds the cellulose and hemicellulose in the tissue of the plant offering it strength and stiffness. These properties are very important for the plant when it comes to protection against pathogens and insects[8]. Often, people describe the lignocellulosic plants as woody, and this is due to roots of the word lignin that is derived from the Latin word *lignum* that means wood. The name of this substance was

given by Swiss botanist Augustin Pyramus de Candolle in 1813. At that time and many decades after the lignin was considered an undesired product especially in the pulping process, even though it is one of the most plentiful organic polymers on the planet[9, 10].

Lignin is also called phenylpropanoid polymer as its structure is consisted of two parts: aromatic part and C3 chain [9]. Unlike cellulose that has a linear, definite chain described by a succession of the same monomer, D-glucose, the structure of the lignin is represented by the polymerization of the three monolignols: p-coumaryl alcohol, coniferyl alcohol and sinapyl alcohol (Figure 2.2). From the Figure 2.2 it can be seen that the number of methoxy-groups linked to the ring makes the difference between these monolignols. After polymerization three main units derive from these alcohols: p-hydroxyl-phenyl propanol, guaiacyl-propanol and syringyl-propanol (Figure 2.3)[11]. They are connected randomly and the ratio of these three units depends on the plant species, location and other factors [11]. It is very important to know the structural chemistry of the lignin before using it for different purposes. Based on the ration of the three monolignols there are three types of lignin:

- *Softwood lignin or also named guaiacyl lignin*- this type is consisted almost from coniferyl alcohol (>95 %) and p-coumaryl alcohol. Sometimes the sinapyl alcohol is present, but in insignificant amounts[7, 12];
- *Hardwood lignin or syringyl-guaiacyl lignin*- the ratio of coniferyl alcohol and sinapyl alcohol sometimes tends to 1, but in many cases, it is less than 1. There are species with their structure consisted of an amount of sinapyl alcohol three times higher than coniferyl alcohol. The p-coumaryl alcohol is present in small amounts[7, 12];
- *Grass lignin or HGS lignin (hydroxyl phenol, guaiacyl and syringyl)*- this type is consisted of all three alcohols, but p-coumaryl is found in higher amount[12].

The approximate content of each alcohol in different plant categories can be seen in Table 8.2, Appendix.

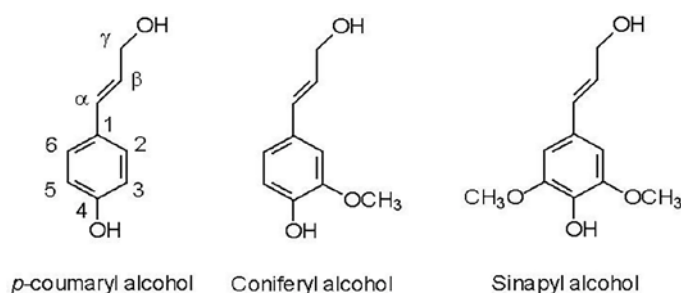


Figure 2.2 Structure of the three lignin monolignols[13]

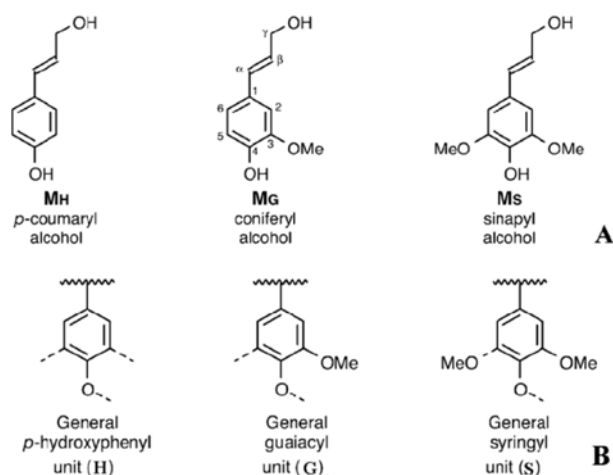


Figure 2.3 Three main lignin units obtained after polymerization[14]

The linkages between the three lignin units play a very important role in the depolymerization processes, considering that they are the first linkages prone to cracking. They are categorized in two groups: ether linkages(C-O-C) and condensed linkages(C-C). Some examples can be observed in Figure 2.4.

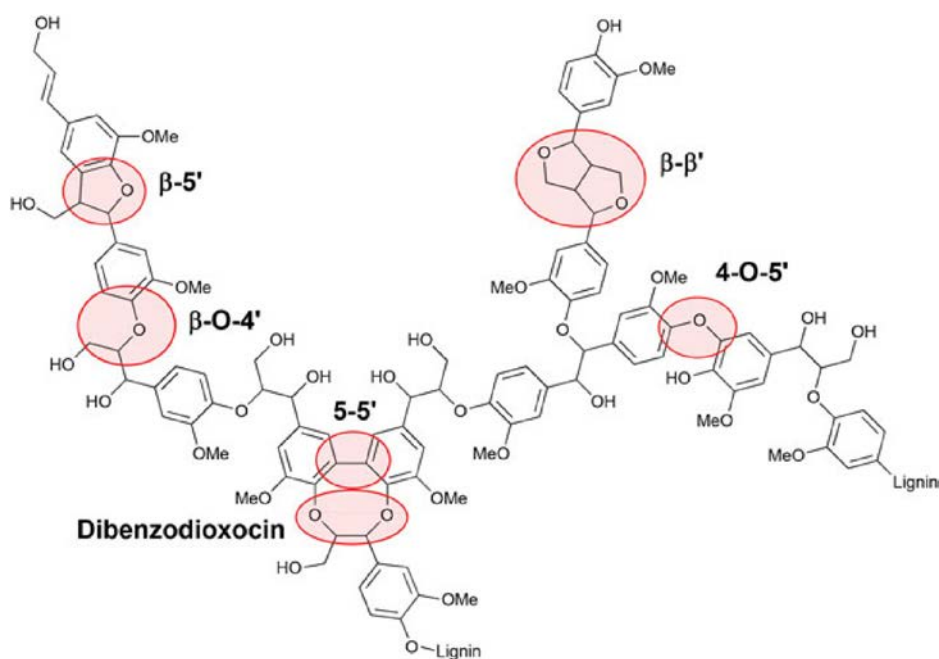


Figure 2.4 Examples of C-O-C and C-C linkages between the three units of the lignin structure[11]

The ether linkages are found in very large quantities in the lignin structure and the β -O-4 is the most dominant one[11, 12]. The frequency of different linkages is presented in the Table 8.3, (Appendix).

2.1.3.1 Types of lignin

Lignin is produced yearly in tremendous amounts as a by-product in different processes, especially in the paper industry and cellulosic ethanol industry[11]. Furthermore, it is a renewable source that involves diverse functional groups which allows production of different valuable chemicals. These are strong arguments that this material has a large potential in people's lives, especially that the world registers an uncontrollable depletion of fossil sources. Of course, lignin is not a very friendly material when it comes to processing, especially in producing biofuels, and this is due to the large oxygen content that should be eliminated in order to increase the HHV of the final products. Many upgrading steps are unwanted as they imply high cost. A solution is focused towards finding out a proper catalyst, a smart design of a reactor and proper process conditions. More and more people become interested in this area and this proves that lignin is an important energy source and a good precursor for a wide range of chemicals and simply burning this valuable material is not a wise solution.

The extraction of lignin from a lignocellulosic source gives it a new name, technical lignin. There are several types of technical lignin and in this paragraph the following types will be discussed: kraft lignin, soda lignin, organosolv lignin and lignosulfonate lignin. These names were given according to the methods of extraction and all the methods are part of the chemical treatment group[11]. In paper and pulp industries it is convenient to dissolve lignin and avoid the degradation of cellulose and hemicellulose and this could be because of the conditions that are more elevated and the reactor exposure to corrosion if using acid for degradation and extraction of cellulose and hemicellulose instead of an alkaline solution for lignin extraction[14]. The solubility of lignin in alkaline solutions is enhanced by its functional groups like phenolic carboxyl and hydroxyl[11]. Sodium hydroxide (NaOH) is used as an alkaline solution. It was reported that a solution of 2 % of NaOH in an ultrasonic atmosphere at 50 °C for 20 minutes can extract up to 91 % of lignin[14]. A black liquor is formed when the lignin dissolves in the solvent. Sodium carbonate (Na_2CO_3) is used to separate lignin from the black liquor and it is called soda lignin. If using sodium sulfate (Na_2SO_4), the lignin becomes kraft lignin[11].

Linkages to polysaccharides can be also broken by using a solution containing sulfurous acid salt or sulfur dioxide. The obtained lignosulfonates are separated from brown liquor by using different methods like: extraction with amines, precipitation in alcohol, ion exclusion and other methods[11]. In many countries this method does not exist as the use of lignosulfonates is limited. However, there are interesting applications of this type of lignin like: chelating agents, dye dispersants and water reducer for concrete setting. The last application is possible due to the anionic activity of the polymer that manifests electrostatic repulsion between cement particles, thus enhancing the fluidity of the cement[15].

The organosolv method is based on an aqueous organic solvent that is capable of breaking the aryl-ether linkages of lignin and to dissolve the obtained fragments. The following solvents can be used: ethanol, acetone, methanol, formic acid, acetic acid, etc. These solvents can be applied individually or by mixing them. As a catalyst, HCl is suitable for this process[11].

2.1.3.2 Physical properties of lignin

- Molecular weight

The structure of lignin is not a regular one defined by a known repetition of one or more monomers. As it was mentioned above, the framework of lignin is modeled by three units that are positioned randomly and it differs from species to species. Moreover, the structure of lignin is different for different tissues of a certain plant, even more, it can differ from cell to cell[12]. According to this, it is very difficult to say the molecular weight for original lignin. Of course, it can be estimated after the lignin separation, but the molecular weight is not the same because different extraction methods and the applied conditions disturb the structure of lignin. The lignin extracted from spruce by applying milling method shows a molecular weight range from 2,100 to 11,000. The high and low molecular weight fractions can reach values such as 40,000 and 5,000 respectively. Lignosulfonates manifest a molecular weight which ranges from 1,000 up to 100,000. In case of Kraft lignin, the values are smaller[6].

- Relative density

The relative density of lignin also depends on the method of extraction and the value is related to the liquid used for measurements, but, in general, it ranges from 1.35 to 1.50[6].

- Color

The lignin we see in most of the cases has a fawn color that can reach deep tan depending on the method of separation. The color of lignin separated by Brauns is light cream. However, an interesting fact about the intrinsic lignin is that it is white or even close to colorless[6].

2.1.3.3 Various application of lignin and its derivatives

Nowadays, by looking around, almost all the products are produced from crude oil: detergents, solvents, different polymers, fertilizers, dyes, cosmetics, pharmaceuticals, fuel for cooking and heating, fuel for transportation and many other applications. In the [Figure 2.5](#) the pathway of crude oil is illustrated. By looking at this picture, one thing is obvious, the society is dependent on the goods that are obtained from crude oil and it is impossible to imagine the life differently. It is very easy to accommodate yourself to a better life: faster transportation, smart technologies, home comfort and so on, but in order to satisfy all these standards that increase day by day, a new carbon source is required due to fuel depletion and climate change. The lignin source is a very complex feedstock, but it incorporates a very useful chemistry. Of course, the oxygen content is high, but not higher than that of cellulose and hemicellulose. If using the lignin for bio-oil production, the oxygen is a major problem, but for the petrochemical industry this is an advantage. It is very interesting that people converted agriculture crops and trees into different chemicals like solvents, dyes, synthetic fibers, but this was only for a short period (at the beginning of 20th century) and then the feedstock was replaced by the fossil material.

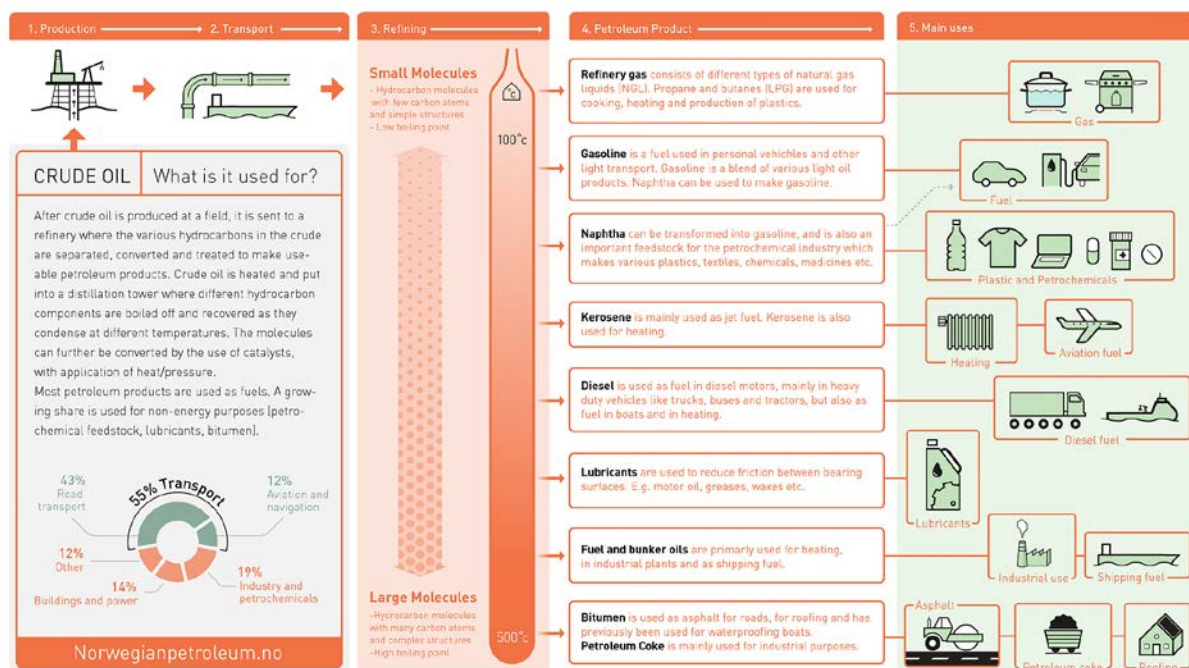


Figure 2.5 The pathway of crude oil[16]

Polymer/Lignin composites

As it was mentioned before, lignin is a very complex material, but its complexity contributes to the protection of the plant, avoiding deformation and bending[11]. These properties are also very important for some materials that people produce everyday: plastics and rubbers. A good example is the industry of tyres. The elasticity and resistance of the tyre are essential properties as it has to support the vehicle weight, especially during movement when both the weight and friction force have to be considered. These two properties are controlled by a process called vulcanization where sulfur is added to crosslink the polymer layers. Too much sulfur is unwanted as it limits the elasticity and the rubber material can crack due to its stiffness. In this way the lignin is investigated as it incorporates a moderate content of sulfur (1.5-3 %)[17]. It was observed that introducing the lignin into the natural rubber increased the tensile properties of the material. A sulfur-free lignin was also studied. As a result, it improved the thermal stability of the natural rubber[11]. A sulfur-free lignin (NovaFiber lignin) was also used in polyethylene in order to stabilize the polymer against UV radiation. It was observed that the mechanical properties were not changed during the 42 days of exposure to UV light. These results were compared with the commercialized HALS (Hindered Amine Light Stabilizer) and lignin-polyethylene composite showed better result. In addition, HALS is a relatively expensive material compared with lignin that is for free. The tensile and morphology properties of high-density polyethylene (HDPE) can be improved by mixing it with lignin. A special catalytic-grafting technique was used in order to enhance the dispersion of lignin in the HDPE matrix. The mechanical properties of low-density polyethylene (LDPE) can be also improved by adding lignin, but it should be esterified in order to increase the compatibility with LDPE. This can be done by using maleic anhydride[11].

Polypropylene (PP) is a widely used product in people's daily lives. Some applications of this precious material are represented in the Figure 2.6. In time, this material is affected

by oxidative degradation and different antioxidants are analyzed in order to see their ability to inhibit this phenomenon. 2,6-di-tert-butyl-4-methylphenol is a commercialized antioxidant used to improve the resistance to the light, but it is not so cheap considering that 30 million tons of PP is consumed yearly and 0.15 wt% of this antioxidant is added. This means that an amount of 45 thousand tons of antioxidant is consumed every year. Based on this, lignin was investigated as it manifests antioxidant properties. An amount of 2 wt% of lignin in a PP-lignin composite showed quite similar antioxidant effect as 2,6-di-tert-butyl-4-methylphenol. A larger quantity of lignin is not recommended as it also can promote the degradation of the composite[11].



Figure 2.6 Different applications of polypropylene[18]

The addition of lignin in the styrene-butadiene rubber (SBR) and polyvinyl chloride (PVC) was also investigated. In order to make the lignin compatible with the SBR, its polarity should be reduced as the SBR is a nonpolar material. The SBR-lignosulfonate composite manifested an improvement of tensile strength at break of 45 %. Some properties of PVC like impact strength and tensile strength were also improved by adding 2 wt% of lignin[11].

Lignin for carbon fibers

Manufacture of carbon fibers from softwood kraft lignin (SKL) and hardwood kraft lignin (HKL) was studied by applying oxidative and thermal stabilization. When comparing the conversion of these two it was observed that the time necessary to accomplish the stabilization was shorter in the case of SKL than the one of HKL and this is due the structure of softwood lignin that is highly branched. The hardwood lignin can be stabilized at a heating rate lower than 0.2 °C and in the presence of oxygen[11].

The softwood lignin can be directly converted to carbon fibers by applying only one step, carbonization. This is possible by using the low molecular mass fraction of a softwood acetic acid lignin[11].

Carbon fiber can be obtained by blending the lignin with different polymers like PP, PET (polyethylene terephthalate). It was found that the addition of polymer in the lignin-polymer mixture contributes to the increase of thermal stability of the carbon fibers._The

miscibility of the lignin with the chosen polymer is very important. In contrast with PP, PET is miscible with lignin and the effect of this aspect can be observed when analyzing the final product. In case of PET-lignin mixture, the carbon fibers have a smooth surface, while the carbon fibers derived from PP-lignin are characterized by a porous surface. In addition, the miscibility enhances the mechanical properties of the carbon fibers[11].

It was also possible to produce very fine carbon fibers from alkali lignin by electrospinning, carbonization and activation. The blending of lignin with polyethylene oxide improved the thermal stabilization. By doing the activation step, the porosity and surface area reached a value higher than $0.7 \text{ cm}^3/\text{g}$ and $1400 \text{ m}^2/\text{g}$, respectively[11].

Lignosulfonate to Surfactants and Dispersants

The surfactants and dispersants are highly demanded products due to the large consumption of detergents, soap, surfactants used as softening agent for fibers, emulsifier for asphalt and many other applications. Sodium, potassium and ammonium lignosulfonates can be used as polyelectrolytes for the treatment of wastewater, as well as for sequestering of heavy metal ions[11].

These lignosulfonates are highly required in the oil well drilling and oil production. The use of surfactants can improve the wettability of the oil reservoir by reducing the interfacial tension between water and oil phase. The dispersants can contribute to lowering the viscosity of drilling mud, which is very important for equipment protection[11].

It is also possible to use the lignosulfonates as dye dispersants, but its dark color influences the color of final product. Lignin is actually a colorless polymer, but when separating it from the cellulose and hemicellulose in the pulping process, for example, the polymer suffers modifications and quinonoid structures appears. These structures confer this dark color to the lignin material[11].

Lignin to Resins/Adhesives

Phenol-formaldehyde resins, as well as all the products mentioned above, are widely consumed and not so cheap to produce different coatings, gels, foams for insulation and, of course, wood adhesives. This process implies very large quantities of phenol and its production from benzene, a petroleum-based compound, makes it a very expensive chemical. In this case, the lignin can be a potential substitute due to its aromatic structure. It was found that by replacing 20 % of phenol with lignosulfonate for production of lignin-phenol-formaldehyde resins the bond strength was increased and it was higher compared to commercial adhesives. In addition, the waterproof property was enhanced due to the hydrophobicity of lignin. The replacement percentage can be increased up to 50 %. This can considerably reduce the total cost[11].

The lignin has many other different applications. A lot of compounds can be detected through fast pyrolysis. One of them that is characterized by a very good selectivity is vanillin. Of course, all of us know about vanilla, a substance with a sweet taste and pleasant smell. But because the natural vanilla is not so cheap, it is also synthesized. This compound is used in food, perfumes and medicines as there are pills with bad taste. The synthesis of a single compound is not a cheap process either, as lignin is a quite complex polymer and many steps are required in order to obtain a pure compound[19]. In the [Figure 2.7](#) many

other applications of lignin can be seen. BTX group, which consists of benzene, toluene and the xylene isomers, is very important for the petrochemical industry. Different products, like nylon-6, polyurethane, polyester fibers, phenolic resins and many other products are produced.

Biofuels

The biofuels production, especially from lignocellulose, is a very researched area of the 21st century. This is due to the structure of lignocellulose that is characterized by a complex and attractive chemistry and serves as a precursor for all materials mentioned above and even more. As the population number is growing very fast, the production of biofuels becomes more pronounced due to the exhaustion of fossil sources. Due to the special aromatic structure of lignin, as well as to the tremendous quantities produced yearly, this renewable source has a high potential in the production of biofuels like gasoline, jet fuel and diesel. Benzene and alkylated aromatic hydrocarbons have a very high octane number compared to paraffins, olefins and naphthenes[20]. When improving the octane number of gasoline, the aromatic hydrocarbons are required, as well as short iso-paraffins, olefins and light naphthenes[21]. It is not simple to obtain gasoline with the commercially required octane number. Many steps like hydrocracking, catalytic cracking and reforming, alkylation and isomerization are used on the crude oil processing plant[21]. It is well known that benzene concentration in the gasoline is very limited due to its carcinogenic effect, and according to American Cancer Society, people are exposed to this compound every day. Benzene is produced in refineries in very large amounts as it is required by the petrochemical plant. It is very volatile and proper storage and transportation are required, as well as strict measures of its manipulation on the petrochemical plant. As it was already mentioned, the commercial gasoline should incorporate an octane number up to 100. Of course, the higher the octane number, the higher the resistance to ignition is and as aromatic hydrocarbons are characterized by high octane number, the probability to be eliminated in the atmosphere without being converted into carbon dioxide and water during the internal combustion is larger. Based on this, people living and working near heavy traffic zones are exposed to this compound. According to all mentioned above, the benzene content in the gasoline was drastically reduced. Of course, lignin is also a precursor for benzene production, but its selectivity can be reduced by using a proper catalyst. It was observed that when using ZSM-5 the selectivity of toluene, ethylbenzene and xylene isomers is much higher compared to benzene[22] and it can be further converted by alkylation or hydrogenation or even separated in order to be used for petrochemical industry.

The aromatic hydrocarbons are also crucial for the aviation fuel as they can increase the lubricity, density and the fuel swelling nature. The last one is a very interesting property; the addition of aromatic hydrocarbons will make the fuel able to penetrate the sealing O-rings of the tanks and will trigger the swelling phenomenon. This will reduce the leakage of very volatile compounds[23]. According to the importance of aromatic hydrocarbons in the jet fuel, lignin can be a very promising feedstock for their production. Bi, Wang [24] produced C₆-C₈ aromatic hydrocarbons on HZSM-5 catalyst in a continuous flow pyrolysis reactor at 500 °C. The total aromatic yield, including naphthalenes and C₉ aromatics, was up to 40 C-mol%. The selectivity of C₆-C₈ aromatic hydrocarbons was almost 80 C-mol%. In order to reach the carbon range of jet fuel (C₈-C₁₅), the alkylation was realized using a

mixture of light olefins. Cyclic alkanes were also obtained by doing the hydrogenation of C₈-C₁₅ aromatic hydrocarbons.

Cycloparaffins and aromatic hydrocarbons are also present in the diesel fuel. As the aromatics are characterized by low cetane number, their content (25 %) is much lower than of n, iso and cycloparaffins (75 %)[25].

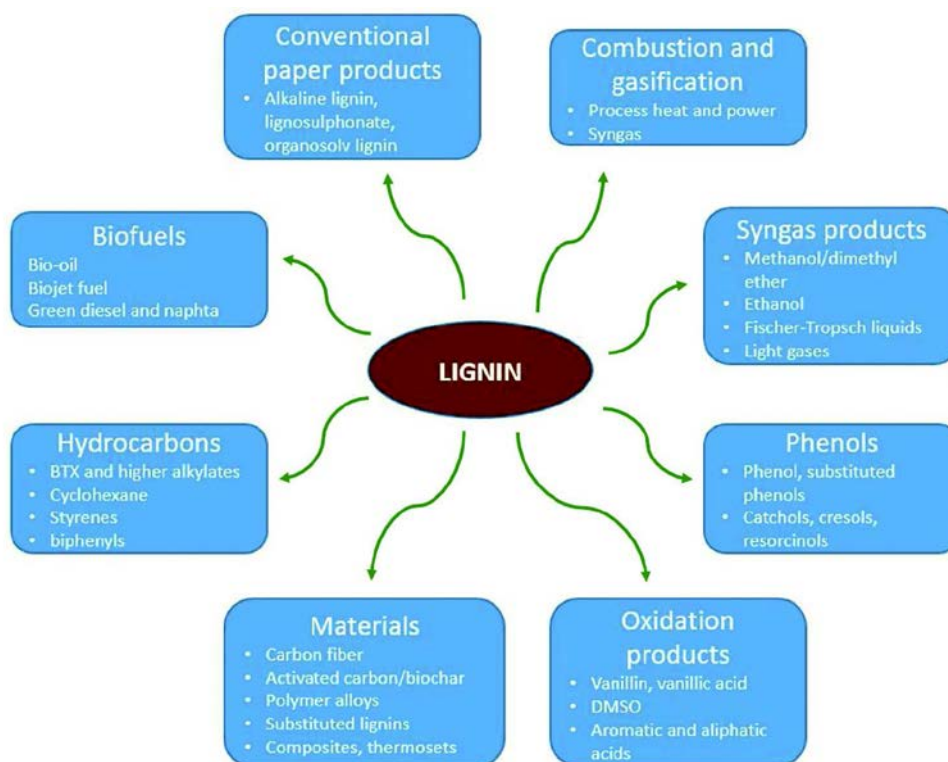


Figure 2.7 Different application of lignin polymer[26]

2.2 Lignocellulose processing

Lignocellulose is a very rich source and it is a part of the solution for solving the energy crisis and not only. There are many publications that describe the material and options of processing, but only a few of them are industrially achievable. This has a valid reason, complexity of lignocellulose, and this is a huge challenge for researches. The positive part of all this is that people are aware of fossil source situation, as well as of climate change and more solutions appear daily. Even though many of them are not achievable, however, they already represent a result and they provide inspiration for many other papers. Here, one aspect should be also considered, the final product. Many technologies are focused mainly on production of one final product. If the final destination is fabrication of one pure compound, then the question should be where the rest of the products are stored, whether they are harmful for the nature or not, if they represent a feedstock for other process or if it is only a by-product that is supposed to be burnt for some energy recovery. These are debatable questions and as examples can serve the paper mills, xylitol plants, ethanol plants and so on[6]. In many processes that involve lignocellulose, lignin is considered a by-product, but its structure, that incorporates very useful compounds, represents a promising solution for production of different materials. As there are refineries for

processing of fossil oil which cover techniques that can handle light fractions and heavy fractions, the same principle should be applied for a biorefinery. Of course, the technical barriers must be overcome, but this is a century of biomass exploitation and creative ideas are welcome for this renewable source.

In order to produce different goods, it is important to do a pretreatment of lignocellulosic feedstock. This process is realized due to the particular properties of each of the three polymers. High conversions of lignocellulose require special procedures for each polymer as their structure differs. The pretreatment is also required due to the crystallinity of lignocellulose which is very high and to convert it directly in useful products is not a solution. For an easier processing, the surface area of this material has to be increased. There are many technologies for the pretreatment of natural lignocellulose and they are categorized as: physical, chemical and biological pretreatment[6].

2.2.1 Physical Pretreatment

The physical structure of lignocellulose is changed by applying different technologies like mechanical grinding, steam explosion, microwave and ultrasonic pretreatment. The first one implies the destruction of the layer that binds the cellulose, hemicellulose and lignin. This process changes the cellulose crystallinity as well as it absorbs very productively the mechanical energy. One effective device is ball milling. It can easily break the hydrogen bonds formed between the crystalline and microfibrillar part. Another interesting technology is the ultrafine grinding. It quickly increases the specific surface area and the dispersibility, thus enhancing the solubility and the chemical activity. By using liquefied gas (under -100 °C), it is also possible to destroy the layer between lignin and hemicellulose and to retain lignin. There are many other technologies, but one aspect is known about the mechanical pretreatment, it consumes large amounts of energy. This strategy can be improved by applying wet grinding[6].

Steam explosion is also an efficient technology and consumes less energy compared to mechanical method. In this process, the depolymerization of lignin and hemicellulose is catalyzed by organic acids that come from acetyl under high pressure and temperature. The propylene ether bonds of lignin framework are broken, and polysaccharide is generated through hydrolysis of hemicellulose. The disadvantage of this method is that lignin is still not removed[6].

Microwave and Ultrasonic Pretreatment are very interesting techniques and very efficient methods for saccharification. Moreover, it is very easy to operate such a process and the treatment time is very short. The microwaves and ultrasound trigger the production of heat in the internal structure of the material. A temperature of 210-220 °C is enough for this process. A higher temperature range will inhibit the enzymatic hydrolysis. The disadvantage of this method is that it is very costly and implies much effort to be realized at industrial level[6].

2.2.2 Chemical Pretreatment

The cellulose, hemicellulose and lignin can be separated by using a specific dissolution agent. Different acidic, alkaline or organic solvents are already involved in handling with the toughness of lignocellulose structure. In case of alkali pretreatment, sodium hydroxide is a very often applied method. It acts as a swelling agent and breaks the hydrogen bonds between the hemicellulose and cellulose. NaOH also reduces the ester bonds between the lignin and hemicellulose by saponification, thus increasing the surface area of lignocellulose. The disadvantage of this delignification solvent is that it dissolves approximately 50 % of hemicellulose. Ammonia solution (10 %) is also a very used agent capable of removing the lignin, but as well as NaOH, it dissolves some hemicellulose, especially at high concentrations.

The separation of lignin from cellulose can be done by applying the organic solvent pretreatment. Solvents like alcohols, phenols, amines at a temperature up to 200 °C are able to dissolve almost 80 % of the lignin. The disadvantage of using these solvents is that they dissolve completely the hemicellulose. In addition, the recovery of solvent is costly, and its handling requires high security measures.

Diluted acid solution is an efficient method for hemicellulose removing. The reaction rate is very fast compared to the cellulose dissolution, and this is because of very low contact area between the cellulose and acid. The dilute sulfuric acid is very often used in the acid treatment of lignocellulose material. However, there are also some disadvantages: the process requires special equipment, especially when concentrated acid solution is required, as well as performant equipment for acid recycling in order to reduce the pollution.

2.2.3 Biological pretreatment

Biological method is assumed to be more convenient for pretreatment of lignocellulose material than physical and chemical methods, and this is because it does not consume much energy and does not require special equipment. In addition, this method is more environmentally friendly as it implies microorganisms for ethanol production, for example. White rot fungi were found to be very efficient for the degradation of lignin. In the [Table 2.1](#) some advantages are presented by using microorganisms. However, this method is still not a convenient one as it consumes a lot of time and it involves high costs when applying it to large scale. In addition, sterile conditions should be maintained[27].

Microorganism	Biomass	Major effects	References
<i>Punctularia</i> sp. TUF20056	Bamboo culms	50% of lignin removal	Suhara et al. (2012)
<i>Irpe</i> <i>lacteus</i>	Corn stalks	82% of hydrolysis yield	Du et al. (2011)
Fungal consortium	Straw	Seven fold increase in hydrolysis	Taha et al. (2015)
<i>P. ostreatus</i> / <i>P. pulmonarius</i>	<i>Eucalyptus grandis</i> saw dust	Twenty fold increase in hydrolysis	Castoldi et al. (2014)
<i>P. chrysosporium</i>	Rice husk	-	Potumarthi et al. (2013)
Fungal consortium	Corn stover	43.8% lignin removal/seven fold increase in hydrolysis	Song et al. (2013)
<i>Ceriporiopsis subvermispora</i>	Wheat straw	Minimal cellulose loss	Cianchetta et al. (2014)
<i>Ceriporiopsis subvermispora</i>	Corn stover	2-3-fold increase in reducing sugar yield	Wan and Li (2011)
Fungal consortium	Plant biomass	Complete elimination of use of hazardous chemicals	Dhiman et al. (2015)

Table 2.1 Biological pretreatment of lignocellulose feedstock[27]

2.3 Thermal cracking of β -O-4 and C_α - C_β

The lignin structure differs from species to species and to predict a pathway of its thermal deconstruction, a deep investigation of network of the chosen species is necessary. As it was mentioned above, the lignin is built up of three main units that are also called monolignols: p-coumaryl alcohol, coniferyl alcohol and sinapyl alcohol. As the interest in the lignin conversion has increased in the recent years, it was found out the approximate composition of different species. However, if the process is decided to be designed at an industrial scale, it will involve lignin from different species, and this is because it is not functional to separate them in too many categories. According to this, three main groups are defined: softwood lignin (mainly consisted of coniferil alcohol unit), hardwood (sinapyl and coniferil alcohol units) and the grass that has all three alcohols in a variable composition. Depending on the type of lignin, the density of aryl ether bonds (β -O-4, α -O-4, 4-O-5) that are the most abundant linkages in the lignin framework also differs. The softwood lignin is described by a density of 58 % compared with the hardwood lignin which counts up to 74.5 % [28]. Moreover, the β -O-4 ether bond was reported to be the predominant linkage with a density of 48-60 % [29]. Considering only the linkages with the highest fraction and a certain type of lignin, the thermal decomposition mechanism can be developed. This is realized by selecting one or a set of lignin model compounds which contain the dominant ether bond and highlight the type of lignin and then the behavior of each compound is investigated under thermal treatment. Thus, by analyzing different radicals and transition states, as well as the final products, the mechanism can be deduced. Klein and Virk [30] investigated the phenethyl phenyl ether (PPE) as it is the prevalent model compound found in the lignin structure. They did the pyrolysis of PPE in the presence and absence of tetralin in order to check if the decomposition of PPE occurs through a free-radical mechanism or through a concerted retro-ene fragmentation. The ene reaction (Alder-ene reaction) occurs between an alkene that has an allylic hydrogen (ene) and a compound which incorporates a multiple bond (enophile). As it can be seen in the Figure 2.8, the allylic hydrogen is transferred to the enophile and the eno suffers a migration of the double bond, thus the new σ -bond is formed [31]. The retro-ene fragmentation is the reverse reaction and it can be analyzed for the PPE in the Figure 2.9. The results obtained by Klein and Virk [30] for the neat pyrolysis and co-pyrolysis with tetralin showed a negligible difference between the product distribution of the two processes. According to this, they decided that the fragmentation of PPE actually occurs through a retro-ene reaction and not through a free-radical mechanism. However, the free-radical reactions are also present due to the minor products that were obtained, but the frequency of occurrence is reduced.

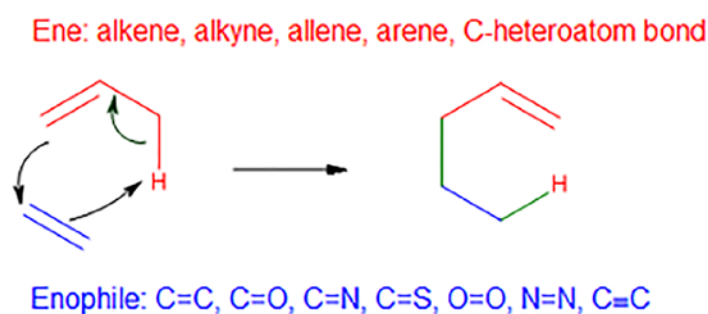


Figure 2.8 Alder-ene reaction [31]

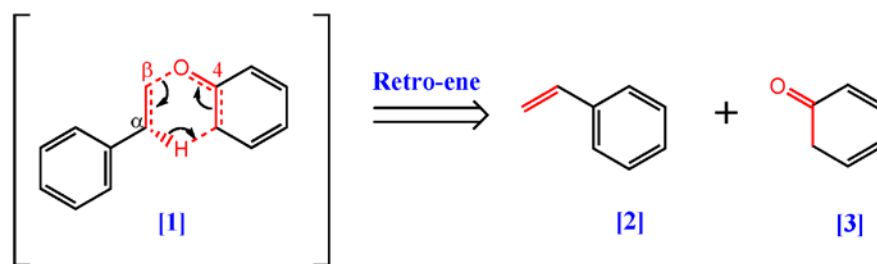


Figure 2.9 Retro-ene reaction of PPE

Choi, Singh [28] also studied the decomposition of different lignin model compounds in order to suggest a reaction network. They investigated the multistep reactions from reactants to intermediates and from intermediates to products by using computational methods (GAMESS package). Then the calculated results were compared with the experimental ones based on the overall mass balance to see which mechanism prevails. The retro-ene mechanism was found to be the most likely mechanism as it was consistent with the experimental results. The free-radical reactions were also studied, but the resulted pyrolytic products were not consistent with the applied mechanism. Moreover, the homolysis of β -O-4 of the 2-phenoxyphenylethanol generates two very unstable compounds and this makes the homolytic process energetically disfavored. Choi, Singh [28] also studied the influence on the two mechanisms of different substituents which are commonly found in the lignin structure. The addition of each substituent was analyzed individually, and it was observed that none of them disturbed the initial proposed mechanism for the unsubstituted 2-phenoxyphenylethanol. The α -O-4 ether bond was also investigated in this study and it was found that lignin model compounds containing this linkage follow the free-radical mechanism. This can be sustained also due to the resulted oligomers that are easily formed from the generated radicals.

Huang, Liu [29]'s study supports both reaction channels: free-radical reactions and the concerted retro-ene fragmentation. First, they calculated the dissociation energy of each linkage contained in the 1-phenyl-2-phenoxy-1,3-propanediol and found that the C_{β} -O and C_{α} - C_{β} are the most sensitive to thermal treatment due to their lower bond dissociation energy compared with other linkages. Thus, the homolysis of both linkages was decided to be analyzed, together with the concerted reactions. It was found that the homolytic dissociation of C_{β} -O (Figure 2.10) and the concerted reaction noted as pathway 3 (Figure 2.11) are the primary reaction channels and then, as secondary reaction channels, the homolytic dissociation of C_{α} - C_{β} (Figure 2.10) and the concerted reactions noted as pathways 1 and 2 (Figure 2.11).

2.4 Thermo-catalytic conversion processes of lignin

As it was already mentioned, lignin is a bio-waste produced yearly in very large quantities. Most of it is produced in the pulp and paper industry, as well as in the bioethanol production process and it is considered a by-product. The resulted amount per year is estimated to up to 50 million tons and it is used as a cheap fuel for some energy recovery by simply burning it. Only 5 % of the total lignin is involved in chemical industry and this is because of its complex framework[32]. The oxygen content in lignin is the major problem when producing bio-oil. The incorporation of oxygenated molecules makes the bio-oil very unstable and thus its properties like viscosity, acidity, volatility and heating value have to be adjusted[33]. Of course, the elimination of oxygen is a quite difficult process and to design a proper catalyst is a very challenging part of this process due to high C/H ratio that deactivated the catalyst very fast. The deactivation can be inhibited by using a hydrogen donor or even hydrogen, but this makes the process not so cheap. There are different thermo/thermo-chemical processes (Figure 2.12) that can convert lignin into bio-oil and the information regarding each process is provided below.

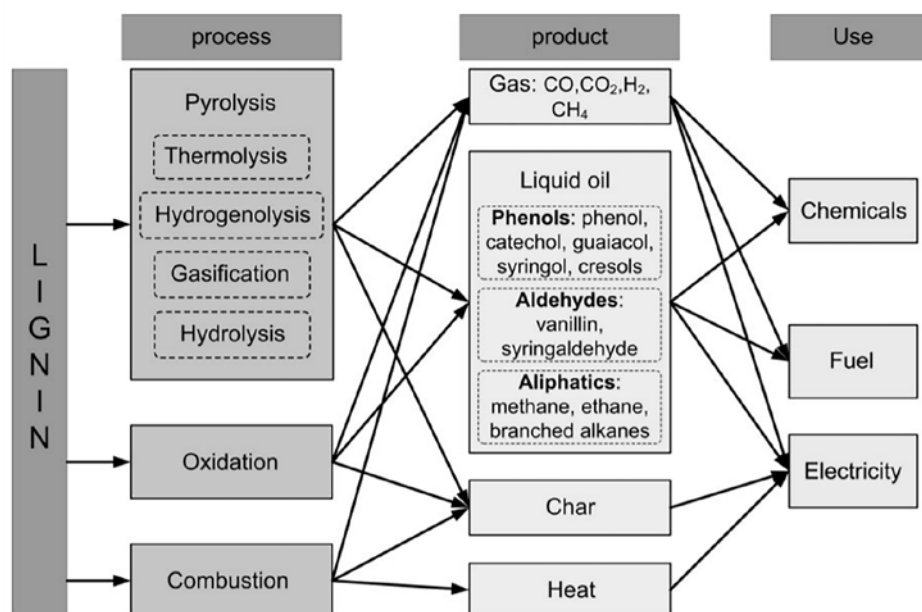


Figure 2.12 Thermochemical conversion processes of lignin into different products[34]

2.4.1 Gasification

The gasification process is a quite old process applied to solid carbon sources in order to produce syngas. By adjusting the composition of the syngas, different chemicals can be obtained, as well as hydrogen and fuels. The gasification of coal was often practiced in Germany during the World War II as liquid fuels were required. The biomass gasification was also realized in that period and over a million of vehicles were powered in Europe. This process occurs at very high temperature (up to 900 °C or higher) and it is based on a partial oxidation mechanism. Different agents like oxygen, carbon dioxide, steam or air are used individually or in a mixture form. The syngas contains CO₂, CO, H₂, CH₄ and N₂. Since this process is an exothermic one, the heat and power can also be produced. In the next

steps the syngas is cleaned and then it can be used in producing fuels by applying the Fischer-Tropsch mechanism. Also, it can be directed to hydrogen production by using water gas shift reaction or to methanol and ammonia synthesis[35]. The gasification process is very tempting because different chemical and fuels can be obtained, but it implies too many steps and the operating conditions are very high. Moreover, there are problems regarding the reactors used in this process. Fixed bed gasifiers are used only for small-scale application and the presence of particles and tar in the gas is still a challenge, especially for the updraft and crossflow fixed bed reactors. Of course, this problem can be attenuated by using a downdraft fixed bed reactor, but it is affected by the high moisture and ash content. Another option is to use fluidized bed reactor as it is very efficient in assuring a proper heat transfer and it is also very flexible and easy to operate. Comparing with the fixed bed reactors, the fluidized bed reactor requires a very small particle size of the biomass and this is not very convenient due to the energy demanded for the reduction, moreover it produces dust. In addition, when using a catalyst, attrition intervenes and a more mechanical stable catalyst is required[35].

2.4.2 Pyrolysis

The pyrolysis is considered an efficient and practical process because it does not consume much time and is capable to produce high yields of bio-oil or biochar. It is realized in the absence of oxygen at temperatures ranging from 300 to 600 °C. The target product depends on the two most important process conditions: temperature and time. If the bio-oil is the wanted product, then the time should be very short, less than 2 seconds, and the temperature should be high. The heating rate must be very high, usually higher than 100 °C/s. In addition, the uniform and rapid heating rates depend on the moisture of lignin which should be less than 10 %, as well as on the dimension of the lignin particles. Of course, the size of lignin particles is chosen according to the design of the reactor. Since the time is very short, the process is also called fast pyrolysis. The slow pyrolysis usually occurs at moderate temperatures and longer time, so the final product is biochar. The gas selectivity can also increase if exhibiting the lignin to temperatures around 600 °C and moderate time interval[36]. Due to the climate change and the fast consumption of fossil fuels, lignin is a potential aromatic feedstock that is produced in large quantities and it is still considered a byproduct in the paper and ethanol industry. It is usually burnt to recover some energy in the extraction of cellulose and hemicellulose. This is not a solution because more valuable fuels with much higher heating value can be produced. Indeed, the pyrolysis still has some problems regarding the char formation that blocks the active sites of the catalyst and thus decreasing the bio-oil yield, but people become more interested in valuing this renewable material, so different catalysts are designed and tested. Of course, it is very difficult to have a good activity and proper mechanical-thermal stability at the same time, but there is much work towards creation of such a material. Compared to cellulose and hemicellulose, lignin is much more resistant to thermal depolymerization and this results in producing of high char yield. In addition, the resulted pyrolytic oil is very unstable due to high oxygen content, thus, a catalytic upgrading is required. The oxygen can be removed from the resulted products by doing hydrogenolysis using, usually, noble metals or by using an adjusting step that implies only catalysts like zeolites or transition metals. The hydrogenolysis will be discussed later, but due to high consumption of the hydrogen donor or gaseous hydrogen, noble metals, as well as energy to generate high pressure, the process becomes quite expensive. Regarding this, people focus more towards fast pyrolysis of lignin coupled with catalytic upgrading.

In order to compare the results from different papers it is very important to check the lignin type used in the process. Different isolation methods influence the structure of lignin. Wang, Ru [37] investigated the lignin separated by four different methods from the same pine wood. It was observed that alkali lignin and the milled wood lignin have the maximum mass loss at lower temperature compared to the organosolv and klason lignin. This is due to the higher content of β -O-4 linkage that has a low thermal stability and can be easily cracked at low temperature values.

The pyrolysis products distribution is also influenced by the reactor type. Diverse reactors are used in this process like fixed bed reactor, circulating fluid beds, bubbling fluidized bed reactor, centrifuge reactors. The fluidized bed reactor is the one designed at an industrial scale as it is very easy to operate and also provides a good heat transfer [21]. When lignin is heated up, its thermoplastic behavior is activated. Regarding this, some challenges like clogging of feeder and downfall of fluidization due to the agglomeration of sand, char and molten lignin appear [36]. However, various bed materials were investigated and it was found that activated lignin char is capable to provide a more homogeneous heat transfer inside the reactor, compared to the sand bed, thus contributing to a higher yield of bio-oil [11].

Many people are using Py-GC/MS as it is very fast and capable to generate product information in pyrolytic process. This instrument is more suitable for qualitative information regarding the process and it is convenient when the screening of the catalysts is required considering that the amount of feedstock/catalyst consumed in the pyrolysis is very low (1-5 mg). When doing the fast pyrolysis in a Py-GC/MS there are two options that refer to different processes. The first one is catalytic fast pyrolysis (CFP) (mixture method), where the lignin is mixed with the catalyst, and the second one is the fast pyrolysis of lignin coupled with the catalytic upgrading (FP-CU) (layer method) (Figure 2.13). Zhang, Resende [33] simulated these two processes at 600 °C using ZSM-5(Si/Al=30) and HY as catalyst. Based on the results, the mixture method gave a higher content of aromatic hydrocarbons compared to layer method. The process based on ZSM-5(30) gave the maximum yield (28 wt%) at a ratio of C/L=3, while HY registered the maximum (17 wt%) at C/L=2. The ZSM-5 seems to be more suitable and this is due to its small pores that act as a trap for the phenolic compounds, converting them into aromatic hydrocarbons. However, one aspect is unclear regarding the ZSM-5, as well as for HY, β and other zeolites with small pore size. The compounds that result in the fast pyrolysis process are too large to fit into the pore of these zeolites. The dimensions of some of the compounds can be seen in the Table 8.4 (Appendix). It is also assumed that the pore size increases upon heating, but the degree of increase at temperatures higher than 400 °C is still unknown. In case of ZSM-5, it was observed that the pore size increased from its normal size (5.6 Å) to 7.64 Å when the catalyst was heated up to 370 °C [38]. Yu, Li [38] studied the mechanism of converting the lignin oxygenated compounds into aromatic hydrocarbons by using four catalysts: ZSM-5, mordenite, β and Y. According to their study, the pore size of catalyst increases from ZSM-5 to Y zeolite. When doing the lignin pyrolysis at 650 °C in a Py-GC/MS, they observed that the oxygenates content is decreasing with the increase of pore size, while the coke content is increasing. This is true because the larger pore gives space for the polymer development. The largest coke generation in the pores of Y catalyst is also possible due to its higher density of Brønsted acid sites. This means that the distance between sites is very small and thus the promoting of polymerization through bimolecular reactions is possible.

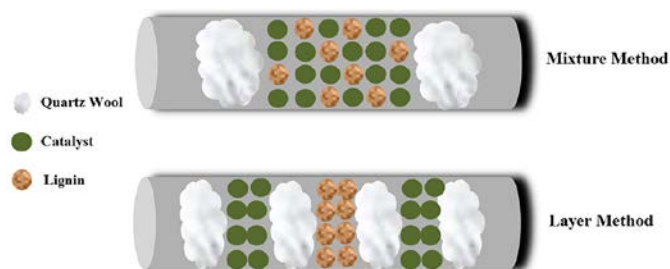


Figure 2.13 Simulation of catalytic fast pyrolysis and fast pyrolysis coupled with catalytic upgrading of volatiles [33]

Since zeolites are suitable catalysts for fast pyrolysis process due to their deoxygenation activity, people are trying to increase the pore size of these catalysts, especially of ZSM-5 and β . By doing this, a larger surface will be available for the large compounds. Bi, Lei [39] managed to expand the pore size by applying the desilication process with an alkaline solution to the microporous zeolites. Moreover, they assumed that this procedure is capable to interconnect the micropores with the mesopores. In this paper the catalytic fast pyrolysis was realized at 500 °C in a Py-GC/MS and the results were analyzed based on the total peak area. It was observed that more oxygenated compounds were converted into aromatic hydrocarbon when using the treated catalyst. Since the β zeolite has a larger pore size than ZSM-5, the treating of β zeolite changed the selectivity of the catalyst, thus more polyaromatic hydrocarbons were produced than BTX.

Lazaridis, Fotopoulos [40] also realized the catalytic fast pyrolysis in a Py-GC/MS, but also in a fixed bed reactor. They tested the three ZSM-5 catalysts with different pore sizes obtained through special treating. The mesoporous ZSM-5 was obtained through alkaline treatment like in Bi, Lei [39] work. The other two catalysts were Nano-ZSM-5 and the normal ZSM-5. Good results were obtained at 600 °C and at ratio of C/L=4. In the Figure 2.14 the distribution of products for the three catalysts can be observed. Based on the peak area results, normal ZSM-5 manifested the highest activity. The nano-ZSM-5 also showed a good activity, and even though it is characterized by a lower amount of Brønsted acid sites, its high interparticle porosity plays an important role in aromatization reactions. In case of Meso-ZSM-5(9 nm), a lower content of aromatic HC was obtained. This result was associated to the decrease of microporosity compared to parent catalyst (ZSM-5(Si/Al=40)). Comparing the result of this work with the one by Bi, Lei [39], the meso-ZSM-5 is supposed to produce more polyaromatic hydrocarbons than the normal ZSM-5 as it has larger pores, but according to the Figure 2.14, it is in fact the opposite. These catalysts were also tested in a fixed bed reactor. The results showed the same trend as in the Py-GC/MS.

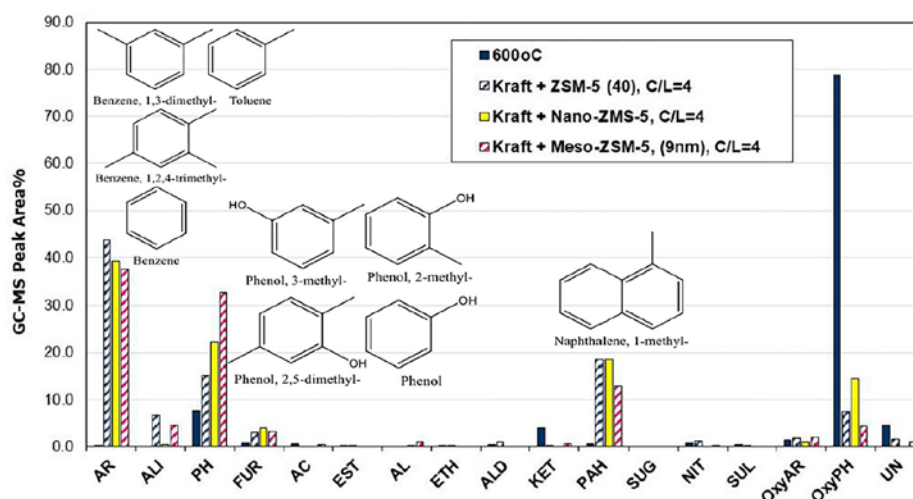


Figure 2.14 The distribution of non-CFP and CFP products for the three zeolites [40]

The improvement of ZSM-5 catalyst activity in the non-CFP coupled with catalytic upgrading step was also studied by Paysepar, Rao [41]. An acidification treatment of ZSM-5 (Si/Al=80) with H_2SO_4 and H_3PO_4 was realized, as well as a Ni (5 wt%) impregnation. The experiments were realized in a fixed bed reactor at 450 °C with 2 g of lignin and 2 g of catalyst. According to the obtained results, the H_2SO_4 -ZSM-5 produces the highest amount of gas due to its stronger Brønsted acid sites compared to ZSM-5. The normal ZSM-5 remains the proper catalyst because it produced the highest bio-oil yield (58 %).

The selectivity of aluminosilicates was also investigated by Ma, Troussard [42]. The pyrolysis was done in a platinum coil pyrolyzer coupled with GC/MS at 650 °C. The catalysts used in their work can be observed in the Figure 2.15. If analyzing the H-ZSM-5, H- β and H-USY, the pore size is increasing as the catalysts are enumerated. According to the information from the already discussed papers, when the pore size increases the coke content is also increasing as it is favored by higher pore space. The results represented in the Figure 2.15 show the opposite. In this paper it is mentioned that more liquid can be produced when the pore size is more compatible with the large compounds.

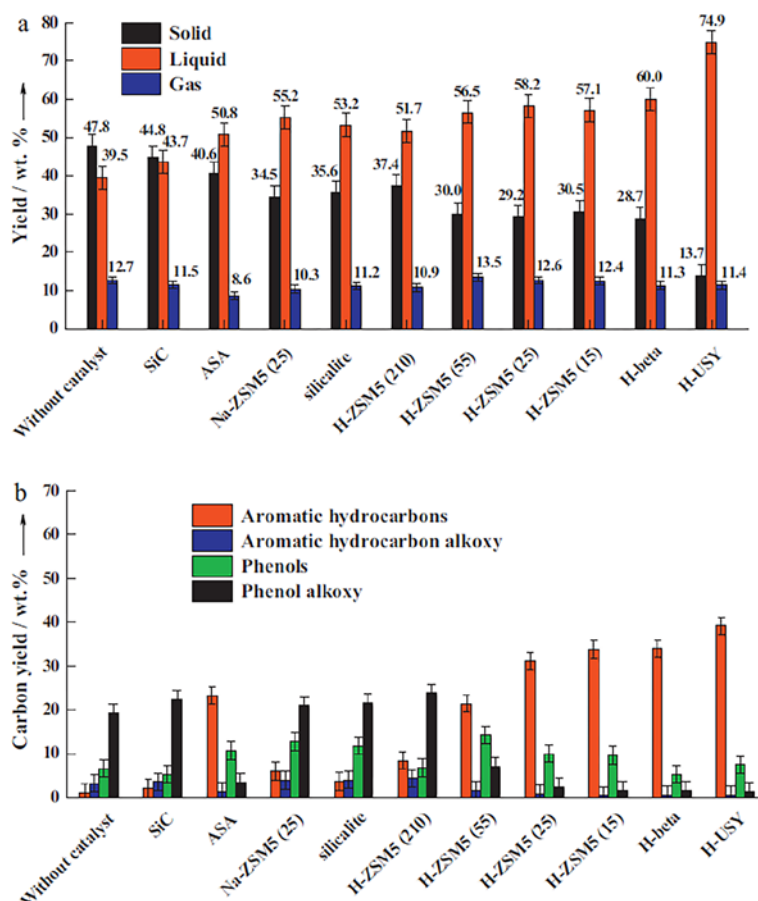


Figure 2.15 The selectivity of silica and aluminosilicate based catalysts[42]

The Py-GC/MS set-up was also used by Mullen and Boateng [43] for the catalytic fast pyrolysis of lignin. The process was realized at 650 °C in the presence of two catalysts: ZSM-5 and CoO (3.5 %)MoO₃(14 %) on alumina. In this study four lignin samples were tested. The results can be seen in the Figure 2.16. As it can be seen, ZSM-5 is much more active than the Co/Mo catalyst. However, if comparing the Co/Mo based catalyst with the non-catalytic fast pyrolysis, especially at a C/L ratio of 3/1, it is capable to convert oxygenated compounds to aromatic HC. In this work it was also observed that p-xylene was produced in higher quantities from Lignol that is rich in S-type compounds. This aspect suggests that a highly branched lignin gives more substituted benzenes. CoMo/Al₂O₃ is a potential catalyst and, in order to improve it, a higher surface area of the support could contribute to a higher dispersion of the active phase and so to a higher conversion of lignin into bio-oil.

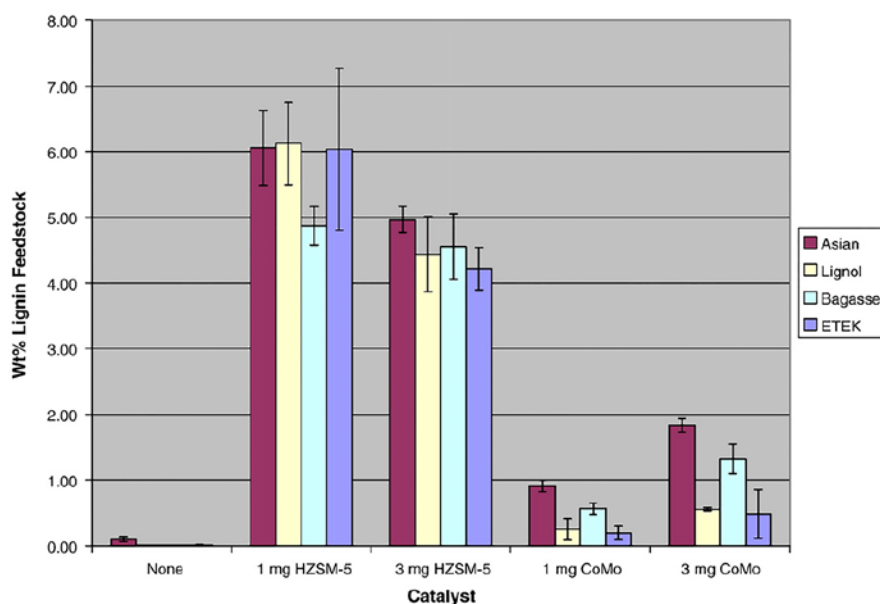


Figure 2.16 Non-CFT and CFP of four lignin sources [43]

Another interesting study regarding catalytic fast pyrolysis of lignin was realized by Chen, Liu [32] where a nano-NiO catalyst was investigated. In this case the process was run at 550 °C with different catalyst loadings. The results are presented in the Table 2.2. According to the provided data, the higher the catalyst loadings, the higher the yields of bio-oil and gas are, while the bio-char yield is characterized by a decrease. When analyzing the gas, it was observed that the content of CO, CO₂ and CH₄ increased and this is due to the catalyst loading that contributed to the degradation of O-CH₃, C-O-C and C=O groups.

Product	AL-0%	AL-5%	AL-10%	AL-15%
Bio-oil	49.92	52.98	53.09	52.15
Gas	7.60	8.31	11.17	12.84
Bio-char	42.48	38.71	35.74	35.01

Table 2.2 The products distribution of the non-CFP and CFP. AL represents Alcell lignin and the % represents the loading of the catalyst* [32]

Zheng, Chen [44] also analyzed the fast pyrolysis process of lignin, but they separated the catalyst zone from the lignin zone. This principle is the same as the one realized by Zhang, Resende [33] (layer method). In other studies, where the same method is applied, the process is very often called ex-situ fast pyrolysis. Zheng, Chen [44] group realized this process in a pyroprobe pyrolyzer where the heating rates were kept at 20 °C/min in order to suppress the coke/char formation. The experiments were run at 700 °C in the presence of MoO₃/γ-Al₂O₃ and Mo₂N/γ-Al₂O₃. Based on the results, Mo₂N/γ-Al₂O₃ manifested a good conversion of oxygenated compounds into aromatic hydrocarbons, especially at a ratio of C/L=4. It was also observed that this catalyst has a high selectivity for benzene and toluene. MoO₃/γ-Al₂O₃ also showed some deoxygenation of the lignin compounds, but

it produced more phenols and some aromatic HC due to its Lewis acid sites. Zheng, Chen [44] proposed a path for the fast pyrolysis process coupled with the catalytic upgrading (Figure 2.17). As it can be observed, the benzene and toluene are formed by eliminating the water and carbon monoxide. The group also suggested this pathway by analyzing the gas. They observed that the amount of water and CO increased when more catalyst was loaded to the process.

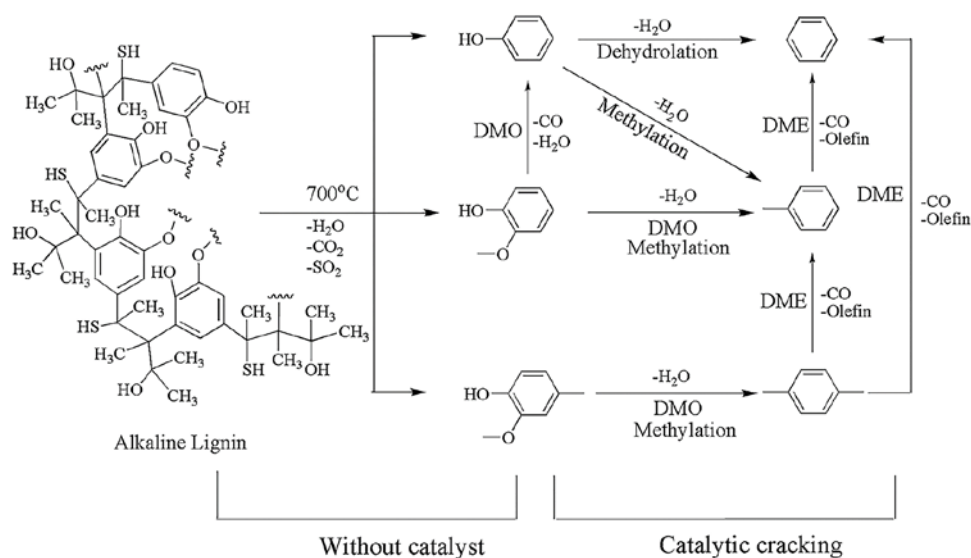


Figure 2.17 The pathway of the non-CFP coupled with the catalytic upgrading [44]

The ex-situ process was also investigated by Yang, Shao [45] in a fixed bed reactor, at 600 °C and in the presence of Fe/ZSM-5. The results for different loadings of catalysts are presented in Figure 2.18. The maximum carbon yield of aromatic hydrocarbons was obtained at 6 % Fe loading, while the yield of olefins at 3 %. According to NH₃-TPD analysis of the catalysts, when increasing the Fe loading, the total acidity was increased, especially the strong acid sites. Based on this analysis, it can be assumed that the strong acid sites promoted the olefins formation, followed by aromatization of these intermediates.

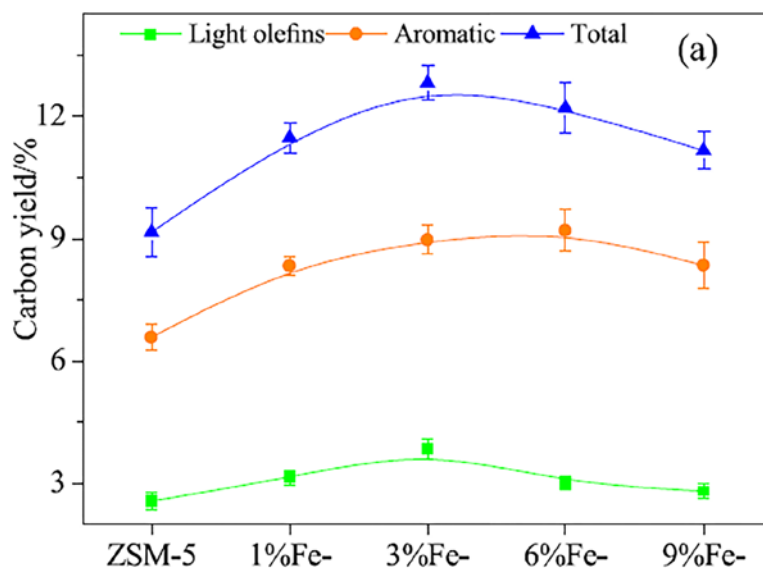


Figure 2.18 Carbon yield variation with different Fe loadings[45]

The Si/Al ratio of the ZSM-5 catalyst and the temperature were also investigated in the catalytic fast pyrolysis process. In order to analyze the effect of Si/Al ratio on the products, Li, Su [46] did the analysis by keeping the temperature (590 °C) and the catalyst to lignin ratio (C/L=5) constant. By increasing the alumina content in the ZSM-5 structure, the Brønsted acid sites content also increases. As the deoxygenation reactions are promoted by Brønsted acid sites, the aromatic content should increase. Four different Si/Al ratios were investigated: 200, 100, 50 and 25. The last one produced the highest amount of aromatic hydrocarbons. When analyzing the temperature effect, it was observed that the aromatic HC content reached a maximum at 650 °C and then a depletion was observed due to a deeper cracking of the aromatic-phenolic compounds into gas products.

Lou, Wu [47] also investigated the effect of temperature in the non-CFP and catalyst in the CFP. It was observed that the amount of phenolic compounds increased with the temperature increase. The highest fraction of phenolic compounds was detected at 600 °C (56.43 %). Sodium chloride and sodium aluminum silicate (permutite) were the tested catalysts. Lou, Wu [47] group observed that NaCl inhibited the coke formation at 5 wt% loading, but then it started to increase with higher loadings. In case of permutite, the variation of solid content was opposite. Both catalysts at 5 wt% loading promoted guaiacol compounds formation, while syringol compounds were not really affected by the catalysts, especially by permutite.

Mesoporous supports with very high surface area were also used in the ex-situ catalytic fast pyrolysis. Karnjanakom, Suriya-umporn [48] studied the stability and the selectivity of Mg-doped Al-MCM-41 catalyst. Different catalyst loadings were analyzed (Figure 2.19). According to the results presented in the Figure 2.19, it can be observed that for non-catalytic process, the amount of HC is very small (≈ 15 %). In the presence of only MgO, this amount is enhanced up to 37 %, showing that MgO involves activity for deoxygenation reactions. The quantity is even more increased by dispersing the metal on Al-MCM-41 that is characterized by a high surface area. By increasing the MgO loading on support, it was observed that the selectivity towards monoaromatic hydrocarbons was increased, while the coke formation was less favored by increasing the loading of MgO. The acidity of Al-

MCM-41 should be tuned in order to avoid further aromatization and polymerization. By impregnation of MgO, basic sites were introduced, and this helped to inhibit the formation of PAH and coke.

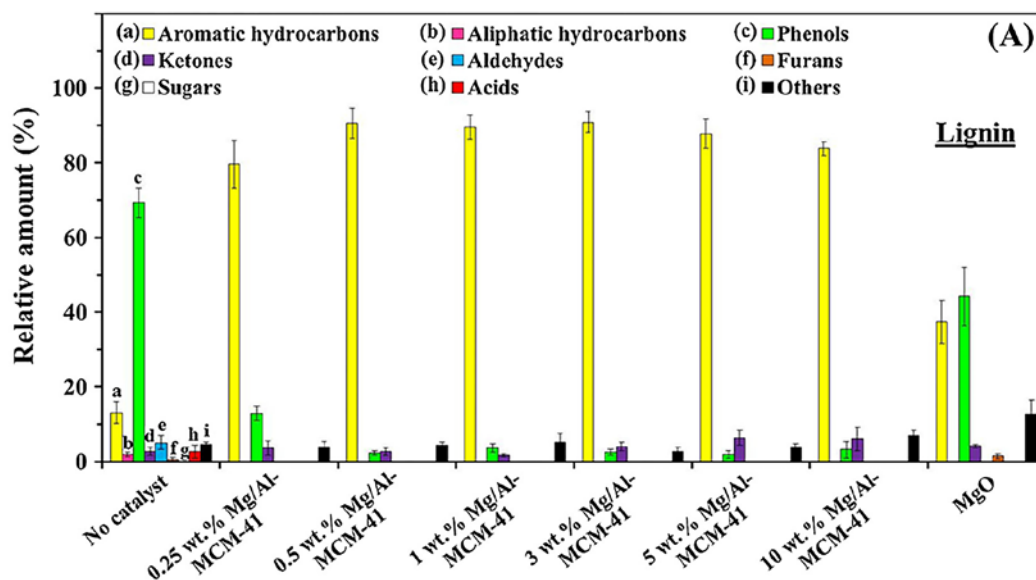


Figure 2.19 The variation of products distribution with different loadings of MgO on the mesoporous Al-MCM-41 and unsupported MgO[48]

Another investigated mesoporous support is MCM-48. The difference between this one and MCM-41 is the structure. MCM-48 has a cubic structure, while MCM-41 has a hexagonal one. Elfadly, Zeid [49] studied the Al-MCM-48 and Zr-MCM-48 in the CFP in a fixed bed reactor. By increasing the aluminum impregnation, the amount of strong acid sites increased. In case of zirconium, the acid sites are distributed only in two groups: weak acid sites (Lewis) and strong acid sites (Brønsted). The highest BTX yield was obtained at 25 ml/min and 600 °C. The influence of C/L ratio was also tested. In case of Al-MCM-48, a catalyst ratio of 3 gave the maximum result (32.5 %) compared with Zr-MCM-48 that registered a maximum (49.4 %) at 2:1 ratio. Zr based catalysts showed good results at a loading of 2.9 % because at this value the highest amount of Brønsted acid sites was detected. In case of Al-MCM-48, the yield increased with increasing the aluminum content. Even though these catalysts presented good activity, after their regeneration, the activity dropped significantly. This is because of heavy coke deposition, pore blocking and deformation of structure.

The effect of impregnation of Co on ZSM-5 in the non-CFP coupled with catalytic upgrading was studied by Xie, Liang [50]. The pyrolysis was realized in a microwave. It was observed that by impregnation of Co on ZSM-5 the yield of bio-oil was increased compared to non-catalytic pyrolysis and only ZSM-5. By analyzing the composition of bio-oil, the addition of catalysts promoted formation of guaiacols and phenolic compounds, especially in case of Co-ZSM-5. These changes occurred due to conversion of 2-furanmethanol and 2-cyclopenten-1-one into more stable compounds like phenolic and methoxyl compounds. The temperature effect was also studied in this paper. The maximum bio-oil yield was obtained at 450 °C and C/L ratio of 2.34 %. By analyzing the gas composition, H₂ was the

dominant one (up to 40 %), then CO₂ with a yield of 25 % and CO with 15 %. Methane was also detected, but in very low amount.

2.4.3 Hydrogenolysis

The H/C ratio range of the lignin is almost the same with the one of crude oil, but lower compared to hemicellulose and cellulose (Figure 2.20). However, when comparing the O/C ratio of these materials, of course, the lignocellulosic polymers dominate as the formation of biomass and crude oil is very different.

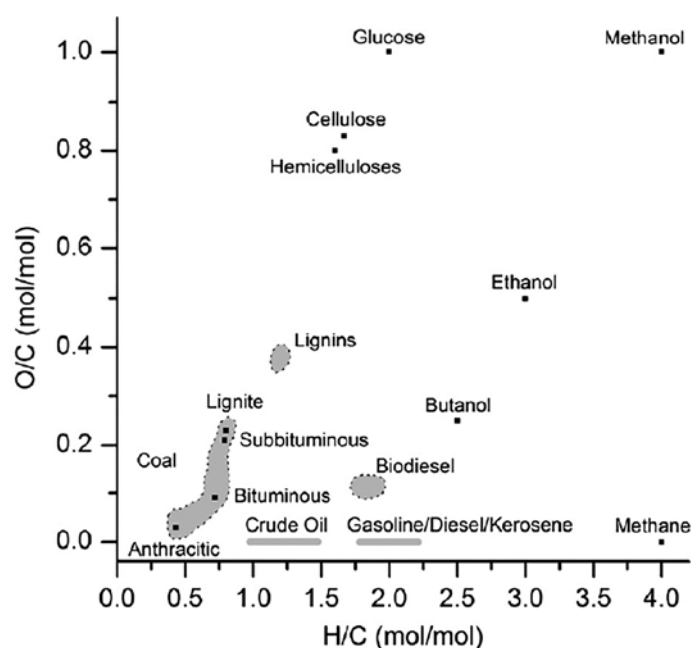


Figure 2.20 The O/C ratio and H/C ratio of the crude oil, conventional fuels, three polymers of lignocellulose and other chemical and petrochemical compounds[51]

It is advantageous to produce conventional fuels like gasoline, diesel and kerosene from crude oil as the oxygen content is extremely low, but as chemistry industry requires different oxygenated compounds to manufacture fibers, pharmaceuticals, solvents, food additives and so on, the crude oil compounds have to be functionalized. In case of the lignocellulose, the situation is opposite as it already incorporates a high content of oxygen and in order to produce fuels, the oxygen should be eliminated as it has negative effect on the stability and other properties of the fuel[51]. According to this, hydrogenolysis is considered a very efficient process to get rid of oxygen if the production of fuels is proposed. This process is based on a reduction reaction that uses hydrogen or hydrogen donor as a reductive agent. In most of the cases this reaction is realized in presence of a catalyst, usually noble metals are preferred. As the ether bonds are dominant in the lignin structure, especially the β -O-4, the cleavage of C-O bond occurs due to its low bond dissociation enthalpy[29, 36]. According to the analysis by Mike Kleinert [52], formic acid was found to be a very good donor of hydrogen in the one-step depolymerization of lignin. At high temperature values, the formic acid decomposes into hydrogen and carbon dioxide.

A hydrogen atmosphere inhibits the formation of solid residue and contributes to a higher liquid or gaseous yield. This reagent was also studied by Rahimi, Ulbrich [53]. A yield of 60 wt% of low molecular mass aromatics was obtained under mild conditions. Another studied hydrogen donor is ethanol. Huang, Koranyi [54] investigates the lignin depolymerization in supercritical ethanol on CuMgAlO_x catalyst. At 300 °C and 4 h the yield of monomeric product mixture was 17 wt%. The usage of ethanol contributed to the stabilization of the reactive phenolic intermediates by oxygen and carbon alkylation of hydroxyl groups and aromatic rings, respectively. It was observed that the catalyst plays also a very important role because it manifested good deoxygenation and a low activity toward ring hydrogenation. The ethanolysis was also studied by the Ma, Hao [55]. In this paper a Kraft lignin in ethanol atmosphere was investigated. The best result for liquid yield was observed at 280 °C, 10.5 MPa and 6 h. The reaction was realized in a batch reactor and as catalyst an activated carbon supported α -molybdenum carbide was used. The overall yield of the ethanolysis process was higher than 100 % and this proved that the ethanol is a reactant and not a hydrogen donor. Through esterification and alkylation reactions the alcohol gave rise to different ethyl esters and alkylated products.

The hydrogenolysis is also very researched on gaseous hydrogen. It is well known that a hydrogen atmosphere contributes to the inhibition of char formation and this increases the lifetime of the catalyst. Different noble metals like Pt, Pd, Rh and Ru are extensively used in the hydrogenation/hydrogenolysis processes[11]. The Ohta, Kobayashi [56] studied the hydrodeoxygenation (HDO) of 4-propylphenol on carbon supported platinum catalyst. The phenolic compound was selected according to the abundancy of phenol types that derive from lignin through the depolymerization process. The catalyst was chosen due to its high activity and durability in the hydrogen assisted reactions. The process involves the hydrogenation of aromatic rings and the hydrogenolysis of C-O bond of cyclohexanols. The pathway of the process, that was deduced according to the obtained products, is presented in the Figure 2.21. The active carbon supported platinum (Pt/AC(N)) purchased from Norit manifested high activity towards propylcyclohexane (97 %), while the one purchased from Wako (Pt/AC(W)), resulted in 73 % propylcyclohexane and 16 % 4-propylcyclohexanol.

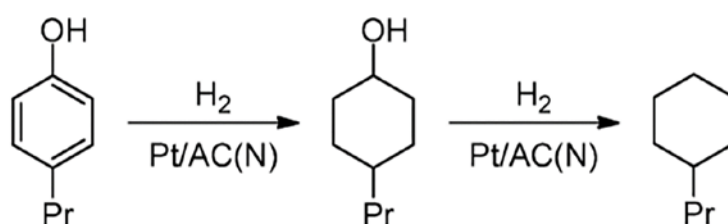


Figure 2.21 Hydrodeoxygenation of phenols pathway[56]

The hydrodeoxygenation process was also investigated on guaiacol as model compound of bio-oil. The reaction was realized in an autoclave-type batch reactor. The guaiacol was mixed with the solvent (dodecane) and then the solution was subjected for 2 h to a temperature of 200 °C and a pressure of 30 bar. As catalysts for this process were selected different Pt supported mesoporous silica such as SBA-15, KIT-6 and aluminum-incorporated SBA-15(Al-SBA-15). Conventional silica was also used in order to see the role

of mesopores. The catalysts without Pt manifested a very low conversion of guaiacol (<3 %). When using Pt based catalysts, the conversion became higher than 90 %. The grafting of aluminum plays an important role as it enhances the production of cyclohexane. When using Pt based catalysts without Al grafting, the benzene ring of guaiacol is hydrogenated in the presence of Pt particles and so cyclohexanol and methoxy compounds are produced. By applying Al-grafting, and by increasing the temperature from 200 to 220 °C, the cyclohexane yield increases considerably. Based on the results obtained for all catalysts, it was observed that mesoporous catalysts play a special role as the cyclohexane yield significantly increased [57]. The HDO of guaiacol on mesoporous silicates was also studied by Selvaraj, Shanthi [58], but transition metal oxides like MoO₃-NiO were impregnated on the mesoporous supports. This work was realized in a fixed bed reactor at different temperatures. The catalysts tested in this process were MoO₃-NiO on SBA-15, Ti-SBA-15 and MAS. These three catalysts were also tested, but in mixture with gamma-alumina (3:1). The conversion of guaiacol reached a maximum at 300 °C (68 %). A remarkable conversion was obtained on MAS. By mixing MAS with γ -Al₂O₃, the guaiacol conversion increased up to 95 %. The cyclohexane was the most abundant compound in the final product. This result was expected as the MAS is characterized by a very high surface area, large H₂ uptake and a high dispersion of metal species. The benzene content was low due to its hydrogenation over Ni active sites.

In contrast to Selvaraj, Shanthi [58] and Jang, Park [57] work, Deutsch and Shanks [59] also investigated the HDO process, but of a complex of oxygenated compounds that include monomers with more than one oxygen atom. The reactions were realized at different temperatures from 150 °C up to 275 °C and 50 bar H₂. As solvent, decalin was chosen and as catalyst, copper chromite. It was observed that the catalyst favors the hydrogenation of the aromatic ring at temperatures higher than 200 °C, as well as hydrodeoxygenation of phenol, resulting in high yields of cyclohexane. Comparing the results with other papers, Deutsch and Shanks [59] noticed that the sulphided NiMo/Al₂O₃ manifests the same selectivity at high reaction conditions, while the CoMo/ Al₂O₃ favors benzene formation. When analyzing the anisole pathway, the benzene, cyclohexanol and cyclohexane were detected. It was observed that the copper has a high activity for demethoxylation reaction. The o-cresol was also studied and its pathway is very similar to the one of phenol. The result of guaiacol analysis is quite the same with the result obtained by Jang, Park [57]. However, Deutsch and Shanks [59] presented one more pathway where the final product is methylcyclohexane. This can be correlated to the catalyst, as well as to hydrogen pressure.

2.5 Zeolites

Zeolites are very special materials with different application. They are highly utilized in the oil industry due to their acidity capable to crack heavy oil fractions. As they are characterized by a definite structure with well-designed pores with the size of molecular dimensions, these materials are used as molecular sieves. In oil refineries the zeolites are used to separate iso-paraffins from n-paraffins. Not all zeolites can be used as they have different thermal and mechanical stabilities. Thus, the most utilized zeolites are Y-zeolite, mordenite, MCM-22, β -zeolite and of course ZSM-5[60]. In the Table 8.5 (Appendix) some applications of these zeolites can be seen. The basic unit of the zeolite materials is a tetrahedron that incorporates the Si or Al atom in the center of the solid body and the four

oxygen atoms that are distributed to its corners. By linking these tetrahedra, different structures can result (Figure 2.22).

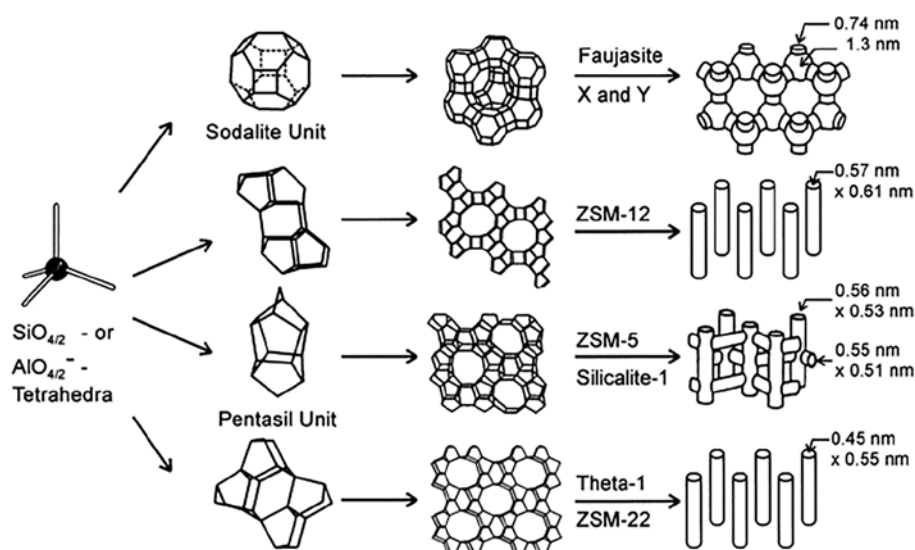


Figure 2.22 The structure and the pore dimensions of Faujasite, ZSM-12, ZSM-5 and Theta-1 [61]

According to IUPAC, the chemical formula for most of the zeolites is the following:



Where the term between the braces refers to guest species that can be cations (M). Due to negative charge of AlO_4 these cations contribute to its balance. The term between the brackets refers to the host framework, x represents the number of Al atoms in the unit cell, y represents the adsorbed water molecules, t is the number of Al and Si atoms in the unit cell and IZA comes from Structure Commission of the International Zeolite Association and refers to the code of the framework type [62]. According to Kulprathipanja [62] the basic unit is called basic building unit (BBU). The integration of the BBUs forms the composite building units (CBUs). Some examples of CBUs can be seen in Figure 2.23. As it can be observed, these structures can be described by their names like cube, sodalite cage, mfi and so on, or a three letter code like d4r for double 4-ring that is actually the cube. The numbers between brackets are also used to name the structure. The power (6) from $[4^6]$ represents the number of rings consisted of 4 sides. The number 4 also refers to the number of Si or Al atoms in one ring. These n-rings (ex. 4-rings) represent the pores of the structure. In a simpler way, the faces of the cubic structure represent the pores of that structure. The polyhedra with the faces formed from six Al or Si atoms or less is also called cages. The polyhedra with at least one face larger than six atoms are named cavities. The CBU frameworks also incorporate channels that represent an expansion in one dimension of the pores and have enough space for the diffusion of the guest species (ex. cations, water). These channels can be distributed in one-, two-, or three- dimensions. It

is very easy to approximate which molecules can fit into the existing pores if knowing the dimensions of polyhedra. In the [Table 8.6](#) (Appendix) the free aperture of different n-rings can be found[62].

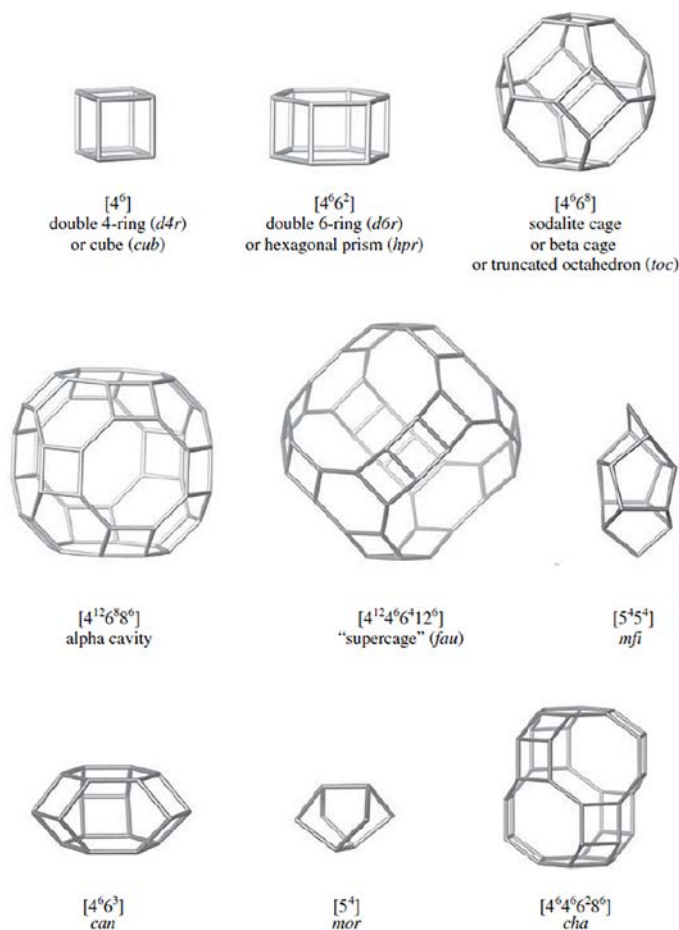


Figure 2.23 Some examples of CBUs with their name and pore symbols[62]

According to Kulprathipanja [62] the most significant zeolites (synthetic and natural zeolites) for different industrial application are:

- Synthetic zeolites: X, Y (FAU), A (LTA), ZSM-5 (MFI), mordenite (MOR), beta (BEA/BEC), MCM-22 (MTW), F (EDI), W (MER), L (LTL);
- Natural zeolites: mordenite (MOR), erionite (ERI), clinoptilolite (HEU) and chabazite (CHA).

Some of the enumerated zeolites will be further discussed.

2.5.1 Faujasite (FAU)

The structure of FAU is formed by joining sodalite cages through hexagonal prism (double 6-rings). This framework can be seen in [Figure 2.22](#). As it can be observed, this

construction develops a supercage that can be accessed through a 3D 12-ring pore. In the [Table 2.3](#) the chemical formula and the synthetic forms can be found[62].

Type material	Faujasite [18, 19]
Chemical formula	$[(\text{Ca}, \text{Mg}, \text{Na})_{29}(\text{H}_2\text{O})_{240}] [\text{Al}_{58}\text{Si}_{134}\text{O}_{384}] \text{-FAU}$
Space group	Cubic, Fd-3m, $a = 24.74 \text{ \AA}$
Pore structure	Three-dimensional 12-ring
Mineral forms	Faujasite
Synthetic forms	Beryllphosphate X, Li-LSX, LZ-210, SAPO-37, siliceous Na-Y, zeolite X (Linde X), zeolite Y (Linde Y), zincophosphate X

Table 2.3 Short information about FAU structure[62]

2.5.2 Chabazite (CHA)

As it can be seen in [Figure 2.24](#), the CHA structure is formed from double 6-ring building units linked by tilted d4r layers. This structure develops a large cavity that can be accessed through a 3D 8-ring pore system. The chemical formula and the synthetic form can be found in [Table 2.4](#)[62].

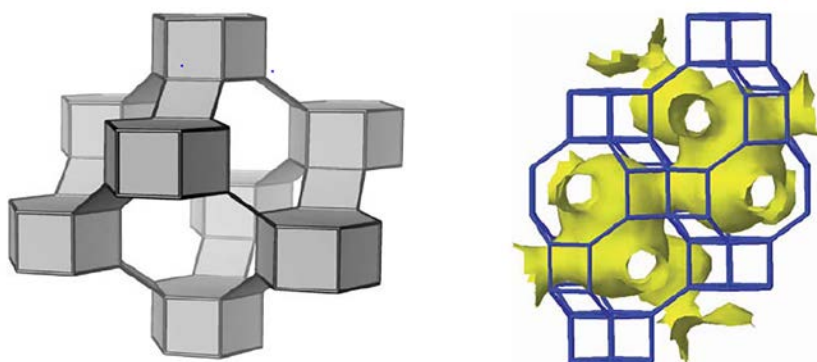


Figure 2.24 CHA framework structure and its channel system[62]

Type material	Chabazite [30, 31]
Chemical formula	$[\text{Ca}_6^{2+}(\text{H}_2\text{O})_{40}][\text{Al}_{12}\text{Si}_{24}\text{O}_{72}] \text{-CHA}$
Space group	Rhombohedral, R-3m, $a = 9.42 \text{ \AA}$, $\alpha = 94.47^\circ$
Pore structure	Three-dimensional eight-ring
Mineral forms	Chabazite, willhendersonite
Synthetic forms	AlPO-34, CoAPO-44, CoAPO-47, DAF-5, GaPO-34, Linde D, Linde R, LZ-218, MeAPO-47, MeAPSO-47, (Ni(deta)2)-UT-6, Phi, SAPO-34, SAPO-47, UiO-21, ZK-14, ZYT-6

Table 2.4 Short information about CHA structure[62]

2.5.3 ZSM-5 (MFI)

The MFI structure is characterized by interconnection of horizontal straight ten-ring channels with vertical zigzag ten-ring channels that are formed from 5-ring units (Figure 2.25). The intersection of these channels form cavities. This framework type is a very siliceous one considering the fact that it is easier to be obtained when the Si/Al ratio is higher. The Si/Al ratios of MFI structure range from around 10 to infinity. In the Table 2.5 some important information can be found[62].

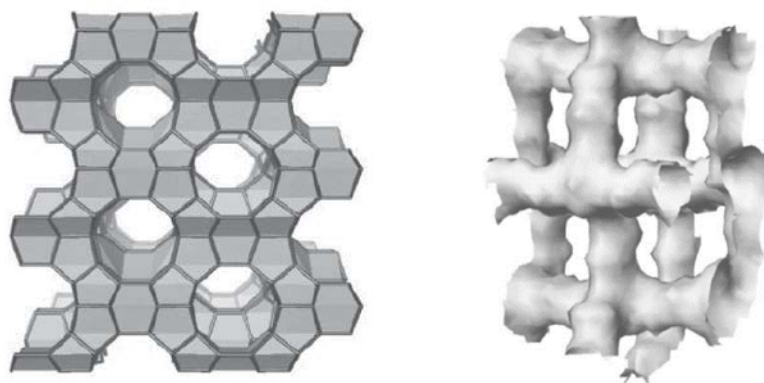


Figure 2.25 MFI framework structure and its channel system[62]

Type material	ZSM-5 [41–43]
Chemical formula	$[\text{Na}_n^+ (\text{H}_2\text{O})_{16}][\text{Al}_n\text{Si}_{96-n}\text{O}_{192}] - \text{MFI}, n < 27$
Space group	Orthorhombic, Pnma, $a = 20.07 \text{ \AA}$, $b = 19.92 \text{ \AA}$, $c = 13.42 \text{ \AA}$
Pore structure	Three-dimensional ten-ring
Mineral forms	Encilite, mutinaite
Synthetic forms	AMS-1B, AZ-1, Bor-C, Boralite C, FZ-1, LZ-105, NU-4, NU-5, Silicalite, TS-1, TSZ, TSZ-III, TZ-01, USC-4, USI-108, ZBH, ZKQ-1B, ZMQ-TB, ZSM-5

Table 2.5 Short information about MFI structure[62]

2.5.4 Beta polymorphs *BEA and BEC

These two types of zeolites, *BEA and BEC, come from a disordered family of zeolites that is called beta. The *BEA is a beta polymorph A that has not been produced yet in a pure state, while BEC is a beta polymorph C that is produced as a Ge polytype. As can be seen in the Figure 2.26, the two structures are characterized by 3D 12-ring channel system. The chemical formula and other information can be found in the Table 2.6[62].

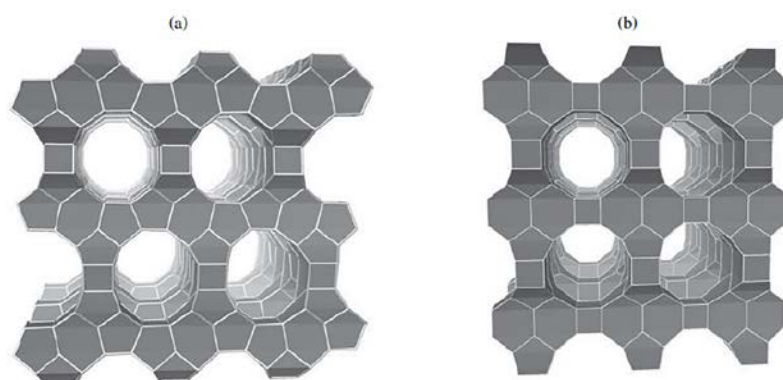


Figure 2.26 *BEA (a) and BEC (b) structures[62]

Type material	Beta polymorph A [51, 52]
Chemical formula	$[\text{Na}^+][\text{Al}_7\text{Si}_{57}\text{O}_{128}] - * \text{BEA}$
Space group	Tetragonal, $P4_122$; $a = 12.661 \text{ \AA}$, $c = 26.406 \text{ \AA}$
Pore structure	Three-dimensional 12-ring
Mineral forms	Tschernichite
Synthetic forms	Beta, Al-rich beta, CIT-6
Type material	FOS-5 (beta polymorph C) [53]
Chemical formula	$[(\text{C}_3\text{H}_9\text{N})_{48}(\text{H}_2\text{O})_{36}][\text{Ge}_{256}\text{O}_{512}] - \text{BEC}$
Space group	Tetragonal, $I4_1/amd$; $a = 25.990 \text{ \AA}$, $c = 27.271 \text{ \AA}$
Pore structure	Three-dimensional 12-ring
Mineral forms	Tschernichite
Synthetic forms	FOS-5 (beta polymorph C), ITQ-14, ITQ-17

Table 2.6 *BEA and BEC structure information [62]

As the ZSM-22 and SAPO-11 zeolites are also considered candidates for catalytic upgrading step in this project, a short discussion regarding their structure will be provided.

2.5.5 ZSM-22 (TON)

The framework of ZSM-22 is described by a one-dimensional 10-ring pore structure. In the [Figure 2.22](#) the channels of this structure can be seen. Due to the unique structure of this zeolite type, it was discovered to be very performant in petrochemical processes like isomerization[63].

2.5.6 SAPO-11

The SAPO-11 zeolite is also characterized by a one-dimensional structure described by 10-ring channels that do not intersect each other. The linear formula of this zeolites is $(\text{SiO}_2)_x(\text{Al}_2\text{O}_3)_y(\text{P}_2\text{O}_5)_z$. The acid sites and the catalytic activity is obtained by replacing the silicon with aluminum and phosphate. Due to the small pore size, this zeolite has low

activity in cracking, but very demanded in isomerization and alkylation processes. As this material has no cavities, its resistance against coke formation is very high[64].

2.6 Synthesis

2.6.1 Incipient wetness impregnation

The incipient wetness impregnation is also called dry impregnation or capillary impregnation and it is based on the determination of the pore volume of a known amount of the material that is decided to be impregnated. The substance that is wanted to be deposited on the analyzed support is dissolved in the determined volume of solvent that was used to find the pore volume of the support. After impregnation, if the solvent volume was approximated correctly, no solution should remain outside the pore space. The advantage of this method, compared with other methods, is that it is cheap, faster and the final property can be controlled in advance. As a disadvantage, the method does not work at high loadings of the precursor due to its limited solubility in the used solvent[65, 66]. After the impregnation step a drying process follows in order to evaporate the solvent.

2.6.2 Calcination

Calcination is a process that takes place at high temperatures, usually in the presence of oxygen or air, and it allows the activation of the catalyst. This process is also called a purification step due to the decomposition and/or burn of different additives, anions (chlorides, nitrates). The structure and the performance of the calcined catalyst is closely related to the temperature, heating ramps and time[65]. If the sample is exposed to high temperatures for a long time, the sintering can occur, leading to a decrease of surface area. It is very important to investigate the mechanical properties of the catalyst especially when it is used in reactions that imply severe conditions. In order to make sure that the catalyst will be mechanical stable in the reaction conditions, the calcination treatment should occur at more severe conditions[67].

2.7 Characterization

2.7.1 Surface area and the pore system - N₂ adsorption

The surface area and the pore size are very important physical properties of a catalyst. A high surface area assures the contact between the molecules of the reactants and the surface of the catalyst, thus increasing the throughput. By increasing the surface area, less catalyst can be involved in the reaction for the same conversion. However, not all the measured area can be available for the reactants if the pore structure is not uniform. For cylindrical pores it can be approximated which of the molecules will fit and which will not, but usually the pores have changes in their structure and this can affect the transportation of the molecules, as well as the reaction pathways[68, 69]. In order to determine the surface area of a solid, the physisorption of an inert gas like nitrogen and argon is realized.

When the monolayer of the inert gas is formed, the total surface can be calculated by having the cross-sectional area of the gas. In case of nitrogen, at 77 K it occupies 0.162 nm² [68]. The quantity of the adsorbate is dependent on the temperature, the equilibrium pressure and on the gas-solid nature. By keeping the same temperature, the adsorption isotherm is:

$$n = f\left(\frac{p}{p^0}\right)_T \quad (1)$$

Where n - adsorbed gas capacity, p^0 - saturation pressure of the adsorptive, p -equilibrium pressure and T -temperature. The interpretation of the adsorption isotherm is realized by analyzing the shape of the curve. According to IUPAC, the physisorption isotherms are classified together with their hysteresis loops (Figure 2.27). The hysteresis loops appear due to the capillary forces that have to be defeated in the desorption step and this is possible at lower relative pressure compared to the one at which the gas entered the pore. When analyzing microporous materials like zeolites and many activated carbons, the isotherm will have the shape represented by the Type I. This type can also manifest the hysteresis loop 4 (H4) and this is due to narrow nanopores that look like slits (Figure 2.28)[69].

The non-porous materials, as well as the macroporous, are characterized by the Type II isotherms. This shape is due to the monolayer-multilayer adsorption that is not restricted at high relative pressures[69].

The Type III isotherm results when weak interaction occur between the adsorbent and adsorbate. In this case there are favorable sites around which the adsorbed molecules will form clusters[69].

The mesoporous materials like oxide gels will generate the Type IV isotherm. Very often the hysteresis loops 1 and 2 are the most common for this isotherm. By looking at Figure 2.28 it can be observed that H1 is associated with uniform pores with both ends opened, while the H2 refers to ink-bottle shaped pores. This type is also characterized by capillary condensation that occurs after monolayer-multilayer adsorption[69].

The isotherm Type V can be described by the same weak interaction that was mentioned in case of Type III isotherm. In this case, after the molecules form cluster, the filling of the nanopores occurs[69].

The Type VI isotherms is generated when the surface area of the solid material is very uniform and the layer-by-layer adsorption occurs. The height of each step refers to the adsorbed layer capacity. This isotherm usually appears when argon is used, for example, as adsorbate and graphitized carbon blacks as adsorbent [69].

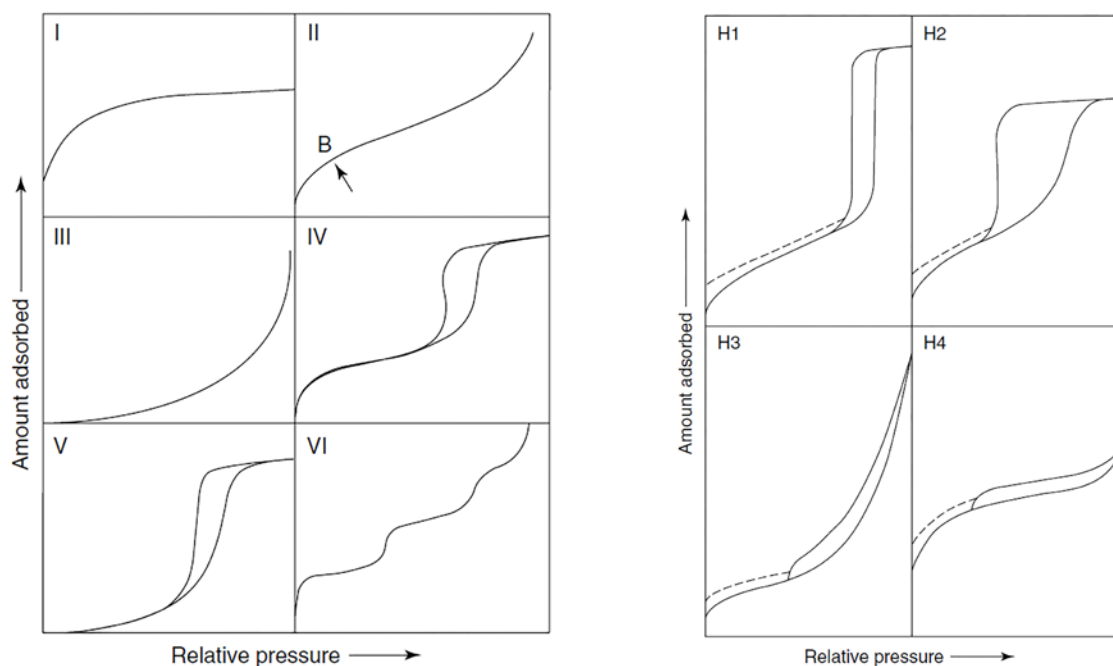


Figure 2.27 Physisorption isotherms (left side) and the hysteresis loops (right side) proposed by IUPAC [70]

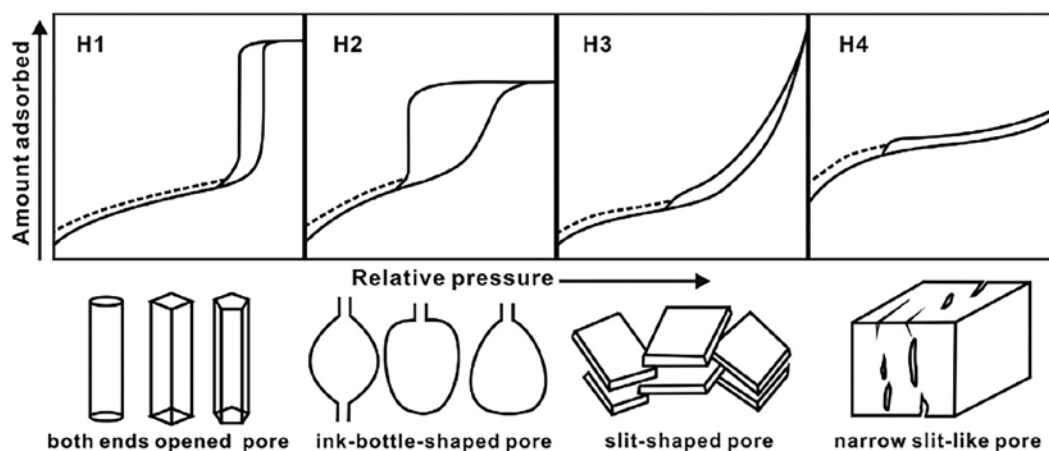


Figure 2.28 Different pore shapes and the associated hysteresis loops [71]

The BET method (Brunauer-Emmett-Teller) is a very common method used in estimation of the surface area of different solid materials like supported and unsupported catalysts. It is not recommended for materials with a very small surface area ($< 2 \text{ m}^2/\text{g}$). The accuracy of adsorption of small amount of gas can be increased by using krypton instead of nitrogen at 77 K. In order to find out the BET surface area, two steps should be followed: the development of the BET plot from the physisorption isotherm and then the deduction of the monolayer capacity, and as the second step, the calculation of surface area based on the cross sectional area of the adsorbed molecules and the resulted monolayer capacity [69]. In the Figure 2.29 the ideal form of isotherm Type II is represented. As it can be seen, the formation of monolayer is accomplished at higher relative pressure, point

B, where the flat zone of the isotherm starts and lasts until the gas molecules will begin to adsorb on the monolayer. In order to derive the BET plot from the physisorption isotherm, the BET equation is used[68]:

$$\frac{P}{V(P_0 - P)} = \frac{1}{V_m C} + \frac{(C - 1)P}{V_m C P_0} \quad (2)$$

Where V is the capacity of the adsorbed gas, V_m is the monolayer capacity and C is an empirical constant. The BET plot can be seen in the Figure 2.30. It is characterized by a linear dependency between the $\frac{P}{V(P_0 - P)}$ and the relative pressure $\left(\frac{P}{P_0}\right)$ [68]. The most common range of relative pressure selected to build the BET plot is 0.05-0.3 and this is due to the good linearity. The last value means the accomplishment of the monolayer[69].

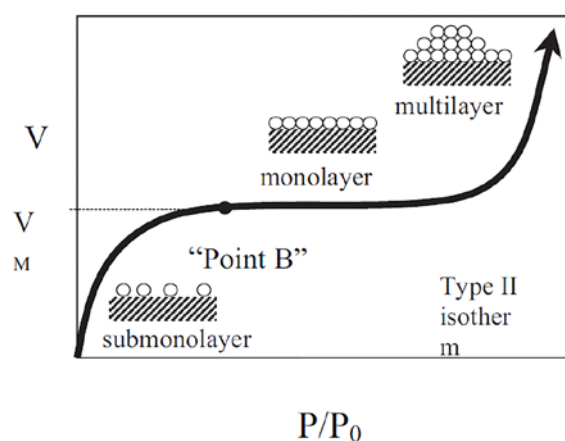


Figure 2.29 The ideal form of Type II isotherm[68]

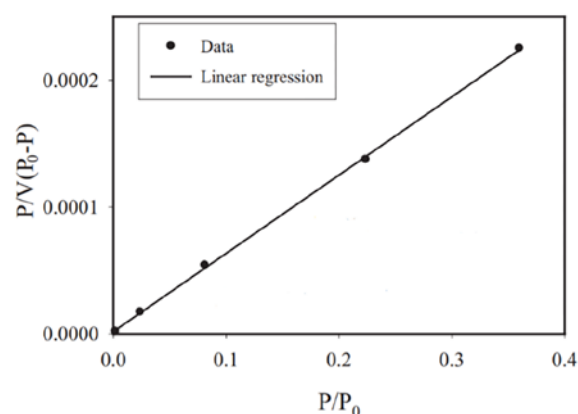


Figure 2.30 The BET plot[68]

The multilayer formation with increasing the relative pressure leads to the condensation of the gas in the pore volume. This phenomenon is also called capillary condensation and it

occurs at a lower pressure than the saturation pressure of the bulk liquid. As it was already mentioned, the Type IV isotherm is described by this phenomenon. It helps to find out the pore volume and the pore size distribution. A widely used method is Barrett-Joyner-Halenda (BJH) and it is based on the modified Kelvin equation that assumes the pore shape to be cylindrical. The equation 3 describes this modified method:

$$r_p = -\frac{2\gamma v_1}{RT} \ln\left(\frac{P}{P_0}\right) \quad (3)$$

Where r_p is the radius of the cylindrical pore, γ is the surface tension of the condensate, v_1 is the molar volume of the condensate and R is the gas constant. The radius of the cylindrical pore is calculated by summation of the Kelvin radius and the thickness of the multilayer film. The equation 3 cannot be applied for very narrow pores and this is because of the adsorption forces that overlap across the pore. Instead of nitrogen, people use argon to find the pore volume of the microporous materials like zeolites.

2.7.2 X-ray diffraction

The X-ray diffraction (XRD) is a very useful and interesting method when the identification of the crystalline phases and determination of particle size of a catalyst are wanted. The crystalline phases are identified by comparing them with the data of the already known structures. The X-rays are defined as being an electromagnetic radiation generated by a cathode ray tube. The wavelengths of these X-rays are quite similar to the distance between the atoms in a crystal (0.1 -100 Å). Before directing the X-rays toward the material that is wanted to be characterized, a filter is used in order to produce only monochromatic radiation. When the incident X-ray reaches the lattice of the sample, it can continue its original direction or it can be scattered by the electrons[72, 73]. The scattered X-rays can interfere constructively or destructively (Figure 2.31). As it can be observed in the Figure 2.31 (a), when the diffracted waves interfere constructively, a new wave will be generated with a higher amplitude. This is possible when the phases of two X-ray waves are separated by an integer number of wavelengths. All this information is incorporated in the equation 4 that is the Bragg's law[72]:

$$n \lambda = 2 d \sin \theta \quad (4)$$

Where n is an integer, λ is the X-rays wavelength, d is the space between two adjacent planes where the atoms are positioned and θ is the angle between the incident beam and the plane. According to the Bragg's law, when two parallel beams diffracted by two adjacent planes are characterized by a path difference equal with $n\lambda$, a constructive interference will occur(Figure 2.32)[72].

Each compound is characterized by a set of d-spacings (diffraction pattern) and the compound is identified based on a library that is equipped with the standard reference patterns [73].

A diffractometer is consisted of three elements: a cathode ray tube that produces the electrons by heating the filament, a sample holder and a detector. When the incident angle is fixed (θ), the sample rotates at an angle value equal to the one of the incident angle while it is bombed with an electron beam. The X-ray detector rotates at an angle value that is twice the value of the incident angle (2θ) while it collects the diffracted X-rays [73].

When analyzing the diffractogram, it is important to know that the peak intensity is proportional with the amount of the phase detected and the peak width is inversely proportional to the crystallite size [72]. The crystal size can be calculated with the Paul Scherrer's equation:

$$L = \frac{K\lambda}{\beta \cos \theta} \quad (5)$$

Where L is the crystal size, K is a dimensionless shape factor with a value close to unity, λ is the X-rays wavelength and β is the width that corresponds to the half-height of the peak [68].

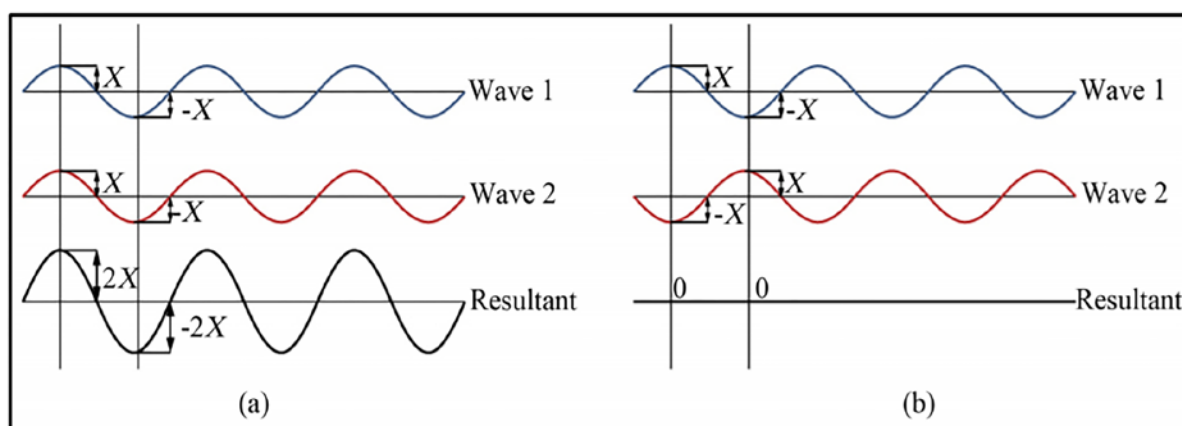


Figure 2.31 Constructive and destructive interferences [74]

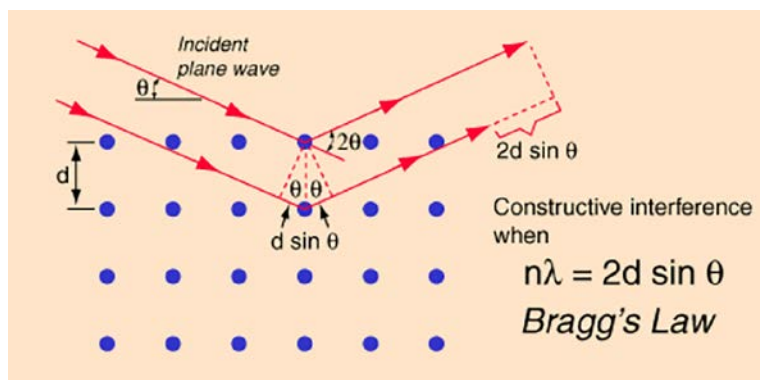


Figure 2.32 Bragg's Law[75]

2.7.3 Temperature Programmed Desorption Technique

The performance of a catalyst is strongly dependent on the chemical species from its surface because they determine its activity and selectivity. In this subparagraph the ammonia temperature programmed desorption technique that helps to identify the amount of acidic sites and their strength will be discussed. The weak point of this technique is that it cannot distinguish between the Lewis and Brønsted acid sites. The difference can be made if using infrared spectroscopy technique and ammonia or pyridine as probe molecules[69, 76]. Ammonia is a very basic substance that is widely used in testing the surface acidity. Moreover, it is characterized by a small molecule that allows it to diffuse easily through different pore structures[76].

In the 20th century the temperature programmed desorption (TPD) was based on the vacuum adsorption of a known gas on the sample that occurred at constant temperature and then, by heating with a chosen heating rate, the desorption of species took place when the energy was sufficient for breaking the chemical bond between the probe molecule and the acidic/basic site. In case of ammonia-TPD, the heat of desorption depends on the proton affinity of ammonia and on the proton mobility of the acidic site. The detection of the desorbed molecule was realized by recording the pressure that increases when the probe molecules start to desorb. In time, the principle of this method remained the same, while some improvements were done for the set-up. Different detectors like flame ionization detector (FID), thermal conductivity detector (TCD), mass spectrometer (MS) and conductometric titration are available for monitoring the desorbed species, as well as skilled apparatus that is capable to keep a good control of the desorption heating rates[76].

The adsorption process is realized at isothermal conditions and usually the temperature is 300 K or higher. Before the sample is exposed to the probe gas, it is pre-treated in vacuum at a proper temperature. In order to identify the active sites, the chemisorption is the process that should be investigated because it is highly specific regarding the surface of the solid and the adsorption is described by a monolayer formation, while the physisorption can occur in multilayer form and the adsorbant-adsorbate bond is characterized by weak forces. Based on this, an inert gas is used to remove the physisorbed molecules. Then the desorption of chemisorbed molecules is monitored by increasing the temperature in a controlled way. It is very important to keep a certain concentration of the probe gas in the gas mixture as the detector sensitivity depends on it. The TPD technique is quite similar to the temperature programmed reduction (TPR), so the concentration of the probe gas should be between 1-10 % for a high sensitivity. If using a TCD as a detector, the difference

between the conductivities of the carrier gas and the probe gas should be high in order to have a good sensitivity of the detector. The mass of the sample is also very important as it can influence the heat transfer. If using large quantities, the resolution and the position of the peak/peaks will be influenced[76].

The TPD desorption profile gives two important classes of data: the area under the obtained curve and the position of the peak maximum. The first one refers to the amount of the adsorbed probe gas. A higher area of the TPD profile means a higher capacity of the adsorbed molecules. The second class refers to the activation energy required by the desorption of the molecule. The higher the activation energy, the more difficult is to desorb the molecule due to strong interactions with the surface sites. Based on this, the temperature of the peak maximum will be higher[76].

2.7.4 Thermal Gravimetric Analysis-Mass Spectrometry

Thermal Gravimetric Analysis (TGA) is a very useable technique used for the investigation of different materials like polymers, metals, plastics, inorganic material and many others. It records the change of mass of the analyzed material as a function of temperature or time if isothermal condition is set. The temperature-time program is very well controlled and it can take place in an atmosphere of different gases like oxygen, air, helium or other gases, moreover it can run under vacuum condition (30 mTorr)[77]. Two types of transformations can be accomplished by using this technique: mass change by losing the mass or mass change by gaining the mass. In the first category are included processes like evaporation, dehydration, desorption, decomposition, and in the second one processes like reaction, adsorption and hydration. The TGA instrument is usually coupled with a mass spectrometer(MS) in order to identify the nature of the volatiles[76], as well as with a differential scanning calorimetry (DSC) which implies the measurement of the energy that can be adsorbed or released by a sample during the heating or cooling process[78]. By using the TGA technique, the stability of the investigated material can be followed. This information is relevant especially for the catalysts that are very fast deactivated in processes like biomass pyrolysis, catalytic reforming, catalytic cracking and requires activation by simply burning the carbon deposition from its surface. Usually the activation process occurs at severe conditions (up to 750 °C) and this is to make sure that all types of coke are removed from the catalyst surface. If using zeolites, elevated temperatures in the presence of water molecules can cause dealumination and thus the acidity is lost in time. Regarding this problem, the TGA can clearly show the range of conditions for using the catalyst.

2.8 Activity

2.8.1 Py-GC/MS

The Pyrolysis (Py) Gas Chromatography(GC)/Mass Spectrometry(MS) (Figure 2.33) is a highly valuable and interesting technique for characterization of different macromolecules that cannot simply be analyzed by GC/MS due to their resistance against vaporization. By

applying the pyrolysis process to these species, the identification of building units of the macromolecule will be possible. Based on their affinity to the material used inside the column of the GC, these units will be retained a certain time, in this way, the resulted compounds in the pyrolytic process will be analyzed one by one by the ionization source of the MS that implies fragmentation of the compound. The MS generates a spectrum of the analyzed species that is unique for each compound and it can be identified by fitting the resulted data with the standard spectra that are already registered in a library. According to the quality of fitting that is calculated by the software of the apparatus, the generated compounds can be found.

Before 1992 this technique was not preferred due to the poor reproducibility, moreover, it could not cope with the instability of different compounds that were stabilized by repolymerization and thus many species could not be analyzed by the instrument. This problem was investigated by Emeritus Professor Shin Tsuge of Nagoya University. He developed a technique based on a small sample cup that free-falls in a micropyrolyzer which is heated up to the target temperature in several milliseconds. The temperature is very well controlled and thus the instrument minimizes the condensation of the reactive species. Due to a much higher performance of the Py-GC/MS reached by the Professor, a Double-Shot Pyrolyzer is commercialized by Frontier Laboratories in 1992[79]. Nowadays, the Py-GC/MS is a very used instrument especially for identification of biomass units. The technique implies a fast procedure for analyzing different macromolecules, moreover, different processes can be simulated and diverse catalysts can be screened. Due to small quantities consumed per one analysis, the technique becomes cheap and at the same time very valuable as many analyses can be done at different temperatures.

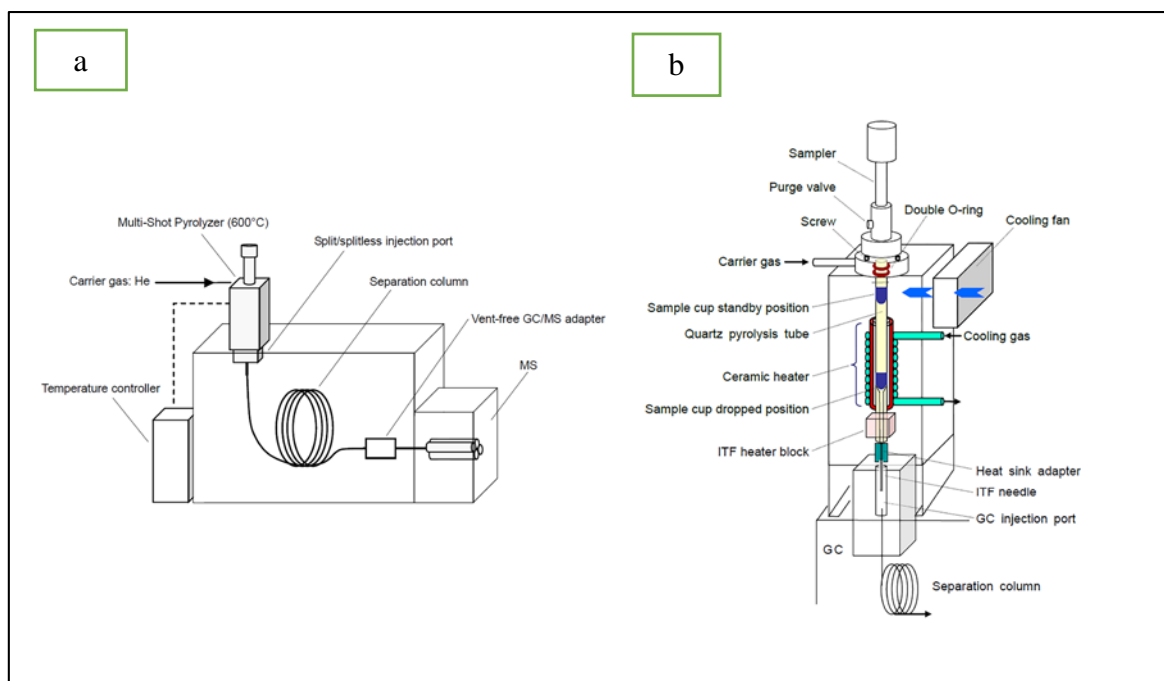


Figure 2.33 **a** - PY-GC/MS system configuration; **b** - Multi-shot pyrolyzer[79]

2.9 GC-FID/TCD

2.9.1 Gas Chromatography/Thermal Conductivity Detector (TCD)

The thermal conductivity detector is a very used detector in the gas chromatography for detection of nitrogen, carbon monoxide, carbon dioxide, oxygen, hydrogen and many other compounds. Its operating principle is very simple, but very interesting and efficient. It is consisted of two parallel channels which are equipped with electrically heated filaments connected in a special electrical circuit which is called Wheatstone bridge. These filaments are cooled down by the gas that is passing through the channels. As each compound is described by its own thermal conductivity, when it passes through the channel, the filament will be cooled down with a specific rate. If the same gas goes through both channels, the bridge will be balanced, if not, the bridge will be unbalanced due to different temperatures of the filaments. When the temperature of the filament changes, the resistance also changes and this will result in producing an electrical signal that is unique for the analyzed compound[80-82]. This technique is very advantageous as it can detect many compounds in only one run and it is non-destructive. However, the filaments should be protected and in this case compounds like acids or halogenates should be used carefully as they can corrode the wires. It is also very important to have the difference between the thermal conductivity of the carrier gas and of the sample gas as large as possible in order to get a better signal result.

2.9.2 Gas Chromatography/Flame Ionization Detector (FID)

The flame ionization detector is also a very practiced detection method in the gas chromatography. It is used especially for the identification of hydrocarbons by breaking their molecules that are transported through the hydrogen/air flame. The ions and electrons formed under the flame are attracted by a polarizing voltage on an electrode and so an electrical signal is generated. The current produced is proportional with the amount of ions generated. An electrometer senses the current and converts it into a digital signal that is transmitted to an output device where the peaks are generated[83-85].

3 Material and Methods

This chapter starts with the elemental analysis and the pretreatment process of the lignin used in this project followed by the preparation of catalysts and the description of the procedures for the all involved characterization techniques and activity test instruments.

3.1 Elemental Composition and Pretreatment of Lignin

The lignin used in this project was supplied by St1 Company. It results as a by-product in the Etanolix plant which produces ethanol from different wastes. The approximated elemental composition of the dried lignin was provided by the company and it is shown in the [Table 3.1](#).

Lignin	Carbon	Hydrogen	Nitrogen	Oxygen
Composition,wt%	61.7	6.2	1.0	31.1

Table 3.1 The elemental composition of lignin

A pretreatment of lignin was realized before using it in the fast pyrolysis process in order to eliminate different impurities and especially the water. It was dried from room temperature up to 100 °C with a heating rate of 1 °C/min and a hold time of 5 hours. Then the dried lignin was grinded and sieved to a particle size range of 100-400 µm.

3.2 Preparation of catalyst

3.2.1 Incipient wetness impregnation and calcination

Herein, five supported catalysts were synthesized. As supports, ZSM-5, β , HY and Al_2O_3 were used and MoP oxides as the active phase. Two alumina supported catalysts were prepared with the loading of MoP of 5 and 10 wt%. The other three supports were impregnated with 10 wt% of MoP.

The incipient wetness impregnation method was used for preparation of the catalysts. The pore volume of each support was determined by slowly dripping water on 1 g of support. When the support became completely wet without any phase separation, the estimated water volume was noted. The water volume measured for each support and the total volume necessary for 15 g of catalyst are presented in the [Table 8.7](#) (Appendix).

As precursors, ammonium molybdate tetrahydrate was used to generate Mo oxide and ammonium phosphate dibasic for phosphorus oxide. The purity and the supplier are shown in the [Table 8.8](#), Appendix. The calculated amount of precursors was dissolved in the determined water amount at room temperature and continuous stirring. Subsequently, the

solution was added drop by drop to the catalyst support. In order to assure a proper impregnation, all the catalysts were left for 3-4 hours in the fume hood and afterwards they were exposed to an overnight drying step at 80 °C to evaporate the solvent. As a final step, in order to eliminate the impurities and to generate the metal oxides, the calcination of all 5 catalysts was realized at 550 °C for 5 hours assisted by a heating rate of 1 °C/min. The mass of the precursors was calculated according to the equations presented in [Equation A3.1](#), Appendix.

3.2.2 Activation of zeolites

Six zeolites were selected for testing in this study: SAPO-11, SAPO-34, ZSM-22, ZSM-5 (silica/alumina ratio of 30, 50, 80 and 280), β and Y. The ZSM-5 and Y zeolites were purchased in their ammonium form (NH_4 -ZSM-5 and NH_4 -Y) and were activated by being calcined at 550 °C for 5 hours and a heating rate of 1 °C/min. The active form of all zeolites is H-X, where H is the cation and the X is the zeolite. Some properties of these catalyst can be found in the [Table 8.8](#), Appendix.

3.2.3 Oxides of transition metals supported on alumina

Five catalysts consisted of oxides of transition metals and an oxide of a non-metal were prepared by Sundli [\[86\]](#) and tested within this study. Each catalyst is consisted of alumina as a support and different metal oxides together with phosphorus oxide as the active phase with a loading of 10 wt%. The first catalyst has as active phase MoP oxides and the other four are formed by adding to MoP Ni, Fe, Co or Cu. The molar ratio between the elements is 1:1 and 1:1:1 respectively. All the catalysts were prepared based on the Pechini method. This method is considered very efficient when a good dispersion of the active phase on the support is wanted, especially in case of using several elements as the active phase. It implies the covering of the support surface with a very thin layer of the active material.

A nickel oxide on alumina catalyst was also tested in this study. The catalyst was prepared by PhD Isaac Yeboah by using the incipient wetness impregnation method for the synthesis of the catalyst.

3.3 Characterization

3.3.1 Surface area and the pore system- N_2 adsorption

The N_2 adsorption-desorption was realized at 77K with a physical adsorption instrument called Micromeritics TriStar II 3020. In order to increase the performance of the adsorption technique each sample was degassed under vacuum at 200 °C overnight in a Micromeritics VacPrep 061. The specific surface area was estimated by applying the Brunauer-Emmett-Teller (BET) method. The decided range of the relative pressure for calculation of the BET area was 0.05-0.3. The Barrett-Joyner-Halenda (BJH) method was used to determine the pore size distribution and the pore volume.

3.3.2 X-ray Diffraction

A D8-Focus instrument was used for performing the X-ray Diffraction of the calcined catalysts. The CuK_α radiation was applied for all samples in order to develop the XRD patterns. The data was collected from 5° to 75° (2θ) with a step size of 0.014° . The DIFFRAC.EVA software was used for data analysis.

3.3.3 Temperature Programmed Desorption Technique

Temperature-programmed desorption of ammonia (NH_3 -TPD) of ZSM-5(30), β and Y zeolites was carried out in an automatic chemisorb analyzer (FineSorb 3010). 0.1 g of each sample was introduced into a U-shaped tubular quartz reactor. Each catalyst was treated by heating it from room temperature to 550°C for 30 minutes with a heating rate of $20^\circ\text{C}/\text{min}$ and then cooled down to 80°C in He ($25\text{mL}/\text{min}$). At this temperature, 10 % NH_3 -He gas was used for chemisorption process for 30 min ($5\text{mL}/\text{min}$) followed by a He purge to desorb the physisorbed ammonia molecules. TPD experiments were performed under a flow of He ($25\text{mL}/\text{min}$) from 80 to 700°C at a constant heating rate ($10^\circ\text{C}/\text{min}$). The desorbed NH_3 was monitored with a thermal conductivity detector (TCD). The analyses were realized in China by the postdoc Xiang Feng.

3.3.4 Thermal Gravimetric Analysis-Mass Spectrometry

The Thermal Gravimetric Analysis (TGA) was performed for all spent catalysts in a TGA Linseis thermal analyzer. A ramp was set from room temperature to 800°C with a heating rate of $10^\circ\text{C}/\text{min}$ followed by an isothermal segment of one hour at the maximum temperature. The analyses were realized under a gas mixture atmosphere consisted of $140\text{mL}/\text{min}$ of air with $60\text{mL}/\text{min}$ of argon. 20-25 mg of sample was placed in a special alumina crucible which is resistant to severe conditions and then installed near the reference crucible. A Mass Spectrometer (MS) was coupled to the TGA in order to register the CO_2 in the evolved gas.

3.4 Activity

3.4.1 Py/GC-MS

The fast pyrolysis and the fast pyrolysis coupled with the catalytic upgrading step were performed on a Micro-Pyrolyzer (EGA/PY-3030, Frontier Laboratories) that is connected to a gas chromatographer (Agilent 7820A) (GC) and a mass spectrometer (5977E) (MS) (Figure 3.1,a). In order to avoid the condensation of the vapor phase, the interface located between the pyrolyzer and the GC is heated up to 300°C . The GC oven was programmed for a 2-minute hold time at 50°C and then one ramp to 200°C with a heating rate of $10^\circ\text{C}/\text{min}$ and a hold of 5 minutes and one ramp to 250°C set up with the same hold time and heating rate. An Ultra ALLOY Capillary Column ($30\text{m} \times 0.25\text{mm} \times 0.25\ \mu\text{m}$, Frontier Laboratories LTD) was used for the GC analysis. Helium was used as a carrier gas of the vapor phase in the GC column with a flow of $2\text{mL}/\text{min}$ and split ratio of 100:1. A range of m/z 29 up to 600 was chosen for the MS data recording and a scanning frequency of 4.9

scans/sec. The scientific library NIST11.L was used for identification of mass spectra peaks. The arrangement of the feedstock and the catalyst in the special sample cup allows simulation of two different processes. The first sample cup from [Figure 3.1 \(b\)](#) simulates the catalytic fast pyrolysis, thus the lignin and the catalyst are mixed. The second sample cup [Figure 3.1 \(c\)](#) simulates the fast pyrolysis of lignin and the catalytic upgrading of the volatiles. In order to realize these two steps, the lignin bed and the catalyst bed should be separated. As it can be seen in the [Figure 3.1](#), the quartz wool is used as a separation material and for covering the surface in order to avoid the loss of used materials and to keep the solid (catalyst/char/coke) inside the cup. For every analysis the mass of the lignin was kept constant (0.5 mg).

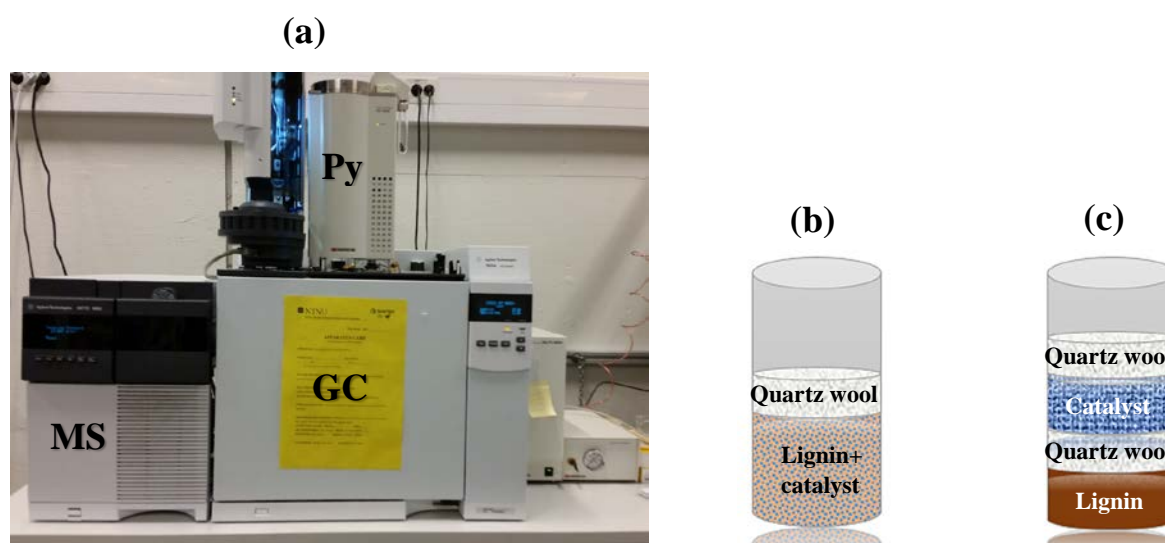


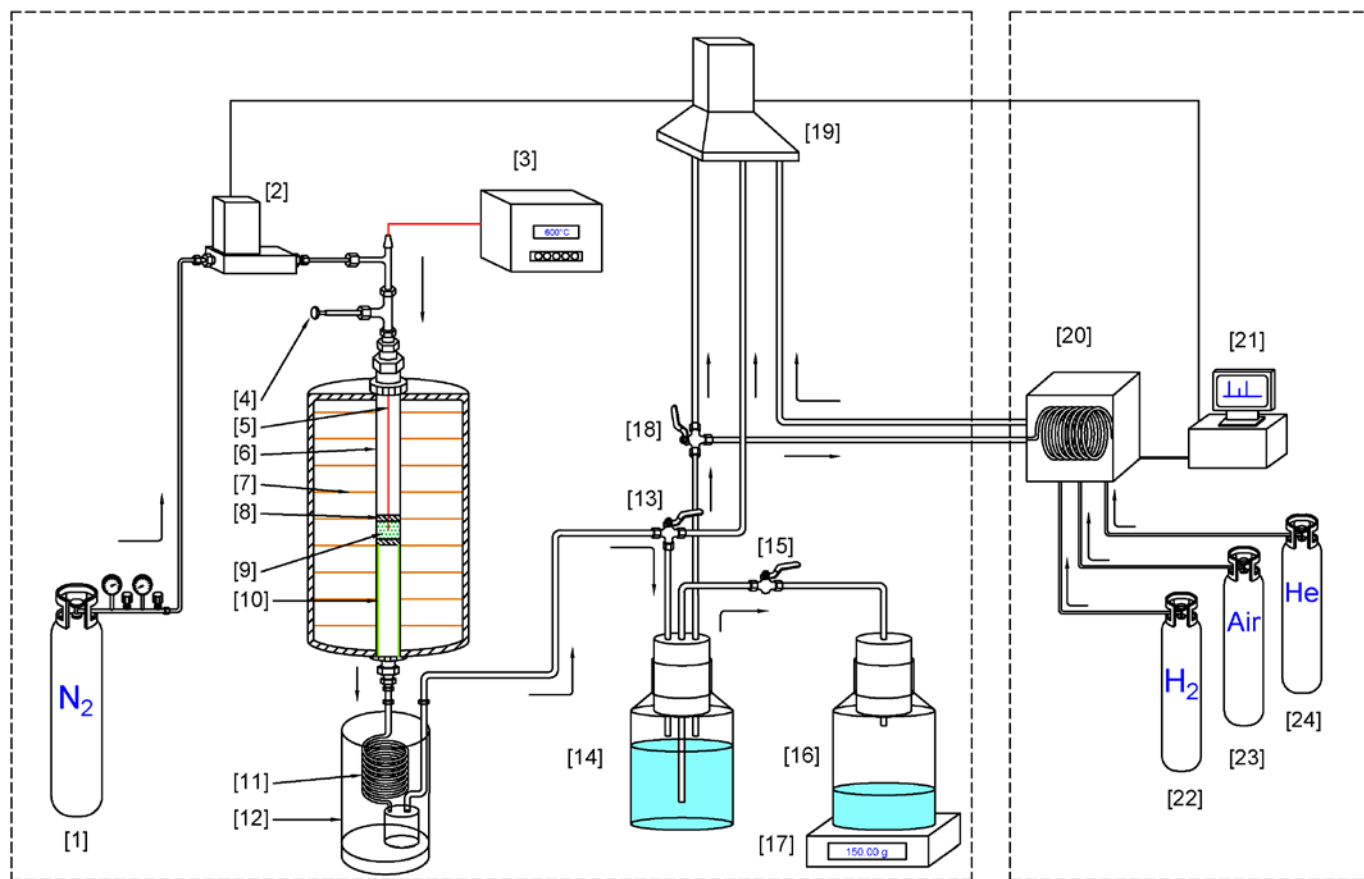
Figure 3.1 (a)-Pyrolyzer-Gas Chromatography/Mass Spectrometry; (b)-Sample cup – simulates fast catalytic pyrolysis; (c)-Sample cup-simulates the fast pyrolysis and the fast pyrolysis coupled with the catalytic upgrading step

3.4.2 Fixed bed reactor

The fast pyrolysis and fast pyrolysis with catalytic upgrading of volatiles processes were also performed on a fixed bed tubular reactor in order to quantify the three main products: gas, liquid and solid, and the compounds of liquid and gas phase. The reactor and the other important elements of the rig are presented in the [Figure 3.2](#). The N_2 (1) was used for creating the inert atmosphere inside the reactor (6), for carrying the products and as internal standard for the gas products. It was fed from the upper tube of the reactor localized outside the furnace (7). The value of the nitrogen flowrate was set with the help of the mass flow controller (2) and the special flow software (21). The reactor was heated up and the temperature of catalyst bed was measured by using the thermocouple (5) (positioned so that it reached the catalyst bed) and the temperature controller (3). The lignin was injected with a special piston mechanism (4). A rubber O-ring was fitted on the piston in order to avoid the gas leakage when it was in the open position (when half of it was outside the horizontal tube). When injecting the lignin (0.1-0.3 g) in the reactor, it was thermally decomposed in different oxygenated compounds (phenolic and phenol alkoxy compounds) on the upper part of the quartz wool (8). Two thin layers of quartz

wool were used. The upper layer was used to separate the catalyst or inert heat carrier (9) (SiO_2 : used for FP with no catalytic upgrading) from the pyrolytic zone and to avoid its contamination with the char. The bottom layer was placed on a cylindrical metal support (10) in order to prevent the catalyst or the inert heat carrier from falling. The liquid products were condensed in a spiral glass condenser (11) placed in a cooling ice bath (12). 0.1-0.3 g of ethylene glycol was used to enhance liquid accumulation. The gas products were collected in the gas cylinder with a triple-hole rubber plug (14). When the gas entered the cylinder, it displaced the water which was driven in the second cylinder (16) positioned on a scale (17). The scale was used to check the gas flowrate. While the nitrogen was flown through the reactor in order to evacuate the air, the 3-way valve (13) was switched to the ventilation (19). It was turned to the gas cylinder right before injecting the lignin. From that moment, the gas was collected for 10-20 min and then the valve (13) was switched back to the ventilation. The time for the gas accumulation was measured in order to know the total nitrogen volume. This value was used for the quantification of the gas products. In order to analyze the gas, the 2-way valve (15) was closed and the 3-way valve (18) was opened and directed to the gas chromatograph (20). The CO , CO_2 , H_2 , CH_4 and N_2 were detected by the TCD, while C1-C6 were detected by the FID. The special GC software (21) was used to set the GC parameters and to analyze the area of the generated peaks. The GC method was run between 3 and 6 times for each pyrolytic experiment and the average value was used in the calculations. The yield of solid was calculated by weighing the reactor (with the catalyst/ SiO_2 and quartz wool inside) before and after the experiment. The weight of char was determined by subtracting the coke (determined by TGA) weight from the obtained solid. The yield of liquid was measured by weighing the spiral glass condenser before and after the experiment. Due to the low amount, the water phase and the organic phase could not be distinguished and separated. Based on this, the liquid obtained in FP and FP-CU was considered fully bio-oil and, thus, the organic compounds were quantified based on the total liquid yield. The organic compounds could be quantified by calibrating the GC-FID and thus the yield of water could be also calculated. However, the calibration was not realized due to the limited time.

All the catalysts, before using them in the FP-CU, were pelletized, grinded and sieved to a particle size range of 250-425 μm . The particle size range of lignin was the same as in the Py-GC/MS (100-400 μm).



Nr.	NAME OF PART	Nr.	NAME OF PART	Nr.	NAME OF PART
1.	Nitrogen tank	9.	Catalyst / inert heat carrier material	17.	Scale
2.	Mass flow controller	10.	Metal support	18.	3-way valve
3.	Temperature controller	11.	Spiral glass condenser	19.	Ventilation
4.	Piston	12.	Ice cooling bath	20.	Gas chromatograph - FID/TCD
5.	Thermocouple	13.	3-way valve	21.	PC
6.	Fixed bed tubular reactor	14.	Gas cylinder with 3-hole rubber plug	22.	Hydrogen tank
7.	Furnace	15.	2-way valve	23.	Air tank
8.	Quartz wool	16.	Water collector	24.	Helium tank

Figure 3.2 The flowsheet of the FP and FP-CU processes

3.4.3 Liquid Analysis: Gas Chromatography/ Flame Ionization Detector (FID)/Mass Spectrometry detector

A GC/FID (Agilent 7820A) and a GC/MS (GC-Agilent 7820A, MS-5977E) were used for identification and quantification of the liquid products obtained in the fixed bed reactor. The GC oven program was kept the same for both instruments in order to maintain the peaks distribution. It was set for a 5-minute hold time at 50 °C and then one ramp to 130 °C with a heating rate of 5 °C/min followed immediately by a second ramp to 250 °C set up with a heating rate of 20 °C/min. An Agilent J&W HP-5 GC Column (30m × 0.320mm × 0.25 µm) was used for the GC analysis. Helium was used as a carrier gas of the vapor phase in the GC column with a flow of 1 mL/min in the GC/FID and 2 mL/min in the GC/MS and split ratio of 10:1. A range of m/z 20 up to 550 was chosen for the MS data recording and a scanning frequency of 2.8 scans/sec. The scientific library NIST11.L was used for identification of mass spectra peaks.

The products analysis was realized with both GC/FID and GC/MS in order to quantify the pyrolytic liquid product. MS was used in order to identify the products and the FID for the quantification of each product. According to Marko R. Djokic [87], the flame ionization detector is characterized by a wide linearity range and broad flexibility when it comes to response factors, while the mass detector is less convenient due to the laborious calibration of each individual compound. In this study, the response factors were calculated based on the effective carbon number approach [87]. Of course, it is more correct to determine the response factors based on a set of defined calibration mixture, but due to the wide range of product obtained in the fast pyrolysis and in the catalytic upgrading, the effective carbon number approach was applied for all the products. Herein, methane was used as a reference compound and the response factor was calculated according to the formula:

$$f_i = \frac{M_i}{\#C_{i,\text{eff}}} \cdot \frac{1}{M_S} \quad (6)$$

Where M_i : molar mass of the compound; M_S : molar mass of methane (reference compound); $\#C_{i,\text{eff}}$: effective carbon number of compound i.

The effective carbon number of a hydrocarbon is equal with the carbon number of the compound, while for the organic groups that contain also oxygen it is calculated based on the formula:

$$\#C_{i,\text{eff}} = \#C_i - n \quad (7)$$

Where $\#C_i$: carbon number of the compound i; n: correction for functional groups.

The correction numbers for different groups were taken from Schofield [88] study. Based on the determined response factor and the FID peak area, the concentration (wt%) of each compound was calculated following the procedure consisted of the following formula:

1. Calculation of area fraction of compound i:

$$A_{f,i}^{\text{FID}} = \frac{A_i}{\sum A_i} \quad (8)$$

2. Calculation of mass fraction of compound i:

$$wt_i = \frac{A_{f,i}^{\text{FID}}}{f_i} \quad (9)$$

3. Normalization of the mass fraction:

$$wt_{f,i} = \frac{wt_i}{\sum wt_i} \quad (10)$$

4. Having the mass of the pyrolytic oil, the mass of each compound was calculated based on the mass fraction.

$$m_i = wt_{f,i} \cdot m_{\text{oil}} \quad (11)$$

3.4.4 Gas Analysis: Gas Chromatography/Thermal Conductivity Detector (TCD)/ Flame Ionization Detector (FID)

The analysis of the pyrolytic gas products generated in the fixed bed reactor was performed on a gas chromatographer (Agilent 7820A) (GC) equipped with a flame ionization detector (FID) and a thermal conductivity detector (TCD). The GC oven was programmed for a 6-minute hold time at 45 °C and then one ramp to 190 °C with a heating rate of 75 °C/min and a hold of 2 minutes followed by a cooling step back to 45 °C. The FID heater was set to 250 °C and the flow of air and hydrogen to 350 mL/min and 35 mL/min respectively. As a makeup, gas helium was used with a flow of 25 mL/min. It was also used as a carrier gas of the gas phase in the GC column with a flow of 35 mL/min and split ratio of 25:1. The TCD heater was programmed at 230 °C. Helium was used as a reference gas with a flow of 45 ml/min, as well as a makeup gas with a flow of 2 mL/min.

The gas products were identified based on the instrument calibration which was realized with a gas mixture of known composition (Table 8.9, Appendix). The quantification of pyrolytic gas products detected by TCD was realized based on nitrogen which was used in the fixed bed reactor to create the inert atmosphere. As methane is identified by both detectors, it was used as a reference gas to quantify the products detected by FID. The equations for calculation of the mass of each compound are shown in Equation A3.11 Appendix.

4 Results & Discussion

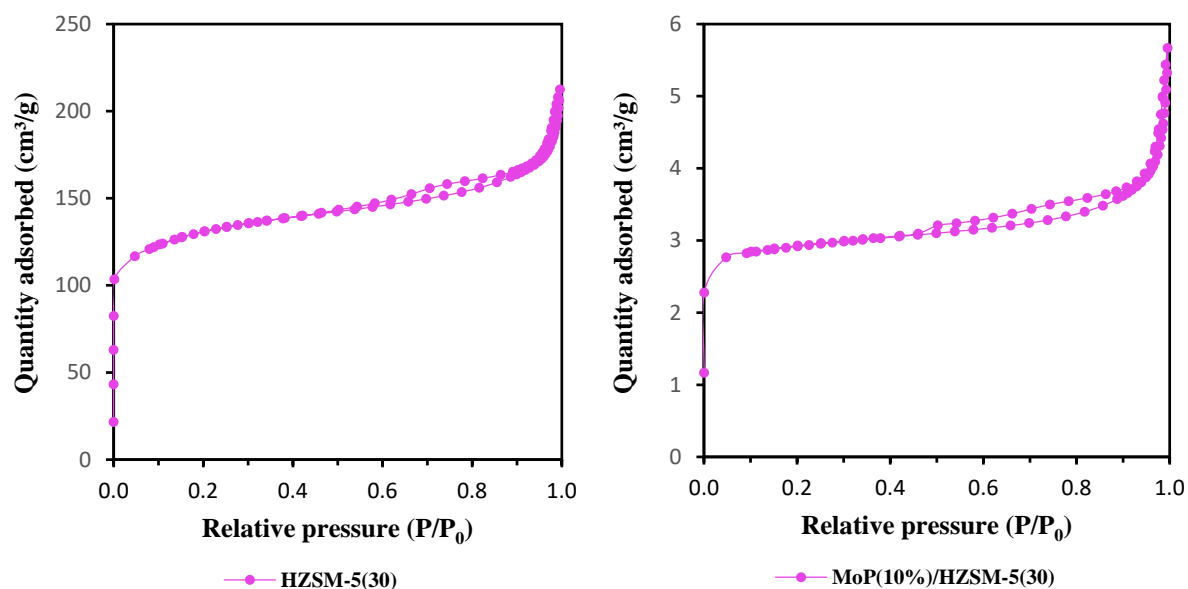
4.1 Characterization

4.1.1 Surface area and the pore system- N₂ adsorption

The N₂ adsorption analysis was realized for the calcined catalysts: HZSM-5(30), MoP(10 %)/HZSM-5(30), MoP(10 %)/ β , HY, MoP(10 %)/HY, SAPO-11 and ZSM-22. Only the surface area was determined for each catalyst. This is because of the micropores of the zeolites that do not give correct results for nitrogen adsorption due to its molecule being too large. As it was already mentioned in the literature discussion of the characterization techniques, the BET equation is used to determine the surface area of the sample. The results are presented in the [Table 4.1](#) and the isotherms in the [Figure 4.1-Figure 4.4](#). The BET plots are presented in Appendix ([Figure 8.3-Figure 8.6](#)) The surface area of β was written in the table only for comparison and it was taken from the product label. If analyzing the figures, it can be seen that all the zeolites have the isotherms with the shape represented by the Type I and the hysteresis loop 4(H4). According to the [Figure 2.28](#), the loop appears due to the very narrow pores. When analyzing the BET plots, it is more difficult to be done for zeolites as they are usually characterized by a negative intercept. According to Thommes, Kaneko [89] this happens due to the strong adsorption of the gas molecules in the micropores and the monolayer is accomplished faster. This means that the BET plot should be realized at lower relative pressure values and in that range more points should be set in the method of the instrument.

According to the values presented in the [Table 4.1](#), it can be seen that the impregnation of the two oxides reduced considerably the surface area of the catalysts. This results as a consequence of the pore blocking or reduced pore size. As the zeolites are characterized by micropores, they can be easily blocked. Of course, high loadings are preferred when it is known that the support has high enough surface area, but the pore size plays a very important role and, in this case, high loadings are not a proper choice for the zeolites. According to this, the MoP was also impregnated on γ -Al₂O₃ that does not have a very high surface area. Two alumina based catalysts with the MoP loadings of 5 % and 15 % were prepared within this project and the MoP(10 %)/ γ -Al₂O₃ was prepared and characterized by Sundli [86]. The N₂ characterization results for γ -Al₂O₃ and MoP(10 %)/ γ -Al₂O₃ were included in this project ([Table 8.10](#), Appendix) with permission of her co-supervisor, prof. De Chen. The N₂ adsorption analysis of MoP(5 %)/ γ -Al₂O₃ and MoP(15 %)/ γ -Al₂O₃ was not realized as it is evident that the surface area of the alumina decreases when the active phase loading increases. In the [Table 8.10](#) (Appendix) it can be seen that the surface area of γ -Al₂O₃ is not so affected like the one of the zeolites and this is because of the γ -Al₂O₃ mesoporous structure.

Sample	Surface area, [m ² /g]
HZSM-5(30)	489
MoP(10%)/HZSM-5(30)	11
H β	640
MoP(10%)/H β	335
HY	854
MoP(10%)/HY	290
SAPO-11	212
ZSM-22	48

Table 4.1 Surface area of the calcined catalysts**Figure 4.1** N₂ adsorption isotherms of HZSM-5(30) (left) and MoP(10%)/ HZSM-5(30) (right)

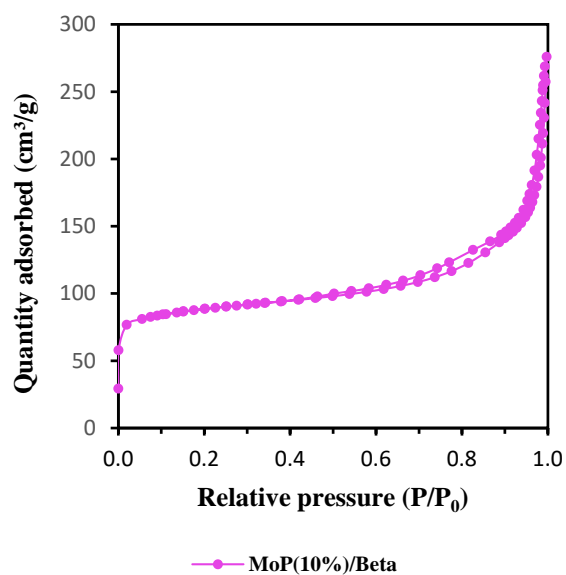


Figure 4.2 N₂ adsorption isotherm of MoP(10%)/ β

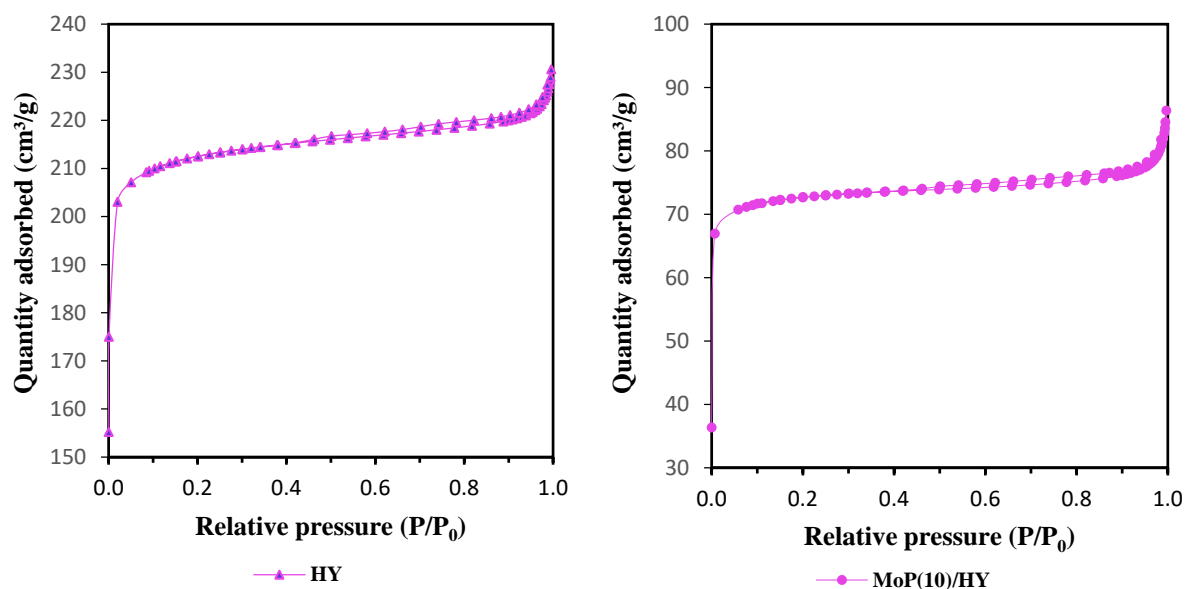


Figure 4.3 N₂ adsorption isotherms of HY (left) and MoP(10 %)/ HY (right)

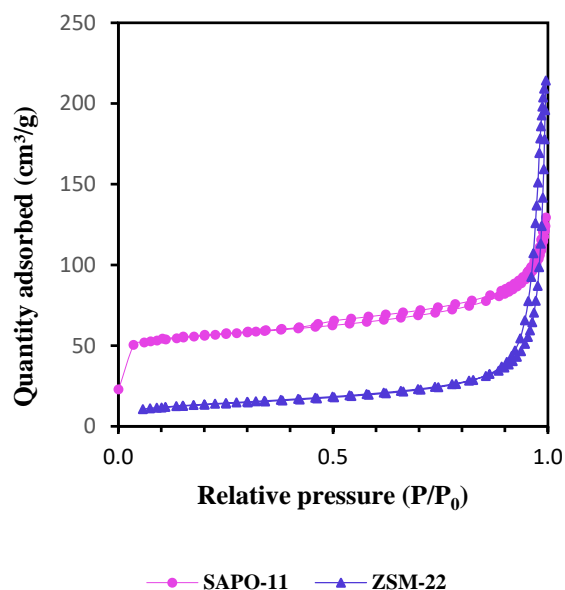


Figure 4.4 N₂ adsorption isotherms of SAPO-11 and ZSM-22

4.1.2 X-ray diffraction (XRD)

The XRD analysis was realized for the calcined catalysts: HZSM-5(30), MoP (10 %)/HZSM-5(30), H β , MoP (10 %)/H β , HY and MoP (10 %)/HY. The results are presented in the [Figure 4.5-Figure 4.7](#). In all three diffractograms it can be seen that the catalysts containing MoP follow the same pattern of their support. In the [Figure 4.5](#), the HZSM-5 registered the peak with the highest intensity at 2θ of 7.8, followed by other large peaks at 2θ of 8.8, 13.2, 14, 14.9, 23, 23, 30,45[39, 45, 90]. The same peaks were detected for the MoP (10 %)/HZSM-5(30), but with a lower intensity compared to its support. According to CAMBRIDGE [72], the peak intensity is proportional with the frequency of the crystalline phase present in the structure of the sample. Thus, the reduced intensity of the peaks for MoP (10 %)/HZSM-5(30) is caused by a loss of crystallinity and this could be due to the modification of the HZSM-5 structure induced by the MoP loading. The absence of the MoP peaks in the diffractogram could be due to the small MoP crystallites that could not be identified by the x-ray diffraction. This indicates that the MoP oxides were highly dispersed on the support[45]. The same discourse can be applied for the other two groups. However, in case of H β and MoP (10 %)/H β , their diffractograms ([Figure 4.6](#)) show that the intensity of the peaks is not so influenced by the MoP loading as in case of HZSM-5 and HY.

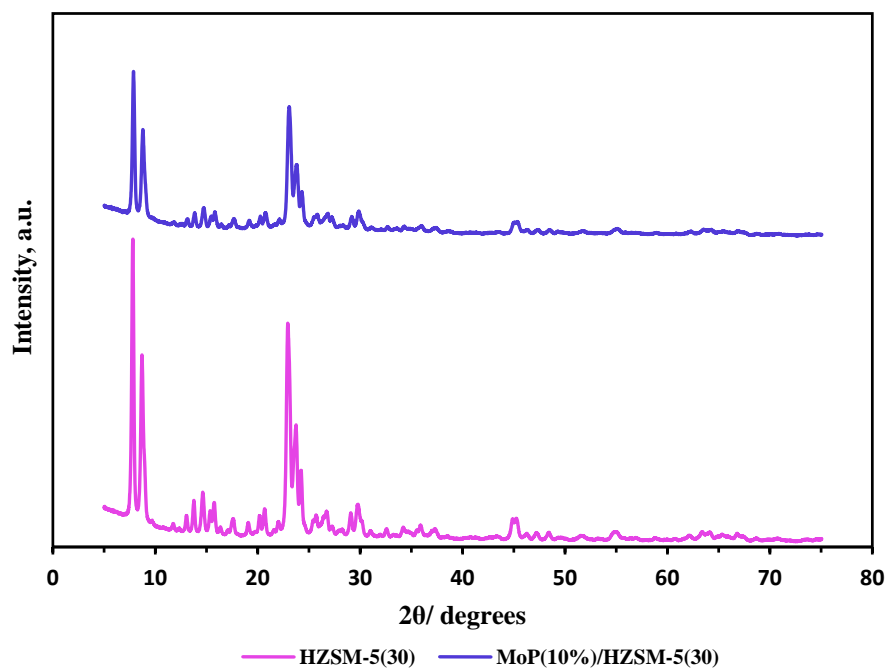


Figure 4.5 The diffractograms of HZSM-5(30) and MoP(10%)/HZSM-5(30)

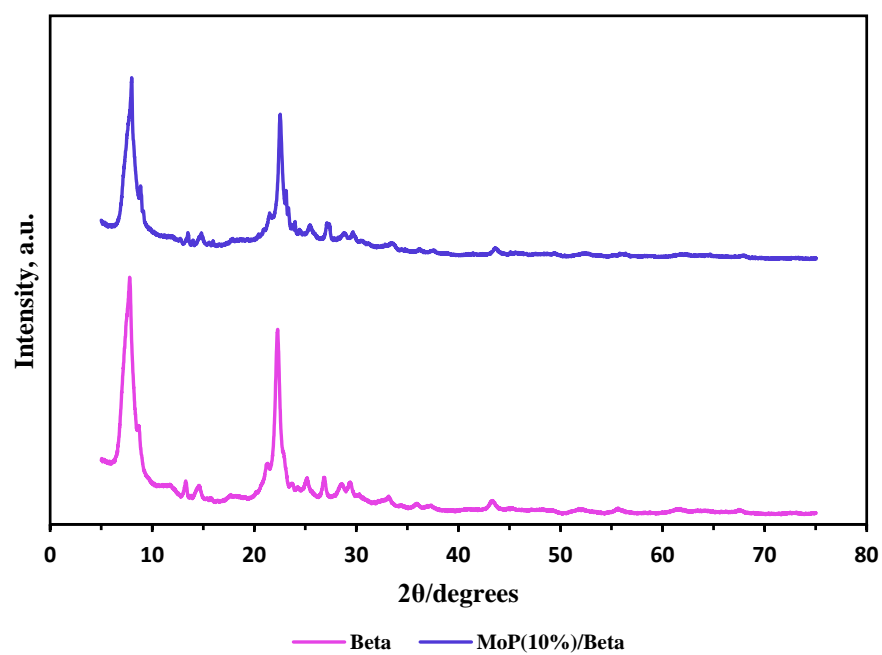


Figure 4.6 The diffractograms of Hβ and MoP(10%)/Hβ

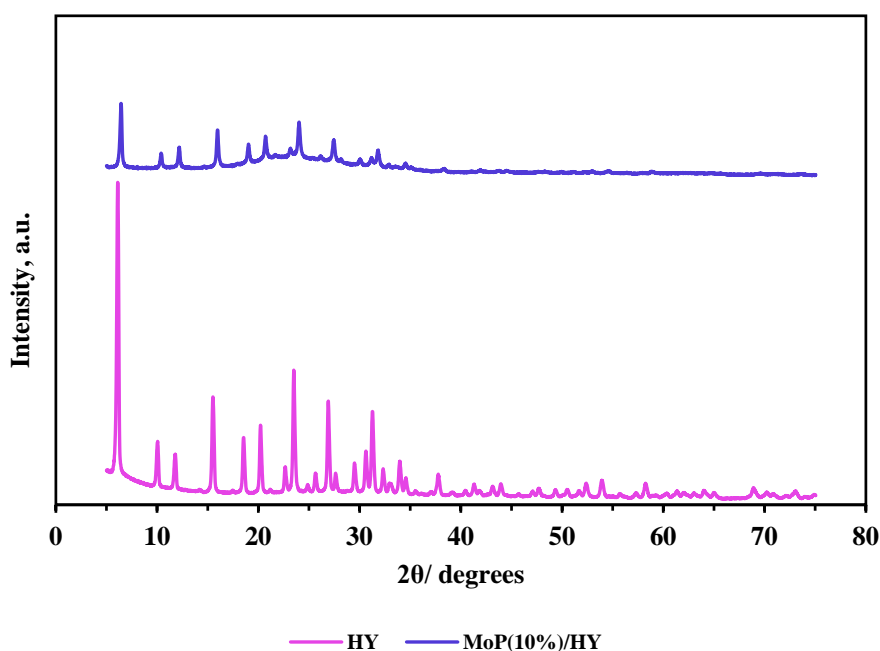


Figure 4.7 The diffractograms of HY and MoP(10%)/HY

4.1.3 Temperature Programmed Desorption Technique (NH₃-TPD)

The acidity of the catalyst is very important for the cracking, dehydration, decarbonylation reactions. As lignin contains a large amount of oxygen, the deoxygenation is a major problem and a catalyst with a proper acidity is required and especially a catalyst with Brønsted acid sites as they promote a good dehydration compared to Lewis acid sites [40, 91]. Zeolites are acidic materials widely used in the petrochemistry plant; thus, different zeolites were also decided to be tested in this project, but in order to compare their activity, it is very important to know the density of their acidic sites and strength. NH₃-TPD technique was applied in order to obtain these characteristics. As it was already mentioned, the weakness of this technique is that it does not distinguish between the Brønsted and Lewis acid sites. However, according to different studies, the Brønsted acid sites dominate in the zeolitic material when the negative charge of the [AlO₄]⁻ is neutralized by protonating it. If replacing the H⁺ with other cations like different complexes containing transition metals, the Lewis sites are generated [39, 92, 93]. According to this, the zeolites used in this project are mostly characterized by Brønsted acid sites as they are described as cation type - H. The results for the HZSM-5(30), HY and Hβ are presented in the Figure 4.8. According to the intensity of the first peak, all three catalysts manifest a high density of the weak acid sites and a less intense peak for the medium-strength acid sites. It was already mentioned that the zeolites can be described by different pore size, channels and cages. Accordingly, Hunger, Heuchel [94] analyzed the density of the acidic sites, moreover, which construction of the zeolite is prone to a higher density of the acidic sites and how strong are those sites. In case of HY, they found that the protons prefer the oxygen positioned in the supercage and sodalite and based on the energy of desorption, the OH groups from the supercage are described by a higher acidity compared with the ones from the sodalite. Considering this, it can be admitted that the first peak of HY positioned at 160 °C was generated based on the acid sites located on the sodalite and the second peak detected at 370 °C resulted based on the sites from the supercage. Hunger,

Heuchel [94] also analyzed the HZSM-5 with Si/Al ratio of 15 and 28 and found that the protons do not have structural preferences, so the OH groups are quite uniformly distributed in the channels of the HZSM-5, moreover, the acidity is equally distributed. According to this, the second peak could be associated to the strong Brønsted acid sites[39]. The first peak positioned at low temperature highlights the presence of weak acid sites or even the adsorbed ammonia through hydrogen bonds[39]. According to Bi, Lei [39], the same thing can be said about H β . The only difference is that the second peak is not well defined, it looks more like a tail from the first peak. However, the strong acid sites can be considered between 300 and 400 °C.

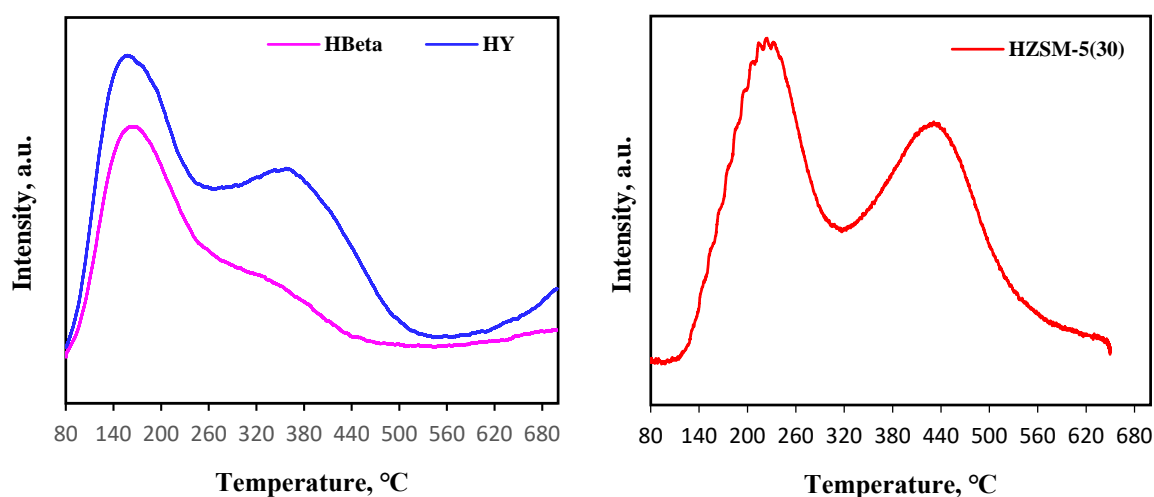


Figure 4.8 The NH₃-TPD results for H β , HY and HZSM-5(30)

4.1.4 Thermal Gravimetric Analysis-Mass Spectrometry

The TG analysis was realized for all spent catalysts in order to see how much coke was deposited. Based on this, the amount of char was obtained by subtracting the amount of coke from the total amount of the solid formed in the FP-CU. Almost all the results were categorized in order to see the effect of Si/Al, pore size and temperature on coke formation. In the [Figure 4.9](#) the effect Si/Al ratio of HZSM-5 is presented. As it can be seen, each curve is characterized by 2 steps of weight loss. The first step can be associated with the release of moisture or other adsorbed species that occurs at low temperature, in this case at a temperature lower than 200 °C. This can be supported by the water peak generated by the MS ([Figure 8.7](#), Appendix). The second one is very large and it highlights the burning of the coke. As it can be seen in the [Figure 4.9](#), the temperature range for this step is between 400 and 700 °C. According to Zhang, Shao [95], this range of weight loss is specific for burning of hard coke. The DSC and the CO₂ ion current graphs ([Figure 4.10](#)) are also presented in order to show the presence of carbon on the catalysts. A small peak of water ([Figure 8.7](#), Appendix) was also observed on this range of temperature that could be generated from the hydrogen present in the coke. If analyzing the effect of Si/Al ratio on the coke formation, it can be seen that more acidic sites that means lower Si/Al ratio promotes the coke formation. According to Yu, Li [38], high alumina loading results in a higher density of the acidic sites. This means that the chemisorbed aromatic molecules will be closer and so the bimolecular coke-forming reactions can be triggered.

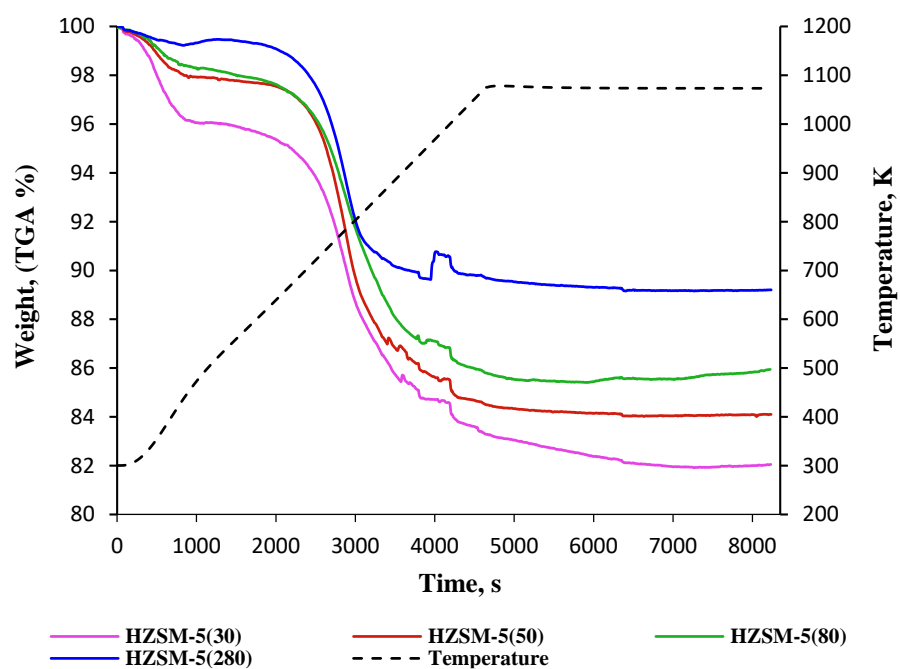


Figure 4.9 Weight loss of the spent HZSM-5 with Si/Al=30, 50, 80 and 280 (FP-CU at 550 °C, C:L=1, N₂ flow=40 mL/min)

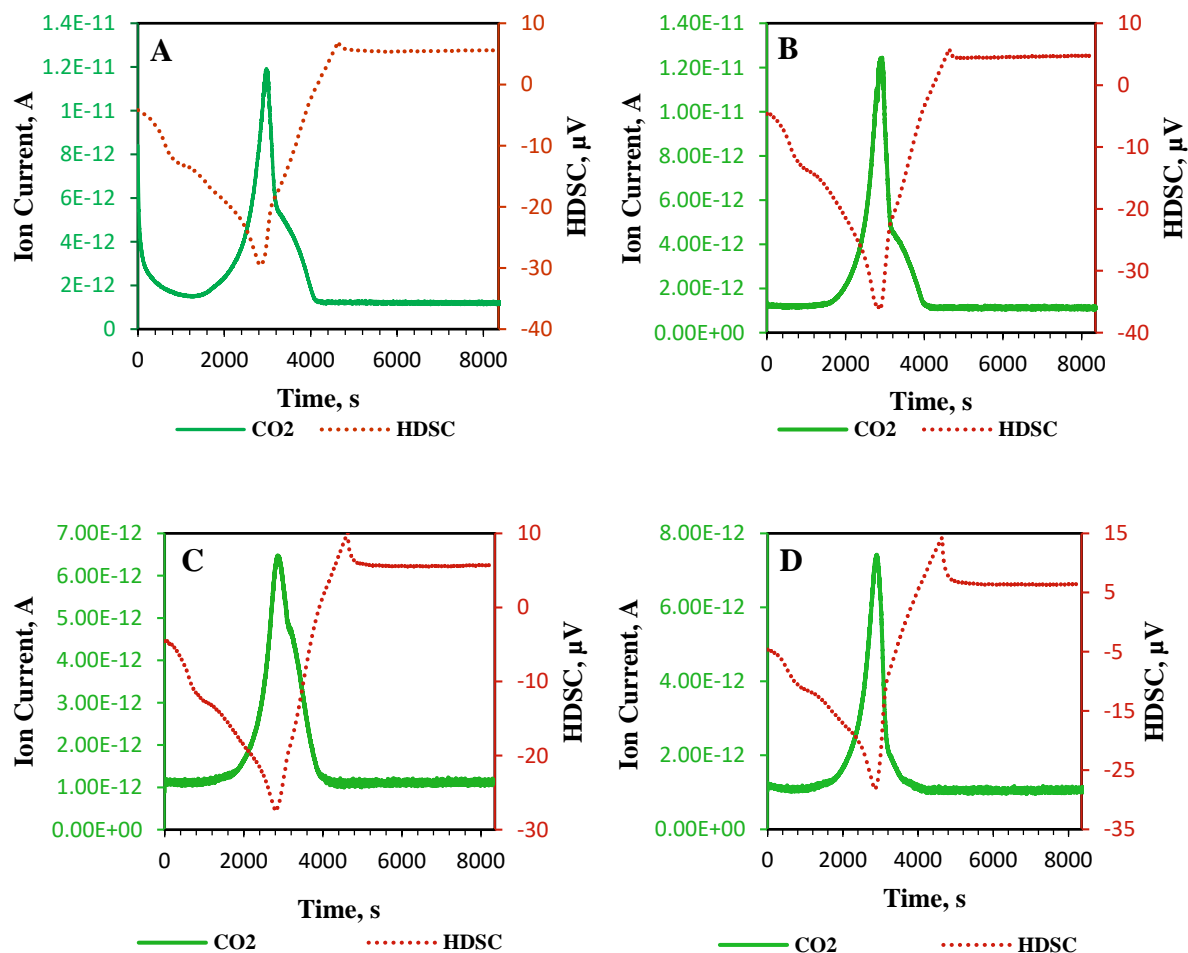


Figure 4.10 The CO₂ ion current (MS) and HDSC of HZSM-5(30) (A), HZSM-5 (50) (B), HZSM-5 (80) (C) and HZSM-5 (280) (D) (FP-CU at 550 °C, C:L=1, N₂ flow=40 mL/min)

The influence of pore size on the coke formation is presented in the [Figure 4.11](#). The same two steps can be seen in the case of different structures of zeolites. The HZSM-5(30) inhibits the coke formation compared to H β and HY. This is because of the space inside the pore that is smaller in case of the first two catalysts. The H β has a smaller pore compared to HY, so less coke is present on the spent catalyst[38, 96]. The HY records the highest weight loss and this is also because of the cages present in its structure. Moreover, as it was mentioned in the TPD results, the OH groups are concentrated in the cages of HY and due to the high density of the strong acidic sites, the coke is generated faster and in higher quantities due to enough space. The DSC and CO₂ ion current are shown in the [Figure 4.12](#). As it can be seen, more CO₂ is produced in the case of HY. Besides CO₂ water was also released at two different temperatures ([Figure 8.8](#), Appendix). The first peak simply highlights the water evaporated and the second one the generated water from hydrogen.

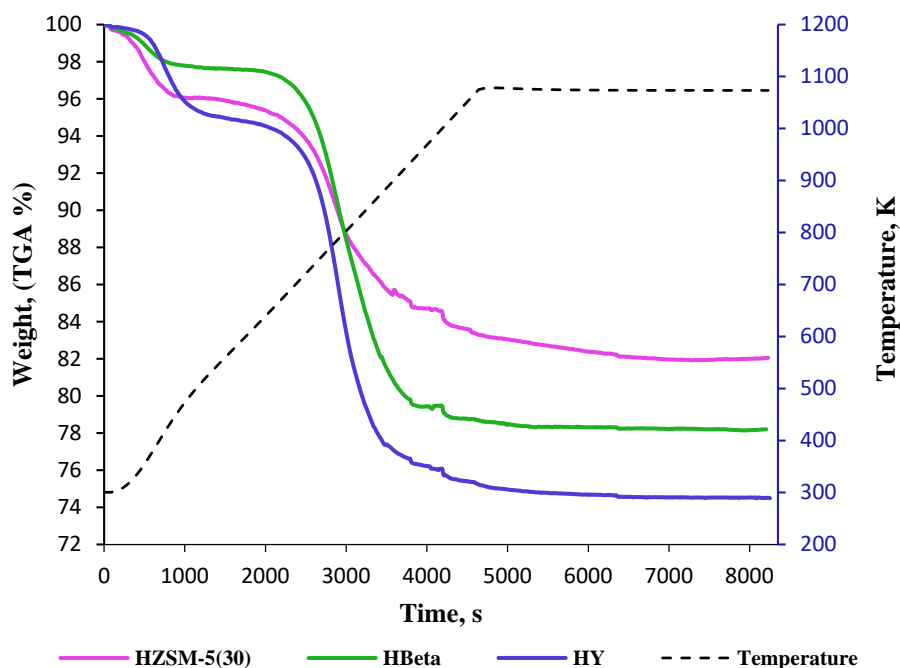


Figure 4.11 Weight loss of the spent HZSM-5(30), H β and HY(FP-CU at 550 °C, C:L=1, N₂ flow=40 mL/min)

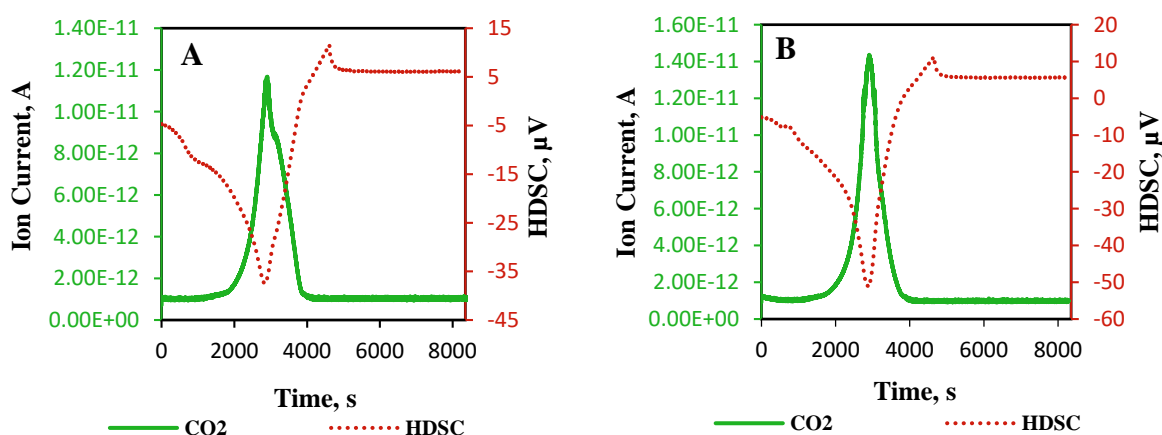


Figure 4.12 The CO₂ ion current (MS) and HDSC of H β (A) and HY (B) (FP-CU at 550 °C, C:L=1, N₂ flow=40 mL/min)

According to Arrhenius equation, the reaction rate is increased by increasing the temperature and, because the coke formation is also a chemical reaction, it means that the amount generated is proportional with the temperature. However, Henrique S. Cerqueira a [97] tested the conversion of m-xylene on USHY zeolite at two different temperatures and found that at lower temperature a higher amount of coke was deposited in the pore structure. The explanation referred to the coke precursors that are easier to be retained in the pore structure at lower temperature. This is because of their low volatility at reduced temperature. When the temperature is increased, the coke molecules are

retained because of their steric blockage. The same explanation could be applied for the results obtained in this project. It can be seen in the [Figure 4.13](#) that the coke content is expanded at lower temperature. Moreover, the coke formed at 450 °C starts to be eliminated at a lower temperature and this is because of the coke structure. Henrique S. Cerqueira a [97] found that the coke formed at low temperature is mostly consisted of methyl substituted aromatic compounds with three rings per molecule and the coke formed at elevated temperature is a methyl pyrenic material. It is less difficult to remove the polyaromatic compounds with fewer rings per molecule than the pyrenic compounds. The CO₂ ion current and HDSC can be seen in the [Figure 4.14](#) and [Figure 4.10 \(A\)](#) and the H₂O ion current in ([Figure 8.9](#), Appendix).

The TGA and MS results for the rest of the spent catalysts are presented in the [Figure 8.10- Figure 8.15](#), Appendix). The coke amount was calculated for each spent catalyst and it is presented in the discussion of fixed bed reactor experiments.

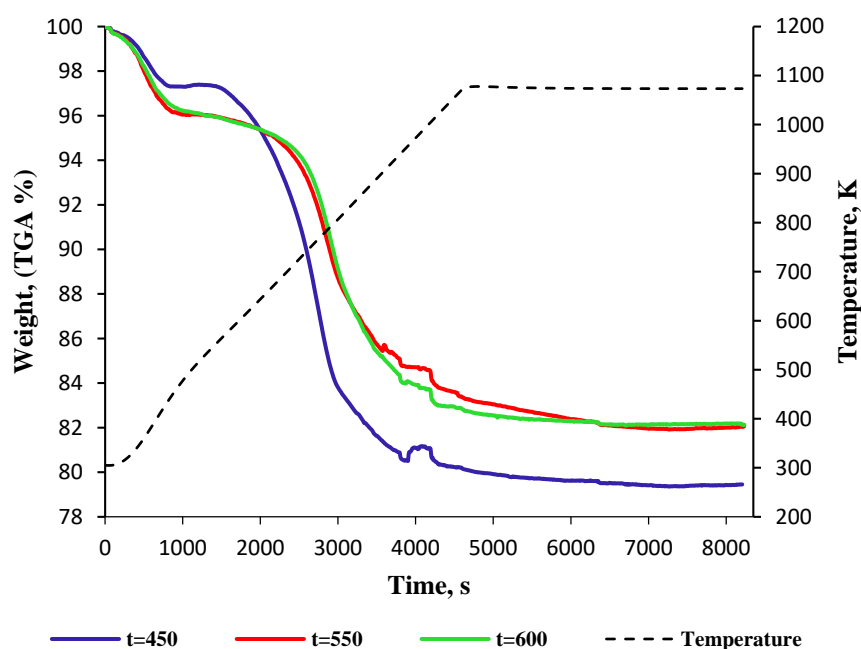


Figure 4.13 Weight loss of the spent HZSM-5(30) involved in the FP-CU at 450, 550 and 600 °C (C:L=1, N₂ flow=40 mL/min)

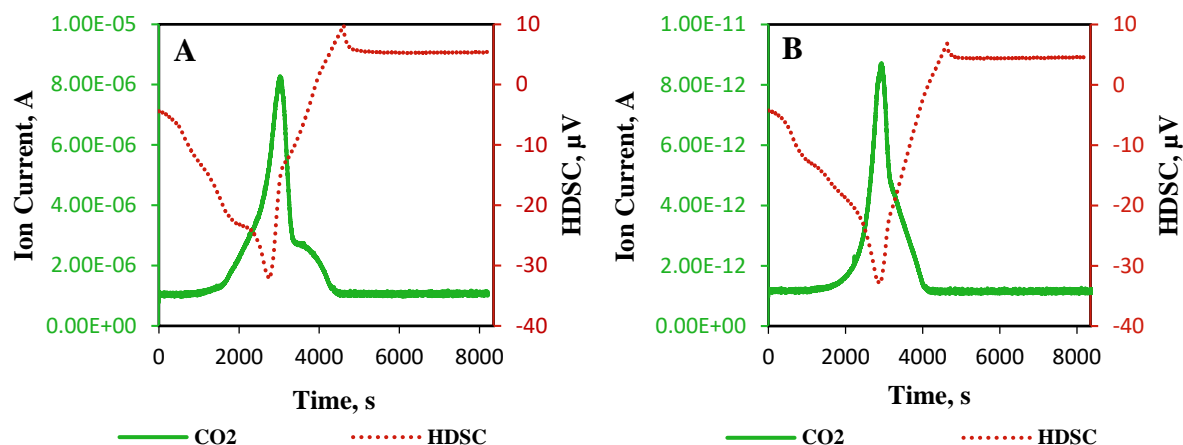


Figure 4.14 The CO₂ ion current (MS) and HDSC of HZSM-5 involved in FP-CU at 450 (A) and 600 °C (B) (C:L=1, N₂ flow=40 mL/min)

4.2 Activity

4.2.1 Py-GC/MS

Different catalysts and pyrolytic parameters were already tested during the specialization project. However, many of the catalysts and parameters were repeated due to the maintenance of the instrument that influenced in a positive way the peak area. The maintenance was necessary due to the carbon deposit and other metal impurities on the reactor. It was replaced with a new one, thus the resulted peaks looked more symmetric with a minimized tail.

Two main processes were developed in the micropyrolyzer: fast pyrolysis (FP) and the fast pyrolysis coupled with the catalytic upgrading (FP-CU). The first one refers to the pyrolysis of lignin without any catalysts and the second one to the pyrolysis of lignin followed by a catalytic upgrading of the generated volatiles. In order to accomplish the FP-CU in the same reactor, the lignin and the catalyst are separated by a layer of quartz wool. In literature this process is also called in-situ catalytic upgrading as the lignin and the catalyst are exposed to the same reaction conditions. The FP-CU was chosen due to the better yield of the oil compounds compared to the catalytic fast pyrolysis (CFP) where the lignin and the catalyst are mixed[22]. In order to compare the results generated by the Py-GC/MS, the weight of lignin was kept constant for all experiments (0.5 mg). The catalyst to lignin ratio of 3 was used for the FP-CU as it showed better yield for oil compounds[22]. In this paragraph the notion of yield refers to the peak area of the compound divided by the weight of lignin and 10^9 (to avoid large numbers). The names of the organic groups are abbreviated and full names are given in the Table 4.2. The structure of Ph, PhA, MAH, DAH and PAH compounds obtained at different temperature in FP and in FP-CU on HZSM-5(30), H β and HY Table 8.11, Appendix. In the Table 4.3 are presented the notations used for carbon number analysis of each organic group.

Abbreviated name	Full name	Abbreviated name	Full name
Ph	Phenolic compounds	Alc	Alcohols
PhA	Phenol alkoxy compounds	Cyc-ene	Cycloalkene
AA	Aromatic alkoxy compounds	Cyc-ane	Cycloalkane
MAH	Mono-aromatic hydrocarbons (one ring)	Cyc-dien	Cycloalkadiene
DAH	Di-aromatic hydrocarbons (two rings)	Fur	Furanic compounds
PAH	Poly-aromatic hydrocarbons (three rings)	Alkan	Alkanes
Mcatec	Methyl catecholic compounds	Alken	Alkenes
Ket	Ketones	Alkad	Alkadienes
		Alkyn	Alkynes
		Ald	Aldehydes
		Cell	Cellulosic compounds
		Cyc-ether	Cycloether
		Unk	Unknown

Table 4.2 The groups generated according to the resulted products

C _n	[No apostrophe-linear organic molecules]	n- no of carbon atoms per molecule
C' _n	['-organic compounds with one ring per molecule]	
C'' _n	["-organic compounds with two rings per molecule]	
C''' _n	[''' – organic compounds with three rings per molecule]	

Table 4.3 The notations for the liquid products analysis

4.2.1.1 Temperature analysis (FP)

The lignin was tested at five different temperatures: 500, 550, 600, 650 and 700 °C. This step was proposed in order to check the value that gives a better yield and a proper products distribution. The last term refers to the products with fewer oxygen atoms per molecule as this is the aim followed herein. The results of these analyses are presented in the [Figure 4.15](#). As it can be seen, the total yield is decreasing when the temperature is increased. This is due to a deeper cracking of the side chains of PhA and Ph compounds generating more gas products. Zhao, Xiuwen [98] also analyzed two types of lignin and investigated the temperature effect on the yield of oil compounds. Each type gave the

highest yield at different temperatures. That makes sense because the lignin structure is variable and depends on the extraction methods and vegetal species. When increasing the temperature, the PhA content is decreased due to the alkoxy groups which are very sensitive at elevated conditions and can be eliminated as CO, CO₂ and other gas products like paraffins and olefins. By partially cracking the sidechains or eliminating them, more Ph compounds result, as well as MCatec compounds. Also, it can be seen that at high temperatures more alkenes and partially saturated cyclic compounds are formed.

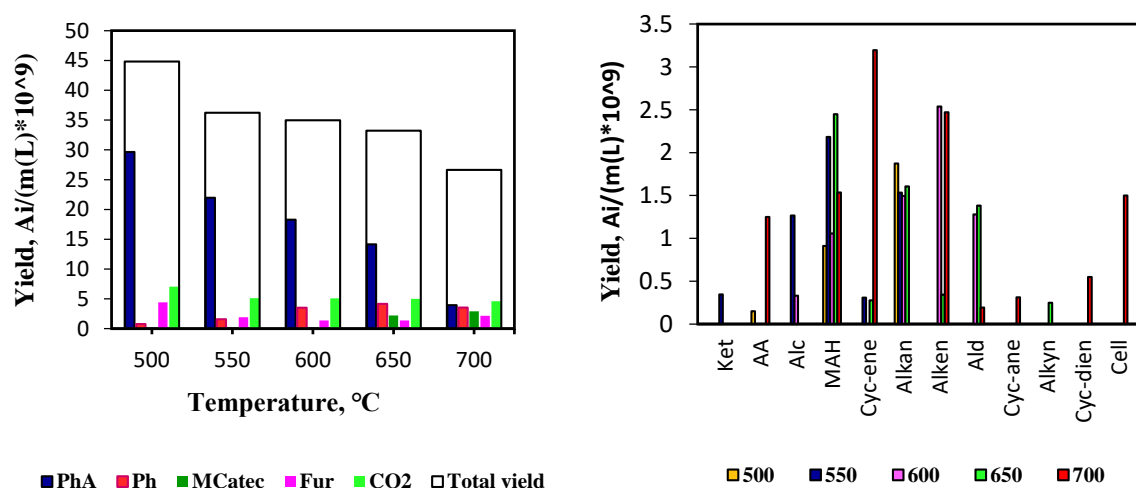


Figure 4.15 The products distributions obtained from lignin in the FP at 500, 550, 600, 650 and 700 °C. Process was realized in a Py-GC/MS at helium flowrate of 2 mL/min.

In the [Figure 4.16](#) the variation of the yield with the temperature of the main PhA and Ph compounds found at different temperatures is presented. It can be seen that phenol, 2-methoxy-, creosol, apocynin and 2-methoxy-4-vinylphenol are generated in high quantities at 500 °C. By increasing the temperature, they are converted into phenolic compounds. Phenol, 2-methyl- could simply result from phenol, 2-methoxy- by substituting the methoxy group with the methyl group. The phenol is also generated in large content and this is because it can result from all PhA compounds, depending on the bond strength of the substituents of each compound. Phenol, 2,4-dimethyl- is also characterized by a large yield, especially at 650 °C. It could derive from all PhA compounds that are substituted in the para position. By replacing the substituent with the methyl group and subtracting the methoxy group, the phenolic compound can be formed. A more detailed pathway of lignin is presented in chapter 5. For the further experiments, the temperature of 550 °C was selected for testing the catalysts. It was selected instead of 500 °C because of higher yield of MAH and Ph compounds. A higher temperature is not wanted as more gas and coke can be generated.

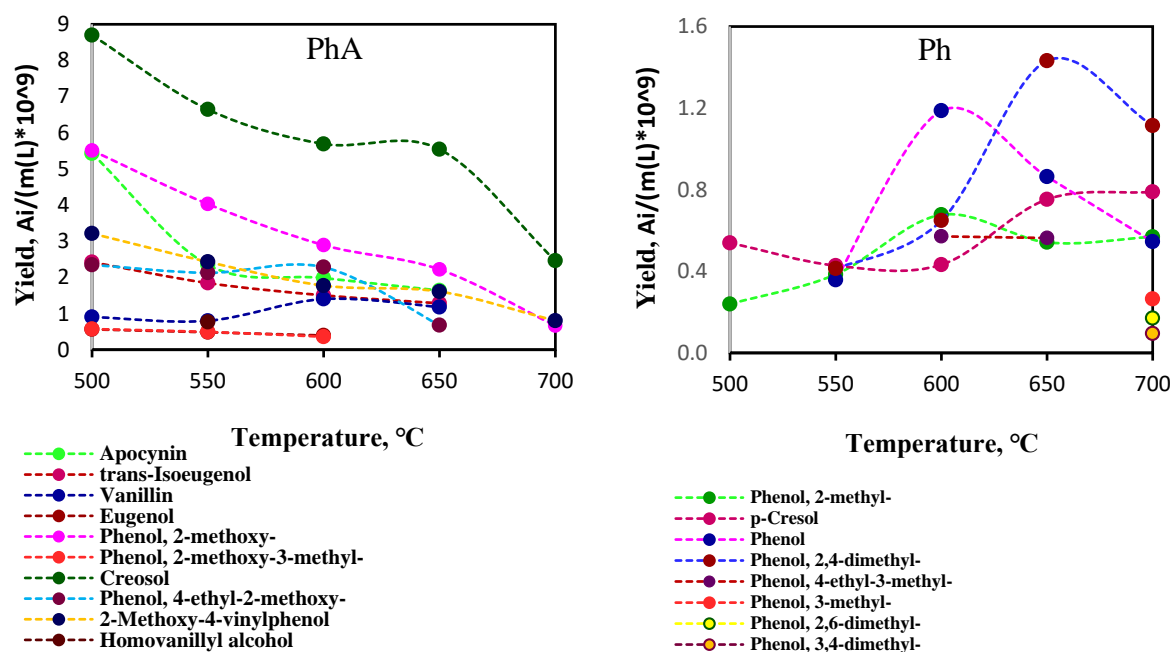


Figure 4.16 The yield variation with the temperature of the main PhA and Ph compounds. FP was realized in a Py-GC/MS at helium flowrate of 2 mL/min.

4.2.1.2 Fast pyrolysis-upgrading of volatiles on metal-non-metal oxides supported on γ -Al₂O₃

The FP-CU on MoXP (X=Co, Cu, Ni, Fe)/ γ -Al₂O₃ catalysts was realized in order to see how the acidic sites act on the oxygenated compounds generated in the pyrolytic step. The alumina support was tested separately as it also participates to the reaction due to its Lewis acid sites[99]. The products distribution of all catalytic tests, as well as of only lignin, are presented in the [Figure 4.17](#) and [Figure 4.18](#). It can be seen that alumina produces a very high content of CO₂ compared to other catalysts. This could be because of the high acidity of alumina. The alumina used in this project is also called PURALOX and it is characterized by a small particle size and a high surface area respectively. By exposing the volatiles to a high acidity, moreover, to the strong Lewis acid sites, a broad cracking of the molecules, especially of the side chains might occur, generating gas. According to Klein and Virk [100], the CO and CH₄ dominate in the gas products. Since the CO could not be detected, it cannot be said that CO₂ is produced in large quantities. However, the Boudouard and water-gas shift reactions could also occur, generating CO₂ from CO and/or water. If analyzing the PhA, it can be seen that the content is very low compared to lignin and more MAH, DAH and PAH are generated. When impregnating the MoP oxides on alumina, the PhA disappears and more Ph compounds are generated, as well as MAH, DAH, Fur and Alc compounds. The MAH group is dominated by the BTX compounds, while the DAH by naphthalenes. This is available for all MoXP catalysts. Chary, Bhaskar [101] studied the acidity of MoO₃ supported on Nb₂O₅. They found from ammonia-TPD analysis that by increasing the molybdenum trioxide loading, the density of the strong acid sites also increased. Sundli [86] did the XRD analyses of the MoXP catalysts and MoO₃ manifested the highest peaks for all calcined and unsupported catalysts. The MoO₃ can be also detected, especially in MoP catalysts due to its light-green color. Based on all mentioned, the MoP can be considered a potential catalyst for the conversion of PhA into Ph, MAH and

DAH. The role of phosphorus oxides is unclear, but it was studied in different papers together with vanadium oxides. According to Spivey [102], VP oxides can exhibit Lewis acid sites of low acidity when they are promoted with Nb. Thus, phosphorus oxide could also participate with its acidic sites, but in a lower proportion.

When adding Co oxide to the MoP, the total yield increased. Ma, Custodis [103] investigated MoO_3 and Co_3O_4 separately and a high yield of liquid was obtained when using Co oxide. However, Sundli [86] detected a cobalt phosphate instead of Co_3O_4 in the diffractogram of the unsupported MoCoP. When analyzing the products distribution, a high yield of Ph is obtained. Ph compounds are formed from PhA by subtracting the methoxy group and modification of the side chain from para position. This can be supported by the high yield of CO_2 and Cyc-ether that is consisted of ethylene oxide. It results from the para position chain which contains more carbon atoms and oxygen. The MAH, DAH and PAH are also present in this case. However, if comparing with the MoP, the MoCoP recorded more DAH and PAH. This could be related to the more acidic sites of the cobalt species which promoted the coke formation.

The addition of Cu oxide to the MoP increased a bit the total yield compared to the lignin, alumina and MoP. The PhA compounds were produced in lower quantity compared to the MoCoP and more CO_2 and acetaldehyde (Ald) were produced. The same as ethylene oxide, the acetaldehyde could result from the side chain from para position of PhA. Besides PhA, the Ph compounds also decreased that could be due to the active sites of Cu species. A deeper cracking could result in more gas and solid. According to Ma, Custodis [103], the solid yield is almost equal to the liquid yield, so it is possible that active sites of Cu species could promote the formation of the solid phase.

The impregnation of Ni together with MoP on alumina recorded a higher yield in the FP-CU process compared to the lignin, alumina, MoP and MoCuP. Chen, Liu [32] studied the activity of nano-NiO at 550 °C and found that with increasing of NiO loading more bio-oil and gas are generated by suppressing the formation of bio-char. The obtained gas was mostly composed of CO, CO_2 and CH_4 . According to Zheng, Chen [44] these gases are probably a result of cracking the CHO, COOH and CH_3 groups. In the Figure 4.18 it can be seen that the alkadiene content is also high. It could result from the side chains of PhA, Ph or from furanic compounds. The furanic compounds are produced in lower quantity compared to the MoP, so they could be converted to alkadienes. As an example, 2-methylfuran could produce 1,4-pentadiene.

The addition of Fe oxide to the MoP resulted in the highest yield compared to the previous catalysts and lignin, but still a large yield of PhA remained unconverted. Moreover, it recorded the lowest yield of MAH if comparing to the other MoXP catalysts. The high yield of ketones could be associated to the cracking reaction of carbonyl group of apocynin (the structure is presented in the table A4.2, appendix). MoP/ $\gamma\text{-Al}_2\text{O}_3$ was selected for further investigation as it converted all the PhA compounds, moreover, it produced a high content of Ph and MAH compounds. In the next subparagraph different loadings of MoP were analyzed.

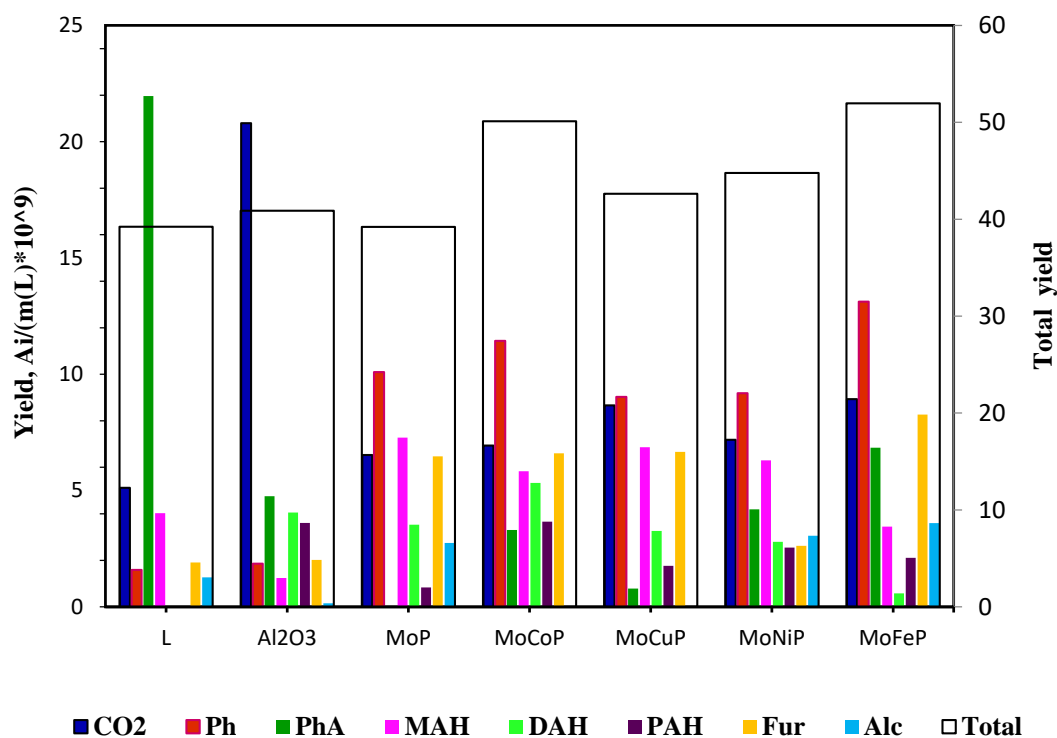


Figure 4.17 The products distribution of FP (L) and FP-CU on γ -Al₂O₃ and MoXP/ γ -Al₂O₃ (X=Co, Cu, Ni or Fe) at 550 °C, Py-GC/MS

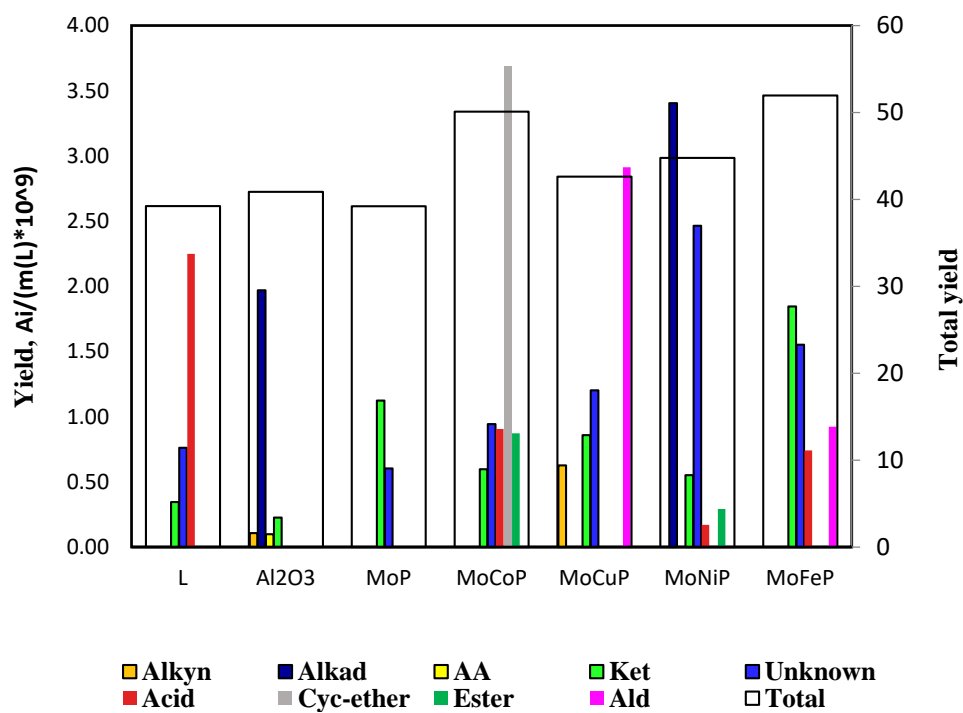


Figure 4.18 The products distribution of FP (L) and FP-CU on γ -Al₂O₃ and MoXP (10 %)/ γ -Al₂O₃ (X=Co, Cu, Ni or Fe) at 550 °C, Py-GC/MS

4.2.1.3 Fast pyrolysis- catalytic upgrading of volatiles on three different loadings of MoP oxides on γ -Al₂O₃

Three different loadings of MoP were tested in order to see the changes in the products distribution. The results are presented in the Figure 4.19. As it can be seen, the MoP with the loading of 10 wt% recorded the highest yield compared to the other two catalysts. The MoP (5 %) generated aromatic hydrocarbons and furanic compounds, but no PhA and Ph. Due to the high content of CO₂ and ethylene oxide (Cyc-ether), probably the PhA and Ph were converted to aromatic hydrocarbons by subtracting the side chains. When analyzing MoP (15 %), the PhA yield is higher compared to one of MAH. This could be caused by a low dispersion of the MoP on alumina surface. Thus, the access of the reactants to the acidic sites is lower and so the PhA compounds could exit the catalyst bed without any conversion. Since the aim of this project is to produce more aromatic hydrocarbon, especially MAH, the MoP (10 %) was selected for testing in the fixed bed reactor.

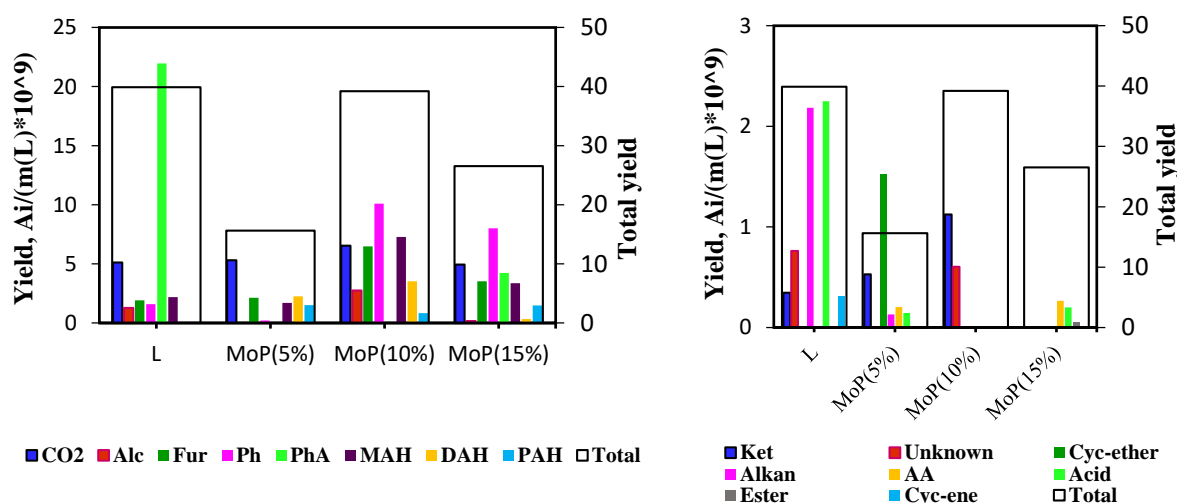


Figure 4.19 The products distribution of FP-CU on MoP (5 %)/ γ -Al₂O₃, MoP (10 %)/ γ -Al₂O₃ and MoP (15 %)/ γ -Al₂O₃ at 550 °C, Py-GC/MS

4.2.1.4 Fast pyrolysis- catalytic upgrading of volatiles on HZSM-22, HZSM-5 (Si/Al=30, 50, 80 and 280), H β , SAPO-11, SAPO-34 and HY

As it was already mentioned in the literature section, the zeolites are very special materials due to their well-defined structure and high acidity. Different researchers investigated their activity in the cracking process of the crude oil and of different types of biomass. In this project the investigation of the effect of the Si/Al ratio of HZSM-5 and different structures on the products distribution was proposed. The results are presented in the Figure 4.20- Figure 4.21. If analyzing first the influence of the Si/Al ratio on the products distribution, it can be seen that the HZSM-5(30) resulted with the highest yield, being dominated by a large content of MAH (BTX) and DAH (naphthalenes). It is also described by a low yield of Ph compounds and what is surprising, the PhA were totally converted in Ph and aromatic hydrocarbons. By increasing the Si/Al ratio, it is obvious that the alumina content is reduced. In this way, the density of the acidic sites is lowered, resulting in a decreasing of the total yield. The HZSM-5(280) is an exception and its increased yield could not be

explained. Lazaridis, Fotopoulos [40] also analysed the effect of Si/Al ratio of ZSM-5 and they found that by decreasing this ratio, the yield is enhanced. However, they also observed that this is available for small C:L ratio. By increasing this ratio, the yield starts to decrease. This can be associated to the retention time of the volatiles in the catalyst bed. If the time is large, it is obviously that side reactions triggered by different carbenium ions will have time to form more coke, thus decreasing the bio-oil yield. When analysing the products distribution, it can be observed that the MAH and DAH dominates for the HZSM-5 with Si/Al ratio of 30, 50 and 80. However, there are PhA and Ph compounds which remained unconverted when alumina content was decreased, especially for the HZSM-5(280). If analysing the figure 59, it can be seen that the content of Ket compounds, mainly consisted of acetone, is quite high for the HZSM-5 with Si/Al ratio of 50, 80 and lower for 280, while for HZSM-5(30) they were not detected. By increasing the alumina content, more sites are generated and thus more PhA are converted to Ph and aromatic hydrocarbons. Based on this the Ket yield might increase due to the cracking of the side chain of more apocynin or even of vanillin, thus recording a maximum at Si/Al=50. At Si/Al ratio of 30, the acidity could be high enough to convert the ketones to other light products.

When comparing the total yield of FP-CU on HZSM-5(30) with the yield of FP of lignin, it can be seen that it is a large dissimilarity. Zhang, Resende [33] also investigated the lignin thermal decomposition in a Py-GC/MS and they also received a large yield of the upgrading step on the HZSM-5(30), especially at the C:L of 3. This is because of the instrument that cannot avoid the condensation of the very unstable intermediates and by forming large molecules, they cannot be analysed by the GC/MS. When using the zeolite, the volatiles are immediately stabilized and more products with low molecular weight can be analysed. Thus, the two yields are not supposed to be discussed based on the Py-GC/MS results. When using a fixed bed reactor, for example, the yield of the gas, liquid and char/coke can be measured and calculated and only after that the yield of FP and FP-CU can be compared. Lazaridis, Fotopoulos [40] studied the FP and FP-CU of lignin in a fixed bed reactor and the total liquid yield recorded in case of FP was higher compared to FP-CU. This makes sense because by deoxygenating of the pyrolytic volatiles, the molecular weight of the bio-oil products is lowered.

The investigation of the structure and pore size of various zeolites was also proposed in this project. As it can be seen in the Figure 4.20-Figure 4.21, the HZSM-22, HZSM-5(30), H β , SAPO-11, SAPO-34 and HY were the decided zeolites to be screened in the Py-GC/MS. If comparing the total yield, the FP-CU of lignin on HZSM-5(30) recorded the highest yield. This is due to its strong Brønsted acid sites distributed uniformly throughout the channels [41, 46, 94], as well as to its 3D 10-ring pores (0.56 x 0.53 nm) that suppress the formation of coke, but enhance the formation of aromatics [38, 104]. However, according to Yu, Li [38], the most of the oxygenated products derived in the FP process are described by a larger molecule size compared to the pore size of HZSM-5. Regarding this aspect, the calculation of the molecule size of the products that resulted in the FP and FP-CU was also realized in this project by using the Materials Studio Software. The name of the products together with their structure and molecule size are presented in the Table 8.11, Appendix. As it can be seen, almost all the aromatic hydrocarbons can exit the zeolite pore on their largest dimension and this highlights the steric effect of ZSM-5 on the reactants which promotes the formation of aromatic hydrocarbons and inhibits the formation of coke. But, if looking at the size of Ph and Mcatc compounds, more than half of them are too large to enter or exit the pore of HZSM-5 and some of the PhA compounds are too large to enter the pore. This information refers also to HZSM-22 (1D-10-ring pore, 0.45 nm x 0.55 nm [61]), SAPO-11 (1D 10-ring pore [64] and typical free apertures: 0.45-

0.60 nm[104]) and SAPO-34 (3D 8-ring pore and maximum free aperture: 0.43 nm[104]). As it can be seen, they even have a smaller size compared to HZSM-5(30), so now the question is how the large molecules fit into the catalyst pore. According to Webster, Drago [105], the pore size of HZSM-5 can be expanded to 7.27 Å at 300 °C and 7.64 Å at 370 °C, thus the molecule can diffuse easily. In addition to this, the intersection of the horizontal 10-ring channels with the vertical zigzag 10-ring channel should be also considered because it offers more space to the formation of larger intermediates and products. Based on Webster, Drago [105] study, the intersection space is increased from 8.17 and 8.88 to 9.08 and 9.09 respectively when it is exposed to high temperature. Considering this, the large molecules formed in that space will be trapped there and this will cause the channel blockage. In addition, the large molecules could also decompose at the surface of the catalyst, especially at the pore opening and the resulted smaller intermediates could proceed with the further conversion inside the pore.

According to the Figure 4.20, the FP-CU on SAPO-34 did not record any aromatic hydrocarbons and this is because of its 8-ring pore which is too small to favour the formation of the aromatics. Based on the Jae, Tompsett [106], this zeolite produces more oxygenates and no aromatic hydrocarbons. If comparing the SAPO-34 results with the FP of lignin, it can be seen that SAPO-34 produces more oxygenated compounds like phenol alkoxy, acids and furans.

The FP-CU on SAPO-11 shows better results compared to SAPO-34, generating more MAH, DAH and Ph compounds. However, if comparing to HZSM-5(30), it does not manifest good activity, even though it is described by a 10-ring pore. According to Lee, Jun [107], the ammonia-TPD of SAPO-11 showed only weak and intermediate-strength acid sites and the pyrolytic products resulted in the CFP of cellulose were dominated by oxygenated products and some hydrocarbons. According to this, the deoxygenation of FP volatiles requires stronger Brønsted acid sites if the aromatic hydrocarbons are wanted to be obtained.

As SAPO-11, HZSM-22 it is also described by a 1D structure with a 10-ring pore, however, its activity is much higher compared to SAPO-11. Wu, Qiu [108] realized the ammonia-TPD of ZSM-22 and found that it is characterized by weak and medium-strength acid sites, but if comparing to SAPO-11, the acid sites of HZSM-22 are stronger due to the higher temperature of the detected peak. Based on this, it can be assumed that the higher yield of MAH and DAH can be associated to the stronger acid sites of the HZSM-22. If comparing the acidity strength of HZSM-22 with the one of HZSM-5(30), it can be seen they are very similar. However, there is a large discrepancy between their activities. This could be due to the much lower surface area of HZSM-22 compared to HZSM-5(30), and to the lower density of acidic sites.

When the influence of the catalyst pore size on products distribution is wanted to be analysed, the set formed of HZSM-5(30), H β and HY is a very convenient option as there is a bigger discrepancy between their pore size. H β is described by a 3D 12-ring pore with a maximum free aperture of 0.8 nm[104] and HY with a 3D 12-ring pore and maximum free aperture of 0.74 nm[61]. HY is also characterized by supercages that record a size of 1.3 nm[61]. According to the Figure 4.20, the yield is decreasing when the pore size is increased. This is due to the larger space offered by the H β and HY which allows the formation of larger molecules. As it can be seen, H β produces more DAH than MAH, as well as a higher yield of PAH compared to HZSM-5(30) and HY. According to Yu, Li [38], HY does not produce many DAH and PAH due to its larger internal pore space that promotes the coke formation. Moreover, the ammonia-TPD of HY recorded a quite high abundance

of the strong acid sites (due to the low Si/Al ratio, Table 8.8, Appendix) and as they are preferentially localized in the sodalite and supercage[94] the coke can be generated very fast. In addition, when the density of the acidic sites is increased, the bimolecular coke-forming reactions are enhanced[38] as the adsorbed species are closer to each other.

A more detailed distribution based on the carbon number of the obtained products was realized for HZSM-22, HZSM-5(30), H β and HY. The results are presented in the Figure 4.22. As it can be seen all the catalysts manifest a high selectivity for the C'6 (benzene), C'7 (toluene) and C'8 (mostly xylenes and some ethylbenzene). The same results were obtained by Zhang, Resende [33] and Lazaridis, Fotopoulos [40] for the HZSM-5. In case of H β and HY, it is expected to see more substituted monoaromatic hydrocarbons as the pore size allows this, however, the results show the opposite. According to Jae, Tompssett [106], the high selectivity for the BTX is related not only to the pore size, but also to the internal pore architecture. The same thing can be said about the zeolites with medium pore size like HZSM-22 and HZSM-5(30). These catalysts are not supposed to manifest so high selectivity for the naphthalene, furthermore, for the naphthalene with sidechains (C''11,12) and PAH (C'''13, 14, 15). But due to the obtained results, it is possible and here the reasons could be also the internal pore construction, the formation of highly substituted MAH, DAH and PAH at the surface, as well as the thermal expansion of the medium pores which can allow the formation of large molecules.

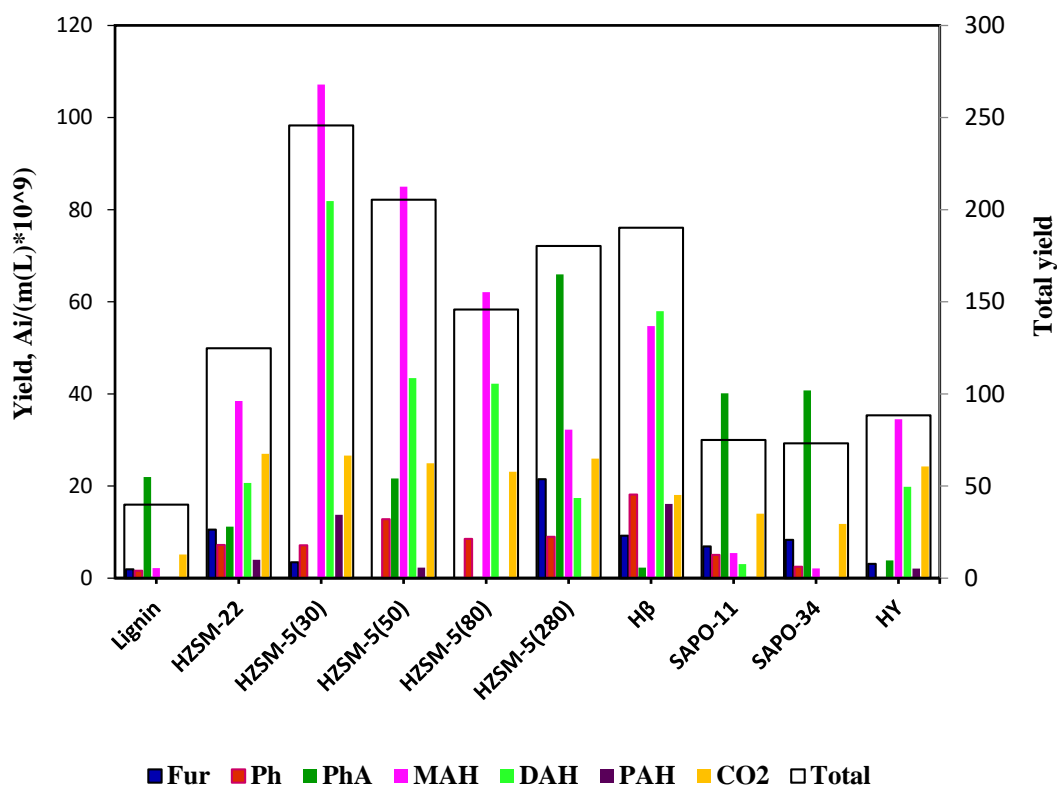


Figure 4.20 The products distribution of FP and FP-CU on HZSM-22, HZSM-5 with Si/Al=30, 50, 80 and 280, H β , SAPO-11, SAPO-34 HY (Py-GC/MS, 550 °C, C:L=3 (0.5 mg (lignin), 1.5 mg (catalyst)))

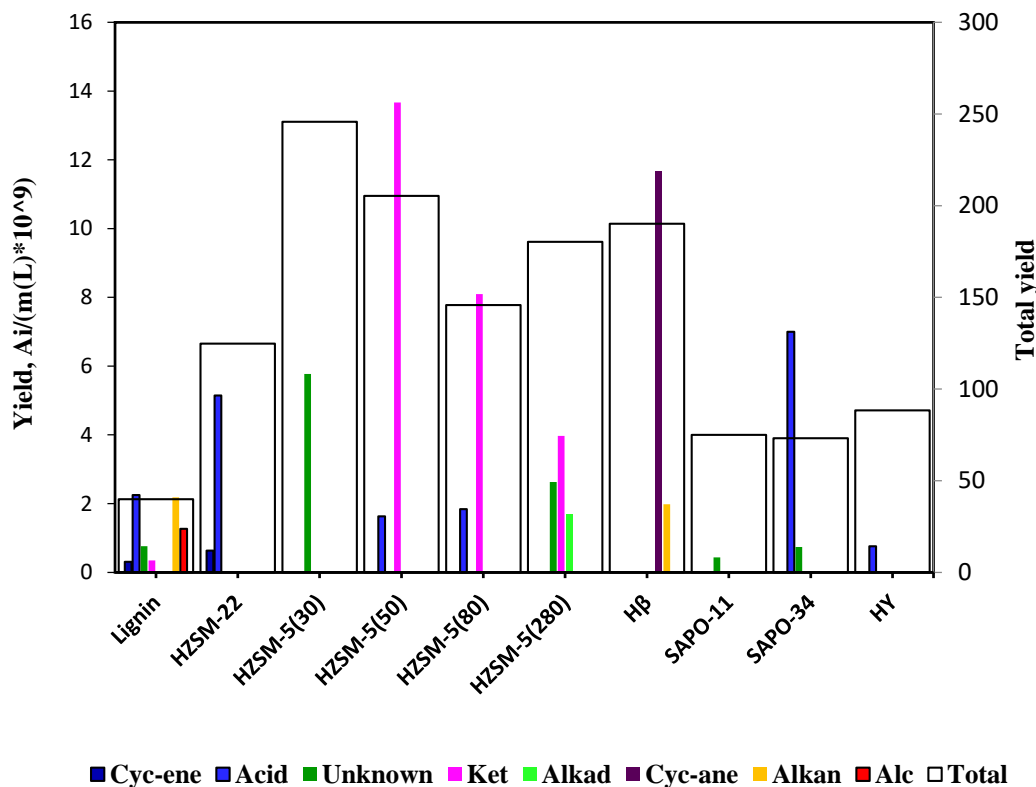


Figure 4.21 The products distribution of FP and FP-CU on HZSM-22, HZSM-5 with Si/Al=30, 50, 80 and 280, H β , SAPO-11, SAPO-34 HY (Py-GC/MS, 550 °C, C:L=3 (0.5 mg (lignin), 1.5 mg (catalyst)))

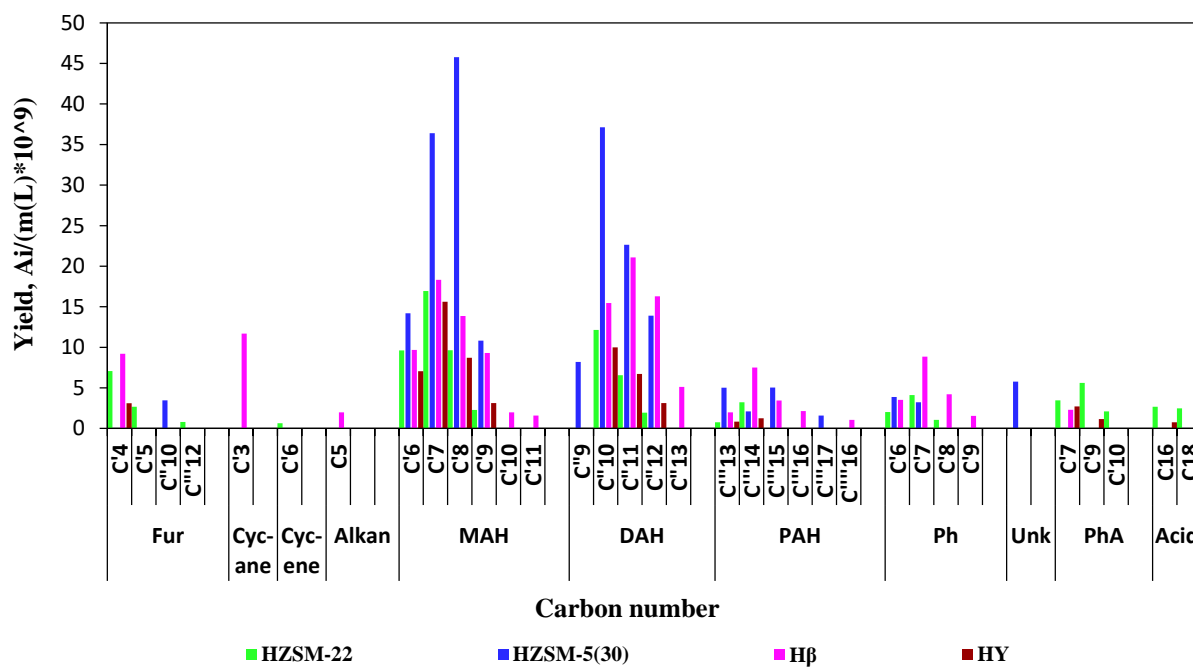


Figure 4.22 The products distribution (carbon number) of FP-CU on HZSM-22, HZSM-5(30), H β and HY (Py-GC/MS, 550 °C, C:L=3 (0.5 mg (lignin), 1.5 mg (catalyst)))

4.2.1.5 Fast pyrolysis-catalytic upgrading of volatiles on MoP(10 %)/HZSM-5(30), NiO(10 %)/HZSM-5(30), MoP(10 %)/H β and MoP(10 %)/HY

The ZSM-5, H β and HY are described by a quite high surface area compared to γ -Al₂O₃. According to this, the impregnation of MoP was decided as it manifested good properties for the deoxygenation of the pyrolytic volatiles. Also NiO was impregnated only on HZSM-5(30) to see any improvement of the products distribution. Based on Chen, Liu [32]' study, the nano-NiO contributed to the increase of the oil yield and minimization of the solid yield. By analysing the results from the Figure 4.23, the total yield is decreased very much for the supported catalysts. In case of NiO, the selectivity to MAH was enhanced, moreover, the PAH hydrocarbons were not detected. This could be due to the lower acidity of the NiO, as well as due to the blocking of the strong sites of HZSM-5(30). If comparing the NiO (10 %)/HZSM-5(30) with the HZSM-5(50) and HZSM-5(80), it can be seen that the effect on products distribution is quite the same. The density of these catalysts is lower compared to HZSM-5(30), thus the bimolecular reactions could be suppressed and so the DAH and PAH could result in a lower content. If comparing MoP (10 %)/HZSM-5(30) with the MoP (10 %)/ γ -Al₂O₃, it can be observed that the yields are almost similar, as well as the products distribution. A large discrepancy is not present even though the surface area of the zeolite is much higher compared to the alumina. This could be due to small pores of HZSM-5 that do not allow a high loading of the MoP. Based on the XRD results, no peaks were detected for MoP oxides which means that it could be dispersed very well. However, the BET results showed a significant decrease of the surface area. This could happen due to the blocking of the pores. The loading of the MoP was also tried on H β and HY as they are characterized by larger pores. However, based on the results from Figure 4.24, the yields were really affected. In case of H β , the products distribution was maintained which means that the activity was reduced by lowering the density of the strong acidic sites. In case of HY the distribution was significantly changed as the oxygenated compounds dominate. This, as in case of HZSM-5(30), could happen due to the blockage of the pores as the surface area of HY (Table 4.1) was also significantly reduced by impregnation of MoP.

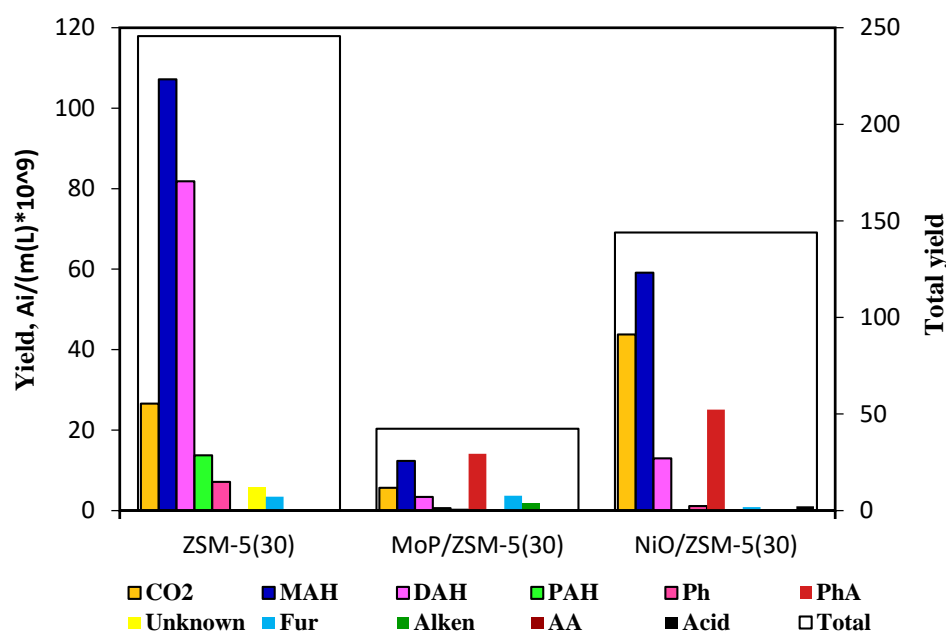


Figure 4.23 The products distribution of FP-CU on MoP(10%)/HZSM-5(30) and NiO(10 %)/HZSM-5(30) (Py-GC/MS, 550 °C, C:L=3 (0.5 mg (lignin), 1.5 mg (catalyst)))

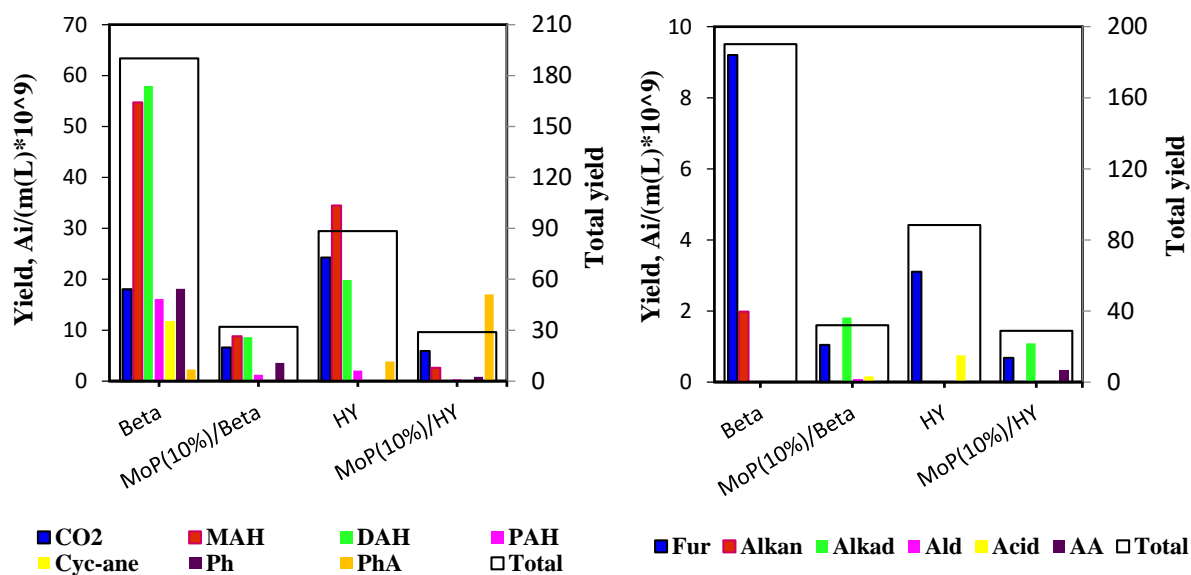


Figure 4.24 The products distribution of FP-CU on MoP (10 %)/H β and MoP (10 %)/HY (Py-GC/MS, 550 °C, C:L=3 (0.5 mg (lignin), 1.5 mg (catalyst)))

4.2.2 Fixed bed reactor

The Py-GC/MS is a very interesting and convenient instrument when a fast screening of different catalysts and organic materials at various temperatures is wanted. However, it is limited as it gives more a qualitative analysis of the final products rather than a quantitative one. According to this, most of the micropyrolyzer experiments were realized in the fixed bed reactor in order to record the gas, liquid and solid yields. The yield of all products was calculated based on the equation 12:

$$\text{Yield}_i(\text{wt } \%) = \frac{m_i}{m_{\text{lignin}}} \cdot 100\% \quad (42)$$

Where m_i is the weight of component i and m_{lignin} is the weight of the lignin used in the FP and FP-CU.

The analysis of the liquid was realized based on the carbon number and number of rings per molecule. The notations are presented in the [Table 4.4](#).

Cn	[No apostrophe-linear organic molecules]	n- no of carbon atoms per molecule
C'n	['-organic compounds with one ring per molecule]	
C''n	["-organic compounds with two rings per molecule]	
C'''n	[''' – organic compounds with three rings per molecule]	

Table 4.4 The notations for the liquid products analysis

The gaseous hydrocarbons were also categorized and the notations are presented in the [Table 4.5](#).

C2	[Ethane and Ethylene]
C3	[Propane and Propene]
C4	[Butane-n]
C5	[Pentane-n]
C6	[Benzene]

Table 4.5 The notations for the gas products analysis

4.2.2.1 Temperature analysis of the FP-CU process on HZSM-5(30)

The FP-CU on HZSM-5(30) was realized at three different temperatures in order to see its effect on the proportion of the three main products: gas, liquid and solid. According to the results presented in the [Figure 4.25 \(A\)](#), by increasing the temperature from 450 to 550 °C, the liquid yield is almost doubled and the gas yield is increased. This means that a higher temperature favours a deeper cracking of the lignin linkages and side chains in the FP bed, proceeded by a stabilization of the oxygenated volatiles in the catalyst bed. When increasing the temperature up to 600 °C, the yield of the liquid was decreased, while the gas yield increased. The same effect of temperature on the liquid was also detected in the Py-GC/MS. This makes sense as the pyrolysis process is based on two main parameters: residence time and temperature. When the temperature is increased and the residence time is lowered, more liquid results. Of course, this is available, but not at a very high temperature. As it can be seen in the [Figure 4.25\(A\)](#), 550 °C is the maximum for the type of lignin used in the project. At a higher temperature, more gas is generated. When analysing the solid yield, especially when using the catalyst, two different solid materials should be considered: the char and coke. The first one forms at low temperature and high residence time[36], the second one depends on the chemical and structural properties of the catalyst, as well as on the temperature and pressure. Based on the total yield of the solid and the TGA analysis, the amount of coke and char was calculated ([Figure 4.25, B](#)). As it can be seen, with increasing the temperature, the coke yield is decreasing. According to Henrique S. Cerqueira a [97], coke precursors are easier to be retained in the pore structure at lower temperatures and this could be an explanation of the decreased coke yield with the temperature. In case of the char, from 450 to 550 °C the yield was decreased, while at 600 °C it was increased. This could be because of the thermocouple which was positioned inside the reactor and even though it was cleaned before each experiment, the collection after the experiment of all the solid deposited on it could not be done so accurately, thus leaving some char on the thermocouple.

In the [Figure 4.25](#), it can also be seen that the mass balance is not accomplished. This could happen due to some char that remained on the thermocouple, as well as due to lignin injected into the reactor. Due to the horizontal piston, it was not possible to push all the lignin inside the reactor. After each experiment, the lignin, which remained in the space at the intersection of the piston and the vertical tube, was collected and the quantity was subtracted from the total amount of lignin placed in the piston tube. Moreover, due to the

plastic properties of the lignin, some of it could stick on the wall of the tube positioned between the piston and reactor. All this is available for all experiments.

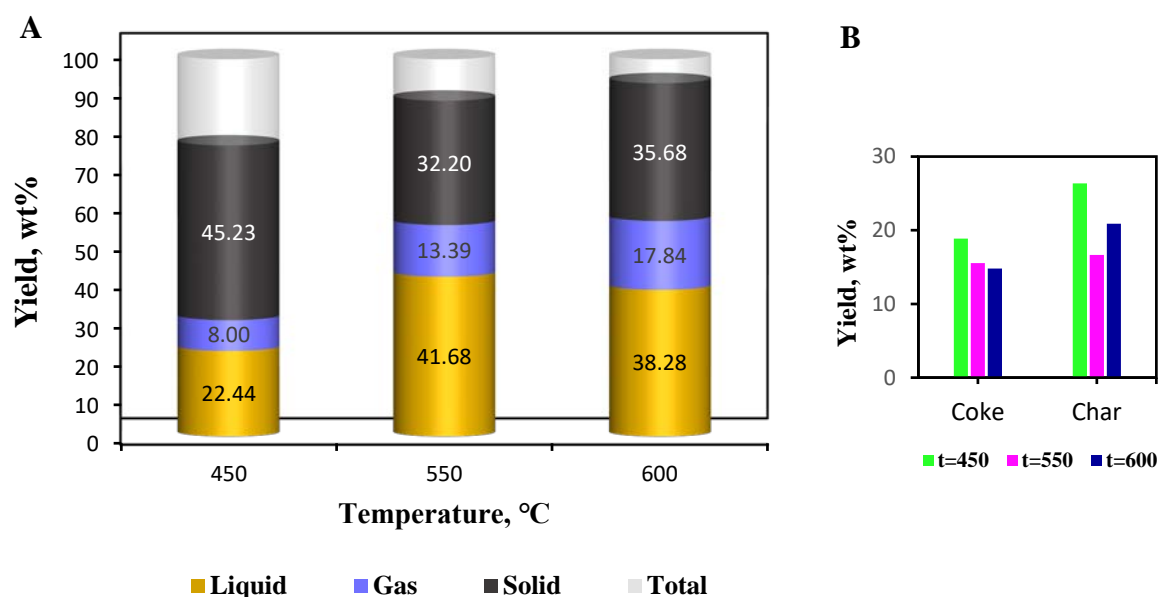


Figure 4.25 Temperature analysis of the FP-CU process on HZSM-5(30) (N_2 flow=40 mL/min, C:L=1). A-fixed bed reactor results. B-Fixed bed reactor and TGA results

Liquid analysis-GC/FID/MS

The temperature influence on the products distribution of the liquid phase resulted in the FP-CU on HZSM-5(30) is presented in the [Figure 4.26](#). It can be seen that with increasing the temperature, almost all the PhA compounds were converted into Ph, MAH, DAH and PAH. The DAH recorded the maximum yield at all three temperatures. If comparing with the data from the Py-GC/MS experiment on HZSM-5(30), the MAH was the most plentiful group. Lazaridis, Fotopoulos [40] also realized the FP-CU of lignin in the Py-GC/MS and fixed bed reactor and the results were similar. However, they used a nitrogen flow of 100 mL/min in the fixed bed reactor. At the beginning, it was thought that this could be the reason of obtaining more DAH and PAH than MAH, as an increase of the residence time of the aromatics in the catalyst bed could promote the formation of more DAH and PAH. Thus, two different nitrogen flowrates were also tested, and the obtained results are presented in the nitrogen flowrate paragraph.

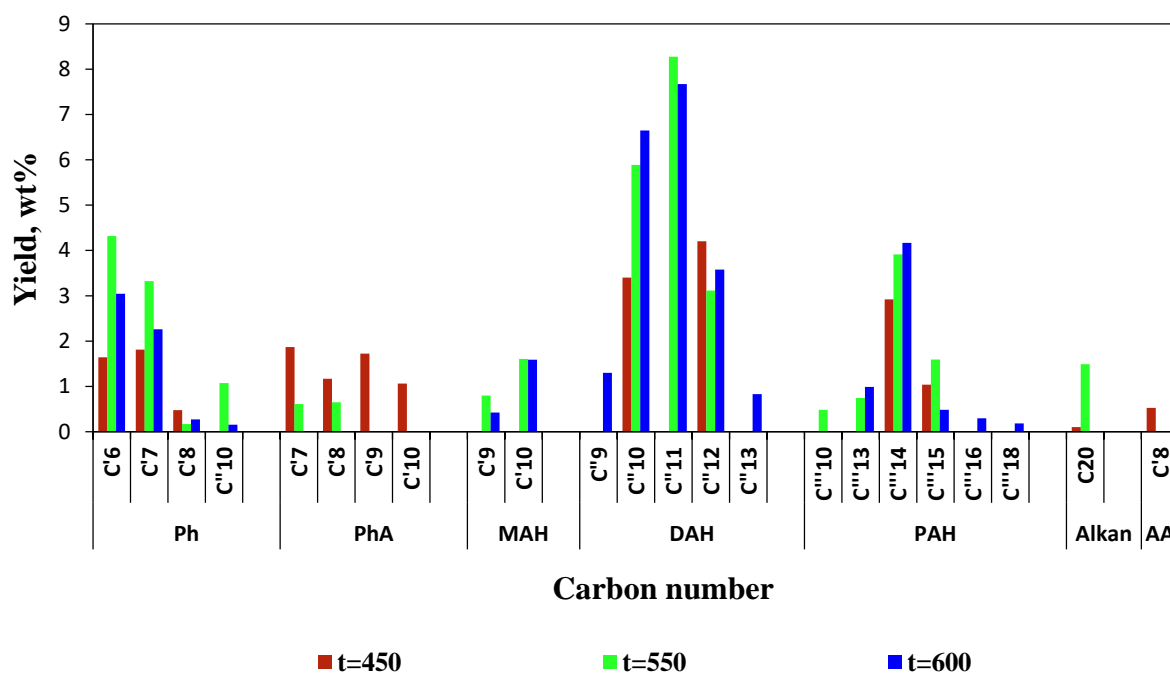


Figure 4.26 Temperature effect on the products distribution of the liquid phase resulted in the FP-CU on HZSM-5(30) (N_2 flow=40 ml/min, C:L=1)

Gas analysis-GC/FID/TCD

The distribution of the gas products at the three different temperatures is shown in the [Figure 4.27](#). As it can be seen, the CO , CO_2 and CH_4 are the most abundant gas products. According to Klein and Virk [100], the methane results mostly from the methoxy group of the PhA, while the CO is produced from the lignin propanoid chains which contain the carbonyl group. The carbon dioxide could result via the decarboxylation reactions, but also from the water gas-shift reaction as the water is also produced, as well as from the Boudouard reaction. Of course, the last two reactions are exothermic, thus, thermodynamically they are not favoured by high temperatures. But from the kinetic point of view, the reaction rate increases with the temperature, so it is possible that these reactions actually occur in the pyrolytic atmosphere of the reactor and a large content of CO_2 could result. The C2-C5 hydrocarbons could result from the side chains of the phenol, 4-ethyl-2-methoxy-, creosol, 2-methoxy-4-vinylphenol, eugenol and other compounds presented in the [Table 8.11](#).

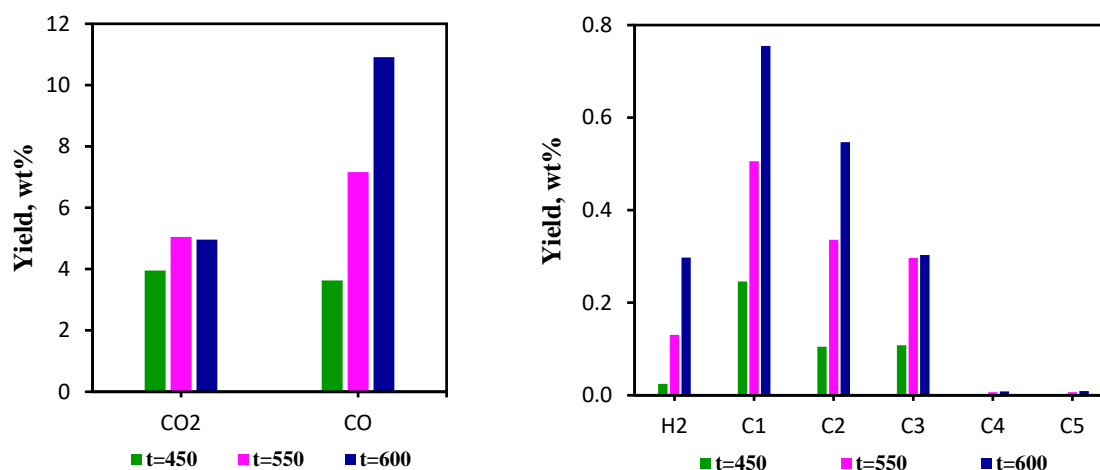


Figure 4.27 Temperature effect on the products distribution of the gas phase resulted in the FP-CU on HZSM-5(30) (N_2 flow=40 ml/min, C:L=1)

4.2.2.2 Nitrogen flow analysis of the FP-CU process on HZSM-5(30)

The effect of the nitrogen flowrate in the FP-CU on HZSM-5(30) was also investigated, by keeping the temperature at 600 °C and the catalysts to lignin ratio of 1. According to the obtained results (Figure 4.28), by increasing the flowrate from 20 to 40 mL/min, the liquid and gas yields were increased, while the solid yield was decreased. As it was already mentioned in the previous subparagraph, a decrease of the residence time of the volatiles in the pyrolytic process contributes to a higher liquid yield and lower char yield (Figure 4.28, B). However, by increasing the flowrate up to 60 mL/min, the gas and solid yield is maintained, while the liquid yield is almost halved. Moreover, almost 25 wt% of products were not quantified. By analysing also the Figure 4.29, it can be seen that the yield of MAH is decreased and it is still much lower compared to the yield of DAH. According to this, it was assumed that due to the high volatility of the MAH, they were probably lost in the gas collection bottle. Based on this, the plastic hose assembled between the spiral condenser and the gas collection bottle was cleaned with a small amount of methanol in order to collect the possibly deposited MAH. The GC/MS analysis showed no peak for the MAH. The experiment at 60 mL/min was repeated, but besides the cooling ice, ethyl acetate was used as solvent in order to enhance the collection of organic compounds. The liquid analysis showed also no peak for the MAH. However, considering that all the DAH and PAH were condensed, as well as the Ph and PhA, the results could be compared in the liquid analysis section.

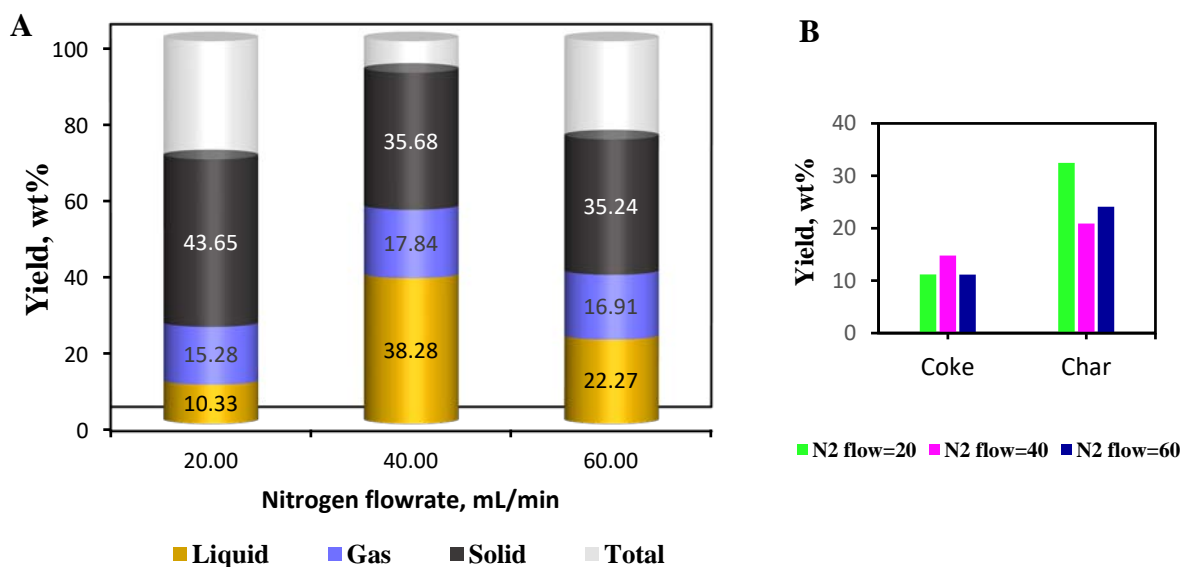


Figure 4.28 Nitrogen flowrate analysis of the FP-CU process on HZSM-5(30) ($t=600^{\circ}\text{C}$, C:L=1). A-fixed bed reactor results. B-Fixed bed reactor and TGA results

Liquid analysis-GC/FID/MS

The influence of nitrogen flowrate on the products distribution is presented in the [Figure 4.29](#). As it can be seen, the nitrogen flowrate of 40 mL/min is the optimum flowrate due to the highest yield of Ph, DAH and PAH, moreover, the PhA compounds were not detected. That means a good conversion into the other resulted products. It can also be noticed that at the nitrogen flowrate of 60 mL/min the compounds from all groups tend to be more substituted and even with more rings per molecule. In the Ph group the C'6 (phenol) and C'7(p-cresol, phenol, 2-methyl-) are the most abundant compounds for all nitrogen flowrates, but when increasing the flowrate up to 60 mL/min, the C'9, C''9, C''10 and C''11 are also enhanced. The same can be said about the DAH with C''14, C''15 and C''16, and PAH with C'''15, C'''16, C'''17 and C'''18. This could be related to the lower residence time of the volatiles in the pyrolytic zone and catalysts bed. Less time means a medium cracking of the side chains and longer side chains could promote the formation of the second ring (C''9,10,11 from Ph). Fewer cracked side chains means less gas and this can be supported by the lower gas yield obtained in the FP-CU at flowrate of 60 mL/min with the one resulted at 40 mL/min.

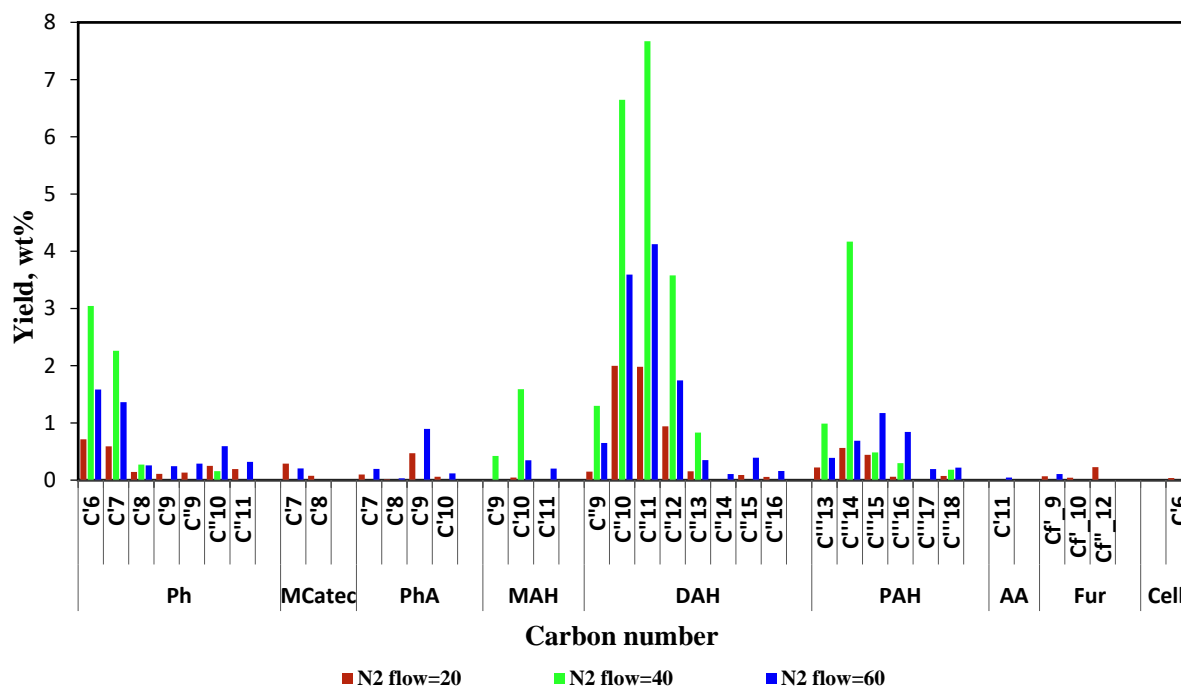


Figure 4.29 Nitrogen flowrate effect on the products distribution of the liquid phase resulted in the FP-CU on HZSM-5(30) ($t=600$ °C, C:L=1)

Gas analysis-GC/FID/TCD

The distribution of the gas products at the three different nitrogen flowrates is presented in the [Figure 4.30](#). As it can be seen, there is not a very large variation when the flowrate is increased. However, at 600 °C and a flowrate of 20 mL/min, the yield of the gas products should be higher compared to the other two flowrates, because at high temperatures and high residence time a deeper cracking occurs, and more gas is generated. Nevertheless, a higher residence time of the volatiles and non-condensable gases in the catalyst bed could contribute to the formation of larger molecules with more rings per molecules, as well as to the coke formation.

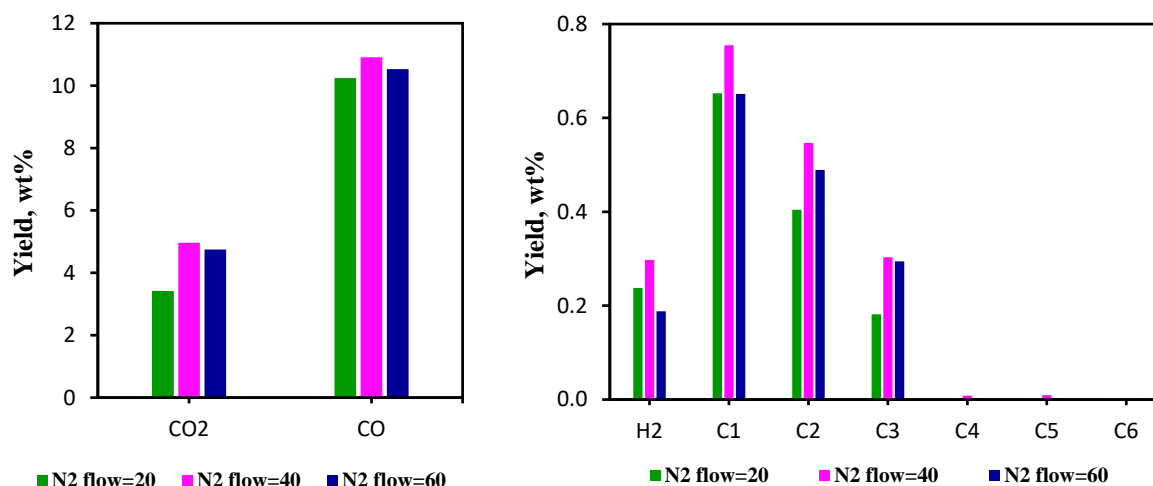


Figure 4.30 Nitrogen flowrate effect on the products distribution of the gas phase resulted in the FP-CU on HZSM-5(30) ($t=600$ °C, C:L=1)

4.2.2.3 Catalyst: lignin ratio analysis of the FP-CU process on HZSM-5(30)

The effect of the catalyst to lignin ratio on the products distribution was also studied in this thesis and the results are presented in the [Figure 4.31](#). For the all experiments the FP-CU was realized at 550 °C and a nitrogen flow of 40 mL/min. In the [Figure 4.31, A](#) it can be observed that the liquid yield is decreasing with the increase of C:L ratio, while for the gas it is the opposite. This variation is due to the deoxygenation and dealkylation properties of the Brønsted acid sites of the HZSM-5(30). By removing the oxygen in form of CO and CO₂, as well as the hydrocarbon side chains from the PhA and Ph, the molecular weight of the compounds will be diminished. Based on this, a lower yield of bio-oil will result, but in a more stable state, while for the gas, an increment will be observed. The solid yield is also increased. If analysing the [Figure 4.31, B](#), it can be seen that the coke yield is increasing with the C:L ratio and this is due to the space velocity which is lowered when the catalyst bed is expanded. The long time exposure of volatiles to the catalytic acid sites promotes the formation of large molecules and coke. In case of char, it should not vary with the C:L ratio[109]. It was assumed that the low char yield at C:L ratio of 0.5 could result from an improper injection of the lignin in the reactor. When a lower amount of lignin is inserted in the pyrolytic zone, less char will result due to the enhanced heat transfer to the lignin particles.

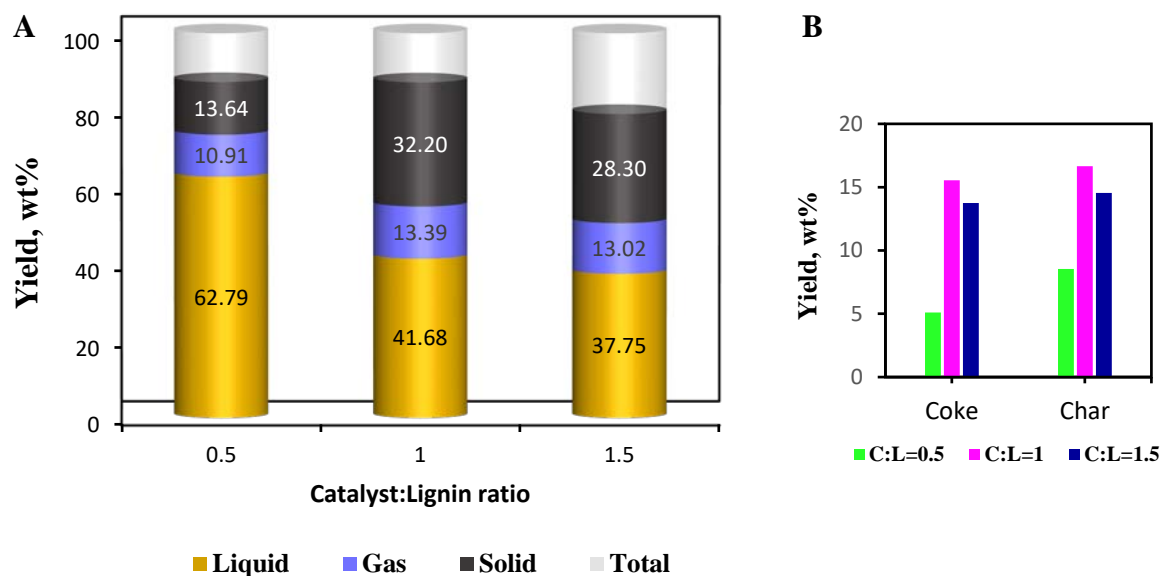


Figure 4.31 Catalyst to lignin ratio analysis of the FP-CU process on HZSM-5(30) ($t=550$ °C, nitrogen flowrate=40 mL/min). A-fixed bed reactor results. B-Fixed bed reactor and TGA results

Liquid analysis-GC/FID/MS

The influence of catalyst to lignin ratio on the products distribution based on the organic groups and carbon number is shown in the [Figure 4.32](#). As it can be noticed, the deoxygenation property of the acid sites of the HZSM-5(30) has a major effect on the products distribution. By realizing the FP-CU on a lower amount of catalysts, more PhA, MCatec and Ph compounds remained unconverted. When the C:L ratio is increased, more DAH are formed due to a lower space velocity of the volatiles in the catalyst bed. However, the C:L ratio of 0.5 recorded a very high peak for the C¹⁵. Of course, this peak was more expected for the higher C: L ratios. Nevertheless, it could result from an irregularity of the catalyst bed. If ignoring the C¹⁵, it can be observed that the yield of PAH dominates for C:L ratio of 1.5. The MAH were not detected at C:L ratio of 0.5 and only a very low amount was detected at C:L ratio of 1.5. Of course, the catalyst to lignin ratio influences the yield of MAH, but not to such an extent that the BTX are not produced or are converted to larger compounds like DAH and PAH.

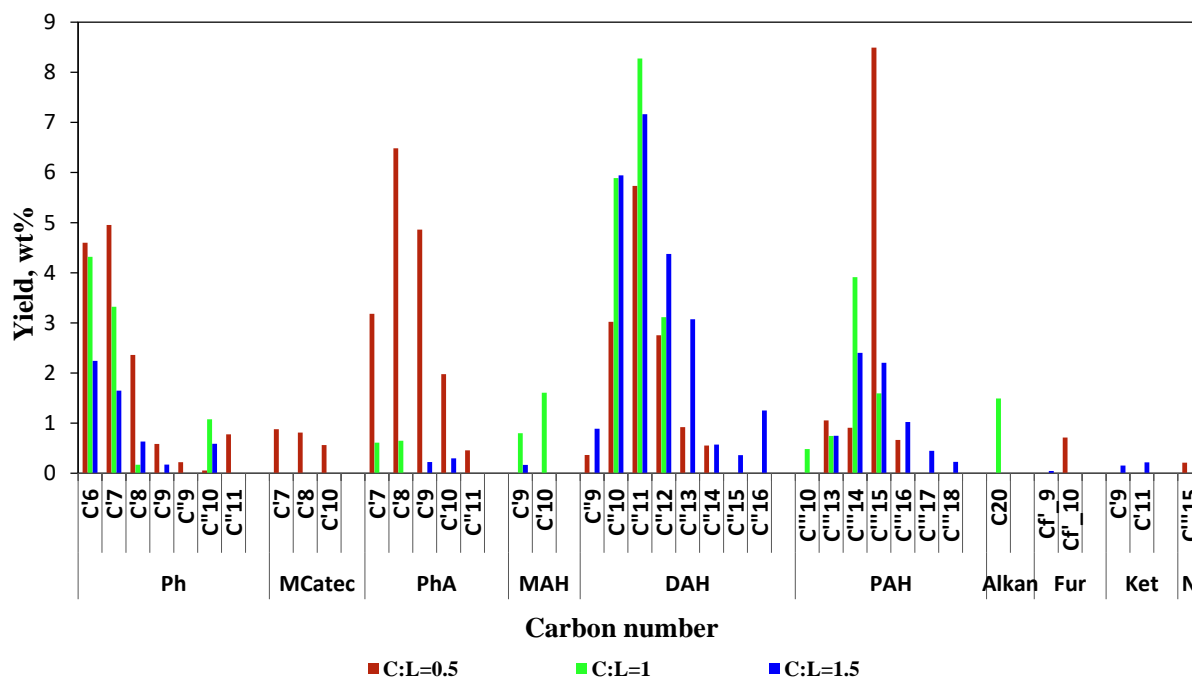


Figure 4.32 Catalyst to lignin ratio effect on the products distribution of the liquid phase resulted in the FP-CU on HZSM-5(30) ($t=550\text{ }^{\circ}\text{C}$, nitrogen flowrate=40 mL/min)

Gas analysis-GC/FID/TCD

The effect of the catalyst to lignin ratio on the products distribution of the gas phase is presented in the Figure 4.33. It can be observed that a higher C:L ratio promoted the yield of almost all the gas products. However, if the ratio is too high, the hydrocarbon side chains will be involved in the formation of the new rings, thus promoting the formation of larger molecules. Considering this the yield of the gaseous hydrocarbons will record a decrease.

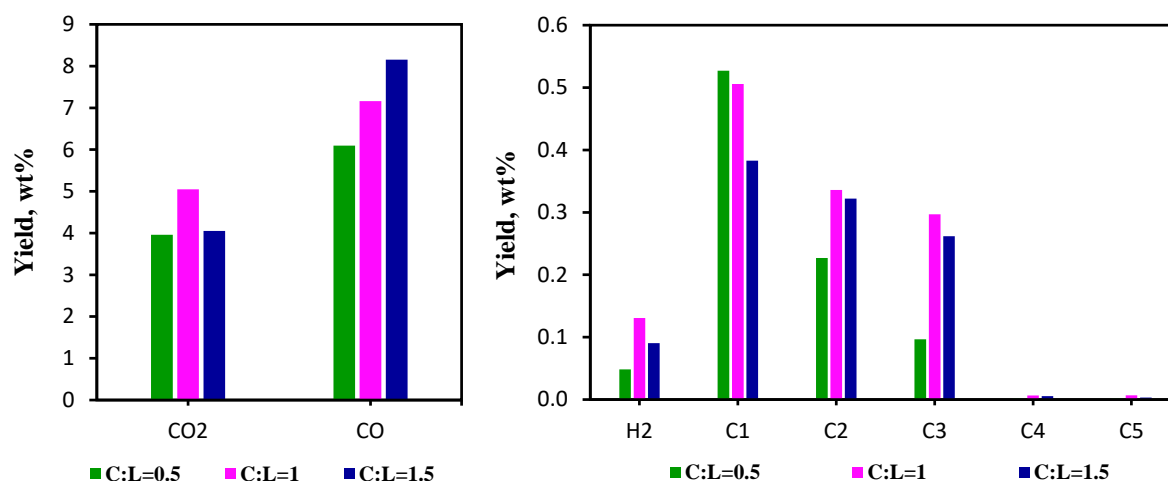


Figure 4.33 Catalyst to lignin ratio effect on the products distribution of the gas phase resulted in the FP-CU on HZSM-5(30) ($t=550\text{ }^{\circ}\text{C}$, nitrogen flowrate=40 mL/min)

4.2.2.4 FP vs FP-CU

The fast pyrolysis and the fast pyrolysis coupled with the catalytic upgrading on HZSM-5(30) were realized at 550 and 600 °C and at a nitrogen flowrate of 40 mL/min in order to see the effect of the catalyst and temperature on the oxygenated volatiles that result in the pyrolytic process. In the FP, for simulation the same conditions in the catalyst zone, SiO₂ was used as an inert heat carrier material [40]. In both processes a ratio of 1 was set for the HZSM-5(30) to lignin and SiO₂ to lignin. The gas, liquid, solid, coke and char yields are presented in the Figure 4.34 (A, B). If comparing the FP and FP-CU at 550 °C, it can be observed that the liquid yield is increased, as well as the gas yield, while the solid yield is diminished. The results obtained in the Py-GC/MS at 550 °C, also show a very small area fraction for the liquid compounds resulted in FP compared to FP-CU on HZSM-5(30) and this is due to the very unstable oxygenated species that tend to re-polymerize if they are not stabilized or cooled down very fast. However, the results obtained by Paysepar, Rao [41] in a fixed bed reactor at 450 °C on a HZSM-5, show an insignificant change of the liquid and solid yield when comparing the FP and FP-CU. It is also not so clear how the all three phases behave in the catalytic fast pyrolysis, even though this domain is more investigated. Lazaridis, Fotopoulos [40] investigated the catalytic fast pyrolysis and the results showed a decrease of the liquid yield and an increase of the solid yield for both instruments (Py-GC/MS and fixed bed reactor). Nevertheless, something is unclear as they used the lignin and the catalyst in a mixed form in the Py-GC/MS and in the fixed bed reactor, the lignin was placed in the piston and the catalyst in the reactor. Thus, if comparing their results with the data obtained by Ma, Troussard [42], an opposite variation of these two phases was recorded. Based on all mentioned, the behaviour of the three phases is unclear and this could be because of the type of lignin, the lignin treatment, the particle size of the catalyst, the reactor and many other factors. According to the results obtained herein at 550 °C, the liquid yield could increase by minimizing the char yield due to the stabilization of the oxygenated species on the Brønsted acid sites of HZSM-5(30). So, when these species are formed, some of them will re-polymerize and form char and the rest will reach the catalyst bed and will stabilize based on the hydrogen donor properties of the HZSM-5(30). When there is no catalyst, it is possible that the formation of char still persists until the species reach the cold zone in the bottom of the reactor and the reactions stop due to the insufficient heat. The gas yield is increased when the catalyst is used, and this is due to the deoxygenation and dealkylation properties of the Brønsted acid sites of HZSM-5(30). By realizing the FP and FP-CU at 600 °C, there is no significant variation of the liquid yield. This could result due to the temperature effect. A higher temperature could generate more stable compounds. This also can be observed on analysing the results of FP at 550 and 600 °C. When the more stable compounds reach the catalyst bed, the dealkylation and deoxygenation reactions produce more gas and less oil due to the lower molecular weight of the resulted products. The variation of the solid yield phase manifests the same behaviour as at 550 °C.

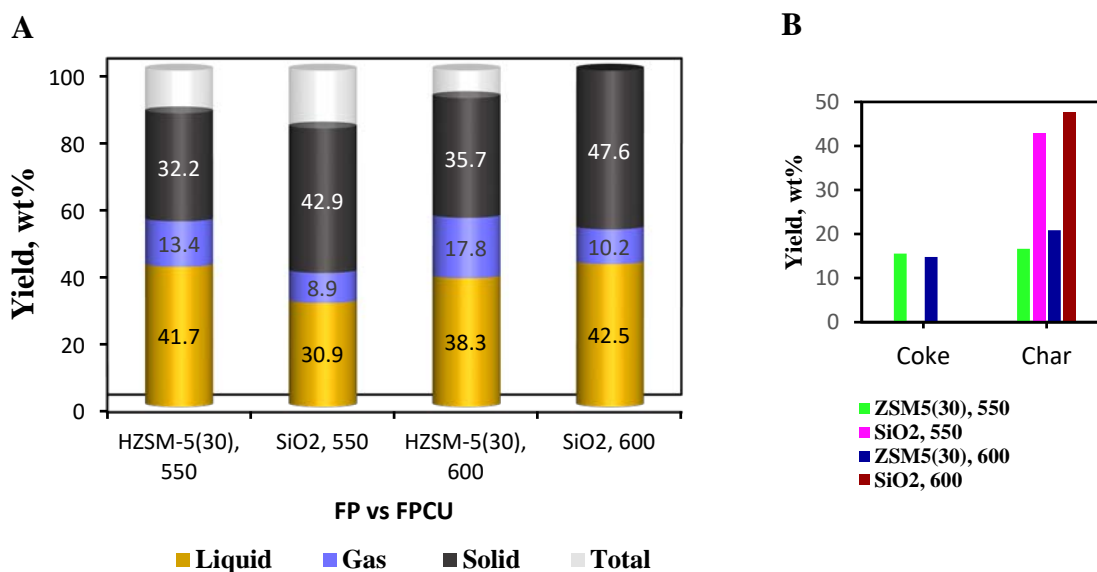


Figure 4.34 The effect of HZSM-5(30) on the oxygenated volatiles resulted in the FP at 550 and 600 °C (nitrogen flowrate=40 mL/min, a ratio of one was set for the HZSM-5(30)/lignin and SiO₂/lignin). A-fixed bed reactor results. B-Fixed bed reactor and TGA results

Liquid analysis-GC/FID/MS

The analysis of liquid products obtained in the FP and FP-CU at 550 and 600 °C are presented in [Figure 4.35](#). If analysing the effect of temperature, it can be seen that at 600 °C more Ph and MCatec compounds are produced compared with the FP results at 550 °C. As it was already mentioned when discussing the [Figure 4.34](#), a higher temperature contributes to the formation of more stable compounds like Ph and MCatec.

The catalyst addition changed significantly the results. Almost all PhA compounds were converted to MAH, DAH, PAH and Ph compounds based on the special activity of the acidic sites of HZSM-5(30), as well as due to its medium pore size which favours the formation of aromatic hydrocarbons. The yield of MAH is low as they could not be identified. However, the investigation of lignin in the fixed bed reactor was continued and the results are presented in the next subparagraphs.

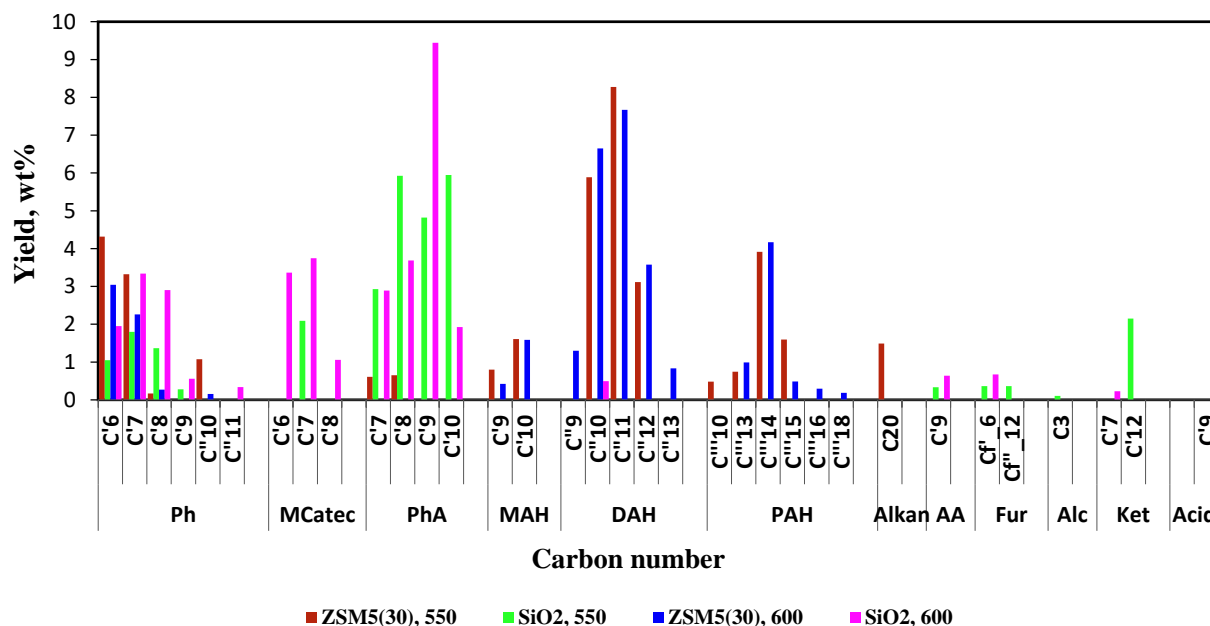


Figure 4.35 The products distribution of liquid phase resulted in the FP and FP-CU realized at 550 and 600 °C. HZSM-5(30) was used in the FP-CU and SiO₂ in the FP. (nitrogen flowrate=40 mL/min, a ratio of one was set for the HZSM-5(30)/lignin and SiO₂/lignin)

Gas analysis-GC/FID/TCD

The analysis of gas products obtained in the FP and FP-CU at 550 and 650 °C are presented in the [Figure 4.36](#). As it can be observed, a higher temperature and the presence of acidic sites contribute to a higher yield of each gas. More CO and CO₂ means more deoxygenated liquid products and more H₂ and C1-C2 means less substituted aromatic hydrocarbons and phenolic compounds with short side chains (toluene, xylenes, naphthalene, 1-methyl-, phenol, p-cresol).

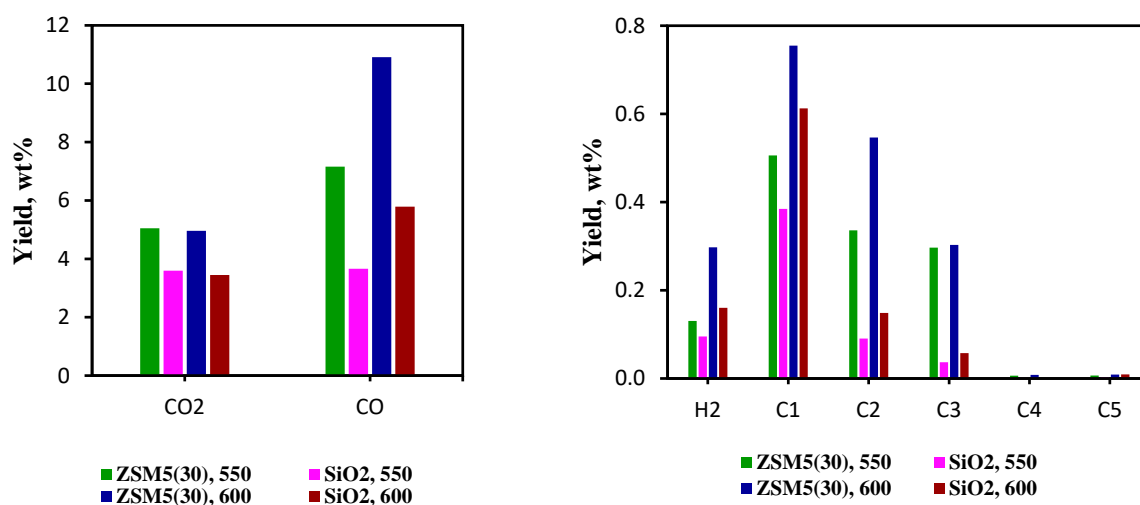


Figure 4.36 The products distribution of gas phase resulted in the FP and FP-CU realized at 550 and 600 °C. HZSM-5(30) was used in the FP-CU and SiO₂ in the FP. (nitrogen flowrate=40 mL/min, a ratio of one was set for the HZSM-5(30)/lignin and SiO₂/lignin)

4.2.2.5 The effect of $\text{SiO}_2/\text{Al}_2\text{O}_3$ ratio of HZSM-5 on the upgrading of the pyrolytic volatiles

The $\text{SiO}_2/\text{Al}_2\text{O}_3$ ratio of HZSM-5 was also studied in order to see how the density of the acid sites influences the upgrading of the pyrolytic volatiles. The FP-CU lignin was realized at 550 °C, a catalyst to lignin ratio of 1 and the nitrogen flowrate of 40 mL/min. According to the results presented in the Figure 4.37 (A), it can be seen that the variation of liquid and gas phase is insignificant. In case of the solid phase, it should increase by increasing the alumina content. When more alumina is incorporated into the zeolite structure, the density of the acid sites is increasing. According to Wang [110], the more dense the acidic sites, the more promoted the bimolecular reactions are, which generate large compounds and coke. If looking at the Figure 4.37, B, the coke yield is increasing with the density of the acidic sites, but as well as the char yield if considering the $\text{SiO}_2/\text{Al}_2\text{O}_3$ of 30, 50 and 80. However, the char yield can be considered quite stable. Even though there is a variation, it could be caused by the molten lignin that stuck to the reactor walls or even some unconverted lignin.

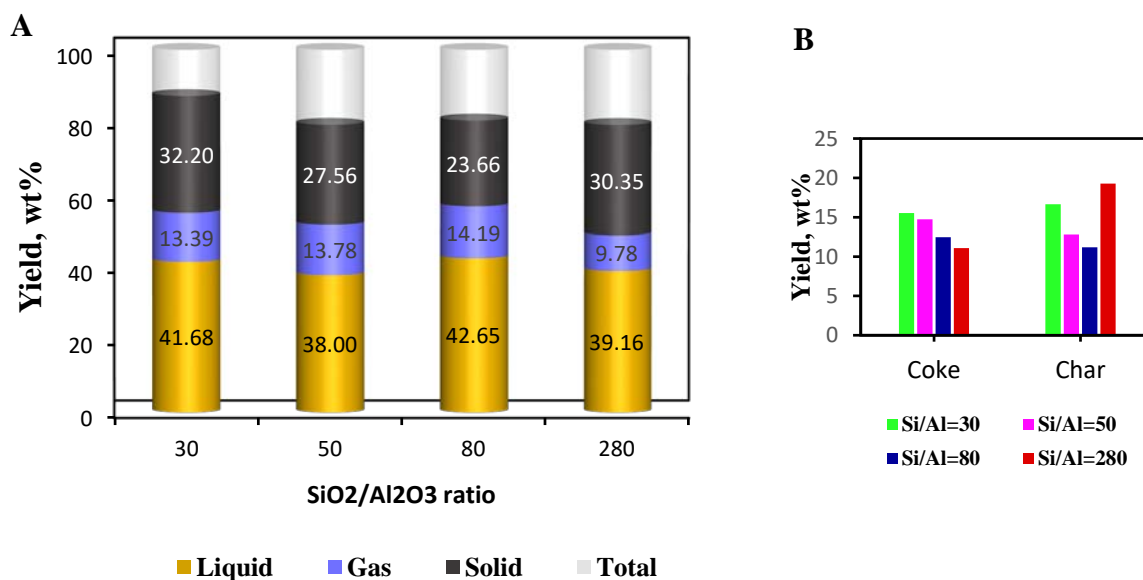


Figure 4.37 The effect of $\text{SiO}_2/\text{Al}_2\text{O}_3$ of HZSM-5 on the distribution of the three main products: gas, liquid and solid. The FP-CU was realized at 550 °C, nitrogen flowrate of 40 mL/min and C:L ratio of 1. A-fixed bed reactor results, B-fixed bed reactor and TGA results

Liquid analysis-GC/FID/MS

The effect of $\text{SiO}_2/\text{Al}_2\text{O}_3$ ratio of HZSM-5 on distribution of liquid products is presented in the Figure 4.38. As it can be seen, by increasing the density of the acidic sites, more aromatic hydrocarbons are generated. Indeed, more than likely, the bimolecular reactions are promoted by the acidic sites when they are arranged closer to each other. This was assumed by taking in consideration the rapid increase of the DAH and PAH yield when decreasing the $\text{SiO}_2/\text{Al}_2\text{O}_3$ ratio of HZSM-5. By comparing these results with the ones generated in the Py-GC/MS, it can be observed that they are very similar. Based on this, it can be assumed that the yield of MAH should be slightly higher than the yield of DAH.

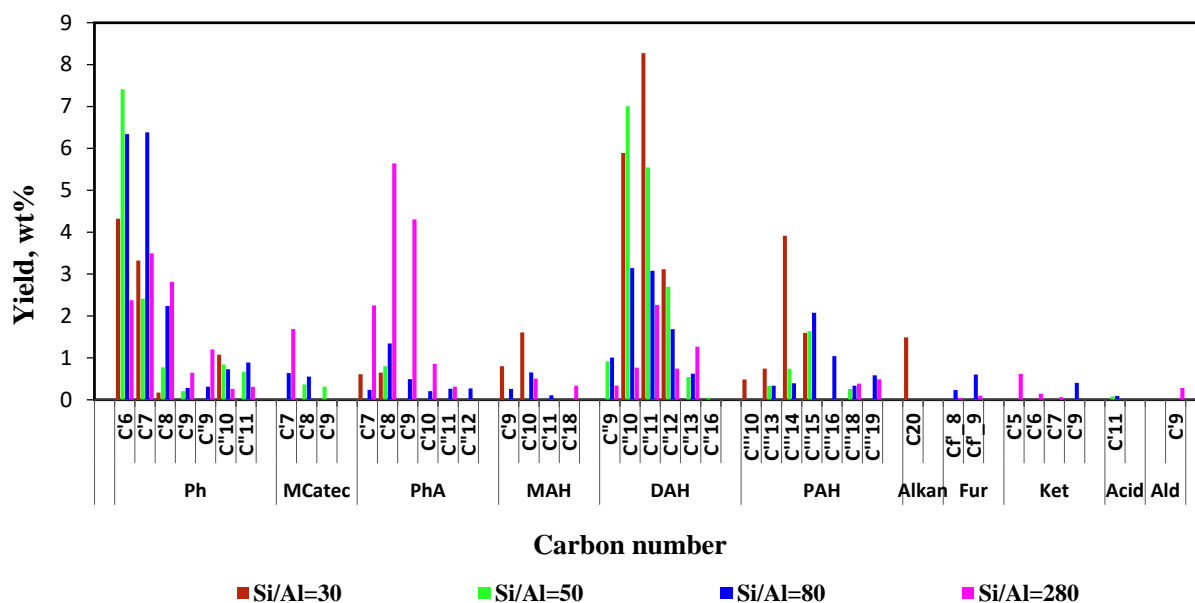


Figure 4.38 The effect of SiO₂/Al₂O₃ of HZSM-5 on the distribution of the liquid products. The FP-CU was realized at 550 °C, nitrogen flowrate of 40 mL/min and C:L ratio of 1

Gas analysis-GC/FID/TCD

The distribution of the gas products obtained at the four SiO₂/Al₂O₃ of HZSM-5 is presented in the Figure 4.39. As it can be noticed, by increasing the density of acidic sites of HZSM-5, the yield of each gas is also increased. This is due to the enhanced deoxygenation and dealkylation reactions.

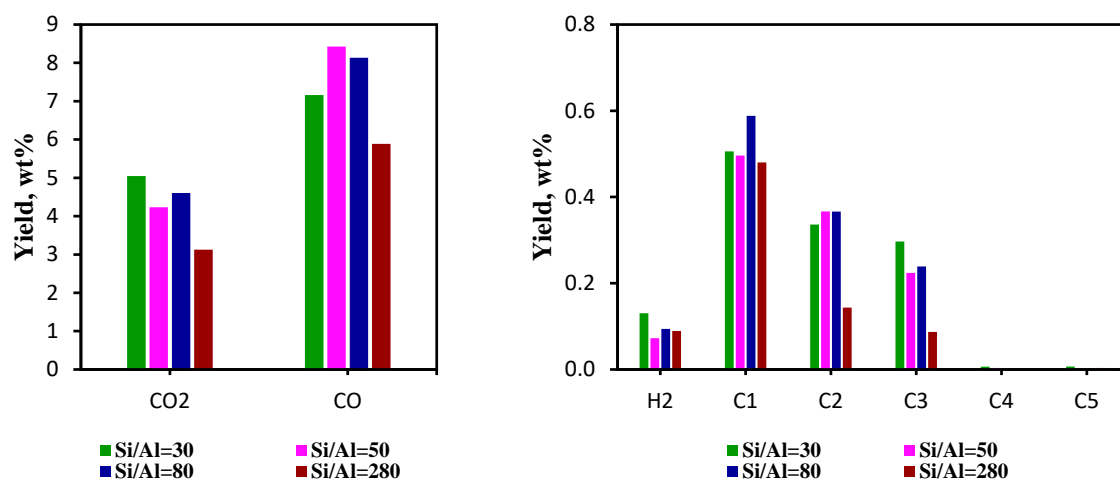


Figure 4.39 The effect of SiO₂/Al₂O₃ of HZSM-5 on the distribution of the gas products. The FP-CU was realized at 550 °C, nitrogen flowrate of 40 mL/min and C:L ratio of 1

4.2.2.6 The influence of the pore size and internal pore architecture on the upgrading of pyrolytic volatiles

The effect of pore size and internal pore construction on products distribution was also studied in the fixed bed reactor at 550 °C, nitrogen flowrate of 40 mL/min and C:L ratio of 1. The yield obtained in the fixed bed reactor and TGA are presented in the Figure 4.40 (A,B). As it can be seen, the large pores promote the formation of a higher liquid content. Ma, Troussard [42] reported the same result when analysing lignin. However, they analysed the pore size in the catalytic fast pyrolysis, but the effect should be the same in the FP-CU process. In their work it is explained that the liquid yield is increasing with the pore size because the large molecules can easily enter the pore and react, thus avoiding the formation of more char. It can be seen in the Figure 4.40, B that the char yield is decreased when the pore is expanded. However, by increasing the pore size, more coke resulted and this is because of the internal pore space which favours the formation of large molecules (DAH, PAH) and coke [38]. A significant variation of the gas was not noticed.

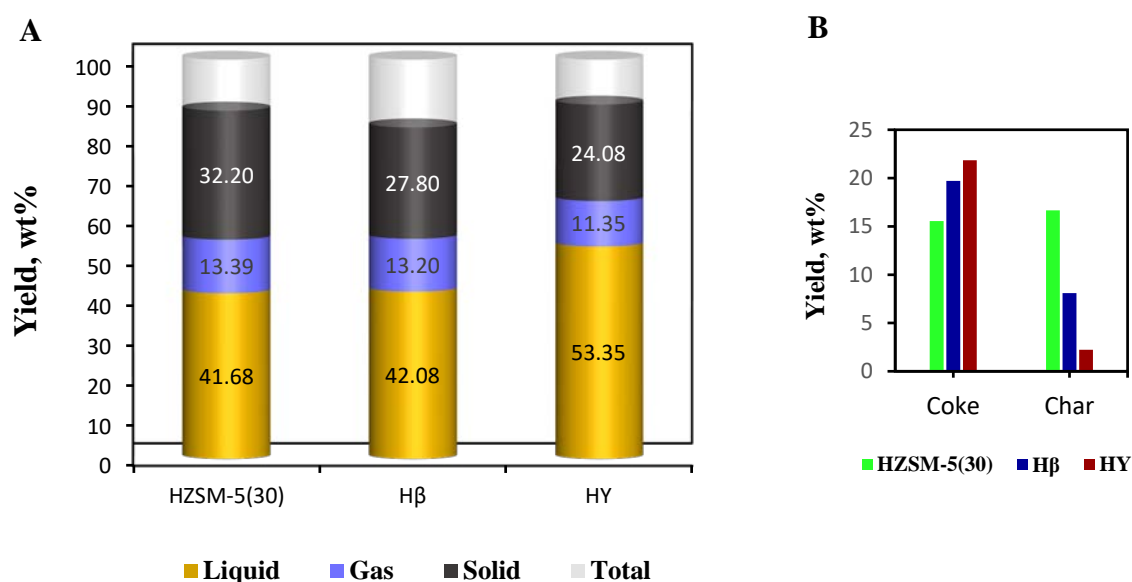


Figure 4.40 The effect of pore size and internal pore architecture on the distribution of the three main products: gas, liquid and solid. The pore size: HZSM-5(30)<Hβ<HY. The FP-CU was realized at 550 °C, nitrogen flowrate of 40 mL/min and C:L ratio of 1. A-fixed bed reactor results, B-fixed bed reactor and TGA results

Liquid analysis-GC/FID/MS

The effect of pore size and internal pore architecture on the products distribution of liquid phase is presented in the Figure 4.41. It can be seen that HZSM-5(30) recorded a good conversion of PhA and Ph compounds into MAH, DAH and PAH. This could be related to its medium pore size that favours the formation of aromatic hydrocarbon. Yu, Li [38] studied the effect of pore size on the products distribution of lignin and found that more aromatic hydrocarbons are formed when using HZSM-5, followed by Hβ and HY. The same can be said based on the results obtain herein. Yu, Li [38] also reported that Hβ produced more aromatic hydrocarbons with 3 and 4 rings per molecule compared with HY. No information

regarding the DAH is specified, but according to the results from Figure 4.41, H β produced more DAH and PAH compared to HY. Due to the supercages in HY structure, the coke formation is more promoted than DAH and PAH. As it was also mentioned in the discussion of the results obtained in the Py-GC/MS, the strong acidic sites of HY are preferably located in its sodalite and cage/supercages structures[94]. According to this, the density of the acidic sites is also higher in those structures, which means that the bimolecular reactions are promoted, thus larger molecules and more coke are generated[38].

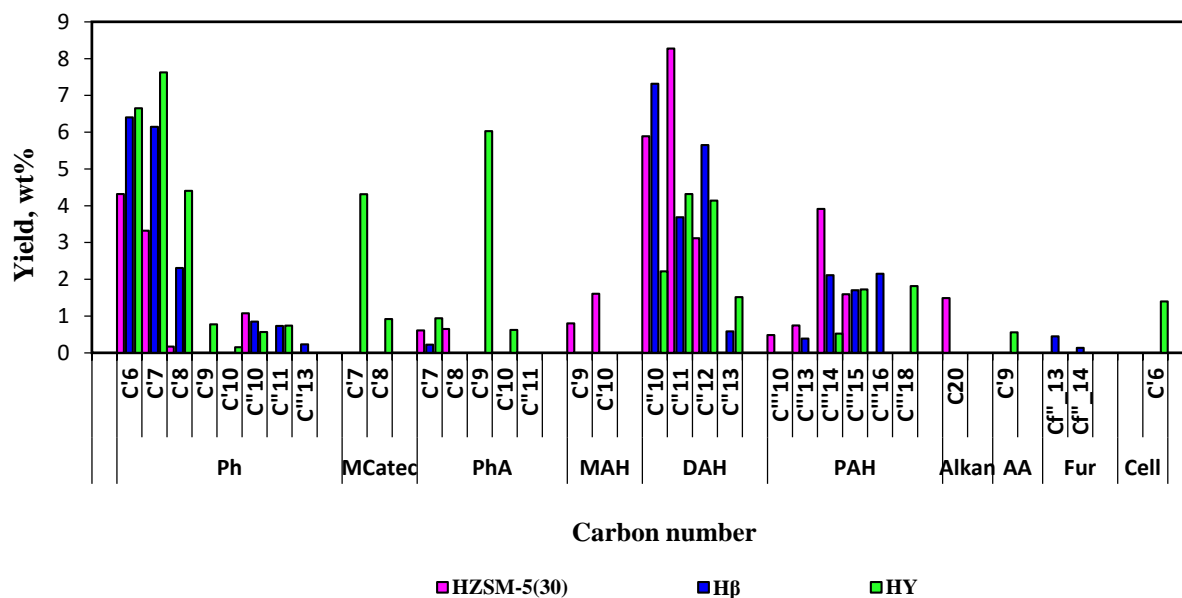


Figure 4.41 The effect of pore size and internal pore architecture on the products distribution of liquid phase. The pore size: HZSM-5(30)<H β <HY. The FP-CU was realized at 550 °C, nitrogen flowrate of 40 mL/min and C:L ratio of 1

Gas analysis-GC/FID/TCD

The distribution of the gas products is shown in the Figure 4.42. As it can be seen, the pore size did not influence the yield of each generated gas product.

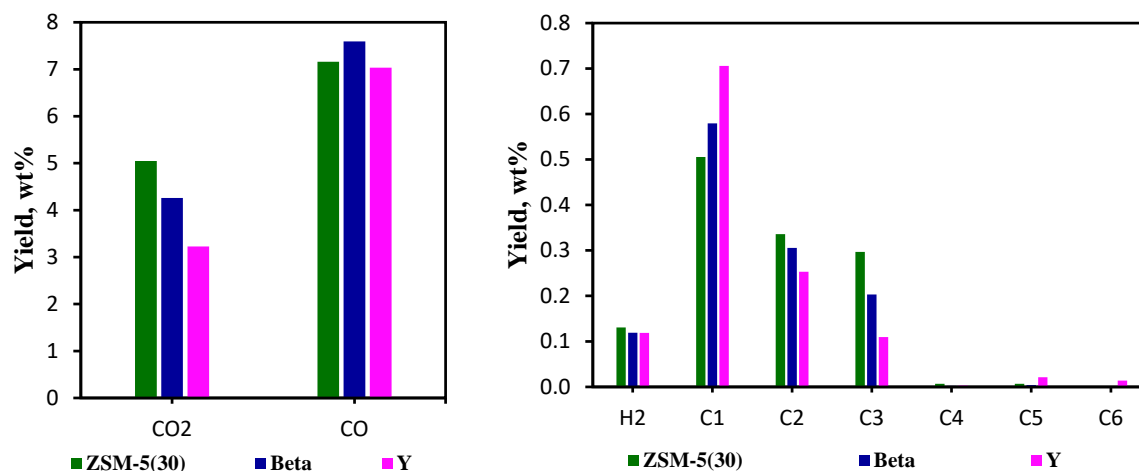


Figure 4.42 The effect of pore size and internal pore architecture on the products distribution of gas phase. The pore size: HZSM-5(30) < H β < HY. The FP-CU was realized at 550 °C, nitrogen flowrate of 40 mL/min and C:L ratio of 1

4.2.2.7 The FP-CU of pine and polyethylene powder- process revision

Almost all the fixed bed reactor results regarding the products distribution were similar to the results obtained in the Py-GC/MS, except for MAH. Various attempts like the modification the temperature, nitrogen flowrate, catalyst to lignin ratio, zeolite type were performed and no progress has been recorder for this group. It was discussed and a different material, which also generates high yield of MAH on HZSM-5, was decided to be studied. This decision was taken in order to see if the problem is related to the lignin structure or to the set-up. Based on Zheng, Zhao [111] and Zhang, Lei [112]'s study, the monoaromatic hydrocarbons are obtained in a quite high quantity from pine and polyethylene (PE) powder. Both materials were tested at 600 °C and nitrogen flowrate of 40 mL/min. The volatiles were upgraded on HZSM-5(30). The catalyst to PE ratio was set 1, while the ratio of catalyst to pine was set 3. The pine was used in a lower amount because it behaves as a highly adhering compound, especially when using small size of its particles (<500 μ m). When the particles stick to each other, the tendency of blocking the intersection of the horizontal piston tube with the vertical gas tube is higher. The products distribution of the liquid phase obtained in the FP-CU process of PE and pine are presented in the Figure 4.43 and Figure 4.44. If analysing the Figure 4.43,A, it can be observed that the MAH were detected in the liquid phase obtained in the FP-CU of PE. The same distribution of products was obtained in the Py-GC/MS (Figure 4.43, B). However, if summing up the yields of all products obtained in the fixed bed reactor, it results a very low yield of liquid phase. The gas and solid yields were also very small (Figure 8.16, Appendix). The overall yield was decreased because a large quantity of PE injected in reactor was molten in the tube placed between the piston and reactor.

When analysing the liquid products resulted in FP-CU of pine (Figure 4.44), the MAH were not detected. According to Yeboah [113], the FP-CU of pine in the Py-GC/MS on HZSM-5(30) recorder a high area fraction for BTX. Considering the results obtained for all three feedstocks, it was thought that the temperature in the reactor could be a problem as the oxygenated compounds are decomposed very hard compared to PE and 600 °C could be not enough for lignin and pine. Another reason could be the nitrogen flowrate. Based on

this, one experiment of lignin at 700 °C and nitrogen flowrate of 100 mL/min was realized. The products were only analysed in the GC/MS, as there was no need for quantification if the MAH were not detected. The GC/MS showed no peaks for MAH (Figure 8.17, Appendix). According to all mentioned, the only parameter that should be checked again is the cooling system. In order to improve the cooling mechanism, acetone was used in the spiral condenser. It is a highly volatile compound and evaporates very fast. As it is known, the evaporation is an endothermic process, thus, in order to evaporate, a liquid requires heat which is taken from the surfaces it comes in contact with. So, when the volatiles will enter the spiral condenser, the acetone will take over the heat and will evaporate by cooling the zone. The FP-CU process was realized at 700 °C and nitrogen flowrate of 100 mL/min. The results of GC/MS analysis of the liquid phase are presented in the Figure 4.45. As it can be noticed, the MAH were obtained in a slightly higher amount compared to DAH and PAH. The higher content of DAH and PAH could result because of a too high temperature. However, by finding out that the cooling part of the set-up was the problem, it can be said that the FP-CU has been operated correctly. More experiments on checking the cooling system at other conditions could not be done due to limited time. Nevertheless, it is good to know that the redesigned set-up is able to generate interesting results, moreover, it can be used by other researchers interested in the pyrolytic process of biomass or other organic feedstocks.

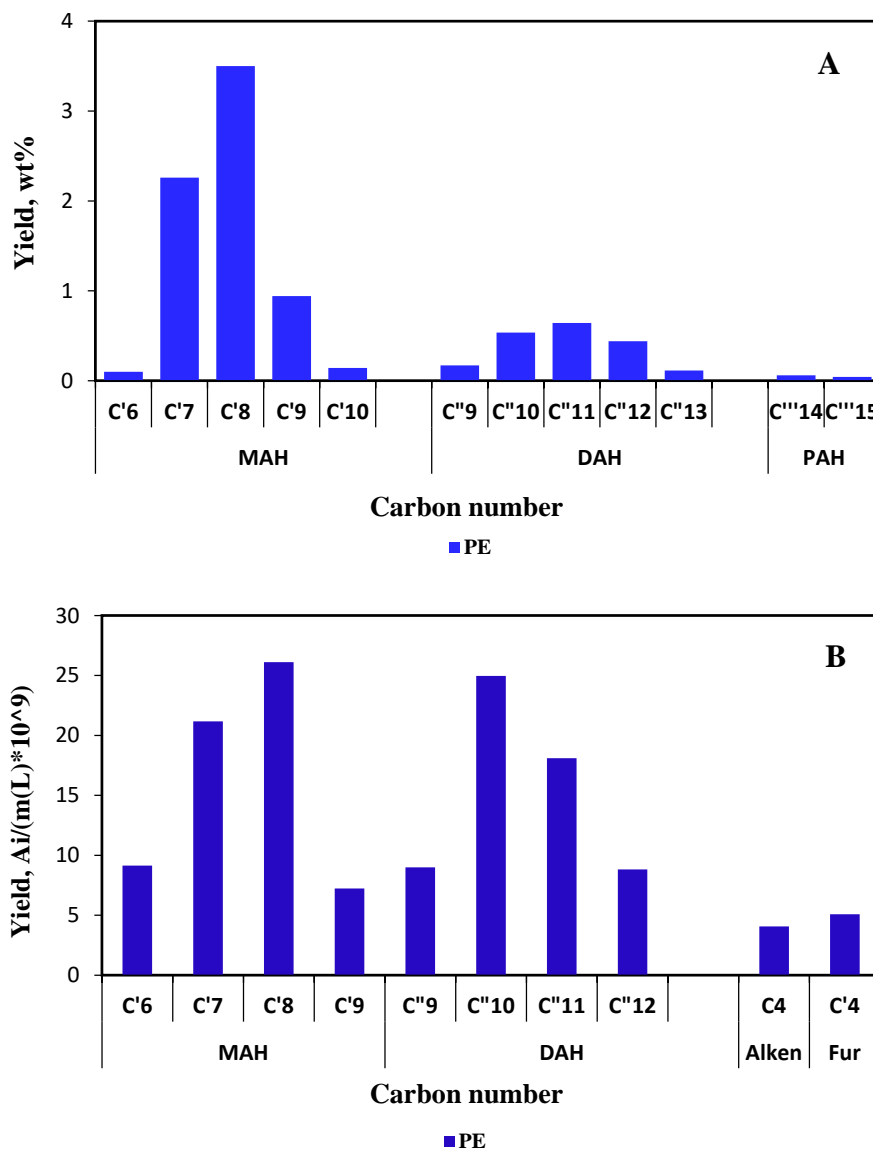


Figure 4.43 The products distribution of FP-CU of polyethylene powder in the fixed bed reactor (A) and Py-GC/MS (B). A: $t=600$ °C, nitrogen flowrate of 40 mL/min and catalyst to PE ratio of 1. The products were quantified based the effective carbon number approach. B: $t=600$ °C, helium flowrate of 2 mL/min and catalyst to PE ratio of 3

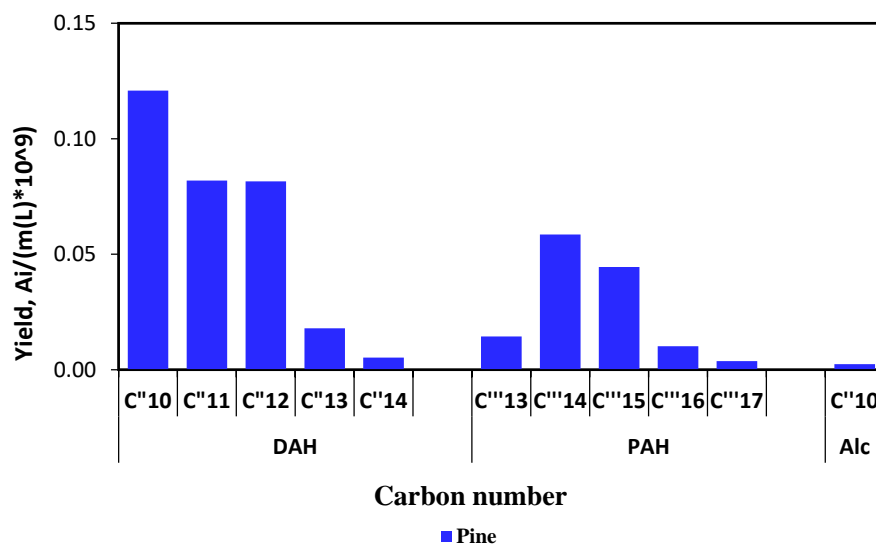


Figure 4.44 The products distribution of FP-CU of pine in the fixed bed reactor. The process was realized at 600 °C, nitrogen flowrate of 40 mL/min and catalyst to lignin ratio of 3. The products of liquid phase were analysed only by GC/MS

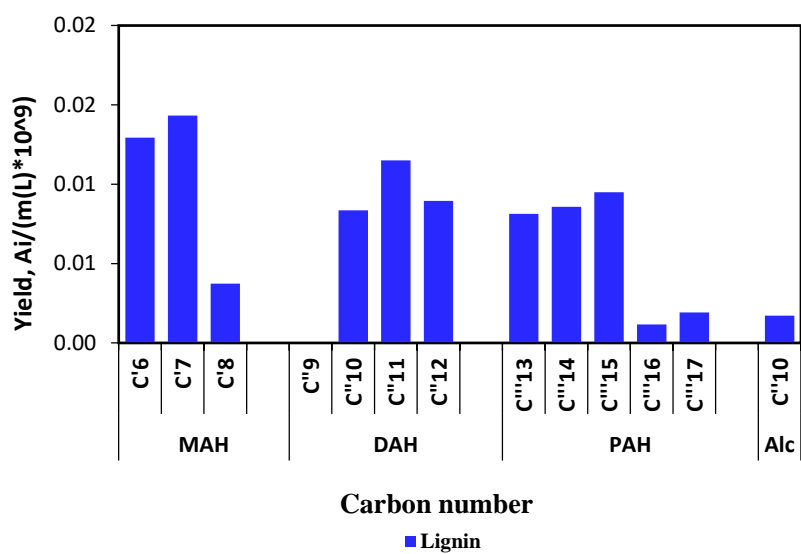


Figure 4.45 The products distribution of FP-CU of lignin in the fixed bed reactor. The process was realized at 700 °C, nitrogen flowrate of 100 mL/min and catalyst to lignin ratio of 1. The products of liquid phase were analysed only by GC/MS

5 Lignin Pathway

5.1 The pathway of lignin fast pyrolysis coupled with in-situ catalytic upgrading

The lignin analysed in this project was provided by St1 and, because it is obtained as a by-product in the ethanol synthesis process from different wastes (bread, supermarket wastes), its structure was unknown at the beginning. However, several analyses in the Py-GC/MS were enough to find out that the lignin structure is a G-type (softwood lignin) due to the guaiacol compounds that were recorded with the highest area fraction. Some H-type compounds were also identified, but they could be derived directly from p-coumaryl alcohol unit or/and from coniferyl alcohol by removing the methoxy group.

In order to derive the pathway of the lignin which is exposed to a thermal treatment like fast pyrolysis and further to a catalytic upgrading, a set of model compounds was chosen. This was decided due to the complex structure of lignin which makes the analysis of the decomposition reactions very laborious. Thus, in order to simplify the deduction of the thermal decomposition pathway, the fast pyrolysis of each model compound was realized. These compounds were chosen from the analysis of the fast pyrolysis of lignin at different temperatures and especially the ones that were the most abundant based on the calculation of their area fraction. Of course, this way of investigation does not fully simulate the lignin thermal decomposition reactions as the initial linkages like β -O-4', α -O-4', 4-O-5', β - β' are not considered. However, this part will be discussed and modelled based on different other studies.

The model compounds chosen for the derivation of the lignin thermal decomposition pathway are listed in the [Figure 5.1](#). The fast pyrolysis of each compound was realized at 550 and 650 °C, as well as at 650 °C with an in-situ catalytic upgrading. As catalyst, HZSM-5 with SiO₂/Al₂O₃ ratio of 30 was selected due to its special deoxygenation properties. As it can be seen in the [Figure 5.1](#), all the compounds (A) obtained in the pyrolytic process highlight the structure of coniferyl alcohol (B), incorporating the methoxy group in the position 3 and the hydroxyl group in the position 4.

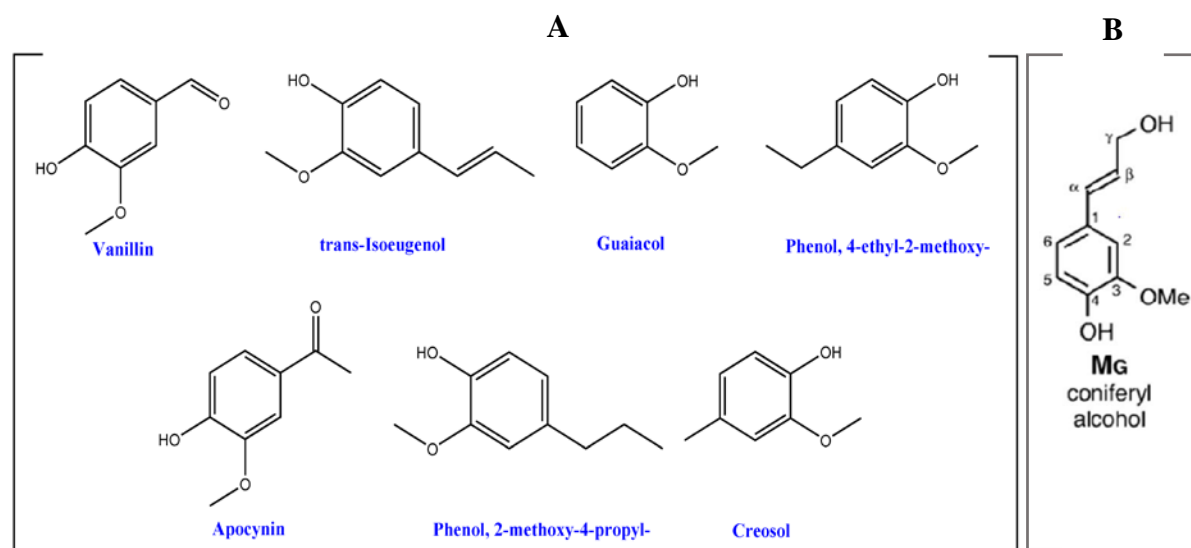


Figure 5.1 The name and structure of the seven lignin model compounds (A) and the coniferyl alcohol monolignol (B[11])

As it was mentioned in the Chapter 2, different model compounds were analysed by different researches. Klein and Virk [30] investigated the unsubstituted model compound called phenethyl phenyl ether (PPE) which contains the β -O-4. Choi, Singh [28] studied also α -O-4 besides β -O-4. This work also followed the effect of different substituents (-OH, -O-CH₃) on the thermal decomposition of PPE. Huang, Liu [29] studied the dissociation energies of the β -O-4 and other bonds of the 2-phenoxyphenyl-1, 3-propanediol. According to all results of the multitude of papers, the β -O-4 is the most sensitive linkage to thermal treatment as it was found to have the lowest dissociation energy. Herein, the model compound chosen is named 1 - (4-hydroxy-3-methoxyphenyl) - 2 - (2-methoxyphenoxy) propane-1,3-diol (Figure 5.2, A) and it was investigated by Choi, Singh [28]. It was selected due to the obtained pyrolytic products which highlight the G-type lignin unit. As a primary decomposition step of the compound A, the concerted retro-ene reaction was selected (Figure 5.3) because it was carefully analysed and found to be the most accurate way of β -O-4 fragmentation based on the overall mass balance and dissociation energy[28-30]. As it can be seen in the Figure 5.3, the product 4 can be easily converted into guaiacol-5 via tautomerization reaction because it is a more stable product. This can be supported by the high area fraction of guaiacol resulted in the fast pyrolysis of lignin and model compounds.

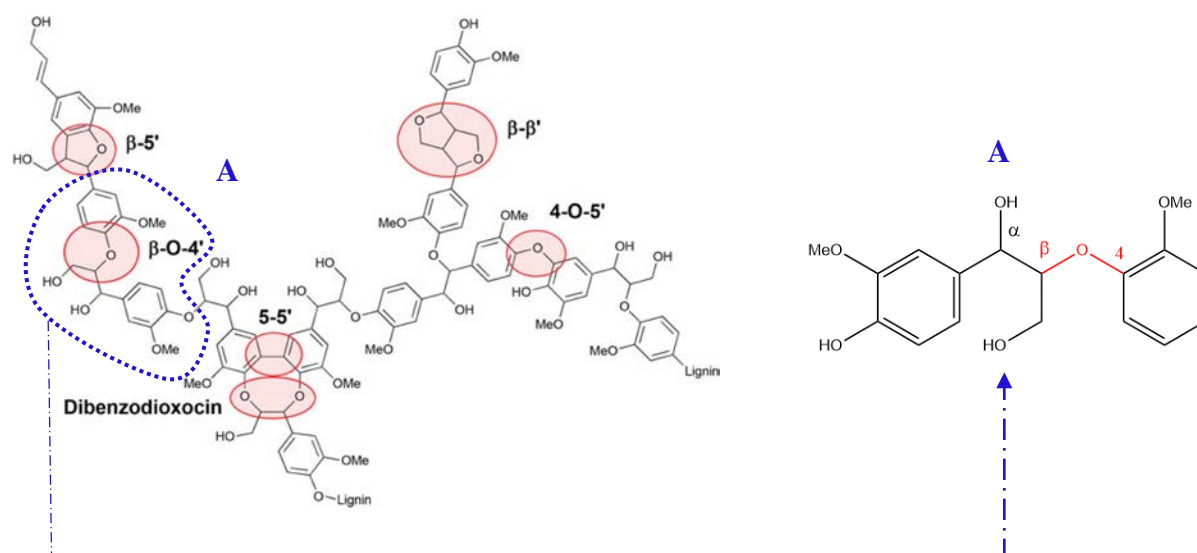


Figure 5.2 The main linkages of lignin network and the model lignin compound (A-1-(4-hydroxy-3-methoxyphenyl)-2-(2-methoxyphenoxy) propane-1,3-diol (Me: methyl group)

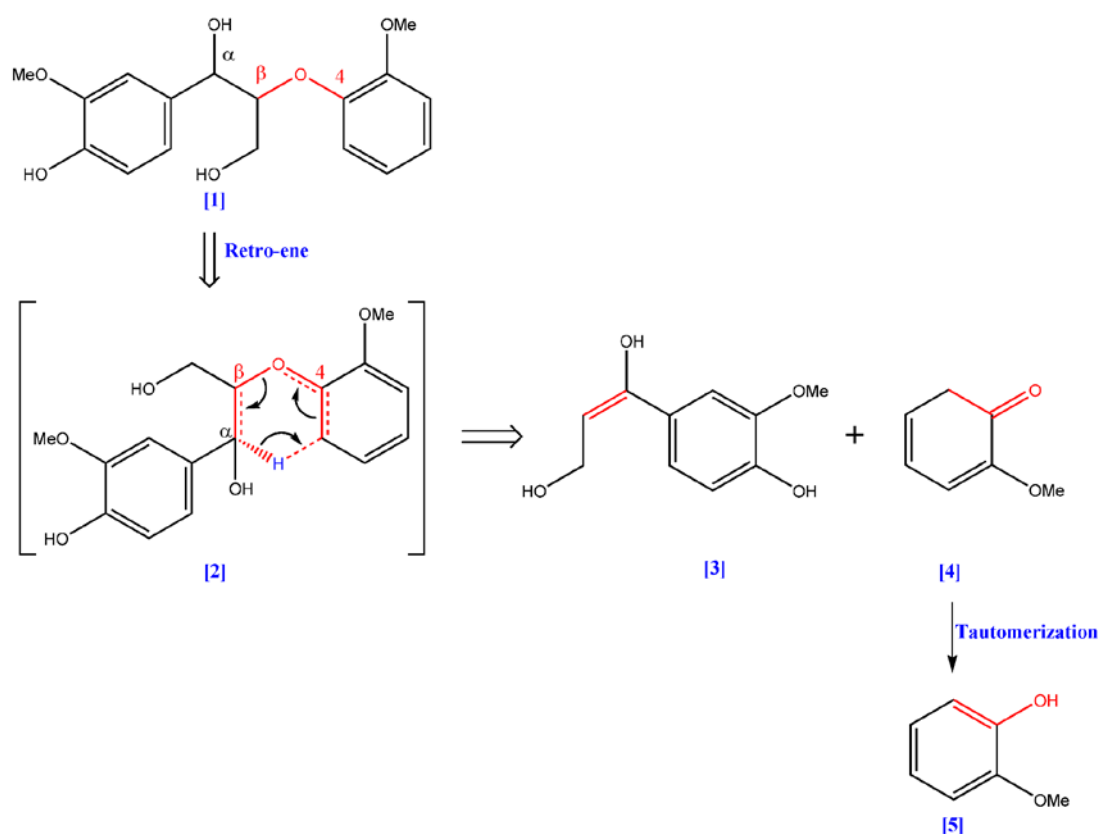


Figure 5.3 Concerted retro-ene (Alder-ene) fragmentation of 1-(4-hydroxy-3-methoxyphenyl)-2-(2-methoxyphenoxy) propane-1,3-diol -1

In the [Figure 5.4](#) are shown the formation steps of vanillin- [7](#), tran-Isoeugenol- [12](#), phenol, 4-ethyl-2-methoxy- [16](#), apocynin- [10](#), phenol, 2-methoxy-4-propyl- [14](#) and creosol- [19](#)

from the compound **3** (Figure 5.3) by following the pathways built up by Choi, Singh [28] and Huang, Liu [29]. As it can be seen, vanillin and apocynin are formed via the intermediate compound **6** that resulted from compound **3** through tautomerization reaction. By subtracting the acetaldehyde or ethylene oxide (oxirane) from the intermediate **6**, the vanillin is produced, while apocynin is formed through deformylation reaction [28, 29]. The trans-Isoeugenol and phenol, 2-methoxy-4-propyl- are formed directly from the compound **3** by subtracting the hydroxyl groups and hydrogenating the double bond in case of product **14**. The elimination of hydroxyl groups results in formation of water, especially from the enol group as Klein and Virk [100] support in their study. According to Choi, Singh [28], at high temperature the intermediate **6** also produces 3-(4-hydroxy-3-methoxyphenyl) propanal-**15** via dehydration, hydrogenation and tautomerization reactions, and 3-(4-hydroxy-3-methoxyphenyl) acetaldehyde-**18** via deformylation, hydroxylation, dehydration and tautomerization reactions. As these compounds are exposed to high temperature conditions, the decarbonylation reaction could occur and phenol, 4-ethyl-2-methoxy- **16** and creosol- **19** could be produced.

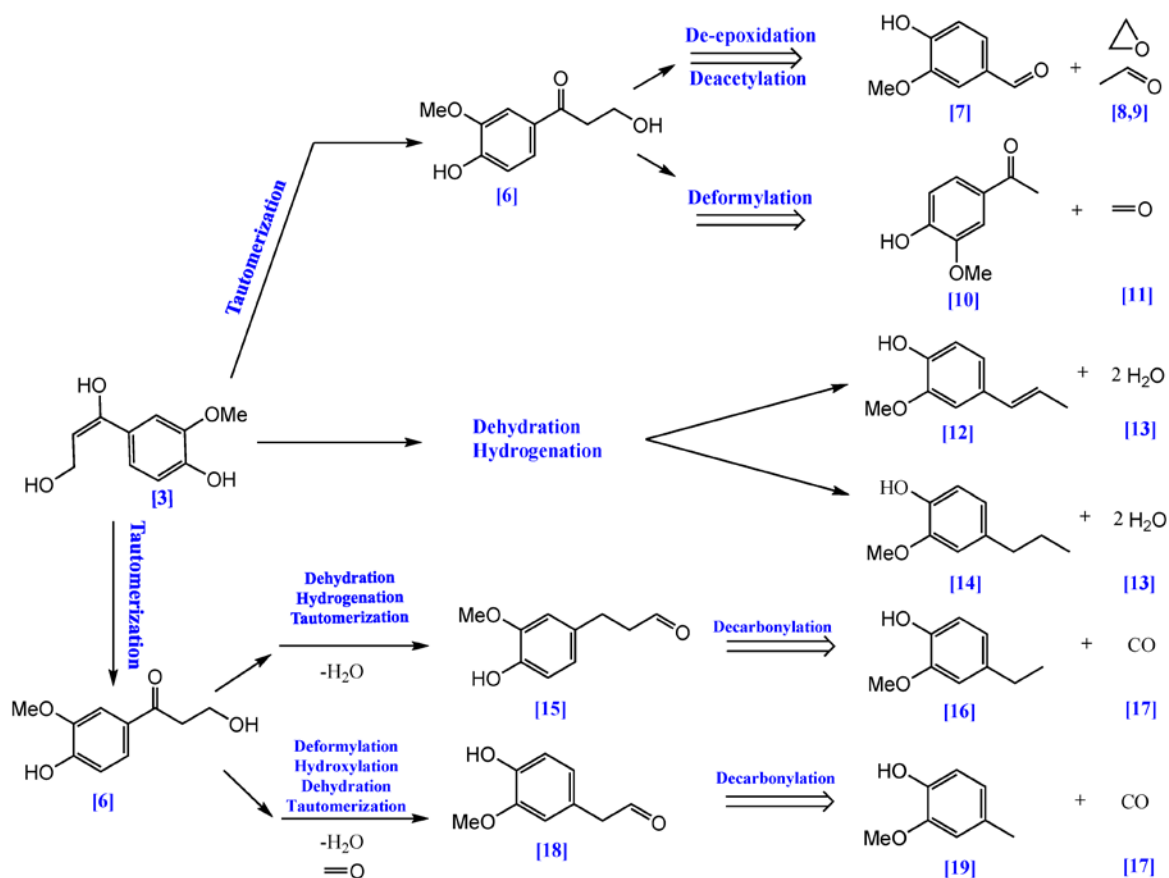


Figure 5.4 The synthesis reactions of vanillin-7, tran-Isoeugenol-12, phenol, 4-ethyl-2-methoxy- 16, apocynin- 10, phenol, 2-methoxy-4-propyl- 14, creosol- 19

Since now, the further development of lignin fast pyrolysis pathway is based on the experimental results obtained within this project, as well as on the results of other studies. As it was mentioned, each compound was exposed to high temperature conditions and to

a catalytic upgrading step. This means that three experiments were realized for each compound while keeping the mass constant (0.4 mg). The purity and the supplier of each reactant can be found in [Table 8.8, Appendix](#). All the compounds are discussed individually and a table with the area fraction expressed in percentage and the structure of each product are presented. Moreover, the pyrograms with the structures of the most abundant products are provided.

5.1.1 Guaiacol

The guaiacol, called also phenol, 2-methoxy-, is a quite thermal stable compound. As it can be seen in the pyrogram A ([Figure 5.5](#)), at 550°C it generates only few compounds with very low area fraction ([Table 5.1](#)). By increasing the temperature up to 650°C, the intensity of the peaks increases due to a higher conversion of guaiacol. According to Nowakowska, Herbinet [[114](#)]'s study, the O-CH₃ bond is the most thermal unstable bond which results in formation of catechol ([5²](#)) and methylcatechols ([5³](#), [5⁴](#)) via route [P1](#) ([Figure 5.6](#)). The catechol is produced in the highest amount (89%) from the radical [5¹](#) compared with methylcatechols because it is easy to stabilize by abstracting a hydrogen atom from another guaiacol molecule than interacting with a methyl radical that has a very short lifetime. This also can be seen in the [Table 5.1](#), the area fraction of catechol is 9% compared with area fraction of 1,2-benzenediol, 3-methyl- and 1,2-benzenediol, 4-methyl- that together recorded 1.7%. However, these percentages were recorded at 650 °C compared with Nowakowska, Herbinet [[114](#)]'s results that were obtained at 475 °C. Of course, this discrepancy could be related to the reactor type. Herein, the micropyrolyzer also included an inert gas flow that did not influence directly the lignin pyrolytic volatiles because they were formed inside of a special small vial which free-falls in the reactor. Whereas the jet-stirred reactor used by Nowakowska, Herbinet [[114](#)] involves a high turbulence of the injected gas and thus a homogeneous reaction atmosphere is assured. Based on other routes investigated by Nowakowska, Herbinet [[114](#)], benzaldehyde, 2-hydroxy- is the second most abundant product obtained via route [P2](#). Nevertheless, in this project, benzaldehyde, 2-hydroxy- is actually the most abundant product and again the reactor could be a reason of this difference. The phenol is also formed through route [P2](#), but also through route [P3](#) and it appears only at 650°C.

The fast pyrolysis process coupled with the catalytic upgrading of guaiacol was also studied in this project because HZSM-5 was found to have promising deoxygenation properties. In the [Figure 5.7](#) a general representation of the final routes is shown. In the pyrogram B ([Figure 5.5](#)) the peaks at 650 °C and 650 °C-HZSM-5 are presented and it can be seen that the catalyst enhanced the conversion of the guaiacol and products obtained via routes [P1](#), [P2](#) and [P3](#). The phenol area fraction is increased in the presence of the catalyst and this could be because of the intensified decarbonylation of benzaldehyde, 2-hydroxy-, and the deformylation of guaiacol. If analysing the [Table 5.1](#), it can be seen that the area fractions of catechol and methylcatechols are also promoted by the Brønsted acid sites of HZSM-5. Phenol, 2-methyl-, p-cresol and phenol, 2,4-dimethyl- also record a relative high area fraction and they could result directly from guaiacol. The first one is also obtained by Nowakowska, Herbinet [[114](#)], but the formation of the second and third compound is also possible as they were obtained in the FP-CU process. Moreover, the -OH is a very strong activator of ortho and para positions of the phenolic ring and this means that the hydrogen atoms can be easily substituted, in this case by methyl groups [[115](#)]. Besides of all the phenolic compounds and catechols, the monoaromatic hydrocarbons (MAH) are also

produced in the catalytic upgrading step and, as it can be observed in the [Table 5.1](#), the BTX group dominates. The benzene could be produced from all phenolic compounds, while toluene could result with high probability from p-cresol, methylcatechols or phenol, 2,4-dimethyl- as these compounds have the methyl group in their structure. In case of p-xylene, it could be produced from p-cresol, 1,2-benzenediol, 4-methyl- or phenol, 2,4-dimethyl- due to the methyl group in the para position. The diaromatic and polyaromatic hydrocarbons are promoted at temperatures higher than 700 °C. They are formed by successively adding the C₂ species like ethyne to the already formed MAH[116]. This route is enhanced by the acidic sites of the catalyst. In case of HZSM-5, it suppresses the formation of coke promoters due to its small pore size.

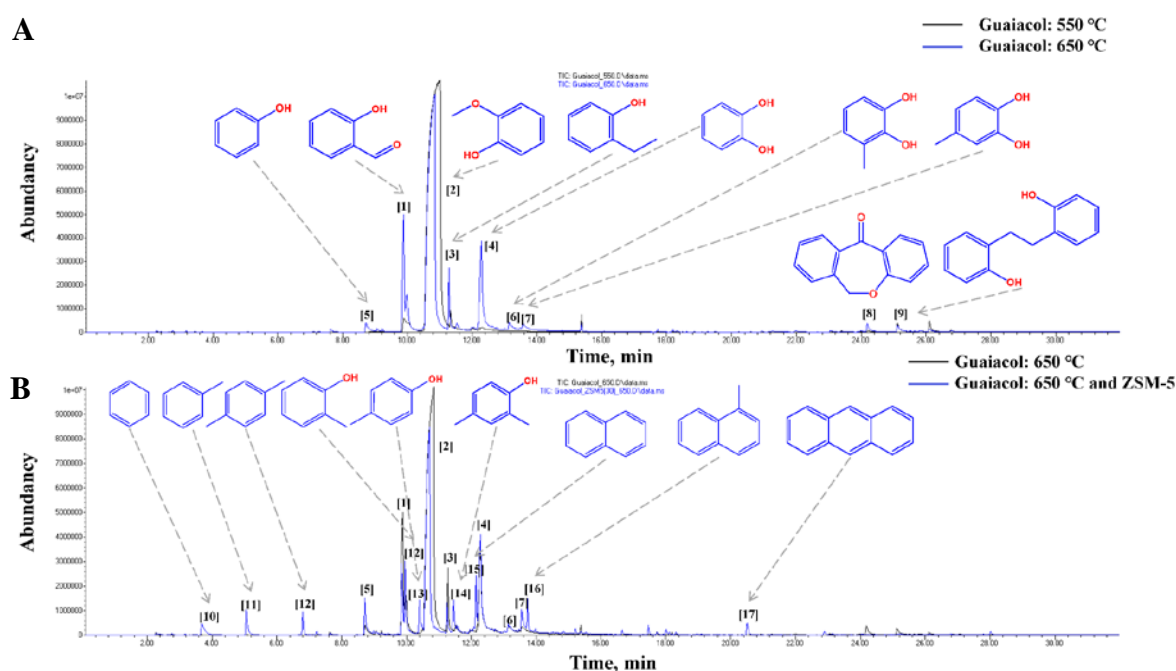
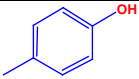
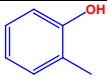
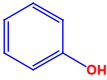
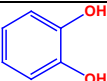
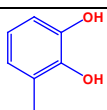
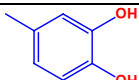
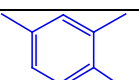
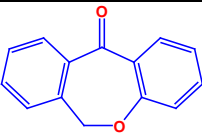
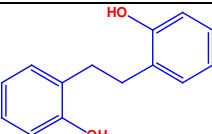

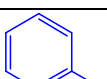
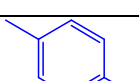
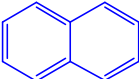


Figure 5.5 Guaiacol: the overlapped 550 °C and 650 °C pyrograms (A) and 650 °C and 650 °C-HZSM-5 pyrograms (B)

Name	Structure	Area fraction (%)		
		550 °C	650 °C	650 °C, HZSM-5(30)
Benzaldehyde, 2-hydroxy-	<chem>Oc1ccccc1C=O</chem>	2.96	13.95	5.30
Guaiacol	<chem>COc1cc(O)ccc1</chem>	94.21	69.56	47.78
Phenol, 2-ethyl-	<chem>CCc1ccccc1O</chem>	2.14	2.78	1.85

Name	Structure	Area fraction (%)		
		550°C	650°C	650°C, HZSM- 5(30)
p-Cresol				3.23
Phenol, 2-methyl-				4.58
Phenol			1.21	3.73
Catechol			9.08	13.19
1,2-Benzenediol, 3-methyl-			1.01	1.26
1,2-Benzenediol, 4-methyl-			0.70	2.14
Phenol, 2,4- dimethyl-				3.04
Dibenz[b,e]oxepin- 11(6H)-one			0.91	
2,2'- Ethylenediphenol			0.79	
Carbon dioxide	$O=C=O$			0.51
Benzene				2.66
Toluene				3.02
p-Xylene				1.49
Naphthalene				2.67

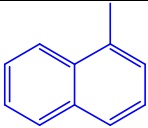
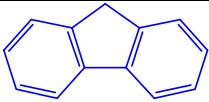
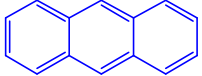
Name	Structure	Area fraction (%)		
		550°C	650°C	650°C, HZSM- 5(30)
Naphthalene, 1-methyl-				1.57
Fluorene				0.62
Anthracene				1.39

Table 5.1 The guaiacol fast pyrolysis and fast pyrolysis coupled with catalytic upgrading products

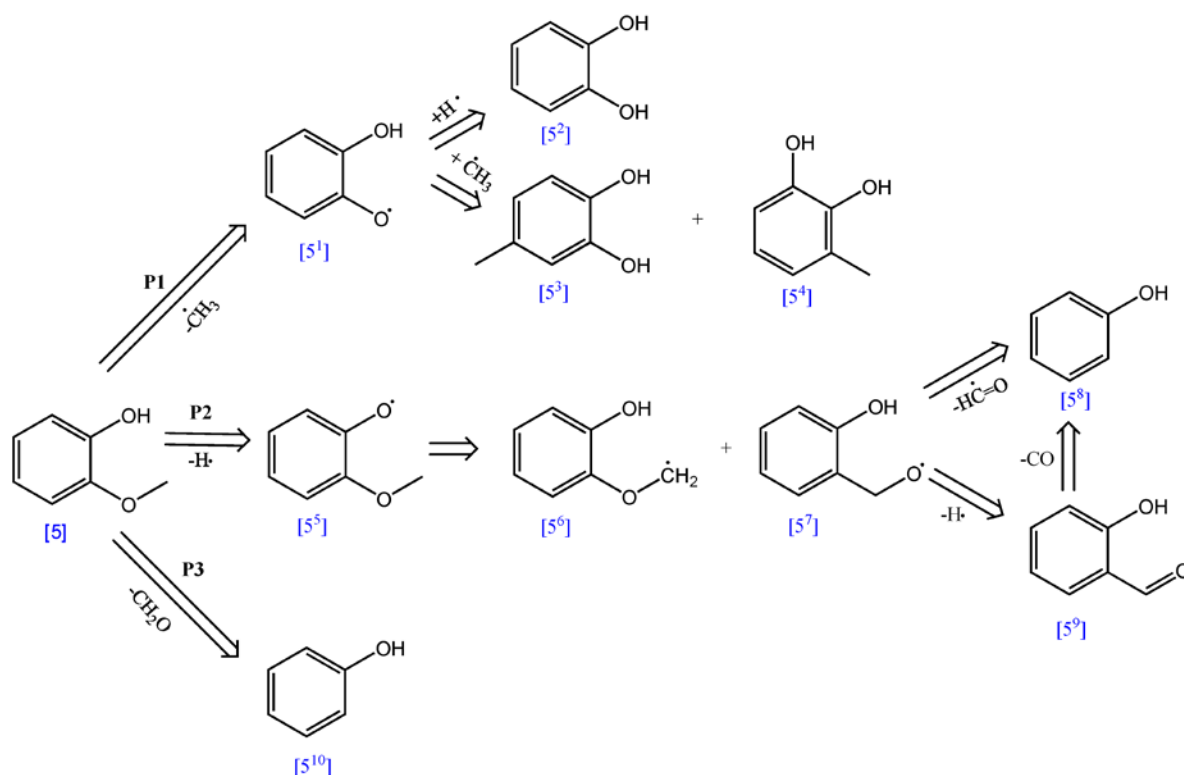


Figure 5.6 The guaiacol fast pyrolysis pathway

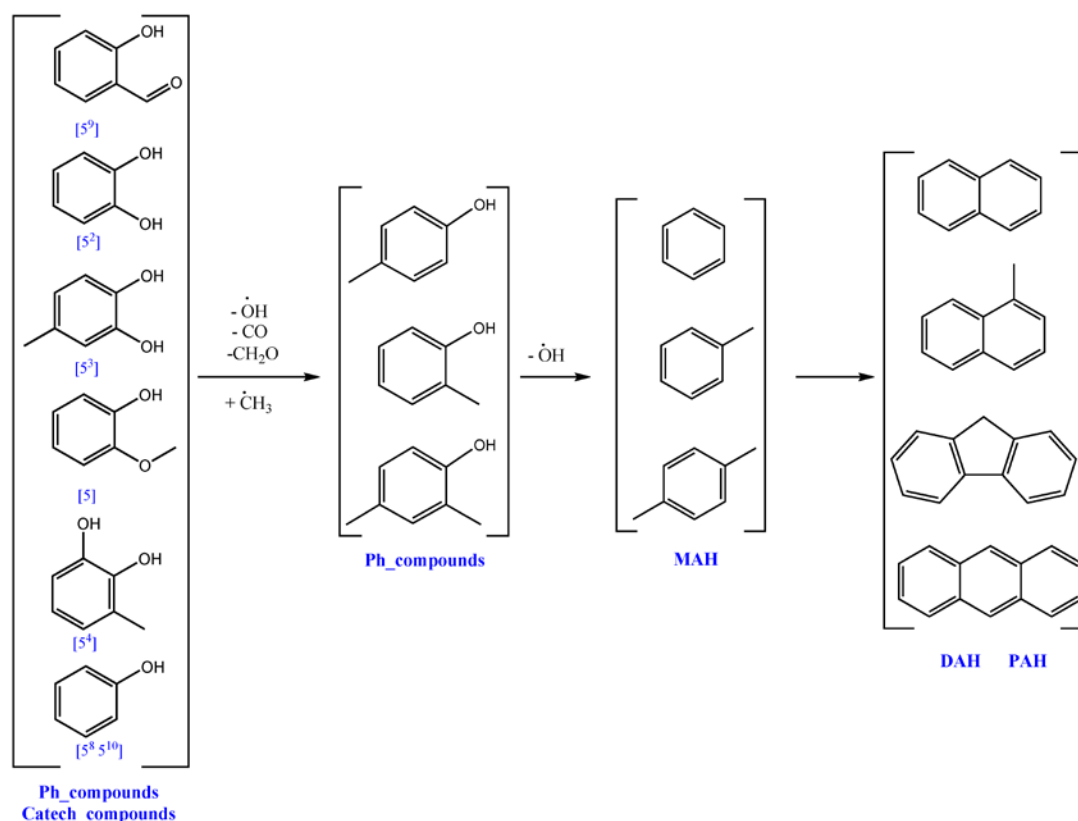


Figure 5.7 The pathway of guaiacol in the fast pyrolysis process coupled with the catalytic upgrading (HZSM-5 with $\text{SiO}_2/\text{Al}_2\text{O}_3=30$)

5.1.2 Creosol

The creosol compound is also called p-methylguaiacol and, by comparing its structure with the guaiacol structure, the methyl substituent located in the para position makes it to differ from guaiacol by a methylene group, thus it can be said that creosol and guaiacol are homologues. According to this, the routes of the creosol fast pyrolysis were decided to be performed in accordance with the pathway of guaiacol. This can be supported by the products distribution obtained in the three experiments of creosol. By analysing the 550 and 650 °C overlapped pyrograms (Figure 5.8), as well as the Table 5.2, it can be seen that 1,2-benzenediol, 4-methyl- (19²), p-cresol- (19⁶, 19⁸) and 2 - hydroxy- 5 - methylbenzaldehyde - (19⁷) are characterized by a high area fraction. The 19² compound is also formed at 550 °C compared with the other two products and this could be because of the route P1 (Figure 5.9) that manifests the highest consumption of creosol. The phenol, 3,5-dimethyl- also recorded a high area fraction, but its formation route is unknown. Of course, if assuming that before cracking the $-\text{O}-\text{CH}_3$ group, it could activate the ortho and para positions and so they could be substituted by the methyl and hydroxyl groups. This is possible only if the hydroxyl group is not already positioned and this is because of its stronger activating properties compared to the alkoxy group. Phenol, 2-ethyl-6-methyl- is also described by a large peak area and its formation is very likely considering that the methyl and ethyl group are located on the positions activated by hydroxyl group.

The general pathway of creosol fast pyrolysis coupled with the catalytic upgrading is shown in the Figure 5.10. As it can be seen, the compounds resulted at 650 °C could be converted to phenol, 2-methyl-, as well as to p-cresol because its area fraction increased in the presence of catalyst, while the area fraction of 2-hydroxy-5-methylbenzaldehyde decreased. According to this, it is very likely that the decarbonylation reaction of the last compound occurred and the p-cresol was produced. All the products resulted in the fast pyrolysis of creosol and in the presence of the catalyst are likely to generate MAH and subsequently DAH and PAH.

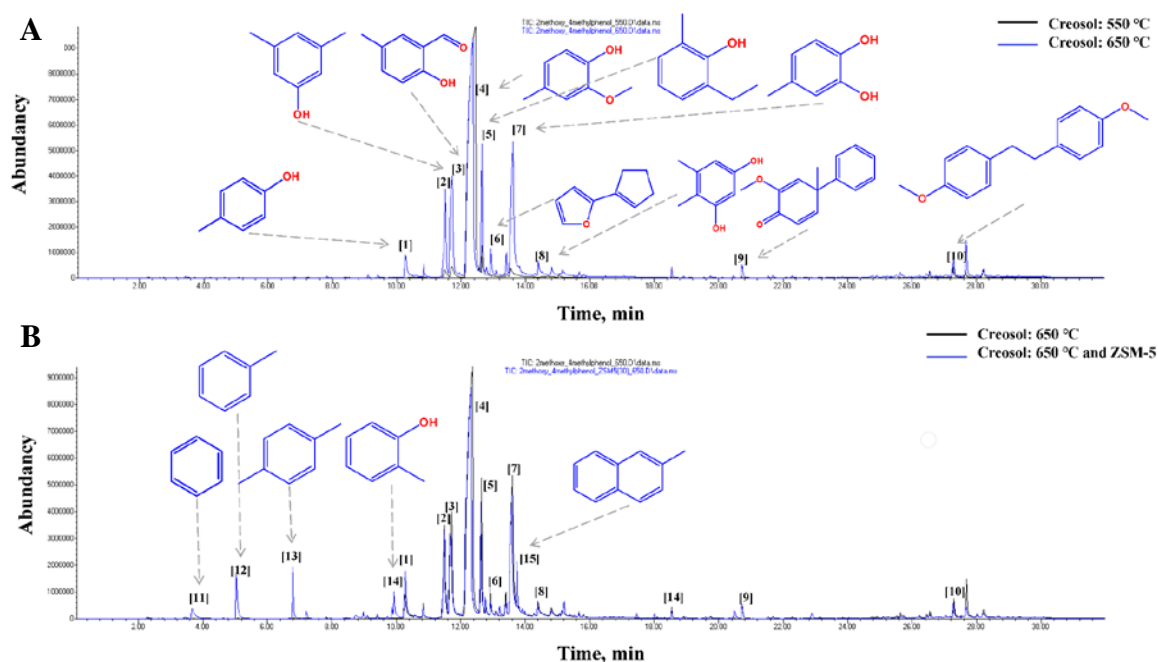
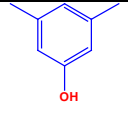
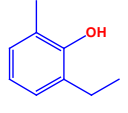
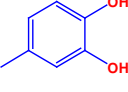
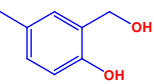
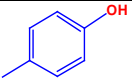
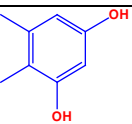
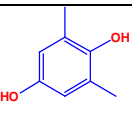
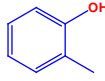
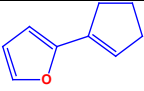
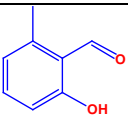
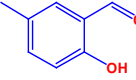
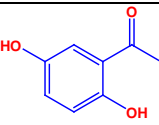
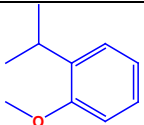
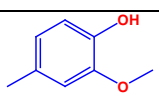
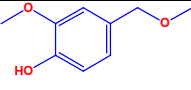
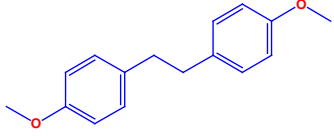
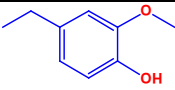


Figure 5.8 Creosol: the overlapped 550 °C and 650 °C pyrograms (A) and 650 °C and 650 °C-HZSM-5 pyrograms (B)

Name	Structure	Area fraction (%)		
		550 °C	650 °C	650 °C, HZSM-5(30)
Phenol, 3,5-dimethyl-		1.24	5.64	7.68
Phenol, 2-ethyl-6-methyl-		3.76	6.34	5.88
1,2-Benzenediol, 4-methyl-		3.17	17.00	12.68

Benzenemethanol, 2-hydroxy-5- methyl-		0.52		
p-Cresol			2.16	3.91
1,3-Benzenediol, 4,5-dimethyl-			3.30	0.93
1,4-Benzenediol, 2,6-dimethyl-			1.31	
Phenol, 2-methyl-				1.49
2-(1- Cyclopentenyl)furan			1.41	0.94
Benzaldehyde, 2- hydroxy-6-methyl-		2.18		
2-Hydroxy-5- methylbenzaldehyde			11.19	9.73
Ethanone, 1-(2,5- dihydroxyphenyl)-		0.51		
o-Isopropylanisole			0.76	
Creosol		86.96	45.36	42.14
Phenol, 2-methoxy- 4-(methoxymethyl)-		0.67		
Bibenzyl, 4,4'- dimethoxy-		0.98	0.95	
Phenol, 4-ethyl-2- methoxy-			1.26	

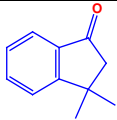
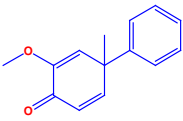
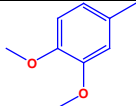
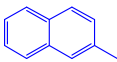
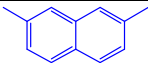
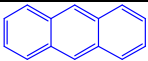
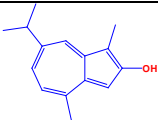
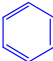
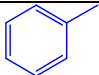
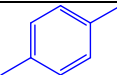
1H-Inden-1-one, 2,3-dihydro-3,3- dimethyl-		1.91
2-Methoxy-4- methyl-4-phenyl- 2,5-cyclohexadien- 1-one		0.74
3,4- Dimethoxytoluene		0.94
Naphthalene, 2- methyl-		2.79
Naphthalene, 2,7- dimethyl-		0.67
Anthracene		0.64
Azulen-2-ol, 1,4- dimethyl-7-(1- methylethyl)-		0.85
Benzene		1.48
Toluene		3.11
p-Xylene		2.14

Table 5.2 The creosol fast pyrolysis and fast pyrolysis coupled with catalytic upgrading products

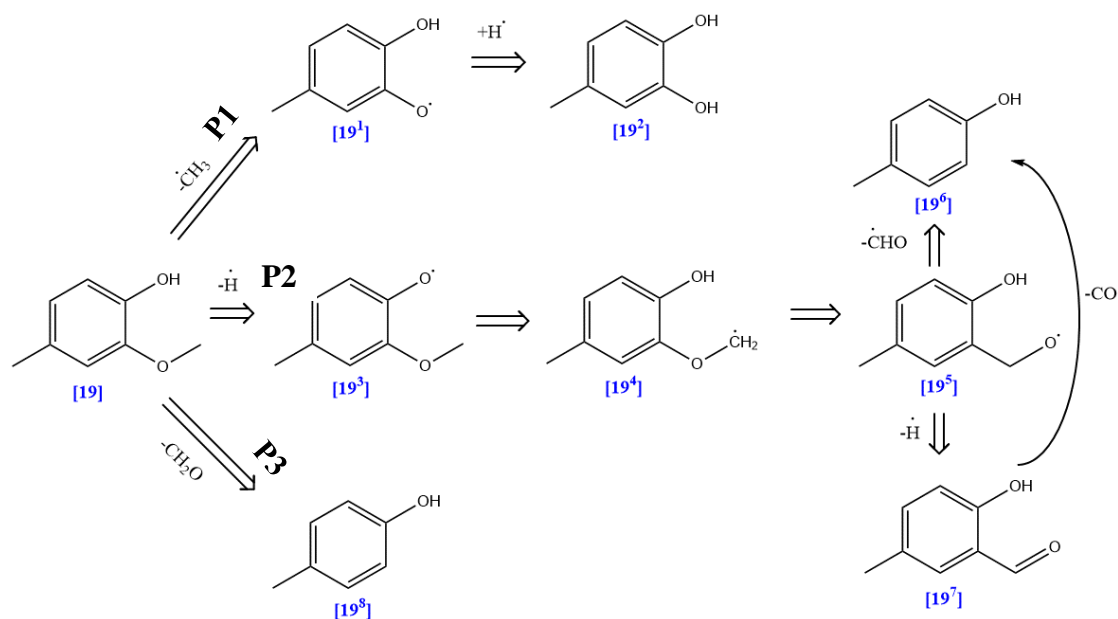


Figure 5.9 The creosol fast pyrolysis pathway

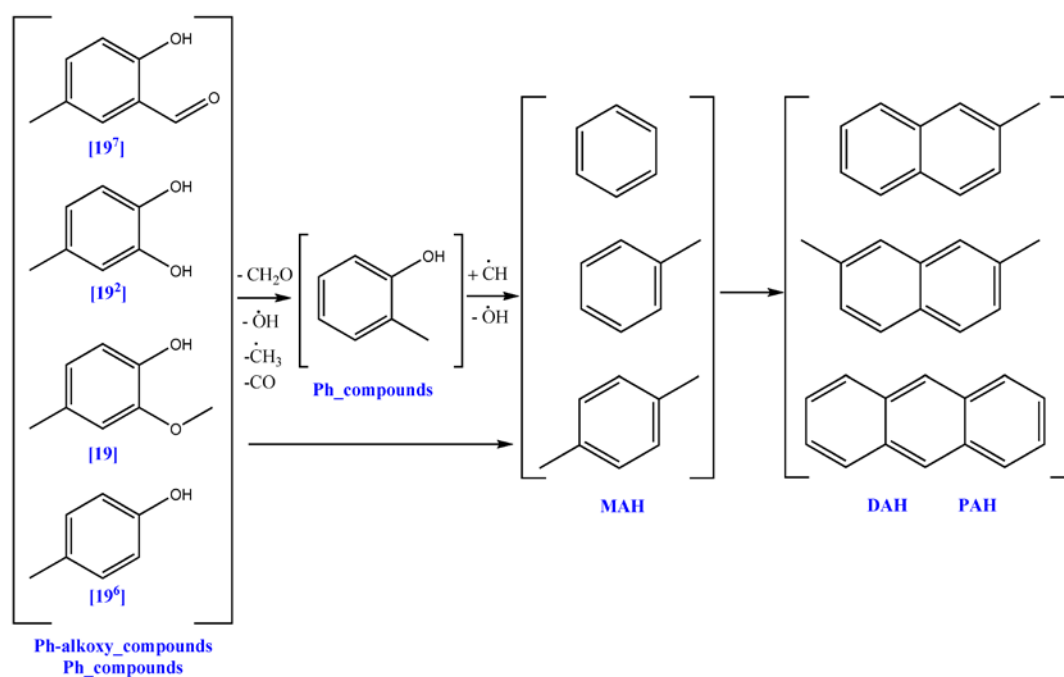


Figure 5.10 The pathway of creosol in the fast pyrolysis process coupled with the catalytic upgrading (HZSM-5 with $\text{SiO}_2/\text{Al}_2\text{O}_3=30$)

5.1.3 Phenol, 4-ethyl-2-methoxy-

The phenol, 4-ethyl-2-methoxy- is also called p-ethylguaicol and according to its structure, it is part of the homologous series with guaiacol and creosol. Based on this, the same routes for 4-ethyl-2-methoxy- fast pyrolysis were applied. The pyrograms and the

table with the resulted products and their area fraction are given in [Figure 5.11](#) and [Table 5.3](#). It can be seen that 4-ethylcatechol and phenol, 4-ethyl- recorded a quite high area fraction and according to the [Figure 5.12](#), they are formed via [P1](#) and [P4](#) routes. In the [Table 5.3](#) it can be seen that ethanone, 1-(2-hydroxy-5-methylphenyl)- [16¹⁰](#) is also characterized by a high area fraction. Its formation route is unknown, but it could be produced via [P4](#) route ([Figure 5.12](#)) from the 2-hydroxy-5-ethylbenzaldehyde- [16⁹](#) which was not identified in the pyrolytic products. The 2-methoxy-4-vinylphenol registered an area fraction of 2.6 % at 650 °C and it could occur through the dehydrogenation step of phenol, 4-ethyl-2-methoxy-. This is very likely due to the hydrogen atoms of the ethyl group which can be easily accessed by the formed radicals compared with the hydrogen atoms of alkoxy and hydroxy groups. Benzene, 1-ethyl-4-methoxy- and benzene, 1-butyl-4-methoxy- were also defined by a relative high peak area. Their formation mechanism has not been found yet, but the first one could be formed by abstracting the alkoxy group and the hydrogen from the hydroxy group and further by stabilizing the molecule, a reaction with a methyl group could occur. The second one could follow the same route with further extension of the ethyl chain with an other one.

The fast pyrolysis with an in-situ catalytic upgrading step of phenol, 4-ethyl-2-methoxy- recorded a quite high area fraction for phenolic compounds like phenol, phenol, 2-methyl-, p-cresol and phenol, 2-ethyl-6-methyl-. Their structures are presented in the general pathway shown in the [Figure 5.13](#). Based on the results presented in the [Table 5.3](#), the area fraction of phenol, 4-ethyl- is slightly decreased when using the catalyst. It could be converted into p-cresol and phenol. The area fraction of 4-ethylcatechol also decreases when using the HZSM-5. It could be consumed in the formation of all phenolic compounds ([Ph_compounds](#), [Figure 5.13](#)).

Monoaromatic hydrocarbons (MAH) are also formed on the acidic sites of the HZSM-5 and they could be derived from the phenolic compounds formed in the pyrolytic process and in the pyrolytic process assisted by the catalytic improvement. The area fraction of the DAH and PAH obtained from phenol, 4-ethyl-2-methoxy- is much higher compared with the ones obtained from guaiacol and creosol. This could be because of the ethyl group that, at high temperature and in the presence of the catalytic acidic sites, produced more acetylene. Thus, the DAH and PAH could be formed via the same mechanisms specified in the guaiacol and creosol discussion parts.

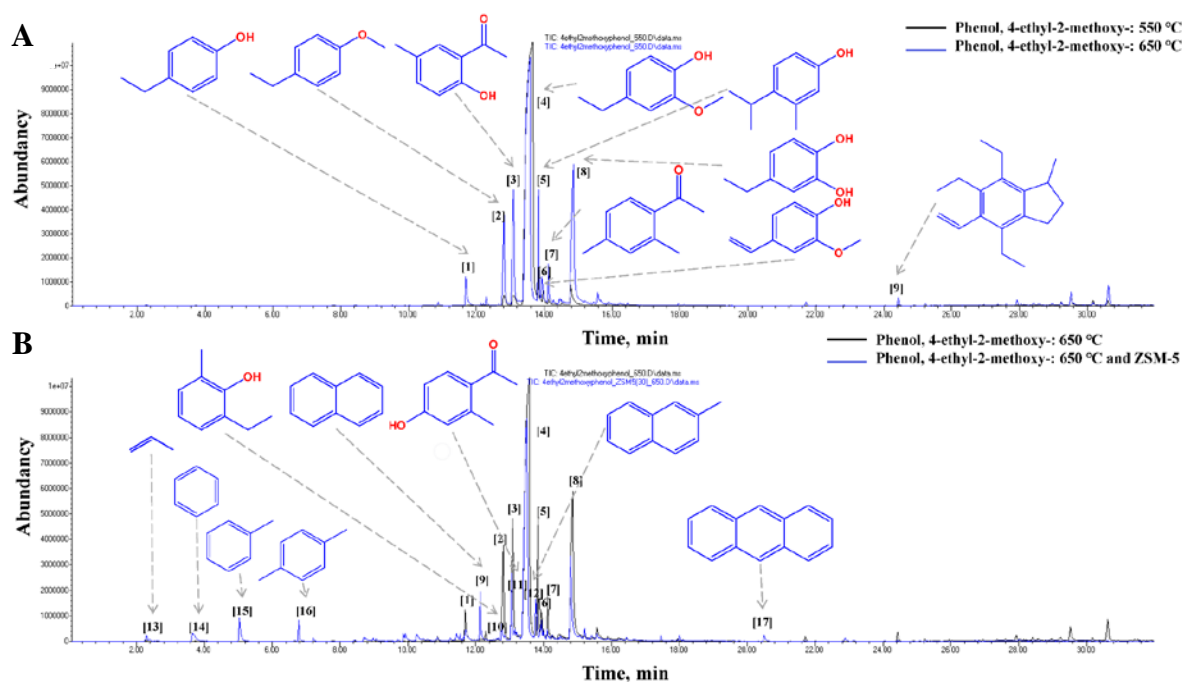
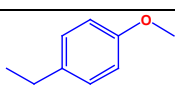
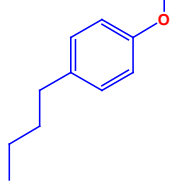
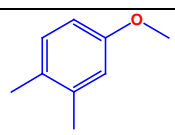
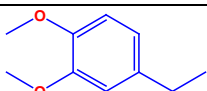
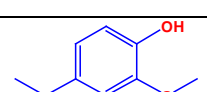
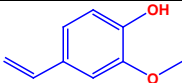
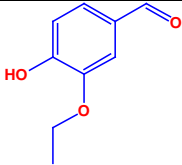
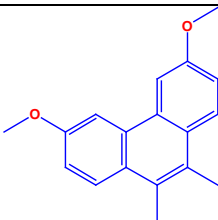
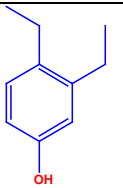
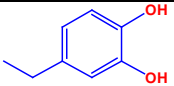
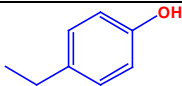
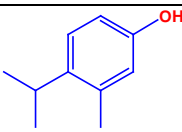
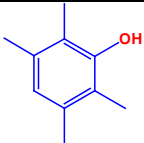
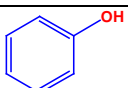
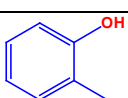
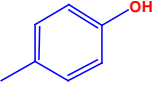
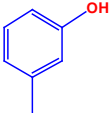
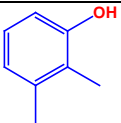
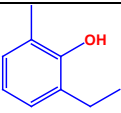
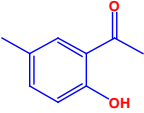
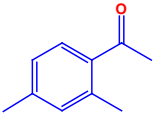
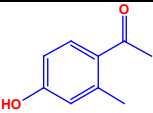
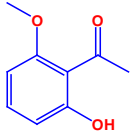
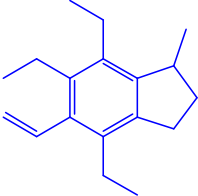
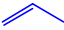
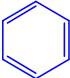
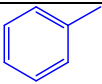


Figure 5.11 Phenol, 4-ethyl-2-methoxy-: the overlapped 550 °C and 650 °C pyrograms (A) and 650 °C and 650 °C-HZSM-5 pyrograms (B)

Name	Structure	Area fraction (%)		
		550° C	650° C	650° C, HZSM- 5(30)
Benzene, 1-ethyl- 4-methoxy-		1.50	6.53	
Benzene, 1-butyl- 4-methoxy-			1.57	
3,4- Dimethylanisole				0.47
Benzene, 4-ethyl- 1,2-dimethoxy-				1.13
Phenol, 4-ethyl-2- methoxy-		91.45	48.95	51.09

Name	Structure	Area fraction (%)		
		550° C	650° C	650° C, HZSM- 5(30)
2-Methoxy-4-vinylphenol			2.60	
Ethyl Vanillin			0.49	
Phenanthrene, 3,6-dimethoxy- 9,10-dimethyl-		0.45		
3,4-Diethylphenol		1.97		
4-Ethylcatechol		2.79	18.27	11.63
Phenol, 4-ethyl-			2.23	1.53
3-Methyl-4-isopropylphenol			5.94	
Phenol, 2,3,5,6-tetramethyl-				0.62
Phenol				1.05
Phenol, 2-methyl-				1.04

Name	Structure	Area fraction (%)		
		550° C	650° C	650° C, HZSM- 5(30)
p-Cresol				1.09
Phenol, 3-methyl-				0.60
Phenol, 2,3-dimethyl-				0.68
Phenol, 2-ethyl-6-methyl-				1.34
Ethanone, 1-(2-hydroxy-5-methylphenyl)-		1.8	10.60	
Ethanone, 1-(2,4-dimethylphenyl)-			2.24	
4-Hydroxy-2-methylacetophenone				5.65
Ethanone, 1-(2-hydroxy-6-methoxyphenyl)-				0.87
Benzocyclopentene, 4,6,7-triethyl-1-methyl-5-vinyl-			0.58	
Propene				0.81
Benzene				2.25
Toluene				2.87

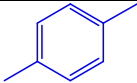
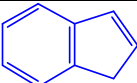
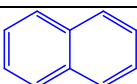
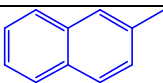
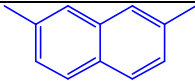
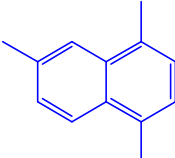
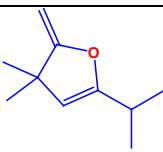
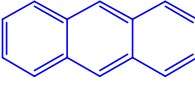

Name	Structure	Area fraction (%)		
		550° C	650° C	650° C, HZSM- 5(30)
p-Xylene				1.69
Indene				0.55
Naphthalene				3.75
Naphthalene, 2-methyl-				4.22
Naphthalene, 2,7-dimethyl-				0.90
Naphthalene, 1,4,6-trimethyl-				1.14
5-Isopropyl-3,3-dimethyl-2-methylene-2,3-dihydrofuran				1.63
Anthracene				0.93
Phenanthrene, 2-methyl-				0.47

Table 5.3 The phenol, 4-ethyl-2-methoxy- fast pyrolysis and fast pyrolysis coupled with catalytic upgrading products

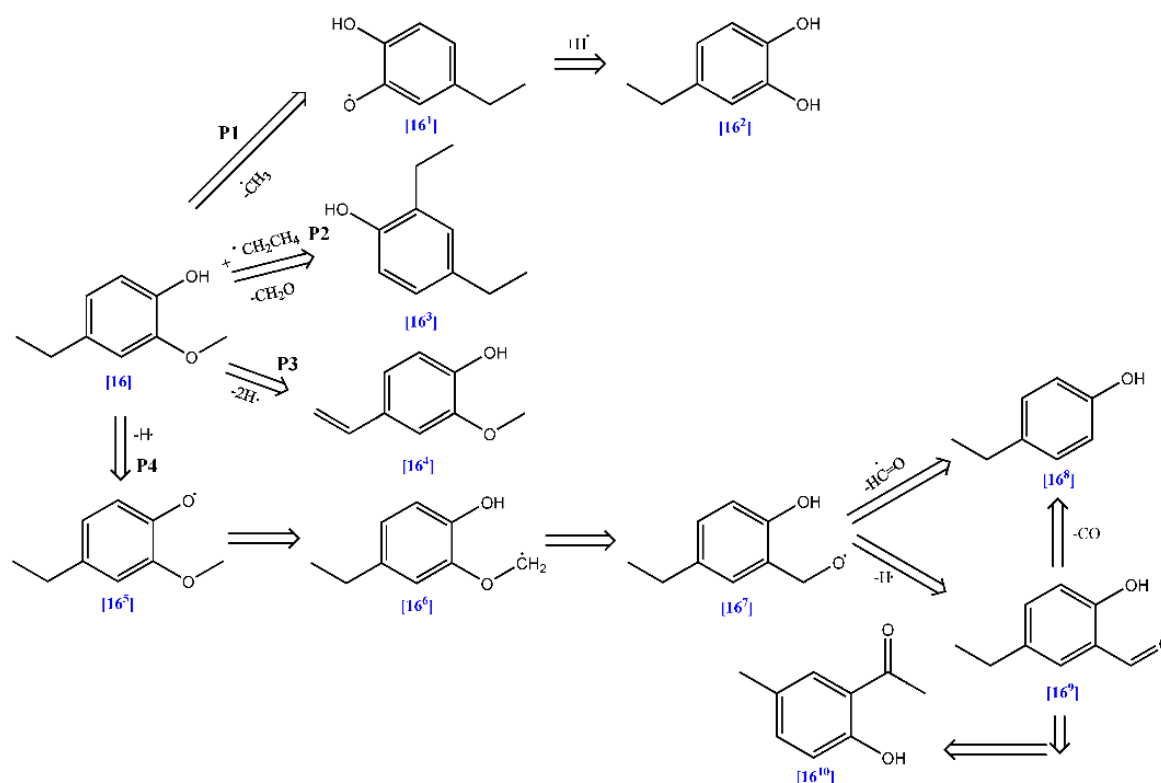


Figure 5.12 The phenol, 4-ethyl-2-methoxy- fast pyrolysis pathway

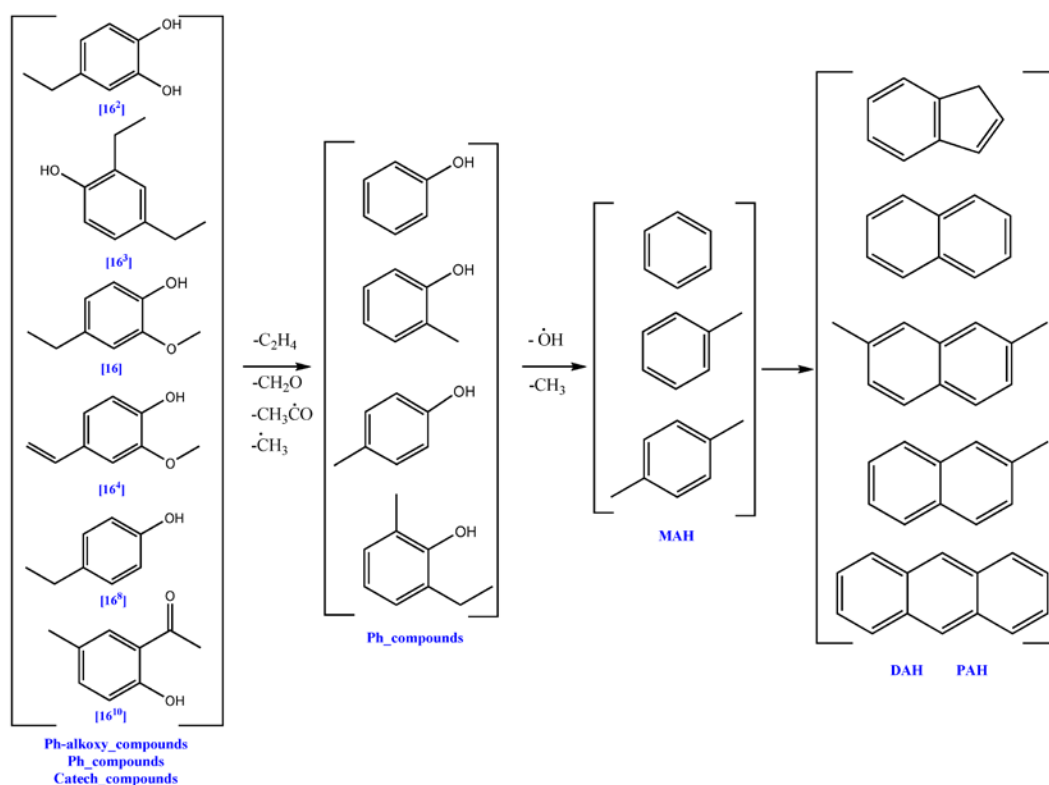


Figure 5.13 The pathway of phenol, 4-ethyl-2-methoxy- in the fast pyrolysis process coupled with the catalytic upgrading (HZSM-5 with $\text{SiO}_2/\text{Al}_2\text{O}_3=30$)

5.1.4 Phenol, 2-methoxy-4-propyl-

The other name of phenol, 2-methoxy-4-propyl- is p-propylguaiacol and it can be said without any doubt that it is part of the homologous series consisted of guaiacol, creosol and phenol, 4-ethyl-2-methoxy-. According to this, the formation routes of the pyrolytic products obtained in this project were kept the same. The pyrogram and the area fraction (%) are presented in the [Figure 5.14](#) and [Table 5.4](#). By following the route [P1](#) from [Figure 5.15](#), the 1,2-benzenediol, 4-propyl- [14²](#) should be obtained. However, its structural isomer 1,3-benzenediol, 4-propyl- was identified with a large area fraction, especially at 650°C. This can not be explained accurately, but it could happen because of the GC/MS instrument that probably considering the same spectra of the isomers, as well as the retention time, the proposed product name could be confused. According to Nowakowska, Herbinet [\[114\]](#), the route [P2](#) should result in formation of 2-hydroxy-5-propylbenzaldehyde-, but only phenol, 4-propyl- [14⁸](#) was detected via this path. Based on the high area fraction of other compounds that were obtained in the pyrolytic process of phenol, 2-methoxy-4-propyl-, it was assumed that these products could be produced via the radical [14³](#) of route [P2](#). For example, 1,3-benzodioxole, 5-propyl- [14⁴](#) could be obtained from radical [14³](#) by simply abstracting a hydrogen atom from the alkoxy group by another radical and then stabilizing through formation of a new C-O bond. The benzene, 1-methoxy-4-propyl- [14⁵](#) and benzene, 1-methoxy-4-(1-methylpropyl)- [14⁶](#) are also identified with a high area fraction and the assumed mechanism discussed in the phenol, 4-ethyl-2-methoxy- section could be applied in the case of these two products. The same can be said regarding the formation of 2-methoxy-4-vinylphenol, as it could form through hydrogenation step of phenol, 2-methoxy-4-propyl- ([P3](#)).

The fast pyrolysis coupled with the catalytic upgrading of phenol, 2-methoxy-4-propyl- resulted in formation of different phenolic compounds, aromatic hydrocarbons, as well as some phenol-alkoxy compounds ([Figure 5.16](#), [Table 5.4](#)). The phenolic compounds like phenol, phenol, 2-methyl-, p-cresol, 2-methyl-6-propylphenol could form from the compounds presented in the first column of [Figure 5.16](#) by cracking the propyl chain or alkoxy group and reacting with other radicals like methyl or propyl groups. As it can be seen, the guaiacol is also formed when the catalyst is used by simply subtracting the propyl chain. This route can be supported by the presence of propene in the products distribution. Of course, the formation of the aromatic hydrocarbons is assumed to be the same as for the previous discussed lignin model compounds.

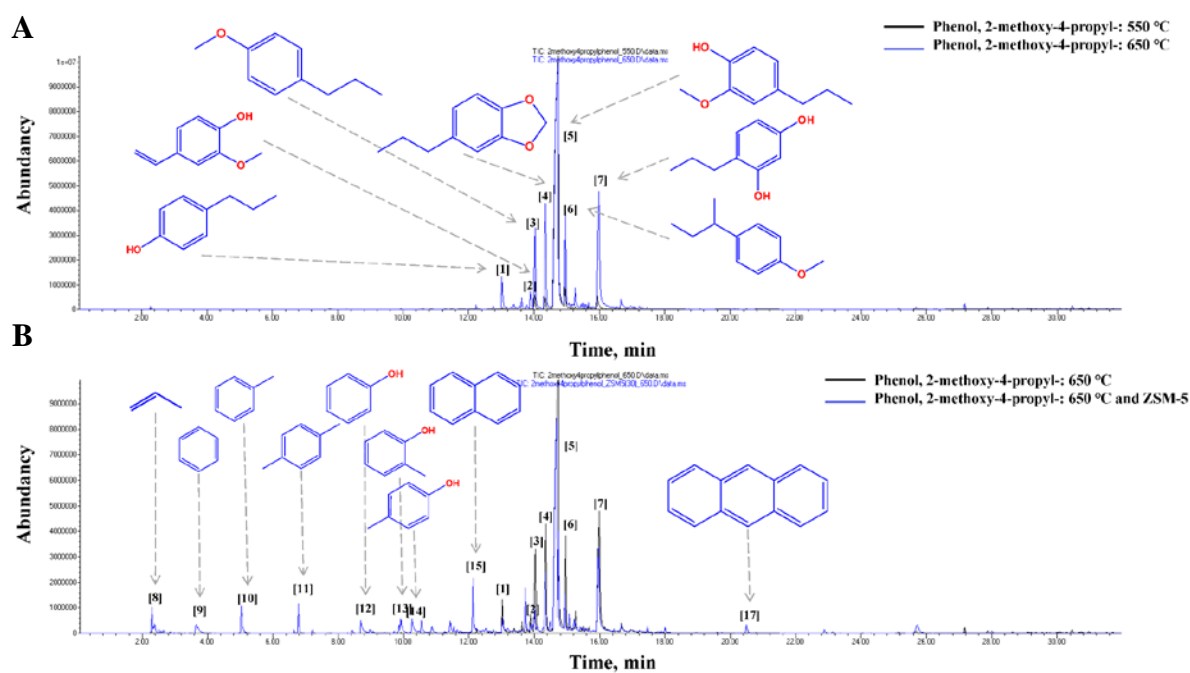
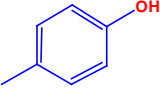
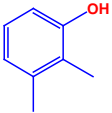
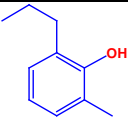
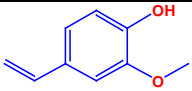
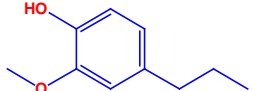
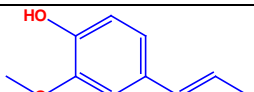
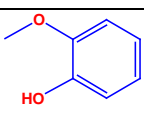
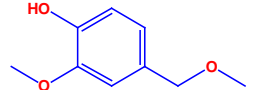
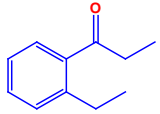
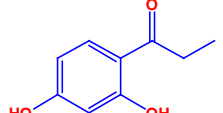
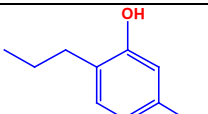
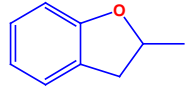


Figure 5.14 Phenol, 2-methoxy-4-propyl-: the overlapped 550 °C and 650 °C pyrograms (A) and 650 °C and 650 °C-HZSM-5 pyrograms (B)

Name	Structure	Area fraction (%)		
		550 °C	650 °C	650 °C, HZSM-5(30)
Benzene, 1-methoxy-4-propyl-		1.86	6.30	1.91
Benzene, 1-methoxy-4-(1-methylpropyl)-		3.33	5.68	2.45
1,2-Dimethoxy-4-n-propylbenzene				1.74
1,3-Benzodioxole, 5-propyl-		1.84	9.03	5.12
Phenol, 4-propyl-			3.62	2.07
Phenol				2.06
Phenol, 2-methyl-				1.61

Name	Structure	Area fraction (%)		
		550°C	650°C	650°C, HZSM- 5(30)
p-Cresol				1.96
Phenol, 2,3-dimethyl-				1.00
2-Methyl-6-propylphenol				0.70
2-Methoxy-4-vinylphenol			1.39	0.80
Phenol, 2-methoxy-4-propyl-		88.78	56.68	41.00
trans-Isoeugenol		0.72		0.52
Phenol, 2-methoxy-				1.14
Phenol, 2-methoxy-4-(methoxymethyl)-				1.23
2'-Ethylpropiophenone		0.90	1.23	
2',4'-Dihydroxypropiophenone			1.07	
1,3-Benzenediol, 4-propyl-		2.56	16.02	10.57
Benzofuran, 2,3-dihydro-2-methyl-				0.87

Name	Structure	Area fraction (%)		
		550°C	650°C	650°C, HZSM- 5(30)
Fluorene				0.95
Anthracene				1.04
Phenanthrene, 2-methyl-				0.53
Indene				0.57
Naphthalene				4.27
Naphthalene, 2-methyl-				3.14
Naphthalene, 2,7-dimethyl-				1.82
Naphthalene, 2,3-dimethyl-				0.66
Propene				2.06
1-Propene, 2-methyl-				1.01
Benzene				2.20
Toluene				2.90
p-Xylene				2.11

Table 5.4 Phenol, 2-methoxy-4-propyl- fast pyrolysis and fast pyrolysis coupled with catalytic upgrading products

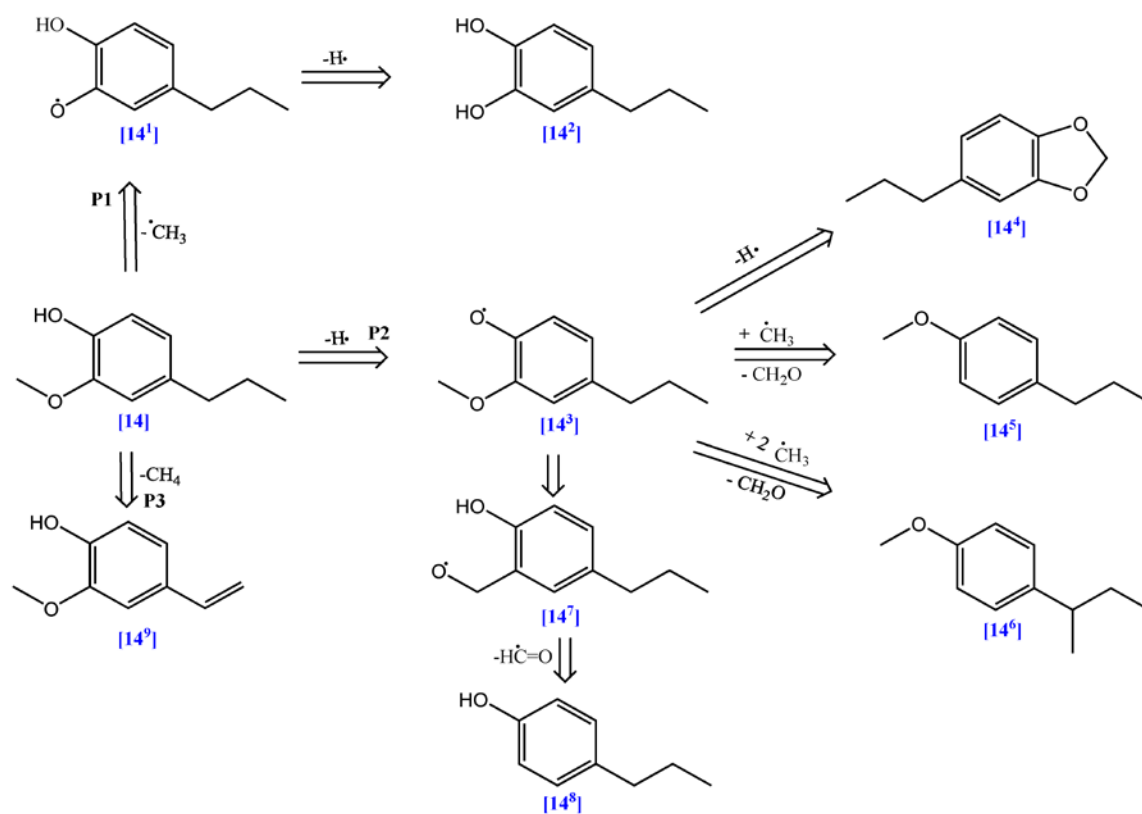


Figure 5.15 The phenol, 2-methoxy-4-propyl- fast pyrolysis pathway

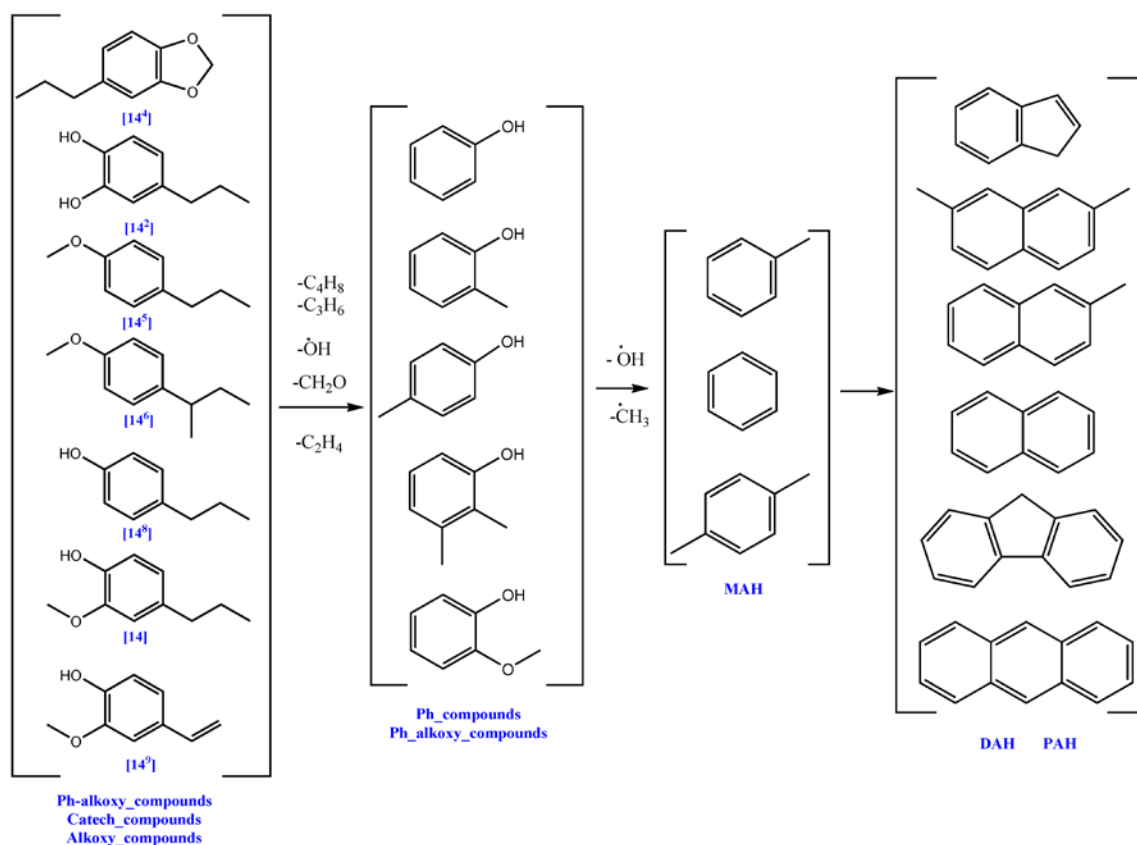


Figure 5.16 The pathway of phenol, 2-methoxy-4-propyl- in the fast pyrolysis process coupled with the catalytic upgrading (HZSM-5 with $\text{SiO}_2/\text{Al}_2\text{O}_3=30$)

5.1.5 Trans-Isoeugenol

The trans-Isoeugenol is also named (E)-Isoeugenol and its fast pyrolysis mechanism was studied by Minami Akazawa1 [117]. The phenol, 2-methoxy-4-(1-propenyl)-, (Z)- 12^2 (Figure 5.18) that was obtained with a very large area fraction (Table 5.5, Figure 5.17) resulted through the isomerization reaction of trans-Isoeugenol. The route of this reaction can be seen in the Minami Akazawa1 [117]'s study (route D and G, fig.3). Eugenol- 12^1 (Figure 5.18) was also formed with a much lower area fraction in the pyrolytic process and it could be produced by following the same mechanism as the one proposed for 12^2 . Vanillin was also produced in this process, but with a much lower area fraction. The same C_6 radical of quinone methide- 12^4 , through which the isomers of trans-Isoeugenol were formed, participated in the formation route of vanillin 12^6 (P2, Figure 5.18). The 2-methoxy-4-vinylphenol was obtained with almost the same area fraction as eugenol. Its route of formation is shown in the Figure 5.18 (P3) and it was also proposed by Minami Akazawa1 [117]. Benzoic acid, 3,5-dimethyl- 12^8 registered an area fraction of 14.58 % at 650 °C, but its formation mechanism is unknown. It is assumed to result from the intermediate 12^5 which was in turn formed via the route P2. The intermediate could undergo the tautomerization reaction and then through the deformylation, dehydroxylation and methylation reactions the benzoic acid, 3,5-dimethyl- could be produced. This could be possible as the carboxyl group is a meta director, so the meta positions would be occupied by the methyl groups. Phenol, 4-(2-propenyl)- 12^{12} could be also obtained via the C_6 radical

of quinone methide by stabilizing it with a hydrogen atom and then proceeding with a deformylation reaction (P4, Figure 5.18).

Different phenolic compounds like phenol, p-cresol, phenol, 2-methyl-, phenol, 2,3-dimethyl- were obtained in the pyrolytic process assisted by the catalytic upgrading step. According to the Figure 5.19, they could be formed by cracking reactions with producing ethene and propene. Only the propene was detected in the products distribution. Other reactions like deformylation, decarbonylation, methylation, as well as decarboxylation could be also involved. The MAH, DAH and PAH could follow the same mechanism as the one discussed for the homologous series. However, the area fraction of DAH and PAH is very high compared with other compounds and their formation could follow another mechanism. Minami Akazawa¹ [117] suggested one mechanism of formation of naphthalenols and it could be faster than the one proposed by Mullery, Hoang [116].

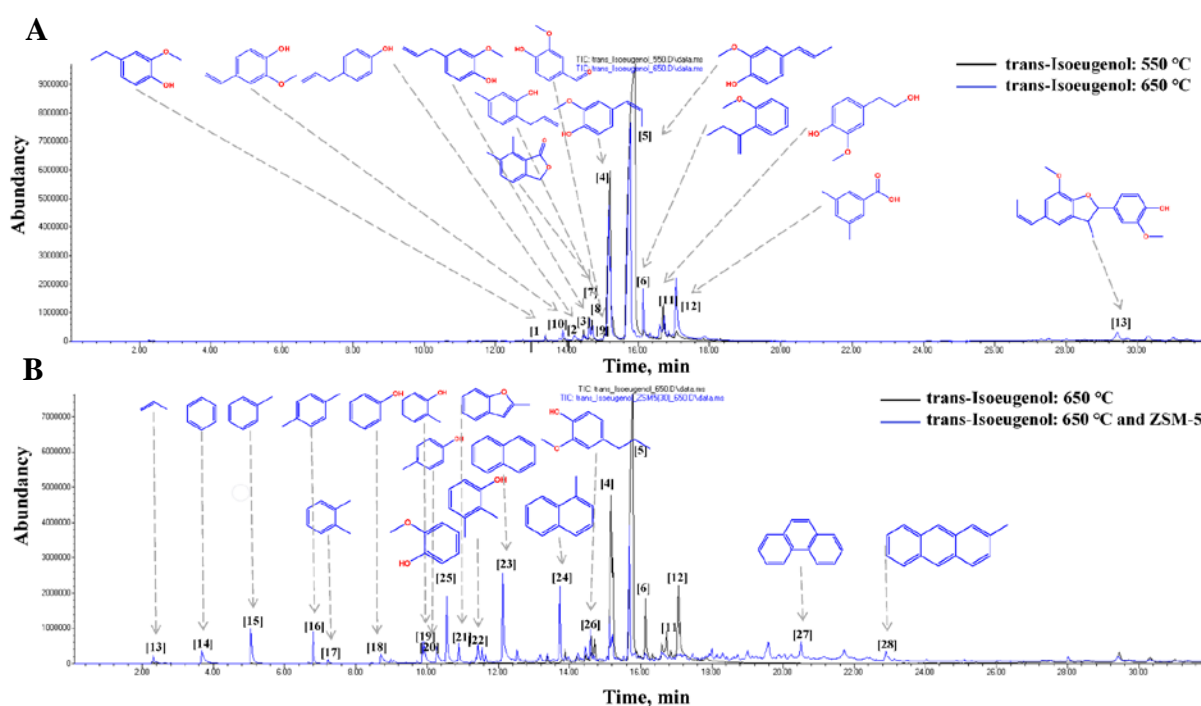
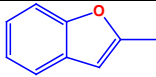
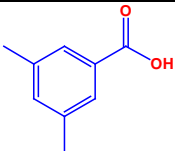
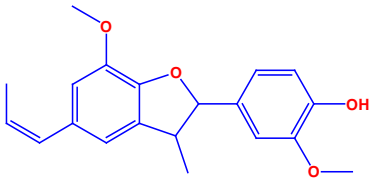
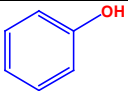
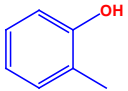
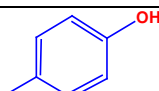
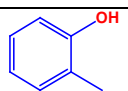
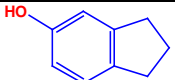
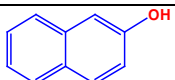
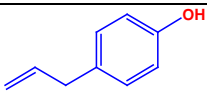
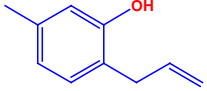
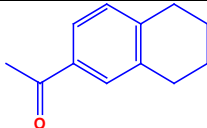
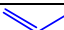
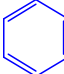
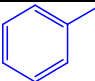
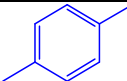
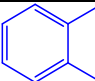
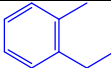
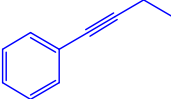
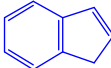
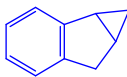
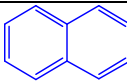
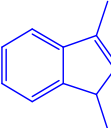
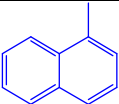


Figure 5.17 Trans-Isoeugenol: the overlapped 550 °C and 650 °C pyrograms (A) and 650 °C and 650 °C-HZSM-5 pyrograms (B)

Name	Structure	Area fraction (%)		
		550°C	650°C	650°C, HZSM- 5(30)
Phenol, 4-ethyl-2-methoxy-		0.48		0.89
Eugenol		1.40	1.01	
Vanillin		0.51	0.60	
Phenol, 2-methoxy-4-(1-propenyl)-, (Z)-		22.10	23.39	
trans-Isoeugenol		72.65	44.21	25.68
2-Methoxy-4-vinylphenol			1.38	
Anisole, o-(1-ethylvinyl)-		2.85	4.64	0.89
Homovanillyl alcohol			2.70	
Phenol, 2-methoxy-				7.33
Phenol, 2-methoxy-4-propyl-				3.41
6,7-Dimethyl-3H-isobenzofuran-1-one			1.66	
Benzofuran				0.53

Name	Structure	Area fraction (%)		
		550°C	650°C	650°C, HZSM- 5(30)
Benzofuran, 2-methyl-				2.14
Benzoic acid, 3,5-dimethyl-			14.58	
Phenol, 4-[2,3-dihydro-7-methoxy-3-methyl-5-(1-propenyl)-2-benzofuranyl]-2-methoxy-			2.29	1.43
Phenol				2.45
Phenol, 2-methyl-				2.95
p-Cresol				3.04
Phenol, 2,3-dimethyl-				2.05
1H-Inden-5-ol, 2,3-dihydro-				1.06
2-Naphthalenol				2.30
Phenol, 4-(2-propenyl)-			1.16	
5-Methyl-2-allylphenol			2.37	

Name	Structure	Area fraction (%)		
		550°C	650°C	650°C, HZSM- 5(30)
5',6',7',8'- Tetrahydro-2'- acetoneaphthone				1.05
Propene				1.10
Benzene				3.47
Toluene				4.73
p-Xylene				2.87
o-Xylene				0.53
Benzene, 1-ethyl-2- methyl-				0.47
Benzene, 1- butynyl-				1.10
Indene				1.76
Cycloprop[a]indene, 1,1a,6,6a- tetrahydro-				0.57
Naphthalene				10.66
1H-Indene, 1,3- dimethyl-				0.55
Naphthalene, 1- methyl-				5.64

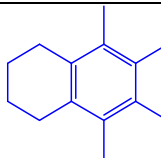
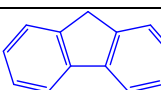
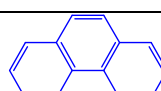
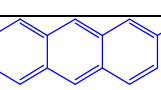
Name	Structure	Area fraction (%)		
		550°C	650°C	650°C, HZSM- 5(30)
Naphthalene, 1,2,3,4-tetrahydro- 5,6,7,8- tetramethyl-				0.74
Fluorene				2.83
Phenanthrene				3.60
Anthracene, 2- methyl-				2.20

Table 5.5 Trans-Isoeugenol fast pyrolysis and fast pyrolysis coupled with catalytic upgrading products

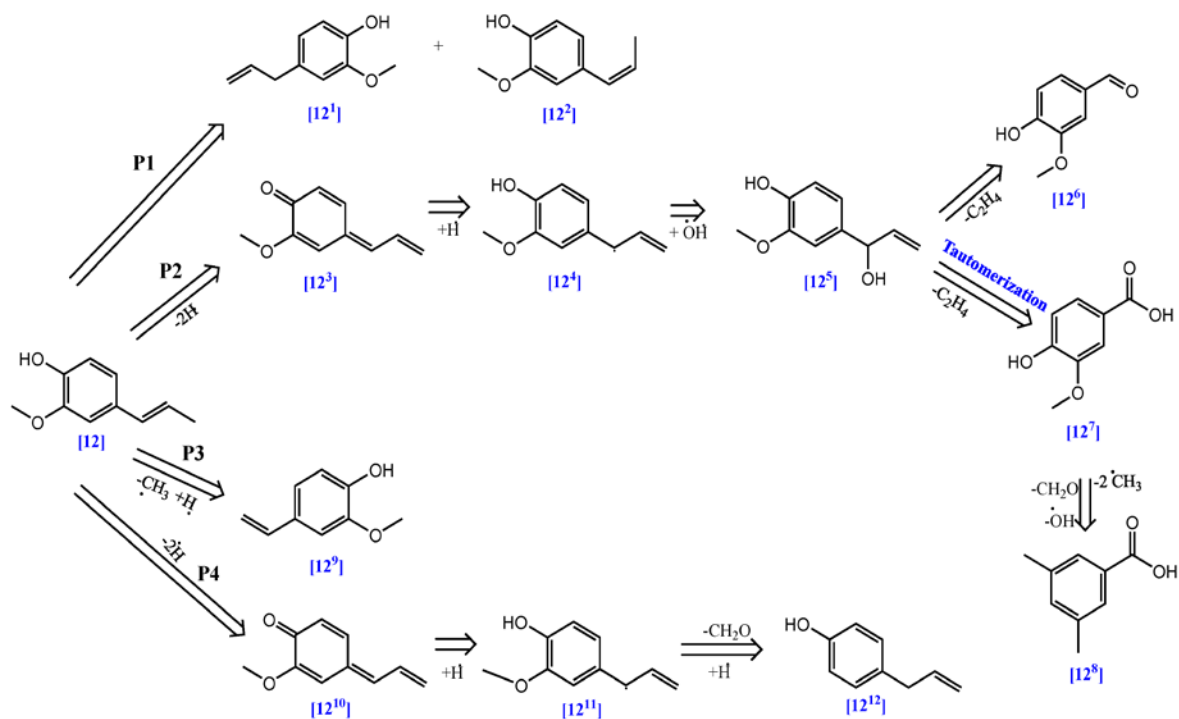


Figure 5.18 The trans-Isoeugenol fast pyrolysis pathway

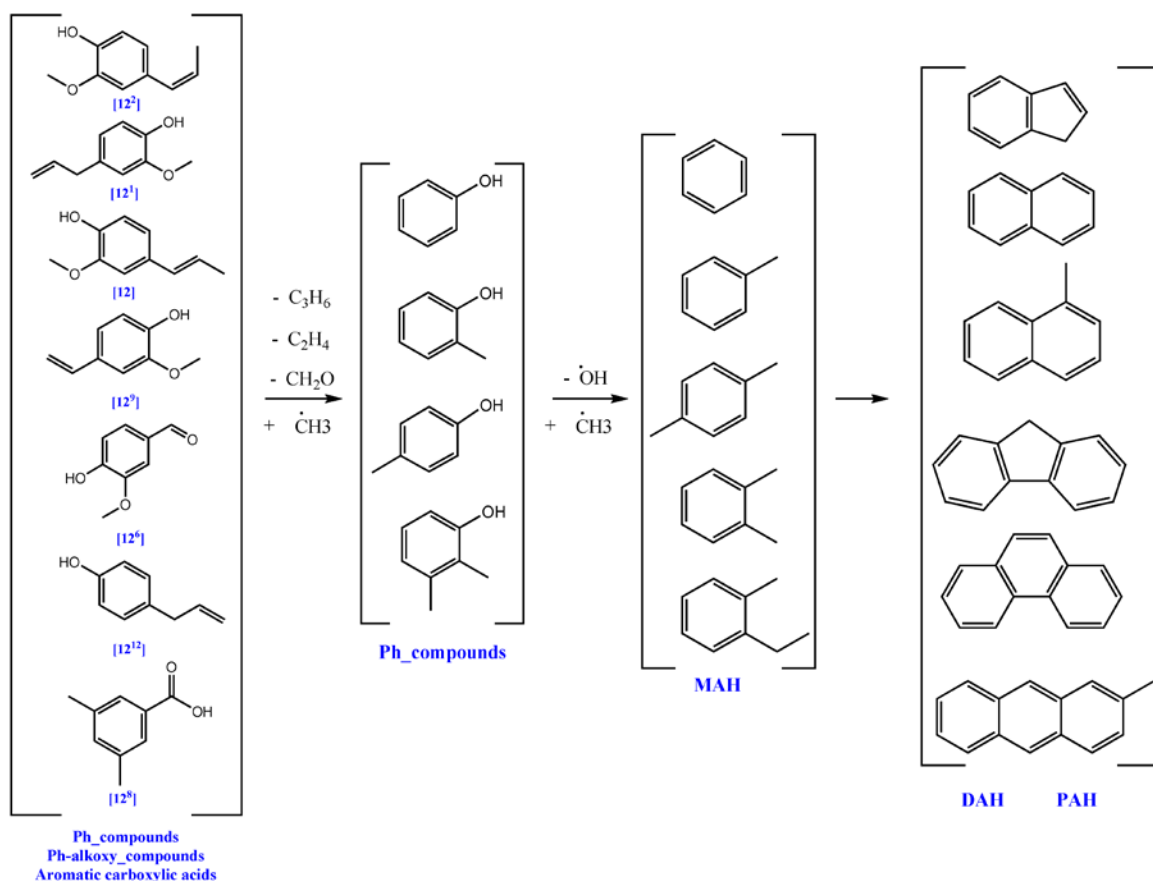


Figure 5.19 The pathway of trans-Isoeugenol in the fast pyrolysis process coupled with the catalytic upgrading (HZSM-5 with $\text{SiO}_2/\text{Al}_2\text{O}_3=30$)

5.1.6 Vanillin

The pathway of vanillin fast pyrolysis was built up based on the routes proposed for the guaiacol thermal decomposition and checked by the area fraction of the products obtained in this project. As it can be seen in the [Figure 5.21](#), the catechol is formed via route P1 and it should be produced in the highest amount. However, according to the [Table 5.6](#), the area fraction of catechol is only 0.58 % at 650 °C. While 5-formylsalicylaldehyde- 7⁶ should be the second most abundant product, it leads with 0.62 % at 550 °C and 6.49 % at 650 °C. In the [Figure 5.21](#), its formation route is presented (P3) which is deduced by Mullery, Hoang [116], but it the same route as the one discussed for the guaiacol (P2, [Figure 5.6](#)). The guaiacol is also formed and it could be formed through route P2 by releasing a molecule of carbon monoxide[100]. Phenol, 2-methyl- appears at 650 °C, but with a low area fraction. It could be formed directly from vanillin through decarbonylation, deformylation and methylation reactions, as well as from 5-formylsalicylaldehyde via decarbonylation and methylation reactions.

In the fast pyrolysis process with the catalytic upgrading step of vanillin different phenolic compounds are formed ([Table 5.6](#), [Figure 5.20 \(B\)](#)). According to the general pathway presented in the [Figure 5.22](#), the phenol could be obtained from each of the compound listed in the column 1, especially from 5-formylsalicylaldehyde through decarbonylation

reaction. The p-cresol could result from 5-formylsalicylaldehyde, as well as directly from vanillin and this is because both of them are able to generate a radical in the para position by releasing a molecule of CO. The stabilization of the radicals with the methyl group results in formation of p-cresol. The area fraction of MAH, DAH and PAH is not very large and the formation routes could be the same as for the compounds discussed above.

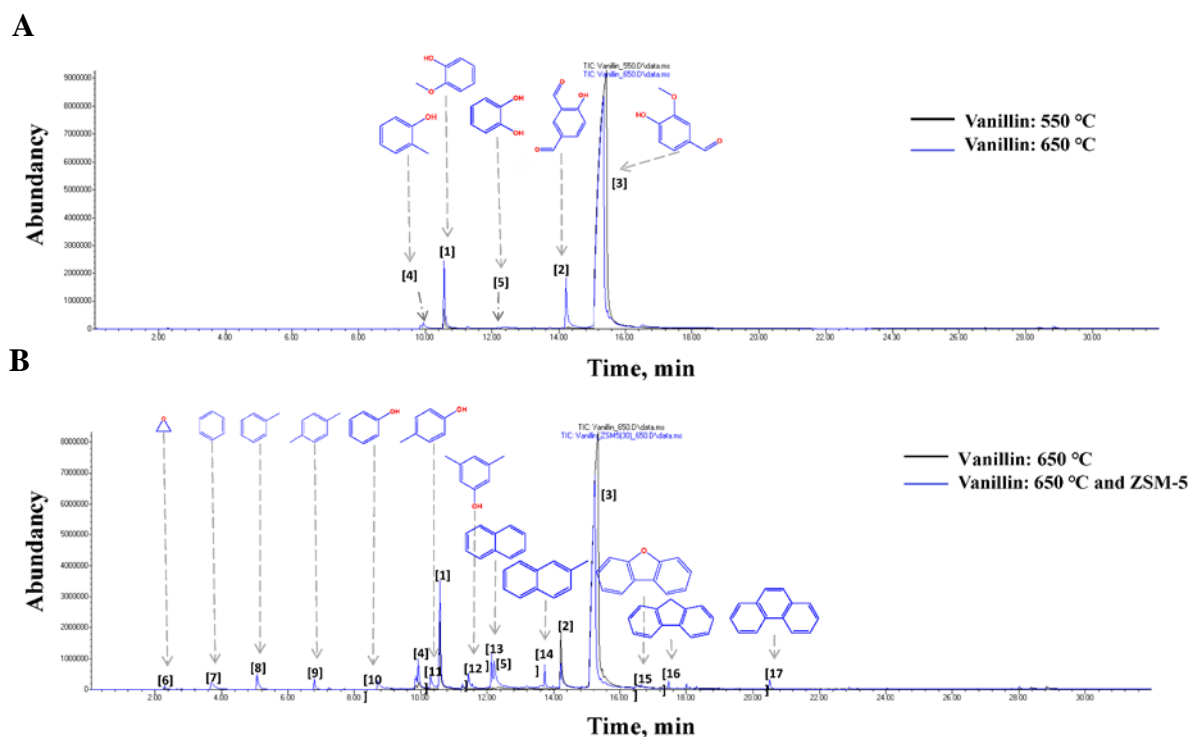
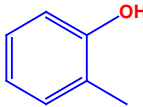
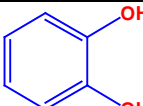
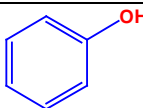
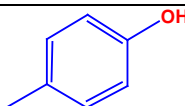
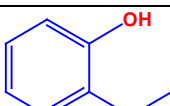
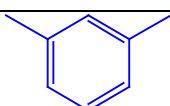
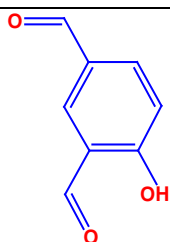
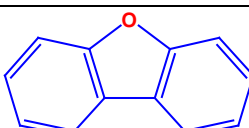
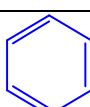
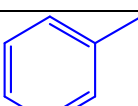


Figure 5.20 Vanillin: the overlapped 550 °C and 650 °C pyrograms (A) and 650 °C and 650 °C-HZSM-5 pyrograms (B)

Name	Structure	Area fraction (%)		
		550 °C	650 °C	650 °C, HZSM-5(30)
Phenol, 2-methoxy-		1.71	5.83	10.68
Vanillin		97.67	86.05	56.46

Name	Structure	Area fraction (%)		
		550 °C	650 °C	650 °C, HZSM-5(30)
Phenol, 2-methyl-			1.05	3.18
Catechol			0.58	5.27
Phenol				1.67
p-Cresol				2.15
Phenol, 2-ethyl-				0.56
Phenol, 3,5-dimethyl-				1.45
5-Formylsalicylaldehyde		0.62	6.49	3.79
Dibenzofuran				0.61
Benzene				1.99
Toluene				2.03

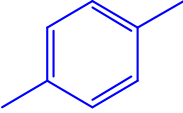
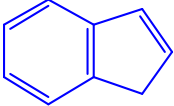
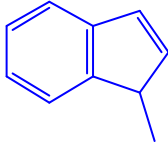
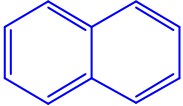
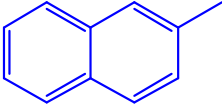
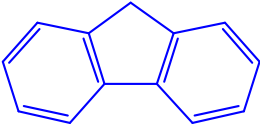
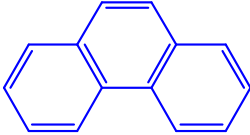
Name	Structure	Area fraction (%)		
		550 °C	650 °C	650 °C, HZSM-5(30)
p-Xylene				0.87
Indene				1.35
1H-Indene, 1-methyl-				0.96
Naphthalene				2.42
Naphthalene, 2-methyl-				1.81
Fluorene				0.64
Phenanthrene				0.98

Table 5.6 Vanillin fast pyrolysis and fast pyrolysis coupled with catalytic upgrading products

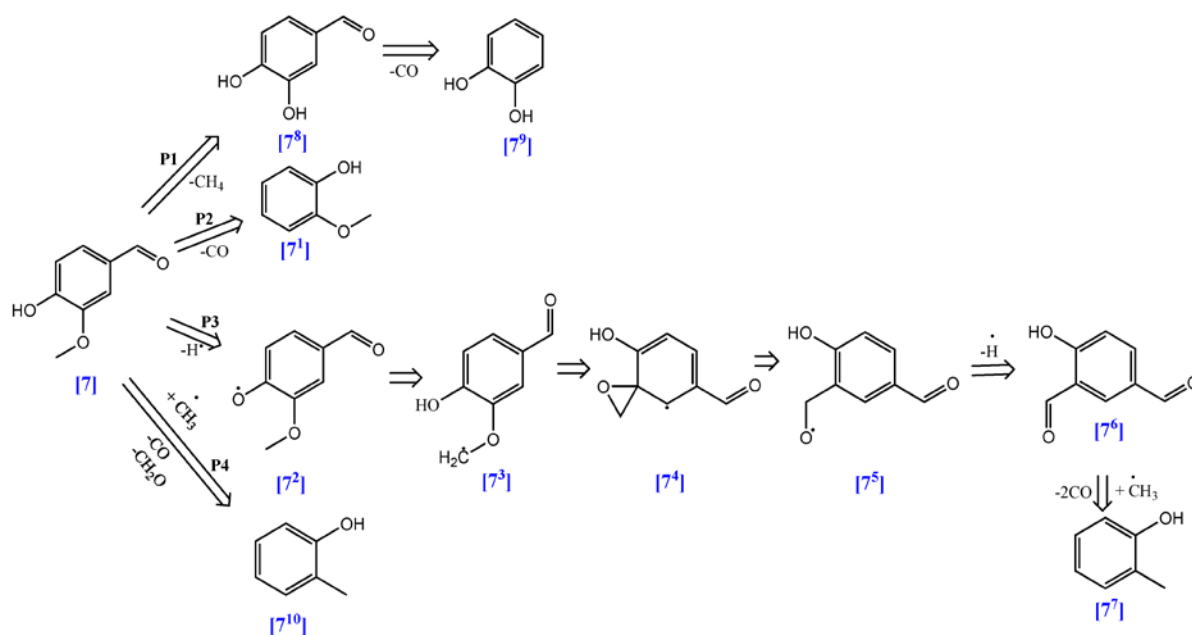


Figure 5.21 The vanillin fast pyrolysis pathway

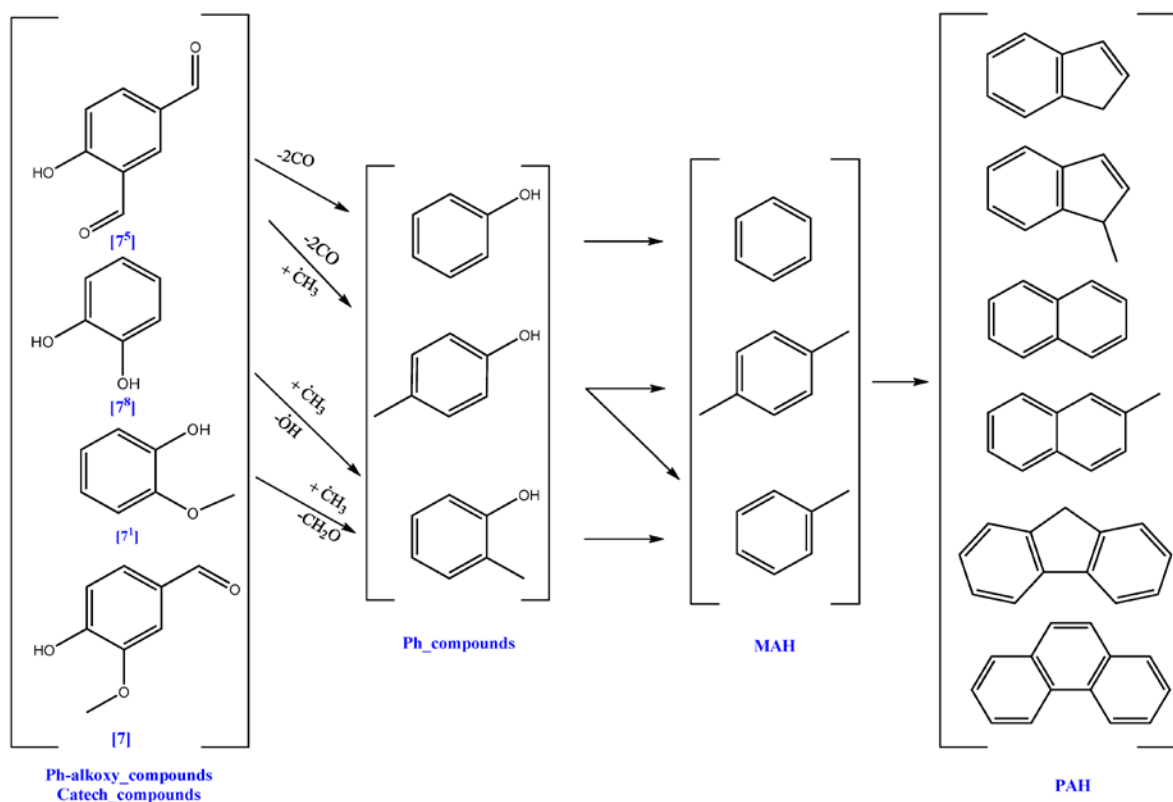


Figure 5.22 The pathway of vanillin in the fast pyrolysis process coupled with the catalytic upgrading (HZSM-5 with $\text{SiO}_2/\text{Al}_2\text{O}_3=30$)

5.1.7 Apocynin

The fast pyrolysis of apocynin generated some products characterized by a low area fraction, but which could be produced via the same route applied in case of guaiacol and the rest of the compounds, and some of them with a high area fraction, but whose routes are unknown and could be assumed. 3,4-Dihydroxyacetophenone- **10**² is formed via route P1 (Figure 5.24) and according to Nowakowska, Herbinet [114] this route produces the largest quantity of catechol in case of guaiacol. Based on the results presented in Figure 5.23 and Table 5.7, the area fraction of compound **10**² is 1.68 % at 650 °C, that is very low. The acetophenone, 4'-hydroxy- **10**⁷ should be the second most abundant compound, however, according to the results, it resulted with a very low area fraction. The 4-acetylbenzoic acid- **10**³ if formed with the highest area fraction and its formation route is unknown, but it is assumed to result according to the route P2.

The products resulted in the fast pyrolysis at 650 °C were improved through deoxygenation reactions catalysed by HZSM-5. According to the results presented in the Table 5.7, guaiacol is characterized by a quite high area fraction and it could result through deacetylation reaction of apocynin (

Figure 5.25). The same reaction could be applied for the 3,4-dihydroxyacetophenone in order to produce catechol. As it is shown in the Table 5.7, its area fraction is almost 5% that is quite high. The other obtained phenols could also result based on the deacetylation reaction, as well as deformylation and decarboxylation. All these mentioned can be supported by the formation of the products like acetone, acetic acid, methyl ester and acetic acid (Table 5.7). The MAH, DAH and PAH could be formed based on the same mechanism as in the guaiacol case.

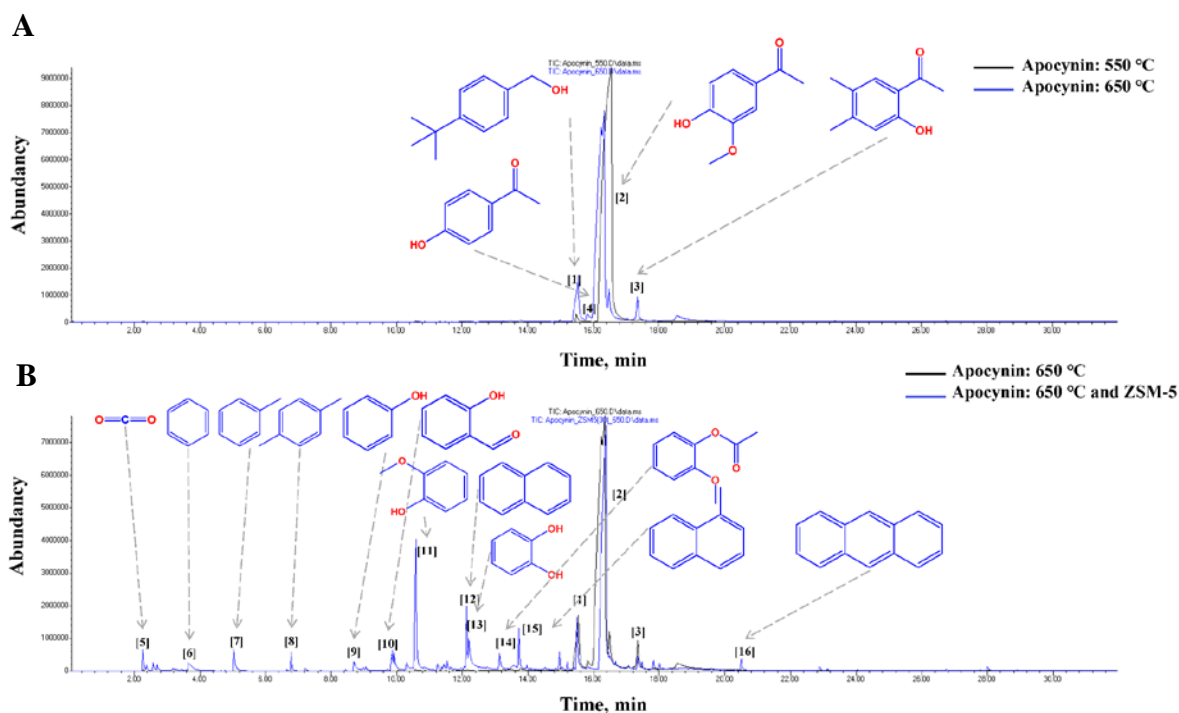
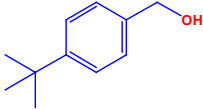
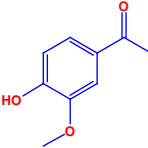
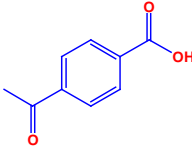
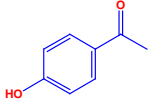
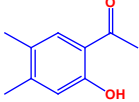
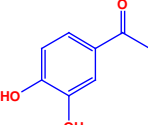

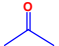
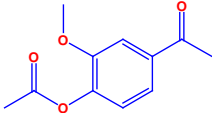
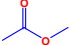
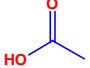
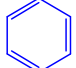
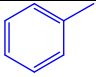
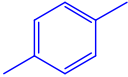
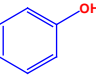
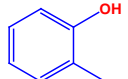
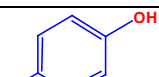
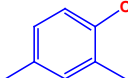
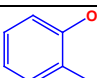
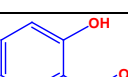
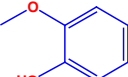
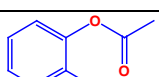
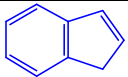
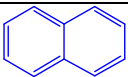
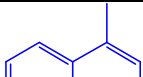
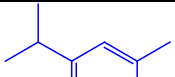


Figure 5.23 Apocynin: the overlapped 550 °C and 650 °C pyrograms (A) and 650 °C and 650 °C-HZSM-5 pyrograms (B)

Name	Structure	Area fraction (%)		
		550°C	650°C	650°C, HZSM- 5(30)
Benzenemethanol, 4-(1,1-dimethylethyl)-		1.03		
Apocynin		98.97	85.84	55.07
4-Acetylbenzoic acid			8.77	
Acetophenone, 4'-hydroxy-			0.84	
2'-Hydroxy-4',5'-dimethylacetophenone			2.87	0.99
3,4-Dihydroxyacetophenone			1.68	
Carbon dioxide				1.23
Acetone				0.48
4-Acetoxy-3-methoxyacetophenone				0.56
Acetic acid, methyl ester				0.62
Acetic acid				0.73
Benzene				2.11

Name	Structure	Area fraction (%)		
		550°C	650°C	650°C, HZSM- 5(30)
Toluene				1.92
p-Xylene				1.07
Phenol				1.26
Phenol, 2-methyl-				1.75
p-Cresol				1.09
Phenol, 2,4-dimethyl-				0.47
Catechol				4.99
Benzaldehyde, 2-hydroxy-				0.54
Phenol, 2-methoxy-				11.05
Phenol, 2-methoxy-, acetate				2.23
Indene				0.97
Naphthalene				3.19
Naphthalene, 1-methyl-				2.15
Benzene, 1-methoxy-4-methyl-2-(1-methylethyl)-				4.13

Name	Structure	Area fraction (%)		
		550°C	650°C	650°C, HZSM- 5(30)
Fluorene				0.52
Anthracene				0.89

Table 5.7 Apocynin fast pyrolysis and fast pyrolysis coupled with catalytic upgrading products

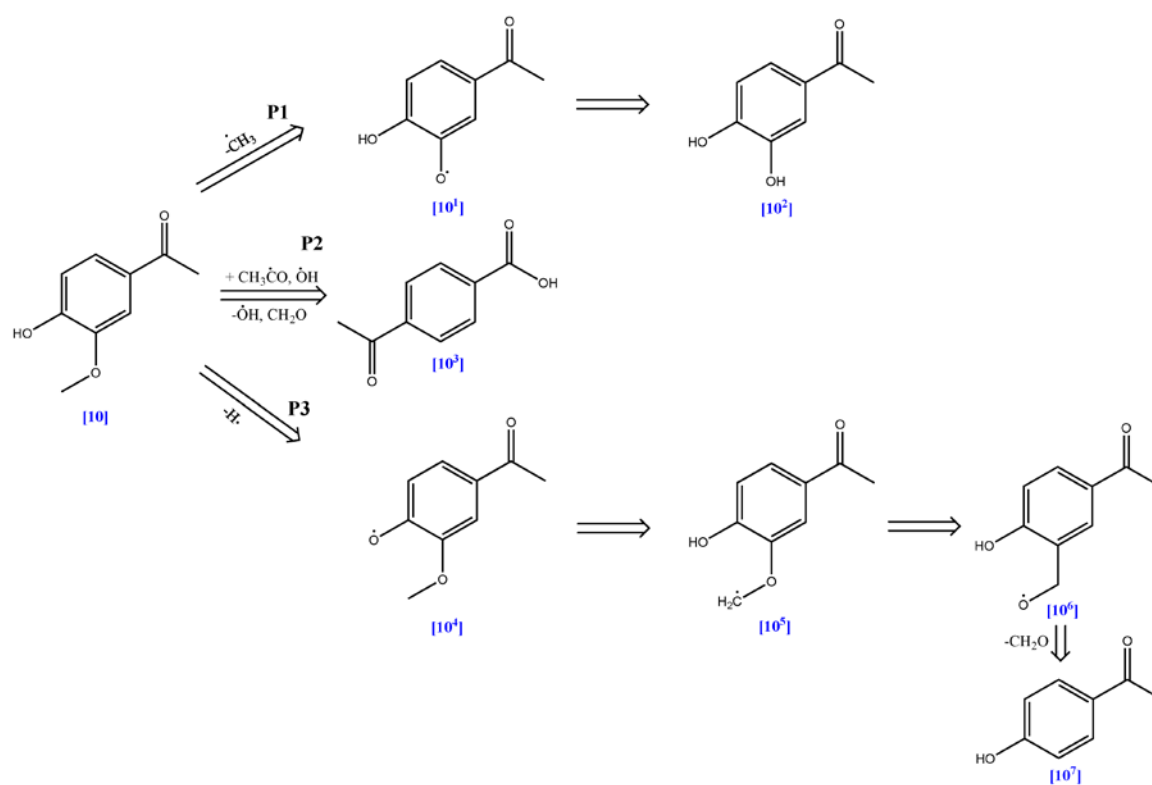


Figure 5.24 The apocynin fast pyrolysis pathway

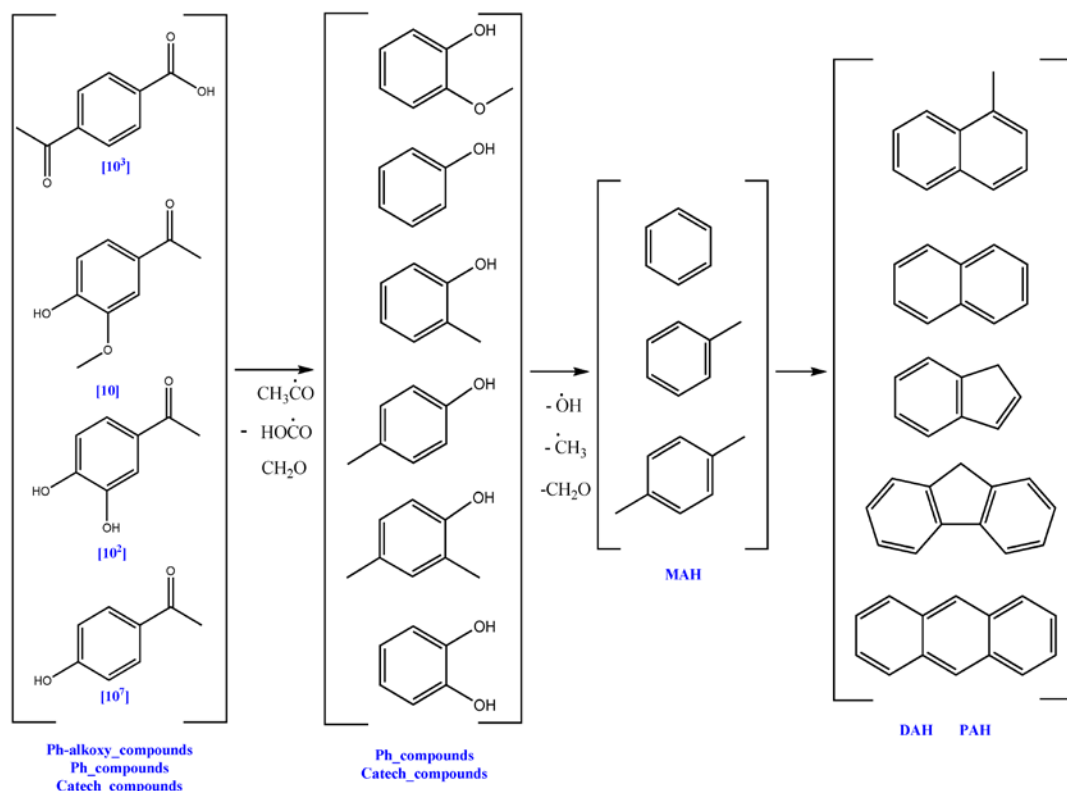


Figure 5.25 The pathway of apocynin in the fast pyrolysis process coupled with the catalytic upgrading (HZSM-5 with $\text{SiO}_2/\text{Al}_2\text{O}_3=30$)

5.2 FP of model compounds vs FP of lignin

It is easier to build up a pathway based on pure compounds rather than finding out the mechanism by directly decomposing the lignin. However, when analysing each abundant compound individually, the pathway deviates from the original one as in the FP of lignin, more species are interacting than in the FP of a pure compound. In the analysis of each model compound, it was noticed that the nature of different substituents in the para position changed the products proportions of the guaiacol pathway proposed by Nowakowska, Herbinet [114], especially the substituents with long chain or oxygen containing chains. The name of the most abundant products obtained in the fast pyrolysis of the seven pure compounds at 650 °C and their area fraction (%) (in the square brackets) are presented in the Table 5.8. In the first column, the percentage of obtaining different products from guaiacol recommended by Nowakowska, Herbinet [114] is presented. As it can be seen, the FP of guaiacol generated almost the same compounds. However, the area fraction of benzaldehyde, 2-hydroxy- is higher than of catechol and this could be because of the higher temperature used herein. The FP of creosol also followed the same pathway, but from phenol, 4-ethyl-2-methoxy- to apocynin only some of the products could be obtain based on the Nowakowska, Herbinet [114] guaiacol pathway. If looking at the area fraction of the seven model compounds, it can be seen that the alkyl chain in the para position contributes to the reactivity of the compound, especially in case of unsaturated hydrocarbon chain of the trans-Isoeugenol. Its high reactivity could be due to the conjugated double bonds of the aromatic ring with the double bond of the side chain. Based on this, the radical of this structure is more stable due to the delocalization of the unpaired

electron through the resonance. This means that the unpaired electron is supported by all the carbons involved in the conjugated structure and not only by one carbon. However, if analysing the products, a large area fraction is occupied by the trans-Isoeugenol stereoisomer. The vanillin and apocynin manifested the lowest activity and this could be also related to the poor stability of the radicals.

By comparing the products distribution obtained in the FP of model compounds at 650 °C (Table 5.8) with the products distribution of FP of lignin at the same temperature (Figure 4.15), it can be observed that the FP of individual compounds generated more catechol and methylcatechols than phenolic compounds (Ph), as well as a large area fraction of benzaldehydes, acetophenones and other oxygenated compounds, while FP of lignin generated more Ph than MCatech and the last compounds were not produced or could not be detected due to the very low area fraction. According to this, it can be assumed that the synergistic effect between the multitude of radicals in the FP of lignin could occur and so producing more phenolic compounds. However, even though the reason of generating more Ph than MCatech is unclear, some reactions of the oxygenated compounds (generated in the FP of model compounds) that could occur in the FP of lignin are presented in the Figure 5.26. It can be noticed that more phenol and p-cresol could be produced through the decarbonylation and dealkylation reactions of benzaldehyde, 2-hydroxy- [1], 2-hydroxy-5-methylbenzaldehyde [4], phenol, 4-propyl- [13] and 5-formylsalicylaldehyde [19], while phenol, 2,4-dimethyl-, the compound produced with the highest area fraction in the FP of lignin at 650 °C, could result from ethanone, 1-(2-hydroxy-5-methylphenyl)- [7], benzene, 1-methoxy-4-propyl- [10], as well as benzoic acid, 3,5-dimethyl- [16] via decarbonylation and dealkylation reactions. The generation of high content of carbon monoxide and a low content of ethylene can be supported by the GC/FID/TCD analysis of the gas phase resulted in the fixed bed reactor experiments.

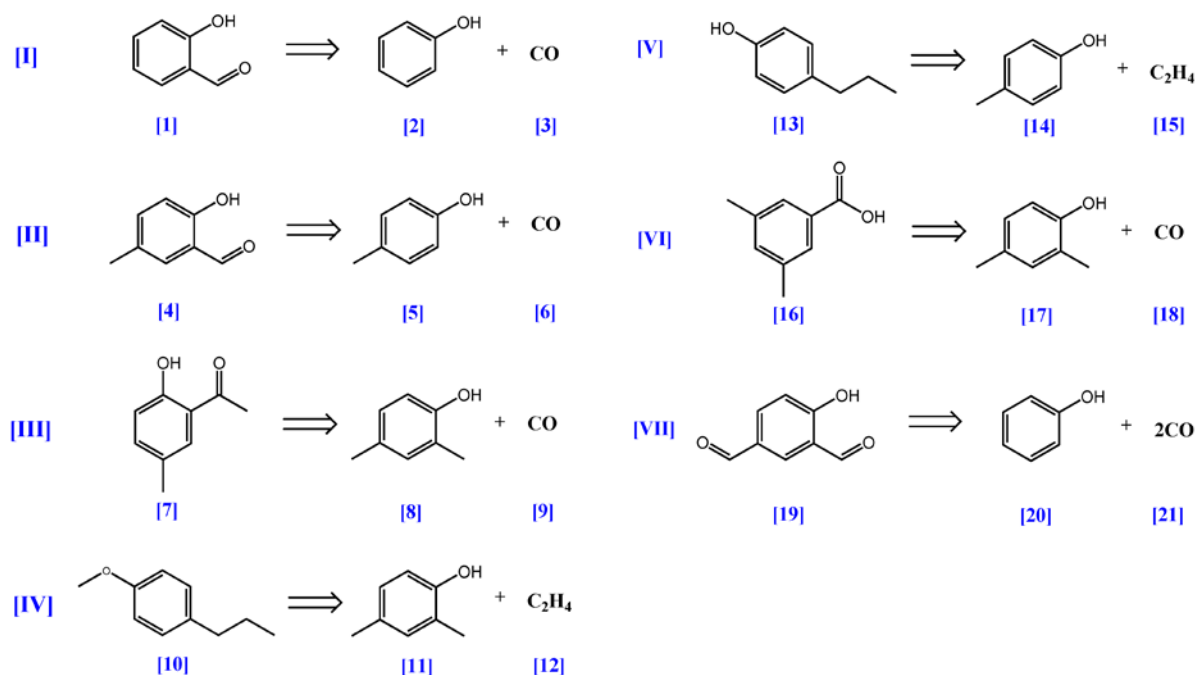


Figure 5.26 The possible reactions of different oxygenated compounds generated with a high area fraction in the FP of model compounds, but not in the FP of lignin

Guaiacol[114]	Guaiacol	Creosol	Phenol, 4-ethyl-2-methoxy-	Phenol, 2-methoxy-4-propyl-	tran-Isoeugenol	Vanillin	Apocynin
	 [69.56]						
Catechol [51.62%]	Catechol [9.08]	1,2-Benzenediol, 4-methyl- [17]	4-Ethylcatechol [18.27]		Phenol, 4-(2-propenyl)- [1.16]	Catechol [0.58]	
Benzaldehyde, 2-hydroxy- [35.34%]	Benzaldehyde, 2-hydroxy- [13.95]	2-Hydroxy-5-methylbenzaldehyde [11.19]				5-Formylsalicylaldehyde [6.49]	
1,2-Benzenediol, 4-methyl- [6.38%]	1,2-Benzenediol, 4-methyl- [0.70] 1,2-Benzenediol, 3-methyl- [1.01]	1,3-Benzenediol, 4,5-dimethyl- [3.3] 1,4-Benzenediol, 2,6-dimethyl- [1.31]		1,3-Benzenediol, 4-propyl- [16.02]			3,4-Dihydroxyacetophenone [1.68]
Phenol [3.28%]	Phenol [1.21]	p-Cresol [2.16]	Phenol, 4-ethyl- [2.23]	Phenol, 4-propyl- [3.62]			Acetophenone, 4'-hydroxy- [0.84]
Phenol, 2-methyl- [3%]	Phenol, 2-ethyl- [2.78]	Phenol, 3,5-dimethyl- [5.64] Phenol, 2-ethyl-6-methyl- [6.34]	3-Methyl-4-isopropylphenol [5.94]		5-Methyl-2-allylphenol [2.37]	Phenol, 2-methyl- [1.05]	2'-Hydroxy-4',5'-dimethylacetophenone [2.87]

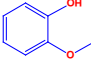
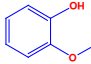
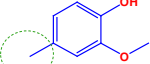
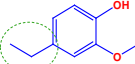
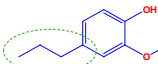
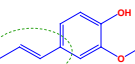
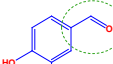
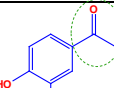
Guaiacol[114]	Guaiacol	Creosol	Phenol, 4-ethyl-2-methoxy-	Phenol, 2-methoxy-4-propyl-	trans-Isoeugenol	Vanillin	Apocynin
	 [69.56]	 [45.36]	 [48.95]	 [56.68]	 [44.21]	 [86.05]	 [85.84]
			2-Methoxy-4-vinylphenol [2.60]	2-Methoxy-4-vinylphenol [1.39]	Eugenol [1.01] Phenol, 2-methoxy-4-(1-propenyl)-, (Z)- [23.39] 2-Methoxy-4-vinylphenol [1.38]		
			Benzene, 1-ethyl-4-methoxy- [6.53] Ethanone, 1-(2-hydroxy-5-methylphenyl)- [10.60] Ethanone, 1-(2,4-dimethylphenyl)- [2.24]	Benzene, 1-methoxy-4-propyl- [6.30] Benzene, 1-methoxy-4-(1-methylpropyl)- [5.68] 1,3-Benzodioxole, 5-propyl- [9.03]	Anisole, o-(1-ethylvinyl)- [4.64] Homovanillyl alcohol [2.7] Benzoic acid, 1,3,5-dimethyl- [14.58]	Phenol, 2-methoxy- [5.83]	4-Acetylbenzoic acid [8.77]

Table 5.8 The most abundant compounds generated in the FP of the seven model compounds at 650 °C. The area fraction (%) is presented in the square brackets

6 Conclusions

The lignin fast pyrolysis and lignin fast pyrolysis assisted by a subsequently catalytic upgrading of the volatiles were studied in this work. The effect of different process parameters and different catalysts on the products distribution of the bio-oil, as well as on the yield of gas, liquid and solid were investigated. The main findings are summarized in this chapter.

By evaluating the temperature influence on the products distribution in the Py-GC/MS, it was noticed that at a lower temperature (500 °C), the content of PhA was much higher compared to Ph and MAH. In the 550-650 °C temperature range, an increase of Ph, MCatec and MAH was observed. In more severe conditions (700 °C), the total area was significantly decreased. The generation of more gas could lead to this. The 550 °C value was selected for FP-CU due to the increase of Ph and MAH. In addition, at a higher temperature, more MCatec were formed. Due to their high oxygen content, they are not a desired product. Moreover, at more severe conditions, a significant increase of Ph was not observed. Thus, an extra energy consumption is unwanted if a noticeable improvement is not detected.

In the Py-GC/MS results of lignin FP-CU at 550 °C on metal/metals oxy phosphates γ -Al₂O₃ supported catalysts, MoP (10 wt%) manifested interesting deoxygenation properties because a higher content of Ph, MAH and DAH were formed. Furthermore, no PhA was detected. The impregnation of the second metal increased the formation of more PAH and decreased the conversion of PhA. The effect of MoP loading was also analyzed and results showed that a loading of 10 wt% is the proper one due to the higher content of Ph, MAH and DAH. However, by comparing its results with the deoxygenation properties of HZSM-22, HZSM-5, H β and HY, it was observed that MoP (10 wt%)/ γ -Al₂O₃ is not good enough, therefore its activity was not tested in the fixed bed reactor.

The analysis of various zeolites characterized by different structure and pore size was also accomplished in this work. Due to their well definite construction, the selectivity of the reactants and products was also investigated. The molecule structure of the compounds resulted in the FP and FP-CU was designed and the x, y and z dimensions were measured. It was noticed that the pore size of HZSM-5 and HZSM-22 was suitable for almost all the reactants and products. However, it was also assumed that too large reactants could start reacting at the pore mouth and then smaller species could enter the pore, and the large products could form on the outside the pore. Moreover, based on Webster, Drago [105]'s study, it is possible that all the compounds might fit into the medium zeolite pore as the pore size is increased when the material is exposed to large temperatures. According to medium pore size of HZSM-22 and HZSM-5, a good selectivity for MAH was identified in the Py-GC/MS results. It was also noticed that a lower Si/Al ratio of HZSM-5 promotes the formation of MAH and DAH. The SAPO catalysts did not manifest any selectivity for the aromatic hydrocarbons and this is due to the very small pore size. By analysing the influence of the pore size and internal pore construction on the products distribution, the results of HZSM-5(30), H β and HY were compared. It was observed that the larger pore of H β promoted formation of DAH, while HY manifested quite the same distribution of the products as HZSM-5(30), even though its pore size is larger than of H β . This could be due to the cages and supercages of the HY zeolite which allow the formation of some aromatic hydrocarbons and of a large content of coke. Moreover, the medium-strength acid sites (NH₃-TDP results) and their high density due to the low Si/Al ratio (6) could enhance the

coke formation. Thus, the significant decrease of the total area resulted in the Py-GC/MS could be associated to the faster deactivation of HY considering the deposition of the coke on its active sites. The HZSM-5(30), H β and HY were also tested in the fixed bed reactor.

Due to the large surface area of HZSM-5, H β and HY, the impregnation of 10 wt% of MoP was decided. Based on the XRD analysis, the MoP species were very well dispersed as no peaks were detected. However, the impregnation decreased the crystallinity of the catalyst when comparing the results to the pure zeolite diffractogram. Moreover, the BET results showed a significant decrease of the surface area. This could be due to the blocking of the micropores. The activity test of the three catalysts showed a noticeable decrease of the total area and the PhA content was increased. Due to the poor results, their activity was not tested in the fixed bed reactor.

By analysing the temperature effect on lignin FP in the fixed bed reactor, it was noticed that an increasing in temperature from 550 to 600 °C increased the liquid yield from 30.9 to 42.5 wt% and gas yield from 8.9 to 10.2 wt%. However, when using the HZSM-5(30) to upgrade the pyrolytic volatiles, a small increase of the liquid yield was observed at 550 °C compared to FP-CU at 600 °C. This occurred due to the higher temperature and strong active sites which promote a deeper cracking of the side chains, thus, resulting more gas at 600 °C and less bio-oil compared to 550 °C. In the presence of the catalytic sites, the stable compounds are formed faster and a high temperature is not required.

The effect of Si/Al ratio of HZSM-5 was also studied in the fixed bed reactor. Based on the results, it was noticed that the liquid yield was not influenced, while the coke formation was promoted by a higher density of the acid sites. The HZSM-5(30) manifested the higher selectivity for the aromatic hydrocarbon. The same results were obtained in the Py-GC/MS.

When analysing the effect of pore size and internal pore construction on the products distribution in the fixed bed reactor, it was noticed that the HY indeed generated the largest amount of coke compared to HZSM-5(30) and H β . Its large pores also minimized the char yield and enhanced the liquid yield. However, based on products distribution of the liquid phase, a lot of PhA and Ph compounds were detected. By comparing the H β and HZSM-5(30) results, it was observed that H β produced more DAH than HZSM-5(30) and this is because of its large pores that allow the formation of large molecules, but inhibit more the coke formation compared to HY. The MAH was detected only for HZSM-5(30), however in much lower yield compared to DAH. According to Py-GC/MS, it should be the opposite. This problem was detected in all the experiments. Different process parameters were changed, like temperature, nitrogen flowrate, catalysts to lignin ratio with no change in the MAH yield. Also, a different condenser was used based on solvent solubilisation of organic compounds, however the BTX could not be identified. The problem was identified when a small amount of acetone was used in the spiral condenser. This showed that the problem was in the condensing part and not in the reactor process parameters. Considering the large yield of MAH formed in the FP-CU, by adding this value to the total product yield, the liquid amount will be enhanced, and so will the mass balance.

The lignin pathway was also studied based of FP and FP-CU of seven pure compounds which were generated in the highest quantity in the FP and FP-CU of lignin. It was noticed that the substituent in the para position of the guaiacol structure affected the pathway proposed by Nowakowska, Herbinet [114]. Moreover, some of the products that resulted with a high area fraction (%), when testing the individual compounds, were not detected in the products resulted from lignin. This was associated to the synergy that could occur between the various radicals resulted from the linkages and phenolic structures of lignin.

Thus, promoting the formation of more Ph compounds than MCatec and other oxygenated species that were not detected in the FP and FP-CU of lignin.

7 Bibliography

1. Wikipedia. *Industrial Revolution*. Available from: https://en.wikipedia.org/wiki/Industrial_Revolution.
2. Sawsan Ahmed Elhoury Ahmed, A.A.M.O., *Renewable energy advantages & disadvantages*. 2016.
3. Wikipedia. *Watermill*. Available from: <https://en.wikipedia.org/wiki/Watermill#Applications>.
4. World, U.o.C.S.S.f.a.H.P.a.S. *How Energy Storage Works*. Available from: <https://www.ucsusa.org/clean-energy/how-energy-storage-works>.
5. St1. *Ethanolix Plant* 2015; Available from: <https://www.st1.eu/st1-built-a-waste-based-etanolix-ethanol-production-plant-in-gothenburg>.
6. Chen, H., *Biotechnology of Lignocellulose*. Chemical Industry Press. 2014.
7. Melián Rodríguez, M., et al., *Lignin biomass conversion into chemicals and fuels*.
8. Furkan H. Isikgor*a and C.R. Becer*b, *Lignocellulosic Biomass: A Sustainable Platform for Production of Bio-Based Chemicals and Polymers*.
9. Abe, A., K. Dušek, and S. Kobayashi, *Biopolymers*. Advances in Polymer Science. 2010.
10. *Lignin: the origin of the name*. Available from: <https://en.wikipedia.org/wiki/Lignin#History>.
11. Chunbao Xu, F.F., *Conversion Of Lignin Into Bio-Based Chemicals and Materials*. Green Chemistry and Sustainable Technology, 2017.
12. Henriksson, G., *Lignin*, in *Wood Chemistry and Wood Biotechnology*. 2009.
13. MADSHANSEN, *Biofuels And The Prospect Of Converting Plant Fibres Into Gasoline Using Enzymes*. 2007.
14. Karpe, A., *Biodegradation of winery biomass wastes by developing a symbiotic multifungal consortium*. ResearchGate, 2015.
15. Huang, C., et al., *Preparation of Lignosulfonates from Biorefinery Lignins by Sulfomethylation and Their Application as a Water Reducer for Concrete*. Polymers, 2018. **10**(8).
16. Petroleum, N.; Available from: <https://www.norskipetroleum.no/en/>.
17. Svensson, S., *Minimizing the sulphur content in Kraft lignin*. 2008.
18. Petroquim. Available from: <http://www.petroquim.cl/usos-del-polipropileno/?lang=en>.
19. Gunnar Henriksson, J.L., Liming Zhang, Mikael E. Lindstrom, *Lignin Utilization: Chapter 9 from "Thermochemical Conversion of Biomass to Liquid Fuels and Chemicals" book*. 2010.
20. EnggCyclopedia. *Octane number*. 2011; Available from: <https://www.enggcyclopedia.com/2011/01/octane-number/>.
21. Moulijn, J.A., M. Makkee, and A.E.V. Diepen, *Chemical Process Technology*. 2nd Edition.
22. Dumitrita Spinu, D.C., Kumar Ranjan Rout, Isaac Yeboah, *Bio-fuels from Lignin by Fast Pyrolysis with Coupled Catalytic Upgrading*, in *Specialization Project*. 2018.
23. Al-Nuaimi, I.A., et al., *Optimization of the Aromatic/Paraffinic Composition of Synthetic Jet Fuels*. Chemical Engineering & Technology, 2016. **39**(12): p. 2217-2228.
24. Bi, P., et al., *From lignin to cycloparaffins and aromatics: directional synthesis of jet and diesel fuel range biofuels using biomass*. Bioresour Technol, 2015. **183**: p. 10-7.
25. Diffen. *Diesel vs. Petrol*. Available from: https://www.diffen.com/difference/Diesel_vs_Petrol.
26. Amezcua-Allieri, M.A. and J. Aburto, *Conversion of Lignin to Heat and Power, Chemicals or Fuels into the Transition Energy Strategy*, in *Lignin - Trends and Applications*. 2018.

27. Sindhu, R., P. Binod, and A. Pandey, *Biological pretreatment of lignocellulosic biomass--An overview*. *Bioresour Technol*, 2016. **199**: p. 76-82.
28. Choi, Y.S., et al., *Pyrolysis reaction networks for lignin model compounds: unraveling thermal deconstruction of β -O-4 and α -O-4 compounds*. *Green Chemistry*, 2016. **18**(6): p. 1762-1773.
29. Huang, J., et al., *Density functional theory studies on pyrolysis mechanism of β -O-4 type lignin dimer model compound*. *Journal of Analytical and Applied Pyrolysis*, 2014. **109**: p. 98-108.
30. Klein, M.T. and P.S. Virk, *Model pathways in lignin thermolysis. 1. Phenethyl phenyl ether*. *Industrial & Engineering Chemistry Fundamentals*, 1983. **22**(1): p. 35-45.
31. Wikipedia. *Ene reaction (Alder-ene reaction)*. Available from: https://en.wikipedia.org/wiki/Ene_reaction.
32. Chen, J., C. Liu, and S.-b. Wu, *Catalytic Fast Pyrolysis of Alcell Lignin with Nano-NiO*. *BioResources*, 2015. **11**(1).
33. Zhang, M., F.L.P. Resende, and A. Moutsoglou, *Catalytic fast pyrolysis of aspen lignin via Py-GC/MS*. *Fuel*, 2014. **116**: p. 358-369.
34. Pandey, M.P. and C.S. Kim, *Lignin Depolymerization and Conversion: A Review of Thermochemical Methods*. *Chemical Engineering & Technology*, 2011. **34**(1): p. 29-41.
35. Richardson, Y., et al., *Biomass Gasification to Produce Syngas*, in *Recent Advances in Thermo-Chemical Conversion of Biomass*. 2015. p. 213-250.
36. Fang, Z., *Production of Biofuels and Chemicals from Lignin*. Springer. Vol. 6. 2016.
37. Wang, S., et al., *Pyrolysis behaviors of four lignin polymers isolated from the same pine wood*. *Bioresour Technol*, 2015. **182**: p. 120-127.
38. Yu, Y., et al., *The role of shape selectivity in catalytic fast pyrolysis of lignin with zeolite catalysts*. *Applied Catalysis A: General*, 2012. **447-448**: p. 115-123.
39. Bi, Y., et al., *Catalytic Fast Pyrolysis of Kraft Lignin over Hierarchical HZSM-5 and H β Zeolites*. *Catalysts*, 2018. **8**(2).
40. Lazaridis, P.A., et al., *Catalytic Fast Pyrolysis of Kraft Lignin With Conventional, Mesoporous and Nanosized ZSM-5 Zeolite for the Production of Alkyl-Phenols and Aromatics*. *Front Chem*, 2018. **6**: p. 295.
41. Paysepar, H., et al., *Improving activity of ZSM-5 zeolite catalyst for the production of monomeric aromatics/phenolics from hydrolysis lignin via catalytic fast pyrolysis*. *Applied Catalysis A: General*, 2018. **563**: p. 154-162.
42. Ma, Z., E. Troussard, and J.A. van Bokhoven, *Controlling the selectivity to chemicals from lignin via catalytic fast pyrolysis*. *Applied Catalysis A: General*, 2012. **423-424**: p. 130-136.
43. Mullen, C.A. and A.A. Boateng, *Catalytic pyrolysis-GC/MS of lignin from several sources*. *Fuel Processing Technology*, 2010. **91**(11): p. 1446-1458.
44. Zheng, Y., D. Chen, and X. Zhu, *Aromatic hydrocarbon production by the online catalytic cracking of lignin fast pyrolysis vapors using Mo2N/ γ -Al2O3*. *Journal of Analytical and Applied Pyrolysis*, 2013. **104**: p. 514-520.
45. Yang, M., et al., *Conversion of lignin into light olefins and aromatics over Fe/ZSM-5 catalytic fast pyrolysis: Significance of Fe contents and temperature*. *Journal of Analytical and Applied Pyrolysis*, 2019. **137**: p. 259-265.
46. Li, X., et al., *Catalytic fast pyrolysis of Kraft lignin with HZSM-5 zeolite for producing aromatic hydrocarbons*. *Frontiers of Environmental Science & Engineering*, 2012. **6**(3): p. 295-303.
47. Lou, R., S.-b. Wu, and G.-j. Lv, *Effect of conditions on fast pyrolysis of bamboo lignin*. *Journal of Analytical and Applied Pyrolysis*, 2010. **89**(2): p. 191-196.
48. Karnjanakom, S., et al., *High selectivity and stability of Mg-doped Al-MCM-41 for in-situ catalytic upgrading fast pyrolysis bio-oil*. *Energy Conversion and Management*, 2017. **142**: p. 272-285.
49. Elfadly, A.M., et al., *Highly selective BTX from catalytic fast pyrolysis of lignin over supported mesoporous silica*. *Int J Biol Macromol*, 2016. **91**: p. 278-93.

50. Xie, W., et al., *Ex-situ catalytic microwave pyrolysis of lignin over Co/ZSM-5 to upgrade bio-oil*. Journal of Analytical and Applied Pyrolysis, 2018. **132**: p. 163-170.
51. Jean Marcel Ribeiro Gallo and J.M.C. Bueno, *Catalytic Transformations of Ethanol for Biorefineries*. Brazilian Chemical Society, 2014.
52. Mike Kleinert, J.R.G., Ingvar Eide,*Ann-Mari Hilmen And Tanja Barth *Developing Solvolytic Conversion Of Lignin-To-Liquid (Ltl) Fuel Components: Optimization Of Quality And Process Factors*. 2009.
53. Rahimi, A., et al., *Formic-acid-induced depolymerization of oxidized lignin to aromatics*. Nature, 2014. **515**(7526): p. 249-52.
54. Huang, X., et al., *Catalytic depolymerization of lignin in supercritical ethanol*. ChemSusChem, 2014. **7**(8): p. 2276-88.
55. Ma, R., et al., *Catalytic ethanolysis of Kraft lignin into high-value small-molecular chemicals over a nanostructured alpha-molybdenum carbide catalyst*. Angew Chem Int Ed Engl, 2014. **53**(28): p. 7310-5.
56. Ohta, H., et al., *Hydrodeoxygenation of phenols as lignin models under acid-free conditions with carbon-supported platinum catalysts*. Chem Commun (Camb), 2011. **47**(44): p. 12209-11.
57. Jang, M.S., et al., *Catalytic upgrading of lignin derived bio-oil model compound using mesoporous solid catalysts*. Research on Chemical Intermediates, 2015. **42**(1): p. 3-17.
58. Selvaraj, M., et al., *Hydrodeoxygenation of Guaiacol over MoO₃-NiO/Mesoporous Silicates: Effect of Incorporated Heteroatom*. Energy & Fuels, 2014. **28**(4): p. 2598-2607.
59. Deutsch, K.L. and B.H. Shanks, *Hydrodeoxygenation of lignin model compounds over a copper chromite catalyst*. Applied Catalysis A: General, 2012. **447-448**: p. 144-150.
60. Niwa, M., N. Katada, and K. Okumura, *Characterization and Design of Zeolite Catalysts*. Springer.
61. Teng, W.C., *Removal of volatile organic compound (voc) from air using zeolite based adsorption-catalytic combustion system*. Master of Science, 2007.
62. Kulprathipanja, S., *Zeolites in Industrial Separation and Catalysis*. John Wiley & Sons.
63. Byggningsbacka, R., L.-E. Lindfors, and N. Kumar, *Catalytic Activity of ZSM-22 Zeolites in the Skeletal Isomerization Reaction of 1-Butene*. Industrial & Engineering Chemistry Research, 1997. **36**(8): p. 2990-2995.
64. Material, A. *SAPO-11 properties*. Available from: <https://www.acsmaterial.com/sapo-1354.html>.
65. Jong, K.P.d., *Synthesis of Solid Catalysts*. 2010.
66. Deraz, N.M., *The comparative jurisprudence of catalysts preparation methods: I. precipitation and impregnation methods*. Allied academies: Journal of Industrial and Environmental Chemistry, 2018.
67. NPTEL. *Heterogeneous Catalysis*. 2014; Available from: <https://nptel.ac.in/courses/103103026/10>.
68. I. Chorkendorff, J.W.N., *Concepts of Modern Catalysis and Kinetics*.
69. G. Ertl, H.K., F. Schuth, J. Weitkamp, *Handbook of Heterogeneous Catalysis*. WILEY-VCH. Vol. 1. 2008.
70. G. Ertl, H.K., F. Schuth, J. Weitkamp, *Handbook of Heterogeneous Catalysis, Vol. 1(b-ok.xyz)*.
71. Tang, X., et al., *The effect of the variation in material composition on the heterogeneous pore structure of high-maturity shale of the Silurian Longmaxi formation in the southeastern Sichuan Basin, China*. Journal of Natural Gas Science and Engineering, 2015. **23**: p. 464-473.
72. CAMBRIDGE, U.o. *X-ray Diffraction*. Available from: <https://www.doitpoms.ac.uk/tlplib/xray-diffraction/production.php>.
73. Bunaciu, A.A., E.G. Udristioiu, and H.Y. Aboul-Enein, *X-ray diffraction: instrumentation and applications*. Crit Rev Anal Chem, 2015. **45**(4): p. 289-99.

74. Geesink, H.J.H. and D.K.F. Meijer, *Mathematical Structure for Electromagnetic Frequencies that May Reflect Pilot Waves of Bohm's Implicate Order*. Journal of Modern Physics, 2018. **09**(05): p. 851-897.
75. *Bragg's Law*. Available from: <http://hyperphysics.phy-astr.gsu.edu/hbase/quantum/bragg.html>.
76. Auroux, A., *Calorimetry and Thermal Methods in Catalysis*. Vol. 154. 2013.
77. Anderson Materials Evaluation, I. *TGA Analysis or Thermogravimetric Analysis*. Available from: <http://www.andersonmaterials.com/tga.html>.
78. Anderson Materials Evaluation, I. *Differential Scanning Calorimetry (DSC) Thermal Analysis*. Available from: <http://www.andersonmaterials.com/dsc.html>.
79. LTD., F.L., *Multi-Shot Pyrolyzer Model EGA/Py-3030d Operation Manual*.
80. Sciences, C.-A. *Gas chromatography- Theraml conductivity detector* Available from: <http://www.chromedia.org/chromedia?waxtrapp=mdqucDsHqnOxmOIIcCbCqEjEsB&subNav=jvfeoDsHqnOxmOIIcCbCqEjEsBzB>.
81. Products, A. *GC with Thermal Conductivity Detector (GC-TCD)* Available from: <http://www.airproducts.com/Industries/Analytical-Laboratories/analytical-lab-applications/product-list/gc-with-thermal-conductivity-detector-gc-tcd-analytical-laboratories.aspx?itemId=651A80DACEBF49F4993E7C447B42808E>.
82. Linde, *Thermal conductivity detector (TCD). Specialty Gases & Specialty Equipment*.
83. Linde. *Flame ionisation detector (FID)*. Available from: http://hiq.linde-gas.com/en/analytical_methods/gas_chromatography/flame_ionisation_detector.html.
84. Hinshaw, J.V., *The Flame Ionization Detector*. <http://www.chromatographyonline.com/flame-ionization-detector-0?id=&pageID=1&sk=&date=>.
85. *The Flame Ionization Detector*. Available from: <http://www.ecs.umass.edu/eve/facilities/equipment/Agilent6890/The%20Flame%20Ionization%20Detector.pdf>.
86. Sundli, E.N., *Master thesis* Department of Chemical Engineering, Norwegian University of Science and Technology, 2018.
87. Marko R. Djokic, T.D., Guray Yildiz, Wolter Prins, Kevin M. Van Geem, *Quantitative analysis of crude and stabilized biooils by comprehensive two dimensional gas chromatography*. Journal of Chromatography A, 2012. **Volume 1257**: p. Pages 131-140.
88. Schofield, K., *The enigmatic mechanism of the flame ionization detector: Its overlooked implications for fossil fuel combustion modeling*. Progress in Energy and Combustion Science, 2008. **34**(3): p. 330-350.
89. Thommes, M., et al., *Physisorption of gases, with special reference to the evaluation of surface area and pore size distribution (IUPAC Technical Report)*. Pure and Applied Chemistry, 2015. **87**(9-10): p. 1051-1069.
90. M.M.J. Treacy and J.B. Higgins, *Collection of Simulated XRD Powder Patterns for Zeolites*. ELSEVIER, 2001. **Fourth Revised Edition**.
91. Zhao, C. and J.A. Lercher, *Upgrading pyrolysis oil over Ni/HZSM-5 by cascade reactions*. Angew Chem Int Ed Engl, 2012. **51**(24): p. 5935-40.
92. Li, G. and E.A. Pidko, *The Nature and Catalytic Function of Cation Sites in Zeolites: a Computational Perspective*. ChemCatChem, 2018. **11**(1): p. 134-156.
93. Deka, R.C., *Acidity in zeolites and their characterization by different spectroscopic methods*. Indian Journal of Chemical Technology, 1998. **5**: p. 109-123.
94. Hunger, B., et al., *Characterization of Acidic OH Groups in Zeolites of Different Types: An Interpretation of NH₃-TPD Results in the Light of Confinement Effects*. The Journal of Physical Chemistry B, 2002. **106**(15): p. 3882-3889.
95. Zhang, H., et al., *Characterization of Coke Deposition in the Catalytic Fast Pyrolysis of Biomass Derivates*. Energy & Fuels, 2013. **28**(1): p. 52-57.

96. Huang, J., et al., *Effect of pore size and acidity on the coke formation during ethylbenzene conversion on zeolite catalysts*. Journal of Catalysis, 2009. **263**(2): p. 277-283.
97. Henrique S. Cerqueira a, P.A.a., Jerzy Datka b, Michel Guisnet a,* , *Influence of coke on the acid properties of a USHY zeolite*. ELSEVIER, 1999.
98. Zhao, J., et al., *Thermal degradation of softwood lignin and hardwood lignin by TG-FTIR and Py-GC/MS*. Polymer Degradation and Stability, 2014. **108**: p. 133-138.
99. Gafurov, M.R., et al., *Quantitative Analysis of Lewis Acid Centers of γ -Alumina by Using EPR of the Adsorbed Anthraquinone as a Probe Molecule: Comparison with the Pyridine, Carbon Monoxide IR, and TPD of Ammonia*. The Journal of Physical Chemistry C, 2015. **119**(49): p. 27410-27415.
100. Klein, M.T. and P.S. Virk, *Modeling of Lignin Thermolysis*. 2008.
101. Chary, K.V.R., et al., *Characterization and Reactivity of Molybdenum Oxide Catalysts Supported on Niobia*. The Journal of Physical Chemistry B, 2001. **105**(19): p. 4392-4399.
102. Spivey, J.J., *Catalysis*. Vol. 18. 2005.
103. Ma, Z., et al., *Chemicals from Lignin by Catalytic Fast Pyrolysis, from Product Control to Reaction Mechanism*. Chimia (Aarau), 2015. **69**(10): p. 597-602.
104. Kulprathipanja, S. *Zeolites in Industrial Separation and Catalysis*. Available from: <https://app.knovel.com/hotlink/toc/id:kpZISC0001/zeolites-in-industrial/zeolites-in-industrial>.
105. Webster, C.E., R.S. Drago, and M.C. Zerner, *A Method for Characterizing Effective Pore Sizes of Catalysts*. The Journal of Physical Chemistry B, 1999. **103**(8): p. 1242-1249.
106. Jae, J., et al., *Investigation into the shape selectivity of zeolite catalysts for biomass conversion*. Journal of Catalysis, 2011. **279**(2): p. 257-268.
107. Lee, I.-G., et al., *Catalytic Pyrolysis of Cellulose over SAPO-11 Using Py-GC/MS*. Bulletin of the Korean Chemical Society, 2013. **34**(8): p. 2399-2402.
108. Wu, X., et al., *Enhanced n-dodecane hydroisomerization performance by tailoring acid sites on bifunctional Pt/ZSM-22 via alkaline treatment*. New Journal of Chemistry, 2018. **42**(1): p. 111-117.
109. Castello, D., et al., *Is it possible to increase the oil yield of catalytic pyrolysis of biomass? A study using commercially-available acid and basic catalysts in ex-situ and in-situ modus*. Journal of Analytical and Applied Pyrolysis, 2019. **137**: p. 77-85.
110. Wang, B., *Zeolite Deactivation During Hydrocarbon Reactions: Characterisation Of Coke Precursors And Acidity, Product Distribution*, in *Department of Chemical Engineering*. 2007, University College London.
111. Zheng, A., et al., *Effect of crystal size of ZSM-5 on the aromatic yield and selectivity from catalytic fast pyrolysis of biomass*. Journal of Molecular Catalysis A: Chemical, 2014. **383-384**: p. 23-30.
112. Zhang, X., et al., *Gasoline-range hydrocarbons produced from microwave-induced pyrolysis of low-density polyethylene over ZSM-5*. Fuel, 2015. **144**: p. 33-42.
113. Yeboah, I., *Tandem Catalytic Upgrading of Biomass Fast-Pyrolysis Constituents to Fuels*, in *Department of Chemical Engineering*. 2019, Norwegian University of Science and Technology.
114. Nowakowska, M., et al., *Kinetic Study of the Pyrolysis and Oxidation of Guaiacol*. J Phys Chem A, 2018. **122**(39): p. 7894-7909.
115. Ashenhurst, J. *Activating and Deactivating Groups In Electrophilic Aromatic Substitution*. Master Organic Chemistry 2019 April 25th; Available from: <https://www.masterorganicchemistry.com/2017/09/26/activating-and-deactivating-groups-in-electrophilic-aromatic-substitution/>.
116. Mullery, A.A., et al., *Thermal decomposition pathways of 4-ethylguaiacol under fast pyrolysis and gasification conditions*. Journal of Analytical and Applied Pyrolysis, 2017. **123**: p. 83-91.

117. Minami Akazawa¹, Y.K., Yoshiaki Kato², *Reaction mechanisms of pyrolysis of four different phenylpropanoids*. US Open Pyrolysis Technology Journal, 2015.
118. Max Roser, H.R., Esteban Ortiz-Ospina. *World Population Growth*. 2019; Available from: <https://ourworldindata.org/world-population-growth>.
119. *Ecotricity*. Available from: <https://www.ecotricity.co.uk/our-green-energy/energy-independence/the-end-of-fossil-fuels>.

8 Appendix

A1. Introduction

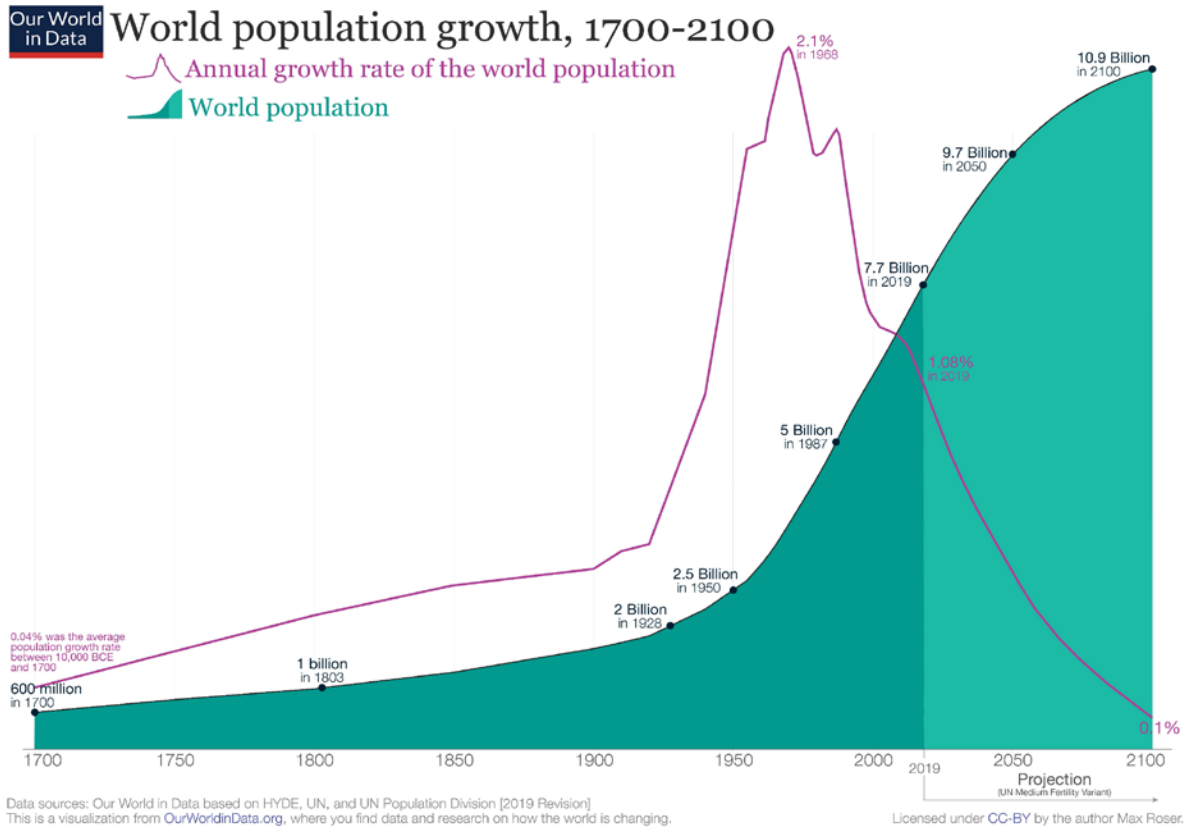


Figure 8.1 The evolution of world population number and of the population growth[118]

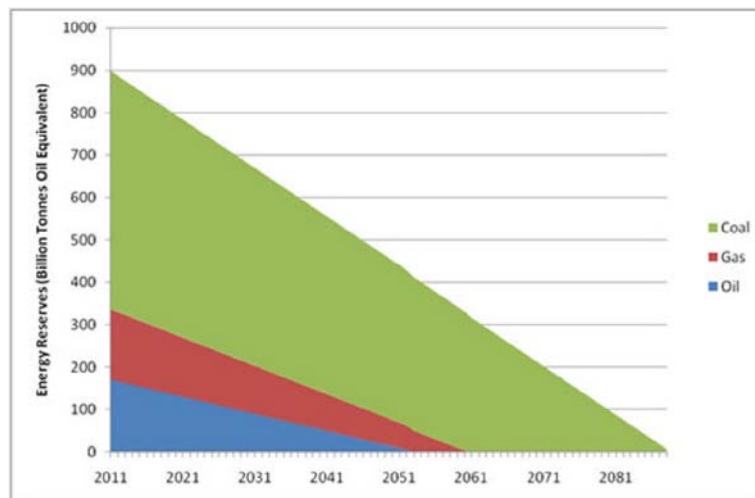


Figure 8.2 The estimated period of depletion of fossil fuel[119]

A2. Literature Survey and Theory

Lignocellulosic Biomass		Cellulose (%)	Hemicellulose (%)	Lignin (%)
Hardwood	Poplar	50.8-53.3	26.2-28.7	15.5-16.3
	Oak	40.4	35.9	24.1
	Eucalyptus	54.1	18.4	21.5
Softwood	Pine	42.0-50.0	24.0-27.0	20.0
	Douglas fir	44.0	11.0	27.0
	Spruce	45.5	22.9	27.9
Agricultural Waste	Wheat Straw	35.0-39.0	23.0-30.0	12.0-16.0
	Barley Hull	34.0	36.0	13.8-19.0
	Barley Straw	36.0-43.0	24.0-33.0	6.3-9.8
	Rice Straw	29.2-34.7	23.0-25.9	17.0-19.0
	Rice Husks	28.7-35.6	12.0-29.3	15.4-20.0
	Oat Straw	31.0-35.0	20.0-26.0	10.0-15.0
	Ray Straw	36.2-47.0	19.0-24.5	9.9-24.0
	Corn Cobs	33.7-41.2	31.9-36.0	6.1-15.9
	Corn Stalks	35.0-39.6	16.8-35.0	7.0-18.4
	Sugarcane Bagasse	25.0-45.0	28.0-32.0	15.0-25.0
	Sorghum Straw	32.0-35.0	24.0-27.0	15.0-21.0
Grasses	Grasses	25.0-40.0	25.0-50.0	10.0-30.0
	Switchgrass	35.0-40.0	25.0-30.0	15.0-20.0

Table 8.1 Lignocellulosic biomass species and their composition[7]

Plant	p-Coumaryl alcohol (%)	Coniferyl alcohol (%)	Sinapyl alcohol (%)
Coniferous" softwood	<5	>95	None or Trace
Eudicotyledonous hard-wood	0-8	25-50	46-75
Monocotyledonous grass	5-33	33-80	20-54

Table 8.2 The approximate content of the three monolignols in different plants[12]

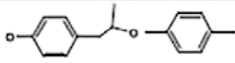
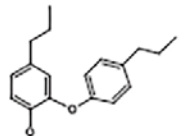
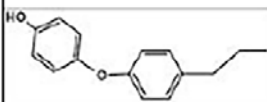
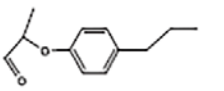
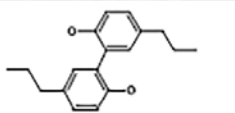
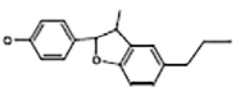
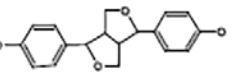
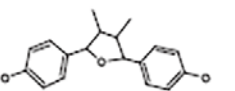
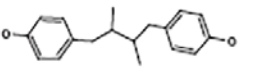
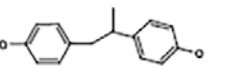
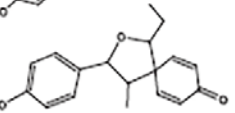
Name	Bonds	Structure*	Frequency softwood (%)	Frequency hardwood (%)
Ether bonds				
β -aryl ether	β -O-4'		35-60	50-70
Diaryl ether	4-O-5'		<4	7?
	1-O-4'		low	low
Glyceraldehyde aryl ether	β -O-4'		<1	<1
Carbon-carbon bonds (condensed bonds)				
Dihydroxy biphenyl	5-5'		10	~5
Phenyl coumarane	β -5'		11-12	4-9
Pinoresinol	$\beta\beta$ '		2-3	3-4
	$\beta\beta$ '		<1	none
Secoisolaricresinol			1-2	none
	β -1'		1-2	1
Spirodienon	β -1'		1-3	2-3

Table 8.3 Frequency of different ether and condensed bonds in softwood and hardwood lignin[12]

No.	Compounds	x (Å)	y (Å)	z (Å)	Critical diameter in literatures (Å)
<i>Oxygenate</i>					
1	Furfural	8.111	6.477	3.400	
2	Phenol	8.098	6.728	3.400	6.701 [34]
3	Phenol, 2-methyl-	8.140	7.426	4.168	
4	Phenol, 3-methyl-	8.728	7.358	4.167	
5	Phenol, 2-methoxy-	9.476	8.101	4.197	
6	Phenol, 6-methoxy-2-methyl-	9.863	7.671	4.218	
7	Phenol, 2-methoxy-4-methyl-	9.272	7.912	4.196	
8	1,2-Benzenediol	7.364	7.325	3.400	
9	1,2-Benzenediol, 3-methoxy-	9.965	7.931	4.197	
10	Phenol, 4-ethyl-2-methoxy-	10.696	8.053	4.197	
11	1,2-Benzenediol, 4-methyl-	8.756	7.693	4.167	
12	2-Methoxy-4-vinylphenol	10.555	8.109	4.197	
13	Phenol, 2,6-dimethoxy-	10.738	7.856	4.218	
14	Phenol, 2,4-dimethoxy-	10.376	8.048	4.197	
15	1,2,3-Benzenetriol	8.760	7.990	3.400	
16	Benzaldehyde, 4-hydroxy-3-methoxy-	10.193	7.331	4.187	
17	1,2,3-Trimethoxybenzene	11.154	9.522	4.197	
18	Ethanone, 1-(4-hydroxy-3-methoxyphenyl)-	10.778	7.950	4.187	
19	Durohydroquinone	9.213	8.802	4.177	
20	Benzene, 1,2,3-trimethoxy-5-methyl-	10.833	10.156	4.197	
21	4-Methyl-2,6-dimethoxybenzaldehyde	10.036	9.489	5.223	
22	Benzaldehyde, 4-hydroxy-3,5-dimethoxy-	10.401	9.765	4.197	
23	Phenol, 2,6-dimethoxy-4-(2-propenyl)-	11.414	10.781	4.218	
24	Ethanone, 1-(4-hydroxy-3,5-dimethoxyphenyl)-	11.014	10.247	4.199	
25	Benzoic acid, 4-hydroxy-3,5-dimethoxy-	10.218	10.103	4.197	
<i>Aromatic</i>					
26	Benzene	7.367	6.702	3.400	6.63 [35], 6.7 [28]
27	Toluene	8.314	6.701	4.172	6.7 [28]
28	Ethylbenzene	9.726	7.157	4.175	6.7 [28]
29	<i>p</i> -Xylene	9.085	6.701	4.168	6.63 [35], 6.7 [28], 6.7 [36]
	<i>m</i> -Xylene	8.937	7.437	4.167	7.4 [28], 7.4 [37], 7.4 [36]
30	<i>o</i> -Xylene	7.969	7.345	4.166	7.3 [35], 7.3 [28], 7.4 [36]
31	Benzene, 1,3,5-trimethyl-	8.952	8.471	4.168	8.35 [35], 8.6 [37]
32	Benzene, 1,2,4-trimethyl-	9.297	7.916	4.167	7.4 [37], 8.0 [36]
33	Benzene, 1,2,3-trimethyl-	8.734	8.318	4.166	7.9 [37], 8.0 [36]
34	Indene	9.085	7.411	4.162	
35	Benzene, 1,2,4,5-tetramethyl-	8.954	7.560	4.167	7.4 [37]
36	Benzene, 1,2,3,5-tetramethyl-	9.121	8.728	4.167	8.6 [37]
37	Benzene, 1,2,3,4-tetramethyl-	9.139	7.701	4.168	7.9 [37]
38	Naphthalene	9.173	7.389	3.402	6.8 [35], 7.19 [38]
39	Benzene, pentamethyl-	9.017	8.449	4.165	
40	Naphthalene, 2-methyl-	10.485	7.752	4.166	7.1 [39]
41	Naphthalene, 1-methyl-	9.611	8.097	4.167	7.65 [40], 8.1 [39]
42	Naphthalene, 2,6-dimethyl-	11.403	7.443	4.170	7.2 [39]
43	Naphthalene, 1,7-dimethyl-	10.481	8.321	4.169	
44	Naphthalene, 1,6-dimethyl-	10.513	7.984	4.168	
45	Naphthalene, 2,3-dimethyl-	10.430	7.482	4.168	
46	Naphthalene, 1,4,6-trimethyl-	10.530	9.194	4.168	
47	Naphthalene, 1,6,7-trimethyl-	10.681	8.256	4.169	
48	Anthracene	11.639	7.397	3.402	
49	Fluoranthene	11.086	9.211	3.401	
50	Pyrene	11.643	9.217	3.401	

Table 8.4 The dimensions of the compounds resulted in the non-catalytic fast pyrolysis (non-CFP) and catalytic fast pyrolysis (CFP) of lignin[38]

Zeolite species		Process	Company
Y (FAU)	USY, CaHY, LaHY	Catalytic cracking	
ZSM-5 (MFI)		Isomerization Alkylation Disproportionation	
	Silicalite	Beckmann rearrangement [2]	Sumitomo Chemical
	Me-MFI (dispersed)	Pyridine bases synthesis [3] Hydration of cyclohexene [4]	Koei Chemical Asahi Chemical
	Me(Cu [6], Fe [7], Co [8])-MFI	NO reduction	Nippon Shokubai
Mordenite (MOR)	Mo-MFI [9]	Aromatization of methane Trans-alkylation, Isomerization, Disproportionation	
	(modified)	Methylamine synthesis [10]	Nitto Chemical
MCM-22 (MWW) β (BEA)		Alkylation of benzene [11] Alkylation of benzene Acylation with acetic anhydride [12]	Mobil
L (LTL) SAPO-34 Titanosilicate	Pt-L	Aromatization [13, 14] Methanol to olefin H_2O_2 oxidation [15, 16]	UOP Eni-Chem

Table 8.5 Different applications of zeolites in industrial processes[60]

T-atoms in ring	Maximum free aperture (nm)	Typical free apertures (nm)
4	0.16	–
5	0.15	–
6	0.28	–
8	0.43	0.30–0.45
10	0.63	0.45–0.60
12	0.80	0.60–0.80

Table 8.6 The free aperture of different n-rings[62]

A3. Material and Methods

Support	Water/1g of support, ml	Mass of catalyst, g	Mass of support, g	Mass of active phase, g	Total volume of water, ml
Al ₂ O ₃	1	15	14.25	0.75	14.25
Al ₂ O ₃	1	15	12.75	2.25	12.75
HZSM-5	0.96	15	13.5	1.5	12.96
H β	1.3	15	13.5	1.5	17.55
HY	0.9	15	13.5	1.5	12.15

Table 8.7 The estimated pore volume of the 4 supports and the total water volume used for the dissolution of metal precursor

Chemical	Details	Supplier
NH ₄ -ZSM-5	SiO/Al ₂ O ₃ = 30, 50, 80, 280	Zeolyst
NH ₄ -Y	SiO/Al ₂ O ₃ =6	
β	cation type –H crystallinity=95% SiO/Al ₂ O ₃ =25 S _{area} =640 m ² /g	
SAPO-11	SiO/Al ₂ O ₃ =0.5 P ₂ O ₅ /SiO=1	
SAPO-34	cation type –H crystallinity=95% SiO/Al ₂ O ₃ =0.5 S _{area} =570 m ² /g Pore volume=0.28	
HZSM-22	SiO/Al ₂ O ₃ =70	
Ammonium phosphate dibasic: (NH ₄) ₂ HPO ₄	Purity = 99.99%	Sigma Aldrich
Ammonium molybdate tetrahydrate: (NH ₄) ₆ Mo ₇ O ₂₄ ·4H ₂ O	Purity \geq 99%	Sigma Aldrich

Chemical	Details	Supplier
2-methoxy-4-propylphenol	Purity \geq 99%	Sigma Aldrich
4'-hydroxy-3'-methoxyacetophenone	Purity \geq 98%	Sigma Aldrich
4-ethylguaiacol	Purity \geq 98%	Sigma Aldrich
Guaiacol	Purity \geq 99%	Sigma Aldrich
Trans-Isoeugenol	Purity \geq 99%	Sigma Aldrich
2-methoxy-4-methylphenol	Purity \geq 99%	Sigma Aldrich
Vanillin	Purity \geq 99%	Sigma Aldrich
Lignin	High purity	ST1 (Etanolix)
Polyethylene	High purity	Sigma Aldrich
γ -Al ₂ O ₃ (PURALOX)		Sasol (Germany)

Table 8.8 The chemicals used within the master thesis

I. Equation A3.1

Calculation of the amount of precursors used in the synthesis of catalyst via incipient wetness impregnation:

$$n_P = n_{M_0} = n \quad (\text{A3.1})$$

$$m_{\text{active phase}} = n_P \cdot M_P + n_{M_0} \cdot M_{M_0}$$

$$m_{\text{active phase}} = n \cdot (M_P + M_{M_0}) \quad (\text{A3.2})$$

$$n = \frac{m_{\text{active phase}}}{(M_P + M_{M_0})}$$

$$m_{\text{precursor}} = n \cdot \frac{M_{\text{precursor}}}{v_{\text{element(Mo or P)}}} \quad (\text{A5.3})$$

Where n: number of moles, [mol]; M: molar mass, [g/mol]; m: mass, [g]; v: stoichiometric coefficient of the element in the precursor.

Gas name	Composition, mol-%
Methane	1
Ethane	0.101
Ethene	0.101
Propane	0.1
Butane-n	0.15
Pentane-n	0.15
Hexane-n	0.098
Propene	0.1
Carbon monoxide	30.4
Hydrogen	63.8
Carbon dioxide	1
Nitrogen	3

Table 8.9 Gas mixture used for GC/FID/TCD calibration

II. Equation A3.II

The equations used for calculation of gas products mass

Equation used for TCD compounds:

$$F_i(\text{mol/h}) = \frac{f_i}{f_{\text{N}_2}} \cdot \frac{A_i}{A_{\text{N}_2}} \cdot F_{\text{N}_2}(\text{mol/h}) \quad (\text{A3.4})$$

$$m_i = F_i \cdot M_i \quad (\text{A3.5})$$

Equation used for FID compounds:

$$F_i(\text{mol/h}) = \frac{f_i}{f_{\text{CH}_4}} \cdot \frac{A_i}{A_{\text{CH}_4}} \cdot F_{\text{CH}_4}(\text{mol/h}) \quad (\text{A3.6})$$

$$m_i = F_i \cdot M_i \quad (\text{A3.7})$$

Where F_i , F_{N_2} and F_{CH_4} - molar flow of compound i, nitrogen and methane respectively, f_i , f_{N_2} and f_{CH_4} - the response factors of compound i, nitrogen and methane, A_i , A_{N_2} and A_{CH_4} - the peak area of compound i, nitrogen and methane, M_i, m_i - molar mass and mass of compound i.

A4. Results and Discussion

N₂ adsorption: BET plots

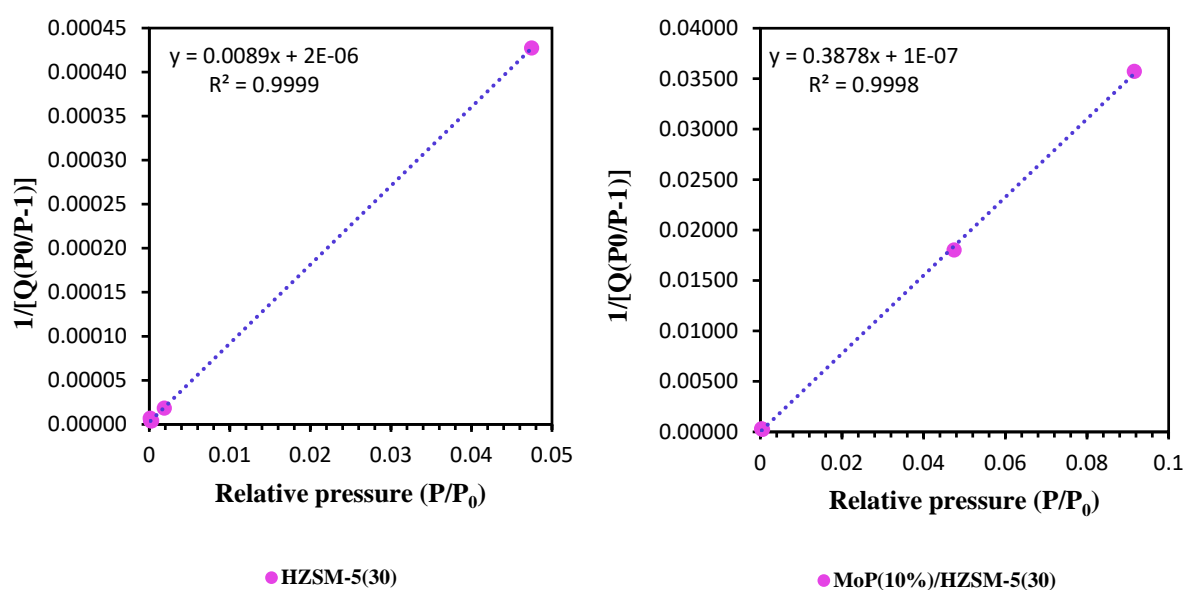


Figure 8.3 N₂ adsorption BET plots of HZSM-5(30) (left) and MoP (10 %)/ HZSM-5(30) (right)

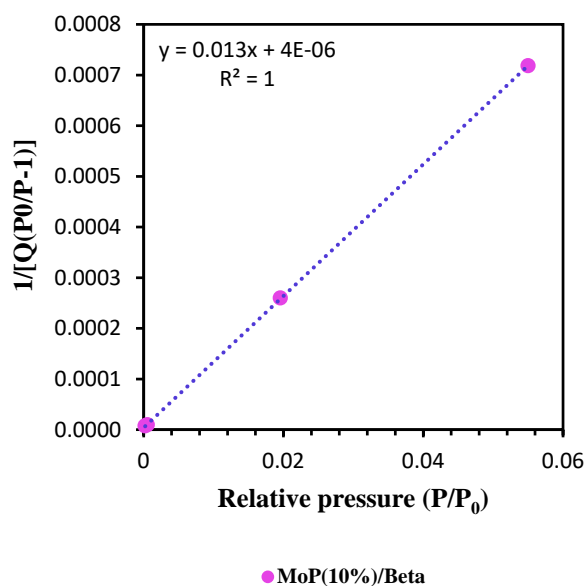


Figure 8.4 N₂ adsorption BET plot of MoP (10 %)/ H β

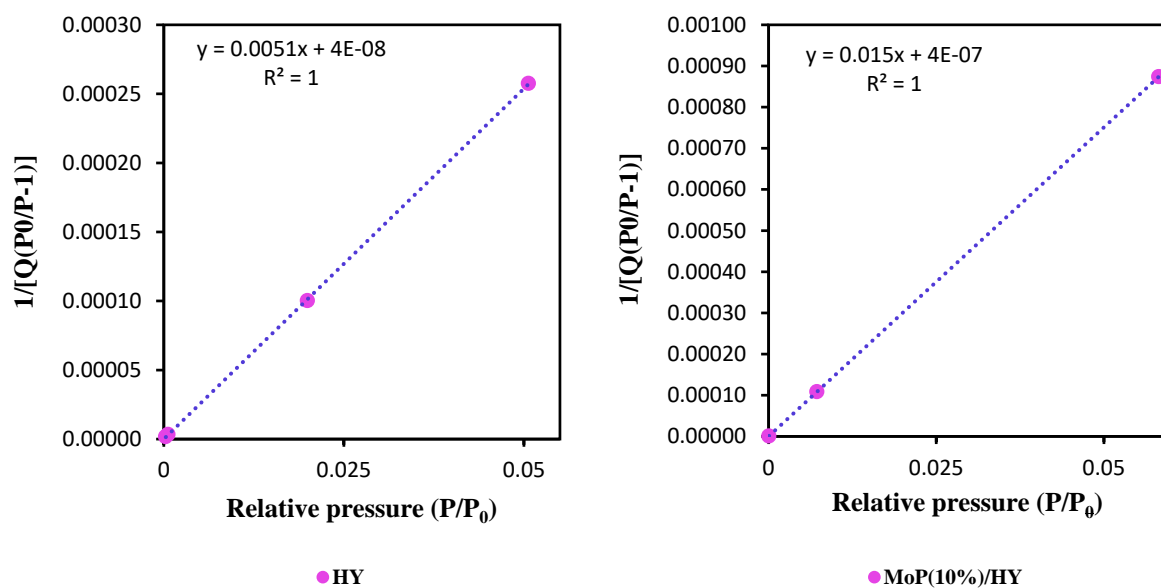


Figure 8.5 N₂ adsorption BET plots of HY (left) and MoP (10 %)/ HY (right)

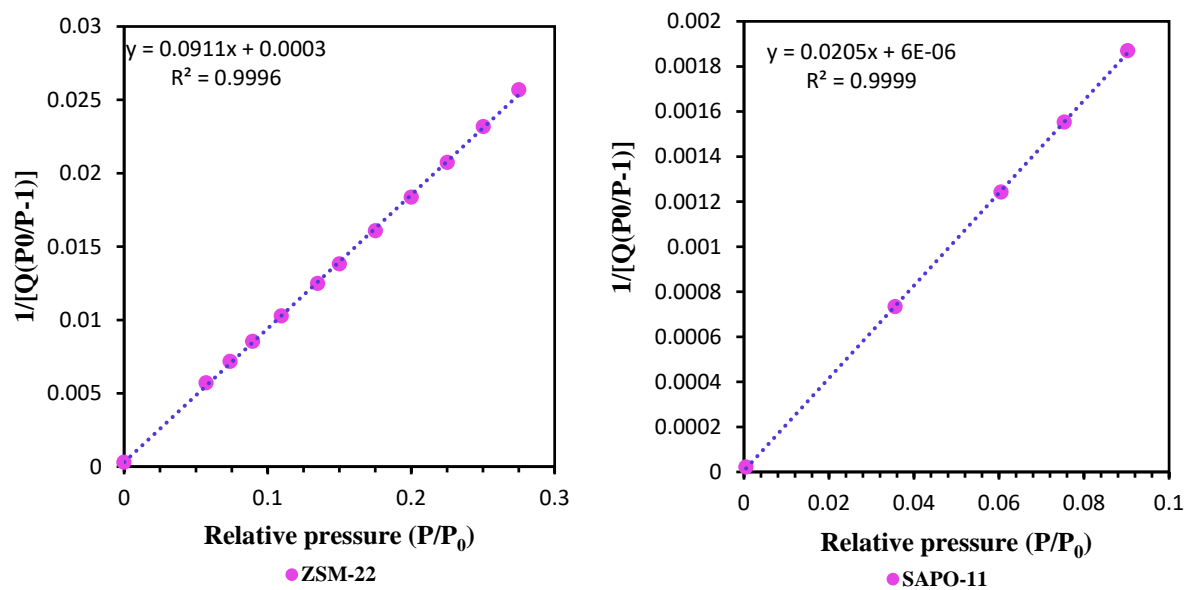


Figure 8.6 N₂ adsorption BET plots of ZSM-22 (left) and SAPO-11 (right)

Sample	Surface area, [m ² /g]
Calcined γ -Al ₂ O ₃	164
Calcined MoP(10%)/ γ -Al ₂ O ₃	149

Table 8.10 The surface area of the calcined support and catalyst: γ -Al₂O₃ and MoP(10%)/ γ -Al₂O₃ Sundli [76]

Thermal Gravimetric Analysis-Mass Spectrometry

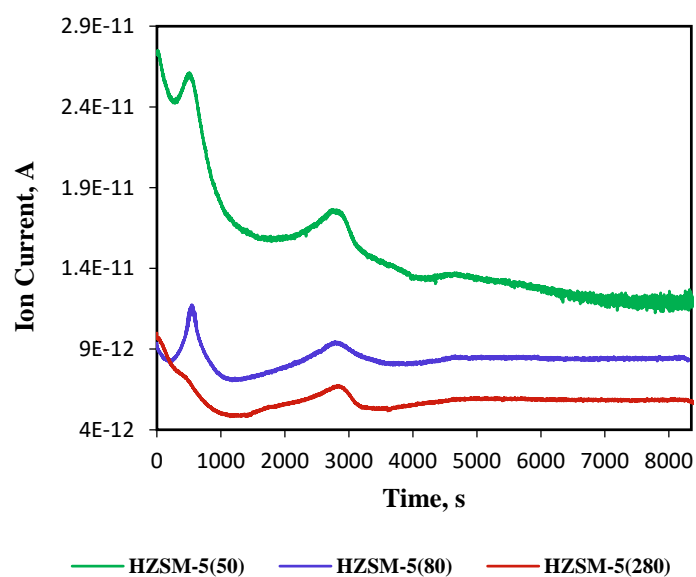


Figure 8.7 The H₂O ion current (MS) and HDSC of HZSM-5 with Si/Al ratio of 50, 80 and 280 (FP-CU: 550 °C, N₂ flow=40 mL/min, C:L=1)

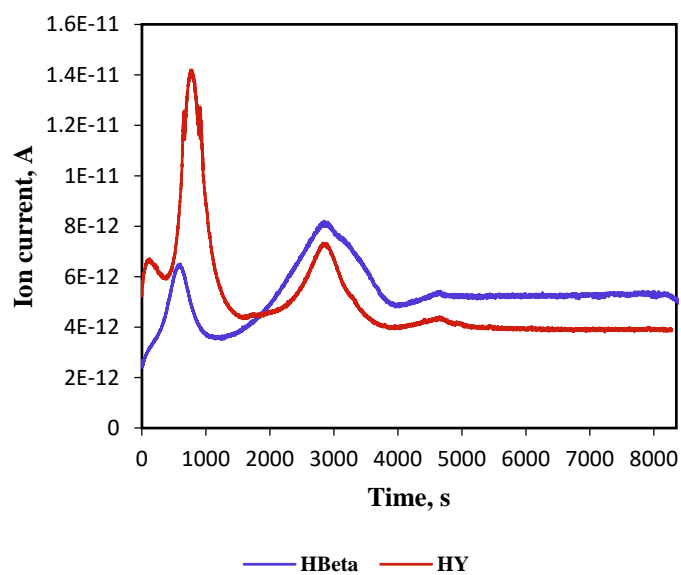


Figure 8.8 The H₂O ion current (MS) and HDSC of Hβ and HY (FP-CU: 550 °C, N₂ flow=40 mL/min, C:L=1)

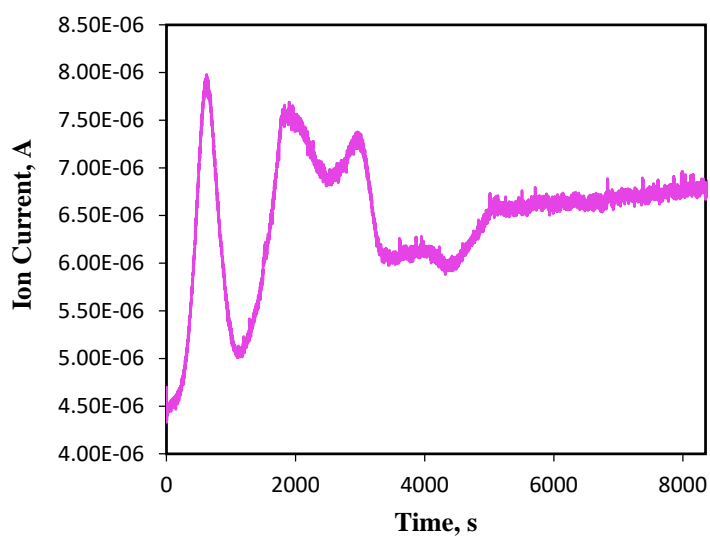


Figure 8.9 The H₂O ion current (MS) and HDSC of HZSM-5(30) involved in FP-CU at 450 °C (N₂ flow=40 mL/min, C:L=1)

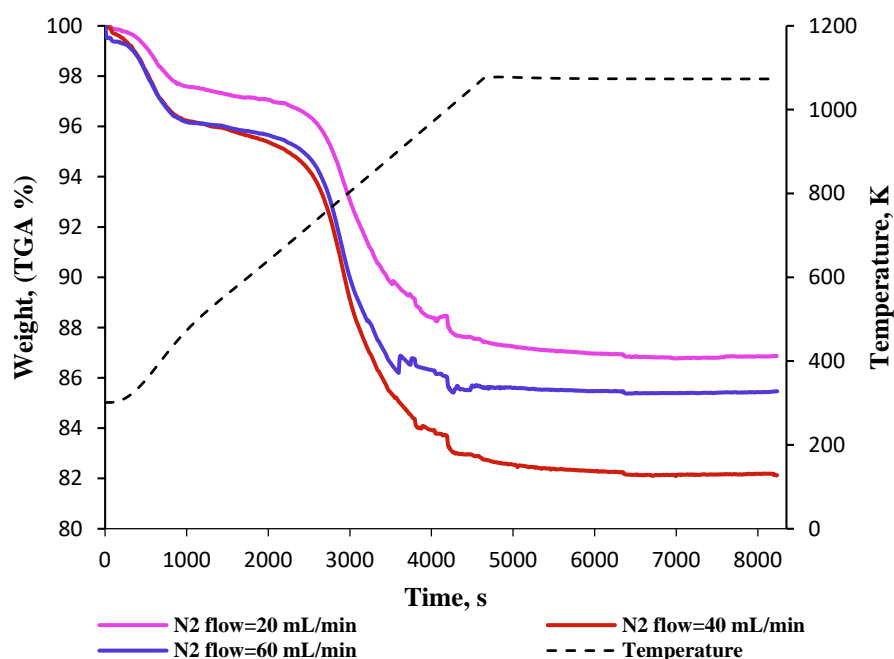


Figure 8.10 Weight loss of the spent HZSM-5(30) involved in the FP-CU at N₂ flows of 20, 40 and 60 mL/min (600 °C, C:L=1)

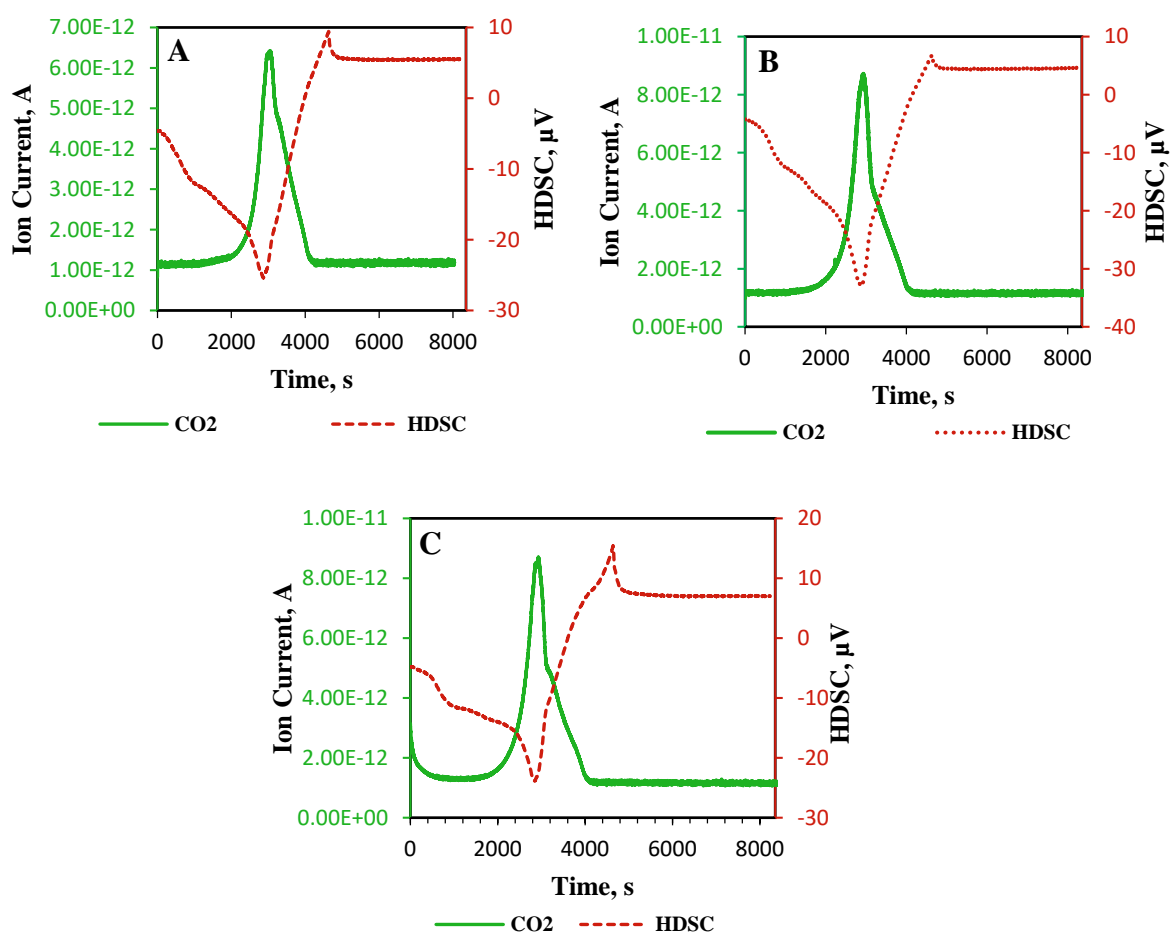


Figure 8.11 The CO₂ ion current (MS) and HDSC of HZSM-5 involved in FP-CU at N₂ flow of 20 (A), 40 (B) and 60 mL/min (C) (600 °C, C:L=1)

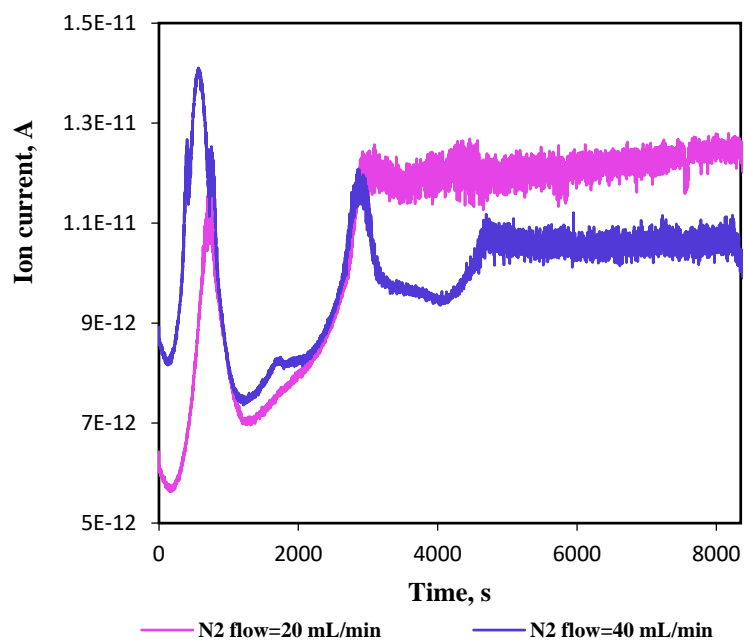


Figure 8.12 The H₂O ion current (MS) and HDSC of HZSM-5 involved in FP-CU at N₂ flow of 20 and 40 mL/min (600 °C, C:L=1)

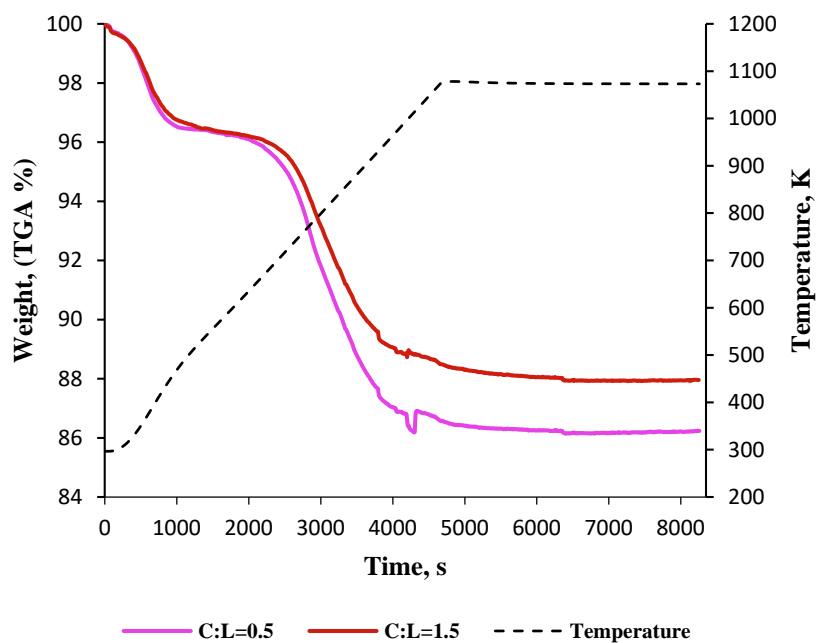


Figure 8.13 Weight loss of the spent HZSM-5(30) involved in the FP-CU at C:L =0.5 and 1.5 (550 °C, N₂ flow= 40 mL/min)

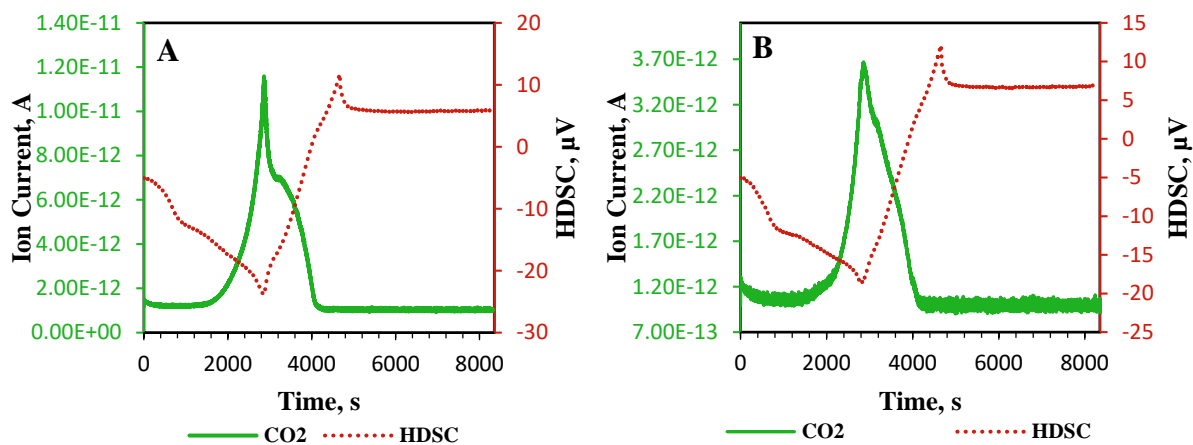


Figure 8.14 The CO₂ ion current (MS) and HDSC of HZSM-5 involved in FP-CU at C:L of 0.5 (A) and 1.5 (B) (550 °C, N₂ flow= 40 mL/min)

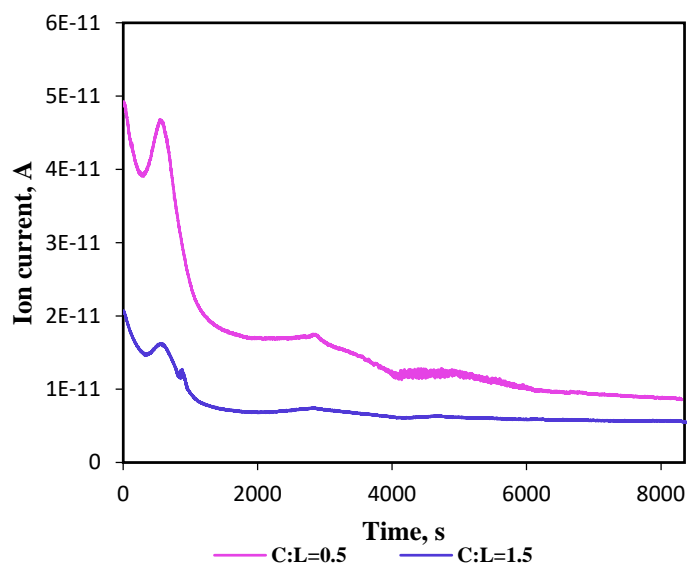
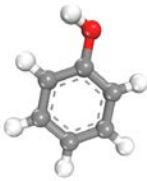
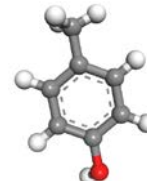
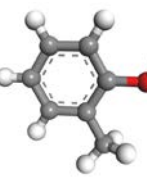
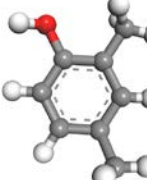
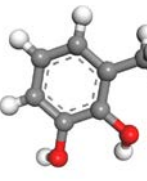
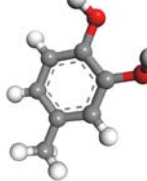
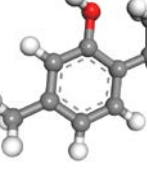
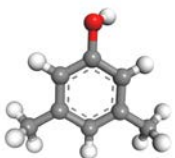
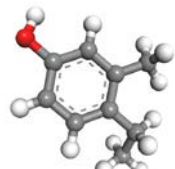
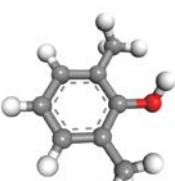
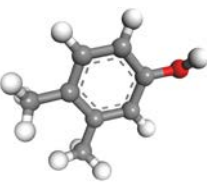
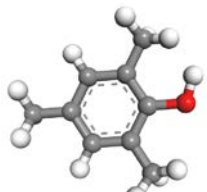
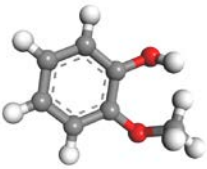
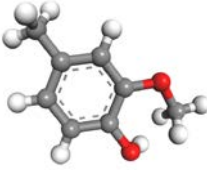
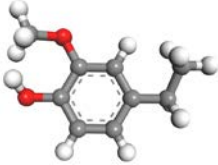
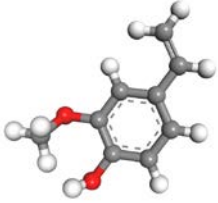
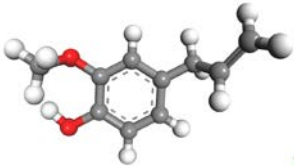
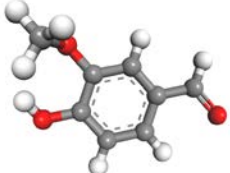
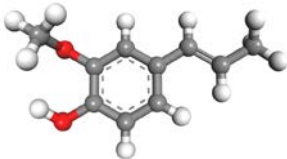
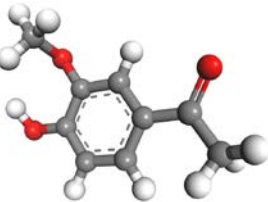
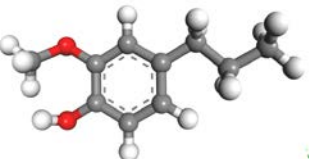
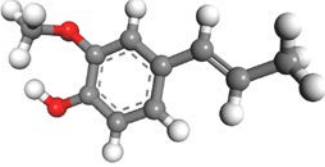
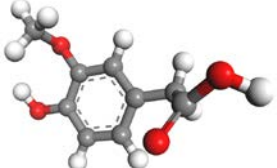
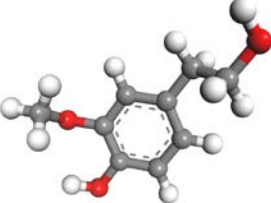
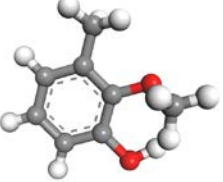
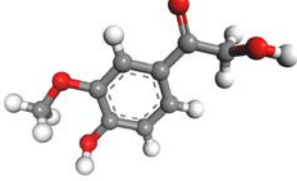
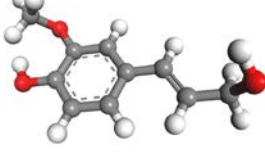
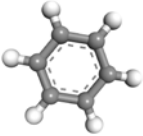


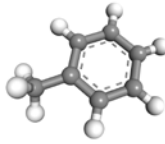
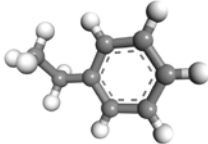
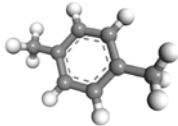
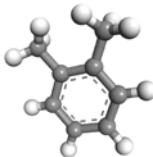
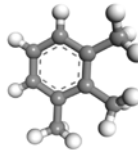
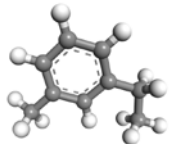
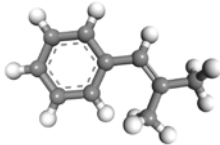
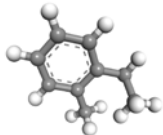
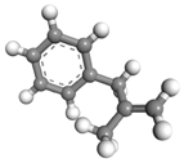
Figure 8.15 The H₂O ion current (MS) and HDSC of HZSM-5 involved in FP-CU at C:L of 0.5 and 1.5 (550 °C, N₂ flow= 40 mL/min)

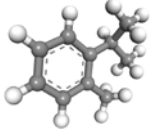
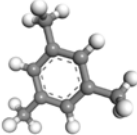
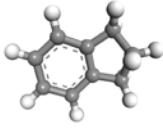
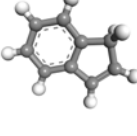
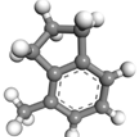
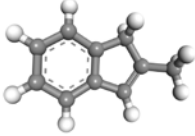
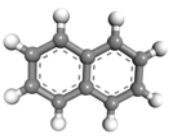
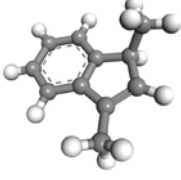
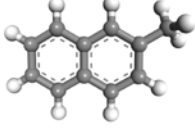
Name of the molecule	Structure of the molecule	Å		
		Size1 (x)	Size2 (y)	Size3 (z)
Phenolic compounds(Ph, MCatec)				
Phenol		1.11	4.64	5.73
p-Cresol		1.861	4.618	6.128
Phenol, 2-methyl-		1.862	5.742	5.758
Phenol, 2,4-dimethyl-		2.28	5.875	7.013
1,2-Benzenediol, 3-methyl-		1.862	5.829	6.18
1,2-Benzenediol, 4-methyl-		1.11	5.211	6.86
Phenol, 2-ethyl-5-methyl-		1.855	5.738	8.508

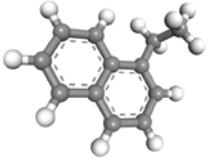
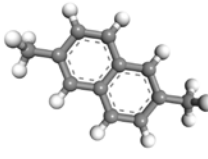
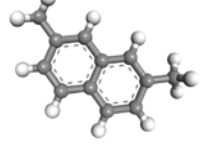
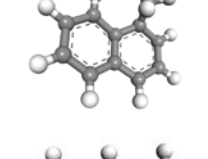
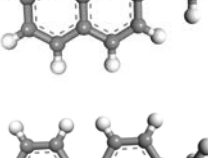
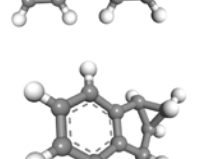
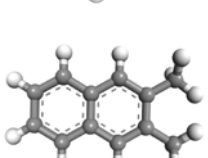
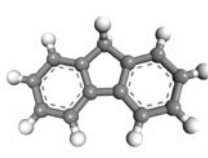
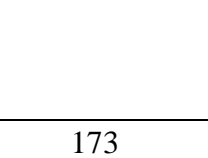
Name of the molecule	Structure of the molecule	Å		
		Size1 (x)	Size2 (y)	Size3 (z)
Phenol, 3,5-dimethyl-		1.862	6.177	6.896
Phenol, 4-ethyl-3-methyl-		3.145	6.217	8.404
Phenol, 2,6-dimethyl-		1.862	5.085	6.215
Phenol, 3,4-dimethyl-		1.862	5.799	6.878
Phenol, 2,4,6-trimethyl-		1.862	6.869	6.871
Phenol-alkoxy compounds (PhA)				
Phenol, 2-methoxy-		2.175	4.641	7.535
Creosol		1.862	5.358	8.251

Name of the molecule	Structure of the molecule	Å		
		Size1 (x)	Size2 (y)	Size3 (z)
Phenol, 4-ethyl-2-methoxy-		2.176	5.778	8.286
2-Methoxy-4-vinylphenol		2.174	6.5	8.233
Eugenol		3.698	5.36	9.305
Vanillin		1.7115	5.985	7.496
trans-Isoeugenol		1.861	5.36	9.482
Apocynin		3.371	5.359	8.557
Phenol, 2-methoxy-4-propyl-		1.862	5.359	10.708

Name of the molecule	Structure of the molecule	Å		
		Size1 (x)	Size2 (y)	Size3 (z)
Phenol, 2-methoxy-4-(1-propenyl)-		1.862	5.36	10.412
Homovanillic acid		3.147	5.359	9.154
Homovanillyl alcohol		3.152	5.36	8.528
Phenol, 2-methoxy-3-methyl-		3.314	5.726	7.288
2,4'-Dihydroxy-3'-methoxyacetophenone		2.178	5.357	10.498
4-((1E)-3-Hydroxy-1-propenyl)-2-methoxyphenol		2.49	5.361	10.267
Aromatic hydrocarbons (MAH, DAH, PAH)				
Benzene		0	4.642	5.36

Name of the molecule	Structure of the molecule	Å		
		Size1 (x)	Size2 (y)	Size3 (z)
Toluene		1.862	4.641	5.757
Ethylbenzene		3.149	4.642	7.52
p-Xylene		1.862	4.641	6.157
o-Xylene		1.862	4.988	5.758
Benzene, 1,2,3-trimethyl-		1.862	5.757	6.845
Benzene, 1-ethyl-3-methyl-		1.863	5.012	7.538
Benzene, (2-methyl-1-propenyl)-		1.862	4.64	8.565
Benzene, 1-ethyl-2-methyl-		3.15	5.818	7.561
Benzene, (2-methyl-2-propenyl)-		3.851	4.641	8.308

Name of the molecule	Structure of the molecule	Å		
		Size1 (x)	Size2 (y)	Size3 (z)
o-Cymene		3.144	5.885	7.642
Mesitylene		1.862	5.759	6.908
Indane		1.892	5.381	6.944
Indene		1.886	5.396	7.175
1H-Indene, 2,3-dihydro-4-methyl-		1.862	6.217	6.938
2-Methylindene		1.862	5.396	7.661
Naphthalene		0	5.36	7.309
1H-Indene, 1,3-dimethyl-		3.165	6.133	7.184
Naphthalene, 2-methyl-		1.862	5.986	8.671

Name of the molecule	Structure of the molecule	Å		
		Size1 (x)	Size2 (y)	Size3 (z)
Naphthalene, 1-ethyl-		3.148	7.31	7.565
Naphthalene, 2,6-dimethyl-		1.862	5.986	9.324
Naphthalene, 2,7-dimethyl-		1.862	5.361	9.601
Naphthalene, 1-methyl-		2.68	5.358	7.308
Naphthalene, 2-ethenyl-		0	5.988	10.326
1,1'-Biphenyl, 4-methyl-		1.863	4.641	10.368
Cycloprop[a]indene, 1,1a,6,6a-tetrahydro-		3.192	5.377	7.04
Naphthalene, 2,3-dimethyl-		1.862	5.36	8.519
Fluorene		1.888	5.617	9.657

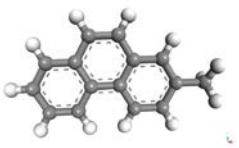
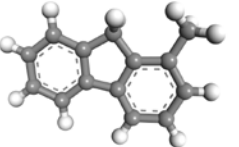
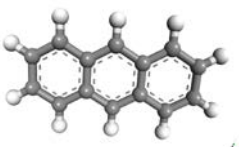
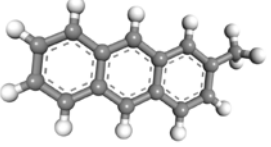
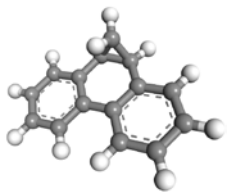
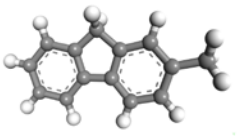
Name of the molecule	Structure of the molecule	Å		
		Size1 (x)	Size2 (y)	Size3 (z)
Phenanthrene, 2-methyl-		1.862	5.987	10.377
9H-Fluorene, 1-methyl-		1.862	5.618	9.656
Anthracene		0	5.36	9.977
Anthracene, 2-methyl-		1.861	5.36	10.914
1H-Cyclopropa[1]phenanthrene, 1a,9b-dihydro-		2.128	5.957	9.974
9H-Fluorene, 2-methyl-		1.864	5.63	10.556

Table 8.11 The structure and the molecule size of the compounds from the PhA, Ph, MAH, DAH and PAH groups obtained at different temperature of FP and in FP-CU on HZSM-5(30), H β and HY

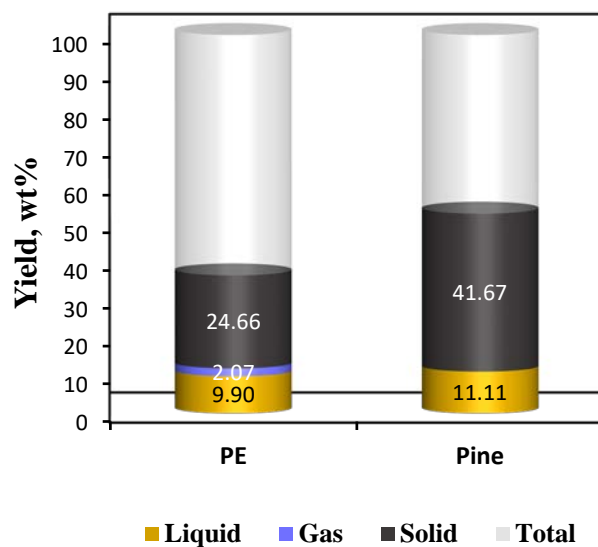


Figure 8.16 The distribution of the three main FP-CU products (gas, liquid and solid) obtained in the fixed bed reactor at 600 °C and nitrogen flowrate of 40 mL/min. The HZSM-5(30):PE ratio was set 1 and HZSM-5(30): pine ratio was set 3.

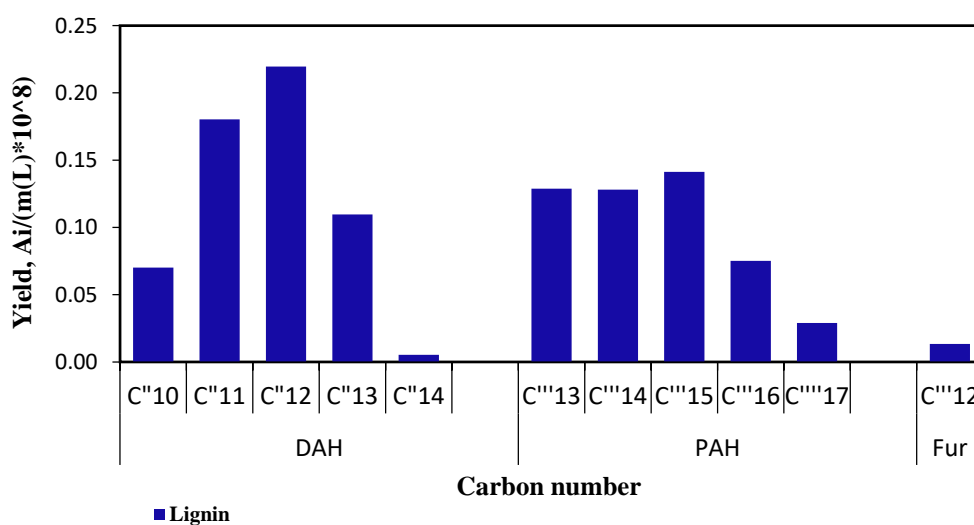


Figure 8.17 The products distribution of FP-CU of lignin in the fixed bed reactor. The process was realized at 700 °C, nitrogen flowrate of 100 mL/min and catalyst to lignin ratio of 1. The products of liquid phase were analyzed by GC/MS.